**Terms and Conditions of Use of Digitised Theses from Trinity College Library Dublin**

**Copyright statement**

All material supplied by Trinity College Library is protected by copyright (under the Copyright and Related Rights Act, 2000 as amended) and other relevant Intellectual Property Rights. By accessing and using a Digitised Thesis from Trinity College Library you acknowledge that all Intellectual Property Rights in any Works supplied are the sole and exclusive property of the copyright and/or other IPR holder. Specific copyright holders may not be explicitly identified.  Use of materials from other sources within a thesis should not be construed as a claim over them.

A non-exclusive, non-transferable licence is hereby granted to those using or reproducing, in whole or in part, the material for valid purposes, providing the copyright owners are acknowledged using the normal conventions. Where specific permission to use material is required, this is identified and such permission must be sought from the copyright holder or agency cited.

**Liability statement**

By using a Digitised Thesis, I accept that Trinity College Dublin bears no legal responsibility for the accuracy, legality or comprehensiveness of materials contained within the thesis, and that Trinity College Dublin accepts no liability for indirect, consequential, or incidental, damages or losses arising from use of the thesis for whatever reason. Information located in a thesis may be subject to specific use constraints, details of which may not be explicitly described. It is the responsibility of potential and actual users to be aware of such constraints and to abide by them. By making use of material from a digitised thesis, you accept these copyright and disclaimer provisions. Where it is brought to the attention of Trinity College Library that there may be a breach of copyright or other restraint, it is the policy to withdraw or take down access to a thesis while the issue is being resolved.

**Access Agreement**

By using a Digitised Thesis from Trinity College Library you are bound by the following Terms & Conditions. Please read them carefully.

I have read and I understand the following statement: All material supplied via a Digitised Thesis from Trinity College Library is protected by copyright and other intellectual property rights, and duplication or sale of all or part of any of a thesis is not permitted, except that material may be duplicated by you for your research use or for educational purposes in electronic or print form providing the copyright owners are acknowledged using the normal conventions. You must obtain permission for any other use. Electronic or print copies may not be offered, whether for sale or otherwise to anyone. This copy has been supplied on the understanding that it is copyright material and that no quotation from the thesis may be published without proper acknowledgement.
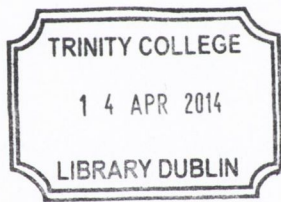
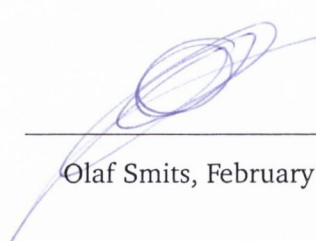# Interferometry and non-equilibrium noise in the fractional quantum Hall effect

Olaf Smits

# Declaration

I declare that this thesis is my own work and has not been submitted as an exercise for a degree at this or any other university and it is entirely my own work.

I agree to deposit this thesis in the University's open access institutional repository or allow the library to do so on my behalf, subject to Irish Copyright Legislation and Trinity College Library conditions of use and acknowledgement.

Olaf Smits, February 2014

# List of publications

This thesis is based on the publications:

O. Smits, J. K. Slingerland, S. H. Simon,
*Tunnelling current through fractional quantum Hall interferometers,*
Physical Review B **89**, (2014), 045308.
DOI: 10.1103/PhysRevB.89.045308
ArXiv e-prints arXiv:1304.6967

O. Smits, J. K. Slingerland, S. H. Simon,
*Non-equilibrium noise in the (non-)Abelian fractional quantum Hall effect,*
ArXiv e-prints arXiv:1401.4581

# Summary

We study theoretical aspects of fractional quantum Hall devices based on tunnelling point contacts. The fractional quantum Hall effect is the prime example of a $(2+1)$ dimensional system with non-trivial topological order. Fractional quantum Hall systems exhibit quasiparticle excitations (anyons) which carry fractional charge and obey a generalized form of statistics. These anyons can be observed and studied in transport experiments using point contacts. In this work we use both perturbative and non-perturbative techniques to study the current through a double point contact interferometer and the properties of non-equilibrium noise in a single point contact.

In a fractional quantum Hall interferometer quasiparticles can tunnel along multiple paths which gives rise to interference effects due to dynamical contributions, the Aharanov-Bohm effect and braiding of edge and bulk quasiparticles. In this thesis we determine the tunnelling current in linear response theory (linear in the tunnelling coupling constant). Our novel result is an expression for the interference current expressed in terms of a hypergeometric function called Carlson's $R$ function which applies to generic quantum Hall edge theories. The expression is a function of properties of the quasiparticle (electric charge, conformal dimension, edge velocities) and of the point contact (distance between the point contacts, source-drain voltage, temperature). We provide a numerical scheme to compute this function. The code used to produce the plots of the current in this thesis is publicly available.

Shot noise experiments measure the noise of a tunnelling current through a single point contact in an effort to determine the fractional charge of the quasiparticles. However, these experiments actually measure the noise in the edge current, instead of the tunnelling current. We develop a non-equilibrium, non-perturbative Kubo formula which relates the edge current to the tunnelling current. Through this expression we obtain a non-equilibrium fluctuation-dissipation theorem which expresses the noise in the edge current in terms of the noise in the tunnelling current. Our results again apply to generic edge theories. We also discuss the linear response theory of the noise, and compare our results to recent experimental work.

*To my parents.*

# Acknowledgements

Wow, it all has come to an end! And what a journey it was. I am hugely grateful to my supervisor Dr. Joost Slingerland for excellent support, guidance and encouragement throughout the past few years. You handed me a very interesting and rich research topic, and allowed me to freely explore the subject and pursue my ideas, all while still keeping me on track. Your continued enthusiasm and attention to detail, even into the late hours during the final week before submission, made this thesis what it is today. Thank you again.

To my parents and family: Anke, Jos, Kitty, my sisters Tamara and Sharon-Joy, and my little niece Lieve. Thank you all for your continued love and support. The trips to Amsterdam always felt like coming home.

To my wonderful girlfriend, Aislinn, thank you for putting up with those weird working hours, listening to my rants about work or when I needed to vent my thoughts. Seriously, your support has been amazing. We can now go and celebrate.

Of course, there's also the guys at the institute, Thomas and Martin. The many coffee breaks made life at the institute a little less quiet. I also need to mention some of the geophysics and astronomy people: Matthew, Andrew, Rachael, Jan, Florian, and all the other people! Special thanks to Jesper, Sebas and Robert for plenty of discussions and feedback, mostly over beer. There are so many other people I could name, but I will keep it short. Thank you Tom, Esther, Alan, Sander, Ines, and everyone else!

# Contents

# Chapter 1

# Topological phases of matter

## 1.1 Introduction

The quantum Hall effect was discovered in 1980 by K. Von Klitzing, G. Dorda and M. Pepper [138]. The effect is observed in effectively two-dimensional electron systems subject to a magnetic field aligned perpendicular to the plane and low temperatures (typically $T \lesssim 25$ [mK] and $B > 3$ [T]). The effect refers to a quantization of the Hall resistance at values of

$$R_H = \frac{1}{\nu} \frac{h}{e^2} \tag{1.1}$$

and a simultaneous vanishing of the longitudinal resistance $R_L$. Quantization in this context means that the measured values of $\nu$ are stable against small deviations of the magnetic field and is independent of the sample geometry. Von Klitzing observed what is now known as the *integer* or *integral quantum Hall effect* as they measured an integer-valued factor $\nu$. For this discovery Von Klitzing was awarded the Nobel prize of 1985 [168]. In between, in 1982, the experimentalists D. Tsui and H. L. Stormer measured in samples grown by A. Goddard the quantization of the Hall resistance [208]. In addition to the integral effect they also measured, unexpectedly, a range of fractional values for $\nu$. This is known as the *fractional quantum Hall effect*. Their most prominent observation is the $\nu = 1/3$ case for which R. B. Laughlin constructed a theoretical framework [145]. For their work Tsui, Goddard and Laughlin were awarded the 1998 Nobel prize [169].

The factor $\nu$ is called the *filling fraction* and is related to the *dimensionless electron density*, which is a dimensionless ratio of the electron density and the magnetic field strength. Figure 1.1 shows measurements of the Hall and longitudinal resistance as a function of the magnetic field strength. As the magnetic field strength is varied the system tends to "lock" into a particular filling fraction where the Hall resistance is quantized and the longitudinal resistance vanishes. These *plateaux* signal the stability of the quantum Hall effect against deviations of the magnetic field.
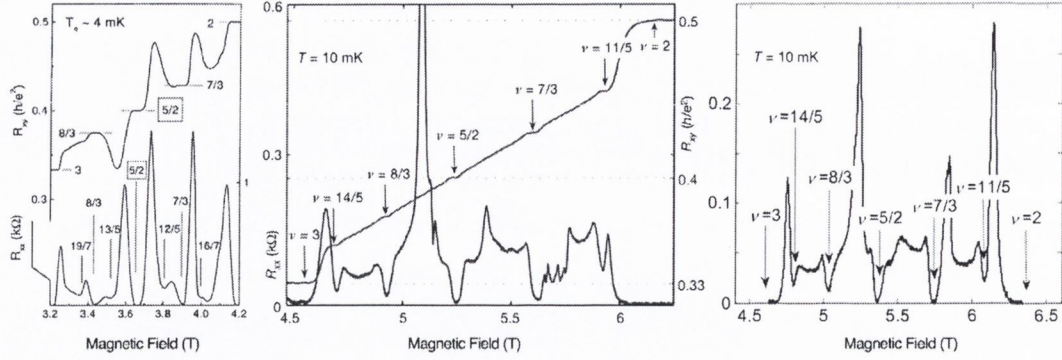
**Figure 1.1:** Examples of measurements of the longitudinal and Hall resistance. Note the formation of plateaux in the Hall resistance as a function of the magnetic field, which occurs simultaneously with a vanishing of the longitudinal resistance. Final plot only shows longitudinal resistance measurements. From left to right plots are taken from [174, 64, 62].

## Principal features of the quantum Hall effect

Figure 1.2 shows an experimental setup known as a quantum Hall bar, commonly used to measure the quantum Hall effect. A current $I$ is injected at the source $S$ which flows through the Hall bar and is collected by the drain $D$. Simultaneously, a magnetic field is applied perpendicular to the plane. As a consequence a voltage difference $V_H$ (the Hall voltage) arises along the transverse direction. This is the classical Hall effect, already discovered in 1879 by E. Hall [104]. The quantum Hall effect arises in effectively two-dimensional systems. This dimensionality reduction is accomplished in special samples which are grown such that a layered structure is formed. Commonly used layered compounds are MOSFET ($Si - SiO_2$) and HEMT ($GaAs - AlGaAs$). At the interface of these layers a quantum well forms. The quantum well "freezes" a direction of movement of the electrons stuck in the well. As a results these electrons are effectively confined to a two-dimensional plane, and the magnetic field is aligned perpendicular to this plane. In addition to the dimensionality reduction the quantum Hall effect requires strong magnetic fields ($B > 3$ [T]), low temperature ($T \lesssim 25$ [mK]) and the so-called ballistic conduction regime in which the mean free path of the electrons is of the order of the system size. The effect is now summarized by the following key features

- **Quantization of the Hall resistance.** This quantization is given by $R_H = V_H/I = \frac{1}{\nu}\frac{h}{e^2}$, where $\nu$ takes on integer or fractional values, and it is incredibly precise (more than one part in a billion).

- An approximately vanishing longitudinal resistance, $R_L = V_L/I \approx 0$ (equivalently, $V_L = 0$, see Fig. 1.1 for rough estimate bounds on $R_L$). This gives rise to **dissipationless flow.**
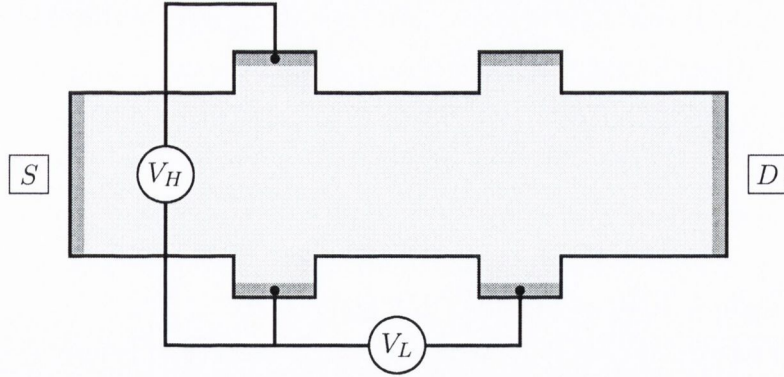
**Figure 1.2:** The experimental setup of a quantum Hall bar. The left and right edges of the system are connected to the source($S$) and drain ($D$). As a consequence a current flows through the system. Probes attached to upper and lower edges measure the longitudinal and Hall resistance (or equivalently the corresponding voltage drop).

- These observations are relatively **stable against perturbations**, such as deviations of the magnetic field, disorder, and the shape and size of the sample.

Related to this is the conductivity tensor $\sigma$ which is defined through the current density response $J_i = \sum_j \sigma_{ij} E_j$ with $E_i$ the electric field that forms inside the Hall bar. The in-plane Hall conductivity is given by

$$\sigma_{xy} = \frac{I}{V_H} = \nu \frac{e^2}{h}.$$  (1.2)

and the diagonal conductivity vanishes $\sigma_{xx} = \sigma_{yy} = 0$.

### Quantum Hall states

Each plateau corresponds to a different electronic phase of matter characterized by the filling fraction $\nu$. There are then two important questions that arise. (1) What is the mechanism responsible for the formation of a quantum Hall plateau, and (2) given a quantum Hall plateau, what are its properties? The first is complex interplay between the Lorentz force, disorder and electron-electron interactions. We briefly discuss this in the next section. The main work presented in this thesis is contained within the second question.

What is important to know is that there is currently no general and universal method that accounts for all observed filling fractions. Laughlin's approach [145] is the most successful description of a quantum Hall state ($\nu = 1/3$) but it does not generalize to generic filling fractions. Other approaches are for instance the composite fermions, hierarchy and more general trial wavefunctions approaches (this includes so-called conformal field theory approaches). But these approaches do not always agree on the nature of a quantum Hall state for fixed

filling fraction $\nu$. For a large class of filling fractions multiple effective theories have been put forward as candidates for the effective field theory. One plateau for which this is the case is the $\nu = 5/2$ state discovered in 1987 [226, 174, 232]. There are at least four different effective theories. It is not clear why one effective theory is favoured over another, and which one is realized in the physical sample.

## Spontaneous symmetry breaking does not apply

To appreciate the complexity associated with the classification of quantum Hall states and the nature of quantum Hall physics we point to one of the great successes of the 20th century: spontaneous symmetry breaking and its classification scheme of phases of matter. In this theory a phase of e.g. a collection of electrons, spins or atoms is characterised by a local order parameter. Upon a phase transition this parameter obtains a non-vanishing expectation value which breaks a symmetry of the system. This gives rise to an effective field theory description of the free energy known as Ginzburg-Landau theory [90]. The classification of phases of matter and phase transitions is accomplished by identifying the corresponding symmetry classes. What is remarkable about the quantum Hall effect is that the different quantum Hall states *cannot* be classified according to this scheme of spontaneous symmetry breaking. All quantum Hall states have the same symmetry and, most importantly, there are no local order parameters which can distinguish different quantum Hall phases [221].

## Topological order

Fractional Quantum Hall states fall into a new paradigm known as *topological order*. This concept was introduced in 1989 by X. G. Wen [214] in the context of spin liquids and high temperature superconductivity. Topological order is a type of quantum order, that persists at zero temperature and gives rise to an incredibly rich field of emergent physics. The low-energy effective theory is an emergent gauge theory, and corresponds to a *topological quantum field theory*. It is responsible for a robust *ground state degeneracy* on Riemannian manifolds with non-zero genus (e.g. a torus). This degeneracy is sensitive to the topology of manifold. The system is topologically protected, meaning local perturbations such as disorder cannot induce transitions within this internal degenerate subspace. The theory contains quasiparticles known as *anyons* which are *fractionally charged* and obey a generalized type of statistics different from Bose and Fermi statistics. In the fractional quantum Hall effect it also predicts the existence of *protected edge states* which are responsible for dissipationless flow of the electric current.

One of the greatest challenges in FQH physics is the theoretical and experimental identification of the topological order associated with a filling fraction $\nu$. Related to this is trying to

understand the emergent physics predicted by this topological order and ultimately devising technological applications, for instance, a *topological quantum computer* [136, 53, 165, 212].

**Overview of this chapter**

The remainder of this chapter is a survey of all that is quantum Hall. Starting with a single particle picture subject to a magnetic field we introduce the main ideas behind the integer and fractional quantum Hall phases, and the special role of the edge. Our focus then shifts to the fractional quantum Hall effect and its interpretation as topological quantum matter. The survey ends with a short overview of the two main topics of this thesis: **fractional quantum Hall interferometry** and **non-equilibrium noise in fractional quantum Hall tunnelling point contacts**.

## 1.2 Aspects of the quantum Hall effect

### 1.2.1 Single particle system

The quantum Hall effect is an intrinsically many-body effect. Still, we can learn a great deal and develop a certain intuition by first considering the single particle case. Both classical and quantum mechanical treatments appear in any given introductory text on the quantum Hall effect, for instance Refs. [177, 155, 38, 92, 236, 124, 96]. Here we primarily use results of the lecture notes by Girvin [92].

**The classical system**

Consider a charged particle confined to a two-dimensional plane and subject to a perpendicularly aligned magnetic field $\mathbf{B} = B\hat{z}$. The dynamics of the charged particle with initial velocity $\mathbf{v}$ are completely determined by the Lorentz force, which reduces to $eB\mathbf{v} \wedge \hat{z}$. The general solution of the classical equations of motion is a *cyclotron orbit*: the particle follows a circular trajectory with an angular velocity $\omega_c$ that is independent of the initial velocity and the radius of the orbit. This angular frequency is called the *cyclotron frequency* and is given by

$$\omega_c = \frac{eB}{m_e c} \ . \tag{1.3}$$

The edge of a finite-size system acts as a barrier for these orbits. Upon an elastic collision with the wall the momentum is reversed and the center of the cyclotron orbit shifts parallel to the wall. The resulting motion is depicted in Figure 1.3 and is called a *skipping orbit*. On average the guiding center of a skipping orbit moves parallel to the wall. Since the orbits are
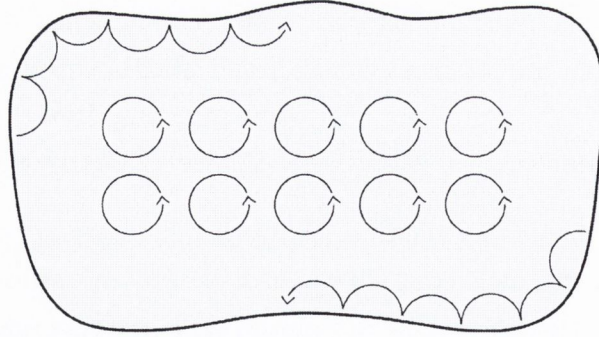
**Figure 1.3:** Figure of cyclotron motion and skipping orbits. The circular orbits is the cyclotron motion. Note that the motion along any given orbit is always counter-clockwise. There are no clockwise orbits due to the absence of time-reversal symmetry. The skipping orbits trace out the edge of the system. The movement along the edge is, again, chiral. Semi-classically there exists a lower bound on the possible radii of classical orbits.

unidirectional due the magnetic field, the net motion parallel to the edge is *chiral*. This reflects the absence of time-reversal symmetry, since the orientation of the magnetic field reverses with respect to this symmetry.

**Landau quantization**

The quantization of the single particle system first appeared in a paper by Lev D. Landau from 1930 [141, 142]. We again use results from Girvin [92]. Typically when a system is quantized the energy spectrum is partially discretised. For free particles this discretisation is a consequence of the boundary conditions imposed by the edge of the system. The energy gap between the different states vanishes as [system size]$^{-2}$. What makes the system of a charged particle in a magnetic field special is that (1) the magnetic field can do no work, meaning all energy is kinetic and the particle is free (yet its classical orbits are not straight lines), combined with (2) the energy levels become partially discretised with a gap that persists on the macroscopic scale. In this case the discretisation occurs because of the boundary conditions imposed by the periodic cyclotron orbits. Semi-classically the electron "wave" is periodic and only a whole number of wavelengths can fit along the circumference of the orbit, which is similar to the idea of the Bohr model. The spectrum of allowed radii is discrete with a gap that is independent of the system size. In particular there exists some smallest possible orbit. We can use Sommerfeld's quantization condition to derive this smallest radius [142, p. 170]. This condition is a constraint on the momentum and coordinates. The predicted lower

bound follows from

$$\oint_{\text{orbit}} \mathbf{p} \cdot d\mathbf{q} = 2\pi\hbar \,. \tag{1.4}$$

We set $|\mathbf{p}| = mv = mR\omega_c$ with $R$ the radius of the smallest orbit. Integrating over $q$ and solving for $R$ results in $R = l_B$ where

$$l_B^2 \equiv \frac{\hbar c}{eB} \,. \tag{1.5}$$

The quantity $l_B$ is called the *magnetic length*. Semi-classically it is the radius of the smallest possible orbit, which also correspond to the lowest energy states. Quantum mechanically the quantity $2\pi l_B^2$ is interpreted as the spread of a coherent wave packet.

To fully appreciate this discretisation we take a step further and look at what happens when the system is properly quantized. The Hamiltonian is given by

$$H = \frac{1}{2m}(\mathbf{p} - e\mathbf{A})^2 \tag{1.6}$$

with $B = (\partial_x A_y - \partial_y A_x)$ and canonical commutation relations $[x, p_x] = [y, p_y] = i$. To obtain the energy spectrum we introduce the gauge covariant momenta $\pi_\mu \equiv p_\mu - eA_\mu$. The different components $\pi_x$ and $\pi_y$ do not commute, in fact $[\pi_x, \pi_y] = -i\hbar eB/c$. These commutation relation are similar to that of a "momentum" $\pi_y$ and "coordinate" $\pi_x$, up to normalization. By writing the Hamiltonian as $H = \frac{1}{2m}(\pi_x^2 + \pi_y^2)$ we recognise the structure of a $1D$ harmonic oscillator, since the two terms appearing in the Hamiltonian do not commute. Diagonalisation of the Hamiltonian results in the energy spectrum of a harmonic oscillator

$$\epsilon_n = (n + \frac{1}{2})\hbar\omega_c \,, \qquad n = 0, 1, 2, \ldots \tag{1.7}$$

These energy levels are known as *Landau levels*. The states in the lowest Landau level ($n = 0$) correspond to the orbits with semi-classical radius $l_B$. The gap between two Landau levels is set by the cyclotron frequency $\omega_c$ which grows linearly with the magnetic field strength. In addition each Landau level is degenerate with a degeneracy of the order of the system size, although to justify this last statement we need to fix the gauge.

To analyse the structure within a Landau level requires a basis for the Hilbert space, which is obtained by fixing the gauge. The two most popular choices are the Landau gauge ($\mathbf{A} = -By\hat{x}$) and the symmetric gauge ($\mathbf{A} = \frac{B}{2}(y\hat{x} - x\hat{y})$), both of which are treated in e.g. Ref. [92]. These choices differ in their residual symmetries, with the Landau (symmetric) gauge retaining translational (rotational) symmetry. A basis for the Hilbert space is constructed using this extra symmetry and a short calculation [92] then gives that for a finite system with area $A$ the degeneracy per Landau level equals

$$\text{Degeneracy per Landau level} = \frac{BA}{\Phi_0} \tag{1.8}$$

where $\Phi_0 = \frac{e}{\hbar c}$ is defined as the unit magnetic flux quantum. The ratio on the right hand side of Eq. (1.8) represents the *number of flux quanta piercing through the system*. The degeneracy is of the order of the system size and grows linearly with the magnetic field strength. Alternatively, we can write the degeneracy per Landau level as $A/(2\pi l_B^2)$. The minimum spread (area) of any localized wave packet corresponds to $2\pi l_B^2$ and so this degeneracy can be formulated as *there is one independent quantum state per Landau level and per unit flux quantum*.

### 1.2.2 Many particle system

The magnetic field strength determines both the macroscopic degeneracy within each Landau level and the energy gap separating the Landau levels. Consider now the many particle case at zero temperature consisting of $N_e$ electrons. We assume that we can ignore the spin degrees of freedom as we expect these to align with the (strong) magnetic field. The *filling fraction* is the ratio of the number of electrons to the degeneracy per Landau level

$$\nu = \frac{N_e}{N_\phi}.$$ (1.9)

This is a dimensionless electron density. The integer quantum Hall effect corresponds to an integer number of fully filled Landau levels. In the fractional case we deal with a single, fractionally filled Landau level and it is possible that this state forms on top of one or multiple fully filled Landau levels.

#### The integer quantum Hall effect

The origin of the integer quantum Hall effect is well understood. It is a combination of the Landau level structure (essentially the Lorentz force at the quantum level) in combination with disorder. The energy gap between two Landau levels separates the ground state from its excitations. Each Landau level acts as a type of flat electron band. In the integer case the chemical potential sits in between two bands (Landau levels) and this resembles the band structure of an ordinary insulator. At the boundary the gap closes and chiral edge states form. These edge states turn the system into a conductor.

The presence of some disorder is required to stabilize the quantum Hall state against small perturbations. For an integer state to form we require the Fermi energy to sit in between two Landau levels. In the absence of disorder this can only be accomplished by the (non-physical) fine-tuning of the chemical potential as it requires a very precise electron density. Disorder causes *localization* of states [2, 179]. Electrons sitting in a localized state do not contribute to the conductivity of the system. Effectively these localized states act as a reservoir for the electrons. When the magnetic field is varied the reservoir can either absorb or supply electrons,
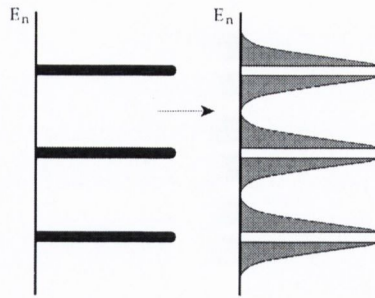
**Figure 1.4:** Sketch of broadening of Landau levels due to disorder. On the right hand side the gray area represents the localized states that do not contribute to the conductivity. The states in the thick white stripes are extended and cause the quantum Hall effect.

thereby keeping the electron density in the *extended states* fixed. It is these extended states which are responsible for the current-carrying properties of the system.

Figure 1.4 sketches the effect of disorder on the Landau level structure. It causes a broadening of the Landau levels and some states become localized. All localized states sit between the Landau levels and fine tuning of the chemical potential is no longer needed.

The integer quantum Hall effect is not the main focus of this thesis. The reason is that the system is actually not an example of a topologically ordered system as we define in Section 1.3. There are no fractionally charged quasiparticles and the system does not develop a ground state degeneracy that is sensitive to the topology of the space.

**The fractional quantum Hall effect**

The fundamental difference between the fractional and integer case is that the interaction between the electrons plays a central role in the formation of the fractional state. The importance of the electron-electron interaction follows from degeneracy of the Landau levels. In the absence of this interaction a fractionally filled Landau level is macroscopically degenerate and there is no energy gap protecting the ground state from its excitations. The lack of a gap implies that electrons can easily be scattered and a vanishing longitudinal resistance cannot occur. Electron-electron interactions are responsible for the formation of a unique ground state accompanied by an energy gap. The exact mechanisms responsible for the emergence of a gap are complicated and there is currently no general microscopic picture that explains why certain fractional quantum Hall states are favoured (more stable) compared to others[1].

---

[1]Specific approaches, such as the composite fermion approach, do provide a physical picture regarding the stability of the state, see e.g. [124] and references therein. But these approaches cannot account for all observed filling fractions.

---

However, we bypass this question and instead focus on the properties of FQH states and the corresponding emergent physics these states provide.

In both the fractional and integer effect the bulk of the liquid has a mobility gap. There are low energy states present in the bulk, but these do not contribute to conductivity properties of the system. We usually ignore this subtlety and speak of an energy gap instead.

### 1.2.3 Importance of the edge

The energy gap separates the ground state from its bulk excitations. Extracting or adding an electron to the bulk of the system requires at least enough energy to cross this gap. Quantum Hall liquids are therefore an example of an *incompressible liquid*, see e.g [155, 34]. The liquid behaves as a puddle of electrons with a tendency to keep its electron density fixed at $\nu$. Therefore, in an incompressible liquid the spectrum of sound waves in the bulk is gapped. Deformation of the liquid through gapless excitations is possible, but only at the edge of the system.

At the edge the liquid allows for gapless excitations which arise due to the force exerted by the boundary of the system. Figure 1.5 shows the (cross-sectional) effect of a confining potential on the Landau levels. At the boundary the energy of the states is pushed upwards and crosses the Fermi level. Halperin showed that these edge states are *extended* [106, 156]. Electrons in these edge states traverse the edge at a (non-zero) velocity $v_c$ and are immune to backscattering. Due to the absence of time-reversal symmetry they are also *chiral* meaning they flow along the edge in a fixed direction. The existence of extended edge states can also be attributed to topological properties of the Brillouin zone. This approach is known as topological band theory and it reveals interesting connections between the integer QHE and other electron states known as topological insulators and topological superconductors [113].

We can now understand the current-carrying properties of the system. In the quantum Hall effect *charge is always flowing along the extended states*. Furthermore, the system physically separates left and right moving states. All left moving states are confined to one edge (e.g. the upper edge), and all right moving states to the other edge[2]. A net total current through the system is generated by causing an imbalance in the left moving versus right moving states. This is depicted in Figure 1.5.

The longitudinal resistance vanishes due to the chirality of the edge states and the absence of backscattering. Extended states exist both in the bulk and at the edge of the system. However, a current injected into the system can only be added at the boundary, since this is where

---

[2]Some fractional states actually contain both chiralities on both edges. However, also in these cases the *net* direction in which charge is moving is again left moving on one edge and right moving on the other.
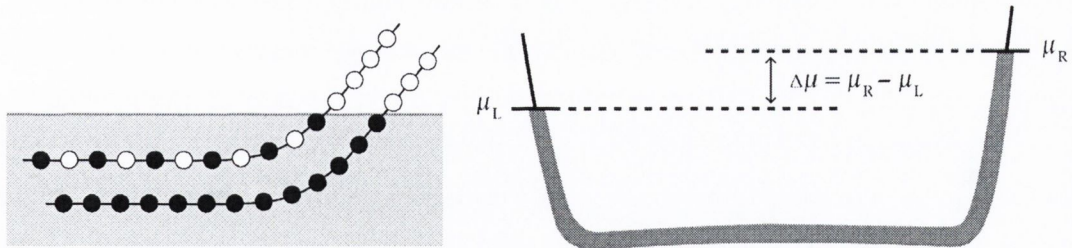
**Figure 1.5:** Left figure depicts the effect of the boundary on two Landau levels one of which is partially filled. In the bulk the states lie well beneath the Fermi level. The confining potential pushes the states situated at the edge upwards. The system allows for gapless excitations at the edge. Right figure depicts an imbalanced filling of the edges. The left/right moving edge is filled up to a chemical potential of $\mu_L$ and $\mu_R$. Since the edge states are extended a current flows through the system equal to $I = \nu \frac{e^2}{h} \Delta \mu$.

the (empty) states are located with an energy close to the Fermi level. For this reason it is often said that *the edge carries the current through the system*. This is partially correct, since in experiments the injected current indeed ends up in the edge of the system. On the other hand the conductivity properties of the system (absence of backscattering and quantization of the Hall conductivity) can only be understood if the bulk is taken into consideration as well. In addition, a local current does flow through the bulk of the system but the *net* current is determined by the relative filling of the edge states. See for instance [54] for further discussions. We explore the properties of the edge states in greater detail in Section 2. This includes a discussion on the total current and local current density operators.

## Quantization of Hall conductivity

The conductivity properties of the system are determined by the combined bulk and edge system. For the quantization of the Hall conductivity in the IQHE Laughlin provides an argument based on *gauge invariance* and spectral flow [144]. This results in the characteristic resistivity $R_H = \frac{1}{\nu} \frac{h}{e^2}$ for the ($\nu$ = integer) case. This argument has the benefit of providing a natural robustness of the conductivity against disorder as it does not require an exact expression for the basis states. A related approach is the Landauer formalism [54] in which the current is determined by integrating over all extended states. This leads to the same conclusion: each Landau level develops a *channel* at the edge, and the conductivity is determined by the number of filled channels (which equals the filling fraction).

Another approach is the famous TKKN paper [205] which computes the Hall conductivity of a quantum Hall state on a torus using the Kubo formula. In this approach the Hall conductivity is (1) given by an integral over all momentum states and (2) this integral is a *Chern*

*number*, which is an example of a topological invariant. This is a powerful conclusion, as it shows that conductivity is a *topological quantum number* and has a natural robustness against deformations of the system. The quantization of the conductivity is an intrinsic property of the electronic phase. The surprising aspect of this approach is that there are no edge states, since the system is considered on a torus, yet we can still determine the conductivity. The reason is, again, that the conductivity is a property of the entire system and not just the edge. For fractional quantum Hall states the quantization of the conductivity is attributed to gauge invariant properties of the effective theory.

### Collective nature of the edge states

Figure 1.5 suggests that it is reasonable to approximate the energy spectrum at the edge by a linear potential. In the integer case [106, 54] this linear approximation results in a $(1+1)D$ Fermi liquid describing the collective nature of the extended edge states. In the fractional case this Fermi liquid is insufficient to account for the range of observed filling fractions $\nu$. One reason is that a Fermi liquid is unstable against interactions in $(1+1)D$ making it unsuitable as a starting point for the FQH edge theory [89].

In a series of papers X.G. Wen [216, 215, 213, 222, 217, 219] conjectured that the edge degrees of freedom span a representation of a Kac-Moody algebra. The (linearised) action which determines the dynamics of this representation is a *chiral Tomonaga-Luttinger liquid* [101, 213, 97, 209, 44]. Wen derived this low energy picture using a hydrodynamical framework.

It was also shown that the edge theory can be viewed as a consequence of *anomaly cancellation* [216, 86, 84]. The effective bulk theory for the electromagnetic field develops an anomaly when the theory is put on a system with a boundary. This *chiral anomaly* is resolved by introducing an edge action with the same anomaly, but opposite in sign. The combined bulk plus edge theory is anomaly free. This anomaly has a natural physical interpretation: it signals that in the effective bulk theory charge is not conserved when a boundary is included. Charge flowing through the bulk eventually ends up in the edge, and we require an edge current to act as a drain of this charge flowing from the bulk into the edge. Electric charge is therefore conserved only in the combined bulk plus edge system.

There is no general theory of the edge of fractional quantum Hall states. Each proposed phase predicts a unique edge theory. There is some degree of universality though. For one, all edge theories are gapless and chiral. Furthermore, in the long wavelength limit the edge theory becomes a *chiral conformal field theory* and is closely related to the bulk phase due to the *bulk-edge correspondence* [213, 222, 200, 201, 33, 34, 52, 85]. However, not all chiral

CFTs are a candidate for a FQH edge theory. There are certain consistency conditions that determine what kind of chiral CFTs can describe an edge theory [85]. One of these is the presence of a $U(1)$ symmetry associated with the coupling to the electromagnetic field. The chiral CFT associated with a $U(1)$ symmetry is called the *chiral boson* [81]. The chiral boson model and its connection to the chiral anomaly are the subject of Section 2.

## 1.3 Topological order

A fractional quantum Hall liquid is an example of a *topological phase of quantum matter* described by *topological order* [219, 221, 220]. We define a topologically ordered state as *a gapped phase of matter which in the long range and low energy limit is described by a topological quantum field theory*. By gapped phase we mean that if we consider the liquid on a compact surface with no boundaries (e.g. a sphere or a torus) then the system has no gapless excitations. However, gapless excitations may arise when we consider a system with an edge. The earliest example of a topologically ordered state is, perhaps surprisingly, the effective theory of superconductivity with a dynamical electromagnetic field [214, 112]. Other examples include gapped quantum spin liquids [137], string net condensates [152], discrete gauge theories [6], BF theory [112], Chern-Simons theory [233], fractional Chern insulators [185] and rotating Bose-Einstein gases [50]. Recently there is also a large interest in topological insulators [164], of which the integer quantum Hall effect is an example. However, these arise in systems of non- or weakly interacting electrons or bosons and do not contain topological order in the sense defined above.

In the fractional quantum Hall effect the collective behaviour of the electrons together with the magnetic field is described by an effective topological quantum field theory known as Chern-Simons theory [233, 65, 165, 15]. In this effective description the energy gap separating the ground state from its excitations is taken to infinity, and the entire theory has trivial dynamics. The Hamiltonian is zero and all properties of the ground state are based on topological properties such as homotopy. Put differently, all correlation functions and observables are invariant with respect to smooth deformations of the space-time manifold. The physics predicted by topological order is far from trivial though. For instance, it predicts a ground state degeneracy which is sensitive to the topology of the underlying space [171]. This degeneracy may be used to distinguish different phases. More generally, the Hilbert space of a Chern-Simons theory is finite-dimensional and all states have zero energy. Other predictions of the topological order are the connection of the bulk wavefunction to conformal field theory [162], the collective behaviour of the protected edge states [217], topological entanglement

entropy [135], fractionalised quantum numbers [204] and bulk-edge correspondence [85, 201, 200]. Last but certainly not least are the quasiparticle excitations of the theory: anyons.

### 1.3.1 Anyons

Excitations arise as topological defects of the liquid and can be formed by extracting or injecting an electron or locally increasing the magnetic flux. These excitations are vortices in the liquid, similar to flux tubes that arise in superconductivity. They carry charge and spin, and may be treated as quasiholes or quasiparticles. What makes the FQHE special is that the "elementary" quasiholes carry *fractional charge* and obey a *generalized form of statistics*, of which Fermi and Bose statistics are special cases. Quasiholes / quasiparticles which obey these types of statistics are called *anyons*. This form of statistics [149, 225] can only arise in an effectively $(2+1)D$ space-time.

#### (Non-)Abelian anyons and Braiding

Anyons fall into two categories: Abelian and non-Abelian. The (non-)Abelian nature refers to the commutative properties of the anyons exchange statistics. An Abelian anyon is essentially an intermediate version of a fermion or boson. Upon the adiabatic exchange of two anyons in real space the wavefunction picks up a phase $e^{i\theta}$. The cases $\theta = 0$ and $\pi$ correspond to Bose and Fermi statistics. In the pure TQFT description the exchange is completely determined by the homotopy properties of the world lines of the anyons. This is called *braiding*. In a physical sample the exchange is assumed to be performed adiabatically. When multiple, identical Abelian anyons are braided the final wavefunction depends on the orientation in which the anyons are exchanged (clockwise or anti-clockwise) but not on the exact order.

Non-Abelian anyons are a different story. In this case the final wavefunction depends more strongly on the exact braiding pattern of the anyons. Consider a quantum Hall state with four non-Abelian anyons (see Figure 1.6). This configuration with fixed coordinates of the anyons is *degenerate*. The wavefunction is an element of a non-local (topological), internal space. Suppose we fix a basis $\{|\Psi_a\rangle\}$ of this internal space. The $|\Psi_a\rangle$'s all have the same spatial configuration of anyons, yet they form an orthonormal basis. The braiding of anyons induces a unitary transformation of the form

$$|\Psi_a\rangle \longrightarrow \sum_b M_{ab}|\Psi_b\rangle \,. \tag{1.10}$$

Here $M_{ab}$ represents the action of that particular braiding pattern on the internal space. The system is said to be topologically protected because *local perturbations cannot induce transitions within this internal space*. In addition when multiple anyons are braided the final

$$|\Psi'\rangle = \sum_a c'_a |\psi_a\rangle$$

$$c'_a = \sum_b c_b M_{ba}$$

$$|\Psi\rangle = \sum_a c_a |\psi_a\rangle$$
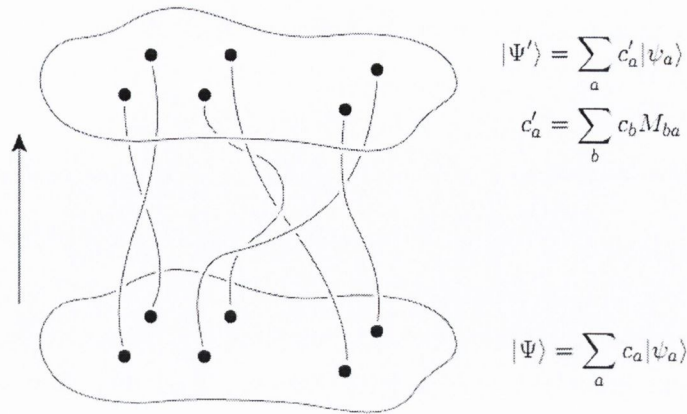
**Figure 1.6:** Braiding of (identical) non-Abelian anyons. The arrow represents the direction of time. At the the initial time there is some configuration of anyons. These anyons are adiabatically braided and interchanged. The final spatial configuration is identical to initial one. However, the braiding induces a unitary transformation on the wavefunction within the internal, topological space.

wavefunction depends on the exact order of the braiding operators, as in general $MM' \neq M'M$. To summarize, non-Abelian braiding statistics refers to the non-commutative nature of exchange operations which is realized by the presence a non-local, degenerate, internal Hilbert space.

### Fusion

A second important property of (both Abelian and non-Abelian) anyons is *fusion*. Two anyons brought in close proximity fuse together and form a third. For Abelian anyons the resulting fusion product is unique. For non-Abelian anyons there may be multiple possible fusion outcomes, which is related to the degenerate internal space mentioned before. If we denote $a$, $b$ and $c$ as types of anyons then the fusion is schematically represented by

$$a \times b = \sum_c N^c_{ab} c, \qquad N^c_{ab} \in \mathbb{Z}_{\geq 0} . \tag{1.11}$$

For Abelian anyons $a$ and $b$ there is a unique anyon $c$ for which $N^c_{ab}$ is non-zero, since the fusion product is unique. Non-Abelian anyons on the other hand have multiple possible fusion outcomes $c$ (multiple non-zero $N^c_{ab}$), and the exact outcome of a fusion process depends on the history of the system. The possible fusion channels are closely related to the degenerate subspace appearing in the exchange relations (1.10). Roughly speaking, a collection of anyons spans an internal, non-local space. In the pure CS theory (the effective theory limit) this internal space is the Hilbert space of the theory with the anyons represented by inserted

Wilson loop operators. All other states are gapped out. The dimensionality of the internal space is determined by the number of fusion channels appearing in the fusion product of the anyons and coefficients of these fusion channels (since $N_{ab}^c$ can be bigger than 1).

**Bulk-edge correspondence**

The bulk-edge correspondence is a natural property of topologically protected systems. The theory which describes the $(1+1)D$ edge of the system is "equal" to the theory which describes the $(2+0)D$ bulk. Before we explain this correspondence we first mention the connection between the bulk wavefunction and conformal field theory. In a famous work by Witten [233, 67] it was shown that the Hilbert space of a Chern-Simons theory corresponds to the space of conformal blocks of a corresponding Wess-Zumino-Witten model. A WZW model is an example of a conformal field theory constructed using a conserved current. In the FQHE this correspondence leads to an interesting property: the ground state wavefunction of a fractional quantum Hall state is given by a conformal block (a correlator) of the corresponding WZW model. This wavefunction is not the "true" wavefunction, but rather that of an idealized system (e.g. no disorder, a special geometry, etc.). The idea is that this wavefunction captures the relevant physics of the corresponding topological order. For instance, the theory predicts the spectrum of anyons, including their electric charge, and the fusion and braiding rules. Conformal field theory is a powerful tool through which the properties of the topological order can be studied as it places stringent conditions on the correlation functions of the theory. Through this connection CFT can be used to devise so-called *representative wavefunctions*, which are candidate wavefunctions that (hopefully) capture the relevant physics of a particular fractional quantum Hall state, see e.g Refs. [162, 183, 184, 3].

The CFT describes the wavefunction for a fixed time slice through its space of conformal blocks. Electrons and anyons are represented by conformal primary operators, and the wavefunction is constructed through a CFT correlator.

The bulk-edge correspondence [85] refers to the idea that the spectrum at the edge of the system is described by the same CFT which is used to generate bulk wavefunctions. The difference is that this edge CFT describes the dynamics of the $(1+1)D$ gapless edge theory and its correlators are not interpreted as wavefunctions. The edge and bulk theory both contain *the same* type of anyons, meaning that for every $(0+2)D$ bulk operator there exists a $(1+1)D$ edge operator, with the same charge and statistical properties. Stone [201, 200] provides an intuitive interpretation of this correspondence. We start with an FQH state on an annulus geometry. The edges are described by a CFT and we consider the inner edge which is carrying an elementary excitation. This elementary excitation is generated through the application of a

conformal primary operator of the edge CFT. Because this inner edge is of finite size its energy spectrum is gapped. By decreasing the size of the inner hole this gap increases. Eventually, the size of the inner edge is so small that only its lowest energy state is accessible – all other states are gapped out. All that is left is a tiny depletion of the electron liquid; a non-dynamical vortex that behaves as a quasiparticle, with the same charge and conformal dimension as the original primary operator that we started with. This procedure can be performed for each primary state in the edge CFT. As a result, for each primary operator on the edge we can construct a vortex-like object in the bulk. The spectrum of bulk quasiparticles is therefore equal to those present on the edge.

Bulk-edge correspondence ensures that the "information" about the topological order of the system is present in both the bulk and the edge of the system. In addition, the edge is responsible for carrying the electric current through the system. These two properties combined imply that experiments involving the edge of the system (i.e. charge, heat or spin transport) are a good candidate for identifying the topological order.

## Modular tensor categories and topological quantum computation

There is a very rich mathematical structure underlying the statistical properties of anyons called a *modular tensor category* (MTC). Such a category models the "topological properties" of a collection of anyons with a consistent set of braiding and fusion rules. A given set of $n$ (non-)Abelian anyons forms a representation of the Braid group $\mathcal{B}_n$. The Braid group by itself is already very rich, for instance due its relation to *knot theory* (see e.g. Ref. [134] for an overview on knot theory from a physics perspective), and the study of anyons and types of topological order is closely related to mapping out the representation theory of the braid group. Fusion of anyons results in mappings between configurations with a different number of anyons. Hence we need to combine the representation theory of the braid groups for all possible numbers of particles $\{\mathcal{B}_n\}_{n=0}^{\infty}$. This is the anyon version of a Fock space with the important difference that the multi-anyon space is not a simple tensor product of single particle Hilbert spaces. In addition, fusion and braiding need to be "compatible" which leads to consistency relations imposed on the braiding and fusion rules [163, 178, 136, 212].

There are also potential technological implications associated with non-Abelian anyons and topological order. The internal space spanned by the anyons has a natural protection against decoherence since local operators cannot induce transitions in this space. This makes the system an interesting candidate for the realization of *topological quantum memory*, as it has an intrinsic protection against its environment. Quantum gates are realized through the braiding relations of the anyons, which is hoped to be a controllable operation. The realization

of a scalable *topological quantum computer* [83, 136, 53, 165, 212] might be just around the corner.

## 1.3.2 (Non-)Abelian fractional quantum Hall states

The prediction of fractionally charged particles was first due to Laughlin [145] for the $\nu = 1/3$ state. This included an effective description of the state using a trial wavefunction. This is the famous Laughlin wavefunction given by

$$\Psi_{\text{Laughlin}}(z_1, \ldots, z_n) = \left[\prod_{i<j}(z_i - z_j)^3\right] e^{-\frac{1}{4l_B^2}\sum_i |z_i|^2}. \tag{1.12}$$

The $z_i = x_i + iy_i$ are complexified coordinates and we consider the system on a disk geometry in the symmetric gauge. The exponential factor is a so-called geometric factor, and arises because the system is analysed on a disk. Stability and incompressibility of the model wavefunction was proven using the plasma analogy [145]. The anyons carry a charge $e/3$, are Abelian [5] and were observed in experiments measuring shot noise [193, 55]. Laughlin's approach may be extended to apply to states at filling fractions $\nu = n + \frac{1}{M}$ with $n$ and $M$ integers, and $M$ odd. In the case of $n > 1$ there are $n$ multiple fully filled Landau levels. Two generalizations of the Laughlin state are the hierarchy [102, 107] and composite fermion [122, 123, 124] approach. These predict states which are all Abelian and have a filling fraction of the form $\nu = \frac{p}{q}$ where $p$ and $q$ are co-prime and $q$ is odd. These two approaches predict different trial wavefunctions and do not agree on the physical mechanism responsible for the formation of a state. However, they do agree on the predicted topological order [182], e.g. the types of anyons present. More recently, the CF approach has also been cast into a conformal field theory language [111, 110, 203].

The $\nu = 5/2$ plateau [226, 174] was discovered in 1987 and is considered, as of yet, the most promising candidate for the realization of a non-Abelian state. The discovery came as a surprise, as the theoretical framework of the "traditional" hierarchy or CF approach cannot account for this particular filling fraction because it has an even denominator. The exact mechanisms responsible for the formation of the state appear to be different in origin as compared to e.g. the Laughlin state. One surprising aspect is, for instance, the absence of a $\nu = \frac{1}{2}$ state in the lowest Landau level, which suggests that an interplay between the electrons in the fractionally and fully filled Landau levels is necessary for the stability properties of the state. In the CF approach the absence of a $\nu = \frac{1}{2}$ can be explained as follows [108]: the effective magnetic field of the composite fermions vanishes at this specific filling fraction. As a result the CF's form a CF Fermi sea of non-interacting fermions. This Fermi sea does not have a gap and so no incompressible liquid is formed. Therefore the fractional plateaux that form

in the second and higher Landau levels could very well be realized by different FQH states as compared to those that form in the lowest level.

Multiple constructions exist as candidates for the topological order and underlying physics of the $\nu = 5/2$ plateau. The Haldane-Rezayi state [103] (based on a variation of the CF approach) and Halperin's (331) state [105] are two Abelian proposals. By far the most famous proposal is the Moore-Read state [162, 183] which is one of the earliest examples of a non-Abelian quantum Hall state. The MR trial wavefunction is constructed using a correlator of a chiral Ising model times a $\hat{u}(1)$ boson. This results in the Pfaffian wavefunction

$$\Psi_{\text{MR}}(z_1, \ldots, z_n) = \text{Pfaff}\left(\frac{1}{z_i - z_j}\right)\left[\prod_{i<j}(z_i - z_j)^2\right]e^{-\frac{1}{4l_B^2}\sum_i |z_i|^2}. \tag{1.13}$$

The Ising model is responsible for neutral degrees of freedom which do not couple to the electromagnetic field. Electrons and quasiparticle operators carry both charged and neutral degrees of freedom, and in general they are of the form $\mathcal{W}_n \otimes \mathcal{W}_c$, with $\mathcal{W}_n$ the neutral part and $\mathcal{W}_c$ the charged part. The Ising model is responsible for the non-Abelian nature of the state. It predicts a non-Abelian anyon with electric charge $e/4$ [162, 166]. A variant of the Moore-Read state is the Anti-Pfaffian [151, 148], which is the particle-hole conjugate of the Pfaffian state. It also predicts an $e/4$ anyon, but with slightly different statistical properties (the two candidates have different topological order).

Pinpointing the nature of the $\nu = 5/2$ plateau still remains one of the greatest challenges of the field. For a recent overview on the nature of the $\nu = 5/2$ state and the current state of the experimental, numerical and theoretical side we point to the review article by Willett [232]. Experiments such as fractional quantum Hall interferometry and shot noise in tunnelling point contacts hope to either rule out or verify part of the topological order. Such experiments measure, either directly or indirectly, the charge and statistics of the anyons. This thesis aims to shed light on theoretical aspects of these experiments, which includes but is not limited to the $\nu = 5/2$ plateau.

We refer to the literature for many other approaches and generalizations that generate trial wavefunctions or other effective models for fractional quantum Hall states [154, 22, 184, 4, 85, 195, 111, 26, 12, 11, 223].

## 1.4 What this thesis is about

Two of the biggest challenges currently faced in the domain of FQH physics are (1) how can we distinguish between different types of topological order, and (2) do non-Abelian anyons exist? One of the most appealing properties of a topologically ordered state is that the effective

theory has no local degrees of freedom. However, it is also this property which prevents the experimentalist from directly probing the order. Topological order can therefore only be identified through indirect means, for instance by identifying the type of anyons present the system, which includes measuring their charge and statistics.

In this thesis we focus on theoretical aspects of two types of FQH experiments that attempt to measure properties of non-Abelian anyons. These are shot noise experiments such as Refs. [193, 55, 95, 187, 94, 100, 114, 49, 46, 47, 115, 116, 64, 45, 13, 60, 62, 61, 63] and fractional quantum Hall interferometry [126, 32, 228, 229, 1, 230, 231, 227]. The edge is central in both of these experiments, since both experiments use the edge current as an experimental probe.

### 1.4.1  The chiral boson

We mentioned that although there is no single action that describes all FQH edges, there are still universal features present in the edge theories of different fractional quantum Hall states. These are the chiral conformal nature, bulk-edge correspondence and coupling to the the electromagnetic field. The coupling is accounted for by the presence of a $U(1)$ gauge symmetry, and the chiral CFT based on this symmetry is the **chiral boson**. Therefore it is expected that one or multiple copies of this theory are always part of the edge theory of a generic fractional quantum Hall state. The chiral boson is the subject of Section 2. We show how the system necessitates a $U(1)$ gapless edge theory through the chiral anomaly, and how the chiral boson resolves this anomaly. Furthermore, we study the quantization of the chiral boson and determine some its correlators.

### 1.4.2  Fractional quantum Hall interferometry

A tunnelling point contact is a constriction in the quantum Hall liquid, which forces the opposite edges together. This generates an overlap of the edge states of the left and right moving edge. As a consequence anyons tunnel between the edges along the point contact, which results in a *tunnelling current* flowing from one edge to other. This current depends on the type of anyon tunnelling. In particular, the current is typically a non-linear function of e.g. the temperature, voltage bias, and the anyon's conformal dimension and electric charge.

In Section 3 we treat the linear response theory of the current through a **fractional quantum Hall interferometer**. The interferometer we consider is, simply speaking, multiple point contacts sequentially aligned, also known as a Fabry-Pérot interferometer. In this section we derive an expression for the tunnelling current using perturbation theory. Our final expression is valid for general fractional quantum Hall edges.

### 1.4.3 Non-equilibrium noise in tunnelling experiments

Shot noise experiments have been successfully employed to measure the fractional charge of the tunnelling anyons. These experiments measure the noise or fluctuations of the tunnelling current. The zero-frequency component of these fluctuations is the shot noise, and can be used (together with the tunnelling current) to extract the fractional charge of the tunnelling anyon.

However, these experiments do not actually measure the tunnelling current directly. Instead, what is being measured is the noise of the edge current, and consequently we require an expression relating the noise in the edge current to the noise in the tunnelling current. In Section 4 we study these relations, and prove them to all orders of perturbations theory. This results in a **non-equilibrium fluctuation-dissipation theorem**. We comment on results from linear response theory and the relevance to experiments in Section 5.

# Chapter 2

# The chiral boson

## 2.1 Purpose of this chapter

This chapter discusses some universal features of the edge theory of a fractional quantum Hall state at a generic filling fraction. In particular we focus on the chiral boson model. This model describes the edge degrees of freedom which couple to the electromagnetic field and are responsible for the charge transport properties of the edge of the system. This work lays the basis for Chapters 3 and 4 in which we study transport properties of tunnelling point contact systems.

The chiral boson by itself is an interesting model which requires some special care. It arises as a consequence of the chiral anomaly, which is a mechanism which necessitates the existence of edge degrees of freedom. Loosely speaking, the bulk electric current of an incompressible Hall liquid does not conserve electric charge at the boundary of the system. This is resolved by introducing an edge current. Charge which flows in the bulk cannot flow through the boundary of the system, and instead ends up in the edge current. On the level of the action this manifests itself as the chiral anomaly. The bulk action is not invariant with respect to the $U(1)$ gauge symmetry of the electromagnetic field. The chiral boson has the same anomaly, but opposite in sign. Therefore in the combined bulk and edge description the anomaly cancels out, gauge symmetry is restored and the total charge is conserved.

The chiral boson is an example of a constrained, bosonized theory. The Hilbert space is constructed using bosonic operators, even though the edge contains both fermionic and anyonic operators. The constrained nature arises because the edge is chiral. In this chapter we study the aspects of this model relevant to the fractional quantum Hall effect. We look at the quantum transport properties of the system, its constrained quantization procedure and we look at some important correlation functions that appear in later chapters.

## 2.2 The chiral anomaly

The chiral anomaly is the mechanism responsible for the existence of protected edge degrees of freedom. A fractional quantum Hall state on a system with a boundary automatically implies the existence of what we call a *charged channel*. This is an effective one-dimensional model describing the collective behaviour of the edge degrees of freedom. The model arises as a consequence of the chiral anomaly and it ensures that the complete (bulk and edge) system is anomaly free. The chiral anomaly states, in short, that the bulk of the system breaks gauge invariance at the edge, meaning electric charge is not conserved and the bulk system is anomalous. This is resolved by the edge theory, which is itself also anomalous. In the combined combined edge and bulk system gauge invariance is restored, the anomalies cancel and charge is conserved.

Our discussion on the chiral anomaly follows closely the work of Refs. [15, 217, 216, 85, 200]. We start with a phenomenological description of the quantum Hall effect by combining the Hall response with $(2+1)D$ electromagnetism. We take the Hall response, i.e. Eq. (2.4), as phenomenological input since this is what is observed in experiments. In this work we do not discuss the exact mechanisms underlying the Hall response, although we discussed in the introductory chapter that it is due to some interplay of the Lorentz force, disorder and the electron-electron interaction. We show how these phenomenological laws naively lead to inconsistencies when we consider a system with a boundary. In particularly in the presence of a boundary the phenomenological laws violate conservation of charge. This is the chiral anomaly which is resolved by taking into account the edge degrees of freedom.

### 2.2.1 Phenomenological considerations

The quantum Hall effect arises in an effective $(2+1)$ dimensional system. Through use of interfaces of certain layered compounds a quantum well is formed. Electrons sitting at the interface are trapped by this quantum well and their motion along the $z$-axis is frozen out. The electrons become confined to a two-dimensional plane, and we model the system as effectively $(2+1)$ dimensional with no spin degrees of freedom.

Consider now the electromagnetic field in $(2+1)D$. It is described by a two-component electric field $(E_x, E_y)$ and a single component magnetic field $B$. We do not consider in-plane magnetic components or perpendicular electric fields. Similarly the gauge potential is a three-
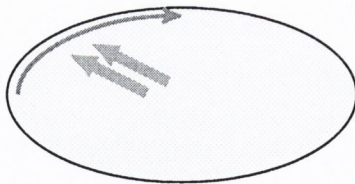
**Figure 2.1:** The simplest depiction of the chiral anomaly. Charge flowing through the bulk eventually encounters the edge of the system. The bulk current is deflected by the edge and charge ends up in the edge current. The bulk and edge currents act as each others source and drain. Charge is conserved only in the combined bulk and edge system.

vector $A_\mu = (A_t, A_x, A_y)$ and the electromagnetic field tensor is

$$F_{\mu\lambda} = \partial_\mu A_\lambda - \partial_\lambda A_\mu \qquad \Longleftrightarrow \qquad F = \begin{pmatrix} 0 & E_x & E_y \\ -E_x & 0 & B \\ -E_y & -B & 0 \end{pmatrix} . \tag{2.1}$$

This antisymmetric tensor is subject to the Maxwell-Faraday equation in (2+1) dimensions

$$\partial_t B = -\nabla \wedge \mathbf{E} \tag{2.2}$$

in units where $c = 1$. The current and charge density also combine into a three-vector, $J_\mu = (J_t, J_x, J_y)$ and no current flows in the $z$-direction. Since the system is closed and charge is conserved we have the continuity equation

$$\partial_\mu J^\mu = \partial_t J_t + \nabla \cdot \mathbf{J} = 0 . \tag{2.3}$$

The characteristic equation of the quantum Hall effect is the Hall transport equation or simply Hall's law. It relates the current density $\mathbf{J} = (J_x, J_y)$ to the external electric field $\mathbf{E}$ as

$$J^i = \sigma_H \epsilon^{ij} E_j \qquad \Longleftrightarrow \qquad \mathbf{J} = \begin{pmatrix} 0 & \sigma_H \\ -\sigma_H & 0 \end{pmatrix} \mathbf{E} \tag{2.4}$$

where $\sigma_H = \frac{\nu}{2\pi} \frac{e^2}{\hbar}$ is the Hall conductivity and $i, j = 1, 2$. The matrix on the right hand side is the conductivity tensor; its inverse is the resistivity of the system. The conductivity tensor has a vanishing diagonal component (dissipationless flow) and a constant off-diagonal (Hall) component $\sigma_H$. When Faraday's law (2.2) and the continuity equation (2.3) are combined with Hall's law (2.4) we obtain a fourth relation known as the Chern-Simons-Gauss' law. We have

$$\partial_t J_t = -\nabla \cdot \mathbf{J} = -\sigma_H \nabla \wedge \mathbf{E} = \sigma_H \partial_t B \tag{2.5}$$

Upon integrating we obtain a relation between the charge density and the magnetic flux. The Chern-Simons Gauss law effectively binds magnetic flux and electric charge

$$J_t(x) = \sigma_H B(x) \,. \tag{2.6}$$

Upon integration of Eq. (2.5) we also encounter integration constants. These are the homogeneous, background electron density $n_e$ and the background magnetic field $\bar{B}$. The current $J_\mu$ and the vector potential $A_\mu$ are fluctuations on top of these backgrounds. The effective theory models the behaviour of the system against this background.

Finally Hall's and the CS-Gauss law can be combined to

$$J^\mu = \frac{1}{2}\sigma_H \epsilon^{\mu\lambda\kappa} F_{\lambda\kappa} = \sigma_H \epsilon^{\mu\lambda\kappa} \partial_\lambda A_\kappa \,. \tag{2.7}$$

This expression reflects the response of charge and current in the Hall fluid to the external (perturbed) electromagnetic field. The relations (2.2) through (2.6) are the phenomenological laws governing the physics of a quantum Hall fluid and any effective theory is required to reproduce them. These laws also naturally give rise to the necessity of an edge current. This becomes apparent when we combine the continuity equation with Hall's law on a finite system $\mathcal{M}$ with some boundary $\partial\mathcal{M}$. The Hall conductivity $\sigma_H$ is constant throughout $\mathcal{M}$ and vanishes outside of it. When we take the divergence of the current this leads to

$$\partial_\mu J^\mu = \frac{1}{2}\sigma_H \epsilon^{\mu\lambda\kappa} \partial_\mu F_{\lambda\kappa} + \frac{1}{2}(\partial_\mu \sigma_H)\epsilon^{\mu\lambda\kappa} F_{\lambda\kappa} = \frac{1}{2}(\partial_\mu \sigma_H)\epsilon^{\mu\lambda\kappa} F_{\lambda\kappa} \neq 0 \,. \tag{2.8}$$

The right hand side is non-zero whenever $\sigma_H$ varies which happens precisely at the boundary $\partial\mathcal{M}$ of the sample. Consequently the boundary invalidates the continuity equation and both the symmetry and the current associated with the continuity equation have become anomalous. Physically, the bulk of the system is gapped which is required for the vanishing of the diagonal conductivity (dissipationless flow). The boundary acts as a confining potential which pushes the energy up and closes the gap locally at the boundary. The anomaly manifests itself as the right hand side of Eq. (2.8), i.e. the non-conservation of the electric current. It is called a *chiral anomaly* as we deal with an anomalous current in a system which breaks time reversal symmetry. The name itself refers to the chiral anomaly of $(1+1)D$ chiral fermions [121]. In the quantum Hall effect these chiral fermions live on the edge of the system. The chiral anomaly can be resolved by combining left and right moving fermions, or, in the case of the quantum Hall effect, by including a lower dimensional theory which produces the same gauge symmetry breaking term, but opposite in sign.

In the QHE the resolution to this paradox is the observation that the current we have been working with is not the total current. There are edge degrees of freedom that need to be taken

into account as well. We introduce an edge current $J^\mu_{\text{edge}}$ which has the same gauge symmetry breaking term, but opposite in sign

$$\partial_\mu J^\mu_{\text{edge}} = -\frac{1}{2}(\partial_\mu \sigma_H)\epsilon^{\mu\lambda\kappa}F_{\lambda\kappa} \tag{2.9}$$

We also set $J^\mu = J^\mu_{\text{bulk}}$ and set the total current equal to $J^\mu_{\text{total}} = J^\mu_{\text{bulk}} + J^\mu_{\text{edge}}$. The total current is now conserved since the anomalies cancel

$$\partial_\mu J^\mu_{\text{total}} = 0 . \tag{2.10}$$

This is called the Callan-Harvey mechanism [128, 200, 201, 240]. Since our bulk picture is already complete through the relations (2.2) to (2.6) the edge current must indeed flow along the edge and it has no component perpendicular to the boundary

$$J^\mu_{\text{edge}} = (J^0_{\text{edge}}, J^\parallel_{\text{edge}}, 0) . \tag{2.11}$$

When considered separately the bulk and edge currents do not conserve electric charge (i.e they are anomalous currents). The edge current acts as a source or drain of charge for the bulk current, and vice versa. When a current flows through the bulk it eventually encounters the edge of the system, see Figure 2.1. Charge cannot flow through the boundary and therefore ends up in the edge current.

### 2.2.2 The effective action

The effective action of the quantum Hall fluid can refer to two closely related concepts. The first is an effective description of the electrons in a quantum Hall liquid; the second is an effective description of the electromagnetic field inside the fluid. We are primarily interested in the latter, but to understand its origin we need to study the former.

The effective action of the electrons is a low energy, long wavelength and low temperature description of a fractional quantum Hall phase. This action captures the low energy features of the phase such as the current-response and quasiparticle excitations, and it arises from a subtle interplay of the Lorentz force, the electron-electron interaction and disorder. In particular, there exists an electrical current $J_\mu$ which couples to the residual electromagnetic field. The partition function is given by

$$Z = \int \mathcal{D}\Psi \mathcal{D}A \, e^{iS_{\text{el}}[\Psi]+iJ_\mu A^\mu + iS_{EM}[A]} . \tag{2.12}$$

The correlators of the current follows from the derivative $\frac{\delta Z}{\delta A^\mu}$. Note that $A_\mu$ is the gauge potential of the perturbed electromagnetic field and does not include the static magnetic background field. For the Laughlin series this action is obtained starting from a microscopic

picture, see e.g. Refs. [181, 238, 154] and the resulting action is a Chern-Simons-Landau-Ginzburg theory (see aforementioned references). Based on this and many other results (see e.g. the review article Ref. [165] and references therein) it is now commonly accepted that all fractional quantum Hall phases are described by a type of Landau-Ginzburg-Chern-Simons theory of the electron degrees of freedom in the low-energy limit.

The effective action of the (perturbed) electromagnetic field arises from Eq. (2.12) by integrating over the remaining electron degrees of freedom. Because $S_{el}[\Psi]$ contains a Chern-Simons term and the coupling of $A$ with the electrons is linear ($A_\mu J^\mu$) the effective action of the EM gauge potential is also a Chern-Simons action. It is given by

$$
\begin{aligned}
S_{\text{bulk}} &= \frac{\sigma_H}{2} \int_{\mathcal{M}} A \wedge dA + \dots \\
&= \frac{\nu}{4\pi} \int_{\mathcal{M}} \epsilon^{\mu\lambda\kappa} A_\mu \partial_\lambda A_\kappa \, d^2x dt + \dots
\end{aligned}
\tag{2.13}
$$

where $\sigma_H = \frac{\nu}{2\pi}$ is the conductivity and we use units where $e = \hbar = 1$. The dots represent higher order terms of $A$ such as the Maxwell action ($dA^2$).

This is, of course, just a simple sketch of how the effective action for $A_\mu$ is obtained and it does not constitute a proof. However, there are very solid arguments in favour of this action. Most importantly, this action reproduces the phenomenological laws of Section 2.2.1. The current is obtained by the derivative

$$
J^\mu_{\text{bulk}} = \frac{\delta S_{\text{bulk}}}{\delta A_\mu} = \sigma_H \epsilon^{\mu\lambda\kappa} \partial_\lambda A_\kappa \,.
\tag{2.14}
$$

This is exactly the Hall response Eq. (2.4) and CS-Gauss law Eq. (2.5). The action also reproduces the chiral anomaly as we will show below.

In addition to reproducing the phenomenological laws we also note that this action is the most relevant term from a renormalization group point of view [216]. Alternative actions, such as a Maxwell term $\int (dA)^2$, are all of higher degree and less relevant in the RG sense. Finally, the coupling constant of the Chern-Simons action ($\sigma_H$) is quantized and can only be an integer: non-integer values break gauge invariance when the system is considered on a compact manifold [56, 165]. This also means that adding weak perturbations of $A$ to the action does not affect the value of the coupling constant. There is no RG flow away from the CS action and the action is itself a fixed point. The coupling constant also represents the conductivity (see Eq. (2.14)) and so its quantization is in agreement with the observed stability of quantum Hall plateaux.[1]

We refer to the literature for an in-depth analysis of the Chern-Simons action [65, 233, 67]. Here we focus the remaining discussion on the chiral anomaly. The gauge field $A_\mu$ corresponds

---

[1]The Chern-Simons theory presented here is actually not general enough to explain the wide range of observed plateaux. We return to this issue in Section 2.3.2.

to a $U(1)$ gauge symmetry associated with the electromagnetic field. The field transforms as $A_\mu \to A_\mu + \partial_\mu f$. The edge breaks gauge invariance of the action. Gauge transformations which do not vanish on the edge generate a boundary term. We fix the coordinates $(t, x, y)$, such that $x$ is parallel and $y$ is perpendicular to the boundary. The action transforms as

$$S_{\text{bulk}} \longrightarrow S_{\text{bulk}} + \delta S_{\text{bulk}}(f) \tag{2.15}$$

$$\delta S_{\text{bulk}} = \frac{\sigma_H}{2} \int (\epsilon^{y\lambda\kappa} \partial_\lambda A_\kappa) f \big|_{\text{edge}} dx dt \tag{2.16}$$

The boundary term spoils gauge invariance and the action is said to be anomalous. This gauge symmetry breaking term arises for any gauge transformation $f$ which does not vanish at the edge. From now on we use $a_\mu$ to denote the gauge potential at the edge, i.e.

$$\frac{\sigma_H}{2} \epsilon^{y\lambda\kappa} \partial_\lambda A_\kappa \big|_{\text{edge}} = \frac{\sigma_H}{2} \epsilon^{\lambda\kappa} \partial_\lambda a_\kappa \,, \qquad \text{where } a_\mu \equiv A_\mu \big|_{\text{edge}} \,. \tag{2.17}$$

We now have two equivalent views of the chiral anomaly. The first is the non-conservation of the bulk electric current. The second is the non-invariance of the bulk action with respect the $U(1)$ gauge symmetry. These are, of course, two sides of the same coin. If the action is invariant with respect to a $U(1)$ symmetry then this implies conservation of electric charge, and vice versa.

The remedy is, as before, the introduction of charged edge degrees of freedom, described by an action $S_{\text{edge}}$ which breaks gauge symmetry in the same manner, but opposite in sign. We set

$$S_{\text{total}} = S_{\text{bulk}} + S_{\text{edge}} \tag{2.18}$$

$$A_\mu \longrightarrow A_\mu + \partial_\mu f \; : \qquad \delta S_{\text{edge}}(f) = -\delta S_{\text{bulk}}(f) \tag{2.19}$$

The total action is again gauge invariant.

## 2.3  Introducing the chiral boson

The chiral anomaly necessitates the existence of an edge current. This current has the same anomaly as the bulk current, but opposite in sign. However, this mechanism does not specify the exact dynamics of the edge degrees of freedom. This is not surprising since the edge theory can contain several non-universal features provided these are consistent with the chiral anomaly.

There are multiple ways to derive the edge action. We will not discuss them in full detail here, but do mention the main ideas. The first approach [217] reduces the set of allowed gauge transformation to those which vanish at the edge of the system, $f \big|_{\text{edge}} = 0$. In turn

---

31

the edge gauge degrees of freedom become "dynamical" and by solving the bulk equations of motion we obtain a solution for its boundary (the edge theory). The second approach is the so-called hydrodynamical approach [217, 153]. The low-energy excitations are confined to the edge due to incompressibility of the quantum Hall fluid, and by using Hall's law an equation of motion is obtained for the charged edge degrees of freedom. A third approach constructs an edge theory with the aim to cancel the chiral anomaly on the level of edge current correlators [215].

The approaches use the same input which are the phenomenological laws, locality of the edge current and the chiral anomaly. They lead to the same conclusion that in the simplest case the edge is described by the action

$$\frac{\nu}{4\pi} \int_{\partial\mathcal{M}} \partial_x\varphi(\partial_t - v_c\partial_x)\varphi \, dtdx \, , \tag{2.20}$$

This action describes *the chiral boson* [81, 213, 44]. The chiral boson $\varphi$ is a real-valued field and its modes satisfy bosonic commutation relations. The non-universal parameter $v_c$ is the velocity of the modes. Upon quantization the modes of the current (to be defined below) form what is known as a $U(1)$ Kac-Moody current algebra [207, 58]. The theory is also known as a chiral Luttinger liquid [213, 44], as two chiral bosons can be combined to form a Luttinger liquid [209].

The chiral boson description of a fractional quantum Hall edge is an example of bosonization [97, 209]. The edge is a fermionic system, yet we use bosonic operators to construct the Hilbert space and determine the correlators. We will explore this connection in more detail in Section 2.6. For now it suffices to note that the model contains both chiral fermions and fractionally charged quasiparticle excitations, all of which are described in terms of the bosonic field $\varphi$. More physically, we interpret the field $\varphi$ as representing the *phase* of the boundary electrons, $\Psi_{\text{el}} \sim e^{i\alpha\varphi}$.

For general $a_\mu$ (recall Eq. 2.17) the action is given by

$$S = \frac{1}{4\pi} \int D_t\varphi D_x\varphi - v_c(D_x\varphi)^2 + \sqrt{\nu}\epsilon^{\mu\lambda}a_\mu\partial_\lambda\varphi \, dxdt \tag{2.21}$$

where $\mu$ and $\lambda$ run over $(t, x)$. It reduces to Eq. (2.20) when $a_\mu = 0$. Upon a gauge transformation we have $a_\mu \to a_\mu + \partial_\mu f$ and the bosonic field transforms as $\varphi \to \varphi - \sqrt{\nu}f$. The final term $\epsilon^{\mu\lambda}a_\mu\partial_\lambda\varphi$ in the action produces the chiral anomaly as we show below.[2] The operator $D_i$ is the gauge covariant derivative which arises from the minimal coupling and it is given by

$$D_\mu\varphi = \partial_\mu\varphi + \sqrt{\nu}a_\mu \, . \tag{2.22}$$

---

[2]In the literature one frequently encounters a different convention for the normalization of the bosonic field given by the replacement $\varphi \to \sqrt{\nu}\varphi$.

This is indeed invariant with respect to a gauge transformation. Note that minimal coupling refers to the construction of a gauge invariant derivative $D_\mu \varphi$. The construction is different from the minimal coupling of a fermionic field, due to the gauge transformation properties. Upon a gauge transformation a fermionic field transforms as $\Psi \to e^{if}\Psi$, while the bosonic field transforms according to $\varphi \to \varphi - \sqrt{\nu}f$. Note that this consistent with the interpretation of $\varphi$ as the phase of the electron, $\Psi_{\text{el}} \sim e^{i\alpha\varphi}$.

### 2.3.1 The chiral constraint

The Lagrange equations of motion and Hamiltonian are

$$\partial_x(D_t - v_c D_x)\varphi = 0 \tag{2.23}$$

$$K_0(\varphi, a_t, a_x) = \int_{\Sigma_i} \left[ \frac{v_c}{4\pi}(D_x\varphi)^2 - \frac{\sqrt{\nu}}{2\pi} a_t D_x \varphi + \frac{\nu}{4\pi} a_x a_t \right] dx . \tag{2.24}$$

The gauge covariant terms $(D_\mu\varphi)$ are gauge invariant by construction, while the final term in the action generates the chiral anomaly. We have upon a gauge transformation

$$\delta S_{\text{edge}} = -\frac{\nu}{4\pi} \int_{\partial\mathcal{M}} (\epsilon^{\mu\lambda}\partial_\mu a_\lambda) f \, dx \, dt . \tag{2.25}$$

This is the now familiar chiral anomaly. In the next section we will quantize this theory. Here we simply note that the system is an example of a constrained system, which requires some special care. Hamilton's equations of motion are given by

$$\boxed{(D_t - v_c D_x)\varphi = 0 .} \tag{2.26}$$

This equation is also referred to as *the chiral constraint* despite the fact that in our approach it is not a constraint but an equation of motion. In the absence of a gauge field it reduces to the first order wave equation $(\partial_t - v_c\partial_x)\varphi = 0$, which shows that $\varphi(x,t)$ is a function of the combination $(x + v_c t)$ i.e. a left-moving wave.

The name "chiral constraint" arises from a different approach used in for instance Ref. [213]. In this approach one starts with a boson containing both chiralities, and extracts the left moving part by imposing Eq. (2.26) as a constraint (i.e. throw away everything that violates this equation). In our approach the chiral constraint arises naturally from the equations of motion. To add to the confusion, the chiral boson is also a constrained system, but the constraint equations do *not* equal the chiral constraint.

A different manifestation of the constrained nature becomes apparent when we compare the chiral constraint (Hamilton's equation of motion) Eq. (2.26) with the Lagrange equation of motion Eq. (2.23). The chiral constraint automatically reproduces the Lagrange equation of motion and we do not require the equation of motion for the momentum of the system.

The reason is that, as stated before, the system is constrained which simply means that in the Hamilton formalism the momentum and coordinates are not independent. We discuss this in more detail in Section 2.5, but it suffices to say that this has to be taken into account when the system is quantized.

### 2.3.2 Generalizations of the edge theory

The remainder of this section is dedicated to studying the chiral boson. We look at how the model is quantized, study the mode expansion of the field, determine the correlation functions, and we construct a physical picture of its relation to the quantum Hall effect (e.g. by determining the edge current and density operators in terms of $\varphi$). However we emphasize that the chiral boson by itself is not sufficient to fully describe the edge theory of generic fractional quantum Hall states.

There are, roughly, three ways in which can obtain a more general picture. First, we can move away from the low energy picture and include higher order terms such as self-interactions of the chiral boson. This leads to non-linearities in the spectrum and possibly edge reconstruction [43, 235].

A second approach is to consider multiple chiral bosons. This picture arises when we deal with multiple filled Landau levels or multiple fractional states layered together [86, 224]. Each Landau level or state gives rise a different chiral boson and the edge action is described by a collection of chiral bosons, which also interact with each other. The general action is given through use of what is known as the $K$-matrix [21, 224]

$$\frac{1}{4\pi} \int K_{IJ} \partial_t \varphi_I \partial_x \varphi_J - V_{IJ} \partial_x \phi_I \partial_x \varphi_J \, dt dx . \tag{2.27}$$

Here $I$ and $J$ run over the different bosonic fields, and there is an implicit summation over repeated indices. The third approach is to include neutral degrees of freedom in the edge theory which are not described in terms of the chiral boson [162, 85]. This neutral channel fully decouples from the electromagnetic field. We will describe this construction in more detail in Chapter 3. The most important feature is that the electron operator decomposes into a neutral ($\mathcal{W}_n$) and charged ($\mathcal{W}_c$) piece

$$\Phi_{\text{el}} = \mathcal{W}_n \otimes \mathcal{W}_c . \tag{2.28}$$

In fact, all operators of the theory follow this decomposition. This is the construction used for non-Abelian quantum Hall states. For instance, in the Moore-Read trial state [162, 183] the neutral piece corresponds to the chiral Ising model, and in the Read-Rezayi series [184] we deal with the parafermion model $\mathbb{Z}_k$. The neutral part is responsible for the non-Abelian nature of the quasiparticle.
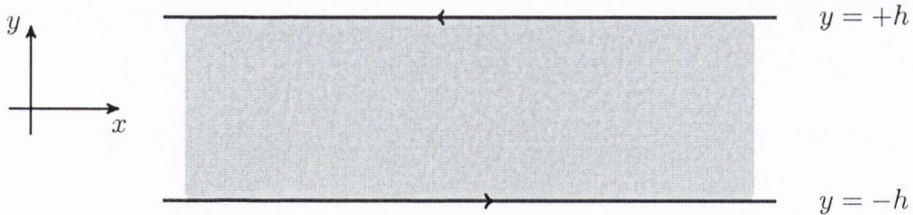
**Figure 2.2:** Sketch of a Quantum Hall bar and the coordinate system. The lower edge corresponds to a right moving chiral boson, and the upper edge to a left moving.

It is also possible to mix these three approaches and, for instance, construct a quantum Hall edge with several neutral and charged channels. But in all cases a charged channel corresponds to the chiral boson.

### 2.3.3 The quantum Hall bar setup

The quantum Hall bar setup is depicted in Figure 2.2. In this simple geometry we deal with two edges of size $L$, denoted $\Sigma_R$ and $\Sigma_L$, both described by the same edge theory. We use Cartesian coordinates $(x, y)$ with $y$ perpendicular to the edges, and the edges are situated at $y = \pm h$. The edge theory consists of a single chiral boson (right-moving on the lower edge and left-moving on the upper) plus a possible neutral channel. We focus the discussion on the charged channel. The total edge action is given by $S_{\text{edge}} = S_R + S_L + S_{n,R} + S_{n,L}$ where $S_n$ is the action of the neutral channel. For the charged channels we have

$$S_i[\varphi_i] = \frac{1}{4\pi} \int_{\Sigma_i \times \mathbb{R}} \left[ \eta_i D_t\varphi_i D_x\varphi_i - v_c(D_x\varphi_i)^2 + \sqrt{\nu}\epsilon^{\mu\kappa}a_\mu \partial_\kappa\varphi_i \right] dt dx \tag{2.29}$$

$$= \frac{1}{4\pi} \int_{\Sigma_i \times \mathbb{R}} \left[ \eta_i \partial_t\varphi_i \partial_x\varphi_i \right] dt dx - \int_{\mathbb{R}} K_0(\varphi_i, a_{t,i}, \eta_i a_{x,i}) dx \tag{2.30}$$

for $i = R, L$ and where $\eta_R = -1$, $\eta_L = +1$ represent the chiralities. Furthermore we recall the gauge covariant derivative $D_\mu\varphi_i = \partial_\mu\varphi_i + \sqrt{\nu}\eta_i a_\mu$. The grand canonical Hamiltonian is given by

$$K_0(\varphi, a_t, a_x) = \int_{\Sigma_i} \left[ \frac{v_c}{4\pi}(\partial_x\varphi)^2 - \frac{\sqrt{\nu}}{2\pi}(a_t - v_c a_x)\partial_x\varphi - \frac{\nu}{4\pi}a_x(a_t - v_c a_x) \right] dx . \tag{2.31}$$

The chiral constraint is $D_t\varphi_i - \eta_i v_c D_x\varphi_i = 0$ for each edge. We consider the grand canonical Hamiltonian as the system is coupled to an external voltage, which acts as a chemical potential. We focus on the case of a DC voltage bias between the edges, a perturbed magnetic field and no bulk current flowing perpendicular from the edges. We set $a_{t,R/L} = U_{R/L}$ constant along the edges and $A_\mu$ is time independent. Then $E_x = 0$, $E_y = \partial_y A_t$ and $B_z = \partial_x A_y - \partial_y A_x$ is the perturbed magnetic field.

### 2.3.4 The edge current

The current density in the system consists of an anomalous bulk and edge current, with opposite anomaly. The sum of these currents forms the total current which is anomaly-free and obeys the continuity equation. The bulk current is given by

$$J^\mu_{\text{bulk}} = \frac{\delta S_{\text{bulk}}}{\delta A_\mu} .$$ (2.32)

with the bulk action given by Eq. (2.13). In our gauge we have for the bulk current

$$J^x_{\text{bulk}} = \frac{\nu}{2\pi}\partial_y A_t - \frac{\nu}{4\pi}\left(a_{t,L}\delta(y-h) - a_{t,R}\delta(y+h)\right) .$$

and the $y$ component vanishes $J^y_{\text{bulk}} = 0$. The delta functions are the surface terms, which arise from integration by parts in the action. For the edge currents the $y$ component also vanishes $J^y_{\text{edge}} = 0$, and for the $x$ component we have

$$J^x_{\text{edge}} = \left(-v_c\frac{\sqrt{\nu}}{2\pi}D_x\varphi_L + \frac{\nu}{4\pi}a_{t,L}\right)\delta(y-h) + \left(v_c\frac{\sqrt{\nu}}{2\pi}D_x\varphi_R - \frac{\nu}{4\pi}a_{t,R}\right)\delta(y+h) .$$

This follows from the action (2.30). The total current density is the sum of these quantities,

$$J^x_{\text{total}} = J^x_{\text{edge}} + J^x_{\text{bulk}} = \frac{\nu}{2\pi}\partial_y A_t - v_c\frac{\sqrt{\nu}}{2\pi}\left(D_x\varphi_L\delta(y-h) - D_x\varphi_R\delta(y+h)\right)$$ (2.33)

This is the total current *density*. To obtain an expression for the total current flowing through the system we integrate the component $J^x$ along a line from the lower to the upper edge. This gives

$$I_0(x) \equiv \int J^x_{\text{total}}(x,y)dy = -\frac{\sqrt{\nu}}{2\pi}(\partial_t\varphi_L + \partial_t\varphi_R)$$ (2.34)

Here we made use of the equations of motion, $\eta_i\partial_t\varphi_i = D_x\varphi_i - \sqrt{\nu}a_{t,i}$. Within our setup and choice of gauge the total current through the system is determined by the quantities $-\frac{\sqrt{\nu}}{2\pi}\partial_t\varphi_L$, which we refer to as the *edge current density* (not to be confused with the edge current $J^\mu_{\text{edge}}$ which is a $(2+1)D$ object). We have

$$\boxed{j_L(x,t) = -\partial_t\varphi_L(x,t)}$$ (2.35)

and the same definition for the right-moving current $j_R = -\partial_t\varphi_R(x,t)$. The total current is completely determined by the edge degrees of freedom. However, this expression does not follow from the edge action itself (i.e. it is not a Noether current of the edge action).

The edge current is the spatial component of a $(1+1)D$ conserved current $j^\mu_i$ ($\mu = 0,1$, $i = R, L$) flowing along the edge. This current is conserved since in this particular system and gauge no charge flows from the bulk into the edge. The components of $j^\mu_i$ are the edge charge density $j^0_i = \rho_i$ and edge current density $j^1_i = j_i$. Together they obey the *continuity equation*

$$\partial_t\rho_L(x,t) + \partial_x j_L(x,t) = 0 .$$ (2.36)

Using $j_L = -\partial_t \varphi_L$ gives $\rho_L(x,t) = \frac{\sqrt{\nu}}{2\pi}\partial_x\varphi_L + h(x)$. We fix $h(x)$ by demanding that the resulting expression is gauge invariant. This gives

$$\rho_L = \frac{\sqrt{\nu}}{2\pi}D_x\varphi_L \ . \tag{2.37}$$

In the gauge $a_x = 0$ this reduces to the more commonly known expression for the edge charge density operator $\rho_L = \frac{\sqrt{\nu}}{2\pi}\partial_x\varphi_L$. An important quantity which follows from the charge density is the *total charge on the edge*. It is the conserved charge associated with the continuity equation and given by

$$\mathcal{Q}_L = \int_{\Sigma_L}\rho_L(x)dx = \frac{\sqrt{\nu}}{2\pi}\int_{\Sigma_L}D_x\varphi_L(x)dx \ . \tag{2.38}$$

These definitions also apply to the right-moving edge.

## 2.4 Decomposition due to the electromagnetic coupling

In the action of the chiral boson Eq. (2.21) the coupling to the external gauge field is linear in $\partial_x\varphi$. This linear term causes a shift in the ground state configuration of the chiral boson. For instance both derivatives of $\varphi$, i.e. $\partial_t\varphi$ and $\partial_x\varphi$, obtain non-zero ground state expectation values in the presence of a gauge field. Our goal in this section is to separate the effect of the coupling to the gauge field from the remaining degrees of freedom, i.e. those degrees of freedom which are not fixed by the gauge field. This is the background field method and significantly simplifies the computation of correlation functions. Put differently, we decompose the classical solution $\varphi$ in terms of a particular and homogeneous solution of the equations of motion. We set

$$\varphi(x,t) = \bar{\varphi}(x,t) + \varphi_h(x,t) \tag{2.39}$$

where $\bar{\varphi}(x,t)$ and $\varphi_h(x,t)$ are the particular and homogeneous solution of the equations of motions, respectively. The coupling to the gauge field is linear and therefore this decomposition completely decouples the homogeneous solution from the gauge field. This is the idea of "completing the square" in the action. On the quantum level this decomposition decouples the quantum fluctuations from the background field configuration. This technique is also used to determine the path integral of quadratic action augmented with a linear potential [79].

We now make this decomposition explicit. The particular solution is a fixed solution to the equations of motion,

$$(\partial_t - v_c\partial_x)\bar{\varphi}(x,t) = -\sqrt{\nu}(U - v_ca_x(x)) \ . \tag{2.40}$$

We solve this equation using the Greens functions method [66]. We introduce the Greens function $g(x,t)$ as the solution to the equation $(\partial_t - v_c\partial_x)g(x,t) = \delta(x-x')\delta(t-t')$. In Fourier space by this is solved by

$$g(\omega, k) = \frac{i}{\omega + v_c k} \tag{2.41}$$

Transforming back requires regularization of the singular behaviour when $\omega = -v_c k$. The regulator is chosen such that we obtain the (physically relevant) retarded propagator. This amounts to adding a term $i0^+$ in the denominator. We obtain

$$g(x,t) = \frac{1}{L}\sum_k \int_{-\infty}^{\infty} \frac{i}{\omega + v_c k + i0^+} e^{i(kx-\omega t)}\frac{d\omega}{2\pi}$$

$$= \frac{1}{L}\sum_k e^{ik(v_c t + x)-0^+ t}\theta(t) = e^{-0^+ t}\delta(x + v_c t)\theta(t) . \tag{2.42}$$

where the sum is over $k = \frac{2\pi}{L}n$ with $n$ integer. Including a possible homogeneous term the particular solution is (taking $0^+ \to 0$)

$$\bar{\varphi}(x,t) = f(x + v_c(t-t_{\text{ref}})) - \sqrt{\nu}\int_{t_{\text{ref}}}^{\infty}\int_{-L/2}^{L/2} g(x-x', t-t')(U - v_c a_x(x'))dx'dt'$$

$$= f(x + v_c(t-t_{\text{ref}})) - \sqrt{\nu}U(t-t_{\text{ref}}) + v_c\sqrt{\nu}\int_{t_{\text{ref}}}^{t} a_x(x + v_c(t-t'))dt' . \tag{2.43}$$

The parameter $t_{\text{ref}}$ is some reference time and $f$ is a homogeneous function we use to fix the boundary conditions on $\bar{\varphi}$. We set $f$ equal to

$$f(x) = -\sqrt{\nu}U t_{\text{ref}} - \sqrt{\nu}\int_{x_{\text{ref}}}^{x} a_x(y)dy . \tag{2.44}$$

where $x_{\text{ref}}$ is a reference point, usually the boundary at $x = +L/2$. We have for the particular solution

$$\bar{\varphi}(x,t) = -\sqrt{\nu}U t + \sqrt{\nu}\int_{x}^{x_{\text{ref}}} a_x(x)dy . \tag{2.45}$$

The homogeneous solution solves $(\partial_t - v_c\partial_x)\varphi(x,t) = 0$ and is any function of the form $\varphi_h(x + v_c t)$. Returning to the decomposition of $\varphi(x,t)$ we merge $f$ with the integral over $a_x$ and obtain

$$\boxed{\varphi(x,t) = -\sqrt{\nu}U t + \sqrt{\nu}\int_{x}^{x_{\text{ref}}} a_x(y)dy + \varphi_h(x + v_c t) .} \tag{2.46}$$

The homogeneous solution $\varphi_h(x + v_c t)$ completely decouples from the gauge field. To see this we substitute this decomposition into the action Eq. (2.30). This gives

$$S[\bar{\varphi} + \varphi_h, a_\mu] = S[\bar{\varphi}, a_\mu] + S_0[\varphi_h] \tag{2.47}$$

$$S[\bar{\varphi}, a_\mu] = \frac{\nu}{2\pi}\int_{-L/2}^{L/2}(U - v_c a_x)a_x dx$$

$$S_0[\varphi_h] = \frac{1}{4\pi}\int_{-L/2}^{L/2}\left[\partial_t\varphi_h\partial_x\varphi_h - v_c(\partial_x\varphi_h)^2\right]dx$$

Here we replaced $\bar{\varphi}$ by its expression in terms of $a_\mu$. The resulting action $S[\bar{\varphi}, a_\mu]$ represents the effective edge action of the electromagnetic gauge potential evaluated at our particular configuration of the gauge field. More importantly, we obtain the edge action of the homogeneous part $S_0[\varphi_h]$, which is (by construction) completely decoupled from the gauge field. The Hamiltonian of the homogeneous part is given by

$$H_0 = \frac{v_c}{4\pi} \int_{-L/2}^{L/2} (\partial_x \varphi_h)^2 \, dx \; . \tag{2.48}$$

### 2.4.1 Effect of decomposition on partition function

The decomposition has a further natural interpretation on the quantum level where it separates the classical background configuration from the quantum fluctuations. This is demonstrated by considering the path integral representation of the partition function

$$Z[\varphi] = \int \mathcal{D}\varphi \, e^{iS[\varphi, a_\mu]} \; . \tag{2.49}$$

We substitute $\varphi$ by its decomposition. Since $\bar{\varphi}$ is fixed and classical it can be taken out of the path integral, provided we shift the integration variable in the path integral ($\varphi \to \varphi_h$). The action splits as in (2.47) and we obtain for the partition function

$$Z[\bar{\varphi} + \varphi_h] = e^{iS[\bar{\varphi}, a_\mu]} \int \mathcal{D}\varphi_h e^{iS_0[\varphi_h]} \; . \tag{2.50}$$

The partition function naturally splits into classical and quantum degrees of freedom. This approach is a method used to solve quadratic actions in the path integral formalism [79].

This decomposition also applies to the correlators. Consider a correlation function of some functional $F[\varphi]$. We have

$$\langle F[\varphi] \rangle \equiv \frac{1}{Z[\varphi]} \mathrm{Tr}\left[ e^{-\hat{K}_0[\hat{\varphi}]/T} F[\hat{\varphi}] \right] = \frac{1}{Z[\varphi]} \int \mathcal{D}\varphi \, e^{iS[\varphi, a_\mu]} F[\varphi] \tag{2.51}$$

The second form in Eq. (2.51) uses the canonical approach (i.e. $\varphi$ is operator valued) and the density operator of a Gibbs state, $\frac{1}{Z} e^{-K_0/T}$. This form is cast into a path integral expression in the last equation. Here we allow for the possibility that the time contour is along the imaginary axis in which case we deal with the Eucledian action and thermal correlators. We now insert $\varphi = \bar{\varphi} + \varphi_h$ in the path integral representation of the correlator. This gives

$$\frac{1}{Z[\bar{\varphi} + \varphi_h]} \int \mathcal{D}\phi \, e^{iS[\bar{\varphi} + \varphi_h, a_\mu]} F[\bar{\varphi} + \varphi_h] = \frac{1}{Z[\varphi_h]} \int \mathcal{D}\varphi_h e^{iS_0[\varphi_h]} F[\bar{\varphi} + \varphi_h]$$

$$= \frac{1}{Z[\varphi_h]} \mathrm{Tr}\left[ e^{-\hat{H}_0/T} F[\bar{\varphi} + \hat{\varphi}_h] \right] \tag{2.52}$$

In the first step a phase factor $e^{iS[\bar{\varphi}, a_\mu]}$ appears in both the partition function and the path integral. These two factors cancel out. In the second step we switch back to a canonical

form (operator valued). However, this time only $\varphi_h$ is promoted to an operator and $\bar{\varphi}$ stays classical. The corresponding density operator is with respect to $H_0$ (instead of $K_0$) since this is the Hamiltonian of $\varphi_h$.

We then arrive at the following expression for a correlator

$$\langle F[\varphi] \rangle = \frac{1}{Z[\varphi_h]} \text{Tr} \left[ e^{-\hat{H}_0/T} F[\bar{\varphi} + \hat{\varphi}_h] \right] . \tag{2.53}$$

Note that by switching to a decomposition into a background field + fluctuations the Hamiltonian appearing in the density operator also changes from $\hat{K}_0$ to $\hat{H}_0$.

## 2.5   Quantization of the chiral boson

We have separated the background field from the remaining degrees of freedom. We now quantize this homogeneous part using Dirac's quantization procedure. This is a generalized form of canonical quantization applicable to constrained systems. Our goal is to motivate the origin of the (somewhat unusual) commutation relations of the chiral boson model. The result is Eq. (2.76).

The constrained nature of the chiral boson can be read off from the action. Consider the action of the homogeneous part of the chiral boson

$$S_0[\varphi] = \frac{1}{4\pi} \int \partial_t \varphi \partial_x \varphi \, dx \, dt - \int H \, dt . \tag{2.54}$$

The kinetic term $\partial_t \varphi \partial_x \varphi$ is only linear in the velocity ($\partial_t \varphi$). If we were to blindly impose the canonical commutation relations between $\varphi$ and its conjugate field $\Pi$, then this immediately leads to inconsistencies. By definition the conjugate momentum is given by

$$\Pi(x, t) = \frac{\delta \mathcal{L}}{\delta \partial_t \varphi} = \frac{1}{4\pi} \partial_x \varphi . \tag{2.55}$$

The Hamiltonian is a functional of the conjugate momentum, $H = H[\Pi(x)]$. Imposing the canonical commutation relation $[\varphi(x), \Pi(y)] = i\delta(x - y)$, $[\Pi(x), \Pi(y)] = 0$ leads to the following equations of motion

$$\partial_t \Pi = i[H, \Pi] = 0 . \quad \text{(wrong)} \tag{2.56}$$

This clashes with the Lagrange equations of motion.

The subtlety ignored here is already evident on the classical level. The conjugate momentum $\Pi$ is not defined in terms of the velocity $\partial_t \varphi$ (but rather in terms of $\partial_x \varphi$). Therefore the velocity cannot be written as a function of the "momentum" $\Pi$ and "coordinate" $\varphi$ and we cannot perform a Legendre transformation which maps the system described in configuration space (spanned by ($\partial_t \varphi, \varphi$)) to one described in phase space (spanned by ($\Pi, \varphi$)).

Put differently, the momentum and coordinates are not independent and the system is said to be constrained. Since quantization is performed using phase space coordinates we need to circumvent the usual Legendre transformation to describe the system using Hamilton's mechanics. This is done through the use of constraints and the introduction of Dirac's bracket.

### 2.5.1 Dirac's quantization procedure

The following discussion of Dirac's quantization procedure [59] is based on treatments in Refs. [202, 117] and ultimately leads to the procedure outlined in [121] for the quantization of certain constrained systems. We consider a Lagrangian linear in the velocity using the dummy model

$$L = \frac{1}{2} q_i C_{ij} \dot{q}_j + V(q_j) \,. \tag{2.57}$$

Here, $C_{ij}$ is a non-singular and antisymmetric two-form with indices $i = 1, \ldots, N$ and $N$ must be even. Summation over repeated indices is implied. This Lagrangian serves as a discrete, prototypical version of the chiral boson. The conjugate momentum $p_i$ is obtained in the usual way and given by

$$p_i = \frac{1}{2} C_{ij} q_i \,. \tag{2.58}$$

The momenta and coordinates $p_i$ and $q_i$ are not independent and the system is said to be constrained.

We define the full phase space $\Gamma$ as the space spanned by *independent* momenta and coordinates, $\{q_i, p_i\}$. The physical system only has access to a subspace $\Gamma_p \subset \Gamma$ of the full phase space. This subspace $\Gamma_p$ is defined through a set of constraint equations, classified as primary and secondary constraints. The definition of the canonical momenta (2.58) provides us with $N$ primary constraints

$$T_j \equiv p_j - \frac{1}{2} C_{ij} q_i \approx 0 \,. \tag{2.59}$$

These equations define the subspace $\Gamma_p$. Secondary constraints do not play a role in our system. The notation $\approx 0$ stands for weakly zero, meaning the equation holds when restricted to the subspace $\Gamma_p$ but not necessarily away from $\Gamma_p$. By definition of $\Gamma_p$ the constraints $T_j$ are all weakly zero. In contrast, the derivatives of the constraints are not weakly zero, since $\frac{\partial T_j}{\partial q_i} = -\frac{1}{2} C_{ij} \not\approx 0$ and $\frac{\partial T_j}{\partial p_i} = \delta_{ij} \not\approx 0$. The fact that the derivatives of the constraints do not vanish is a key feature of a constrained system. This becomes clear when we consider the dynamics of the system.

A priori, the extension of the Hamiltonian from the subspace $\Gamma_p$ to the full phase space $\Gamma$ is not uniquely determined. With $H = p_i q_i - L$ defined in the usual way, we obtain a whole family of Hamiltonians labelled by coefficients $\mu_j$

$$H_\mu = H + \mu_j T_j \; . \tag{2.60}$$

These Hamiltonians are all equal to each other in the weak sense ($H_{\mu'} \approx H_\mu$) since the constraints vanish on $\Gamma_p$. However, the different choices of $\mu_j$ do not give rise to the same dynamics. Minimizing the action $p_j \dot{q}_j - H_\mu$ in the full phase space, and restricting to the subspace $\Gamma_p$ afterwards leads to the (constrained) Hamilton equations of motion,

$$\dot{q}_i = \{q_i, H\} + \mu_j \{q_i, T_j\} = \frac{\partial H}{\partial p_i} + \mu_j \frac{\partial T_j}{\partial p_i} = \frac{\partial H}{\partial p_i} + \mu_i \tag{2.61}$$

$$\dot{p}_i = \{p_i, H\} + \mu_j \{p_i, T_j\} = -\frac{\partial H}{\partial q_i} + \mu_j \frac{\partial T_j}{\partial q_i} = -\frac{\partial H}{\partial q_i} - \tfrac{1}{2} \mu_j C_{ij} \tag{2.62}$$

Here we have introduced the usual Poisson bracket

$$\{A, B\} = \sum_k \frac{\partial A}{\partial q_k} \frac{\partial B}{\partial p_k} - \frac{\partial B}{\partial q_k} \frac{\partial A}{\partial p_k} \tag{2.63}$$

where these brackets are evaluated before the constraints $T_j$ are imposed (otherwise $q_k$ and $p_k$ cannot be varied independently).

The fact that we end up with different dynamics for the Hamiltonians $H_\mu$ is attributed to the derivatives of the constraints which are not weakly zero. We therefore need a criterium that fixes the Lagrange multipliers $\mu_j$. The natural choice is to demand that the constraints remain weakly zero in time. Recall that the time evolution of some function $g(q, p)$ in the complete phase space $\Gamma$ is given by $\dot{g} = \{g, H + \mu_j T_j\}$. We therefore demand that the Lagrange multiplier solve the equation

$$0 \approx \dot{T}_i = \{T_i, H\} + \mu_j \{T_i, T_j\} \tag{2.64}$$

These $N$ equations uniquely fix the $N$ Lagrange multipliers. Using the derivatives of the constraints $\{p_i, T_j\} = -\tfrac{1}{2} C_{ij}$ and $\{q_i, T_j\} = \delta_{ij}$ we obtain

$$\{T_i, T_j\} = C_{ij} \; . \tag{2.65}$$

This fixes the Lagrange multipliers as $\mu_j = -\{T_i, H\}(C^{-1})_{ij}$. We have now arrived at a consistent Hamiltonian formalism of the constrained system. In this approach the physical phase space is described through an embedding in a larger phase space and the constrained dynamics is accounted for through use of extra terms in the Hamiltonian. These terms ensure the dynamics of the system preserve the constraints. Before we proceed to quantize the theory,

it pays off to reformulate our results. For that we introduce a generalized bracket known as the Dirac bracket $\{\cdot, \cdot\}_{\text{DB}}$,

$$\{f, g\}_{\text{DB}} = \{f, g\} - \{f, T_j\}(C^{-1})_{ij}\{T_i, g\} . \tag{2.66}$$

This bracket obeys the usual properties of a Lie bracket, including the Jacobi identity. In terms of this the time evolution is given by

$$\dot{q}_i = \{f, H\}_{\text{DB}} \tag{2.67}$$

where $H$ is the standard Hamiltonian $p_j \dot{q}_j - L$. It is then a straightforward exercise to obtain the brackets for the momenta and coordinates,

$$\{q_i, q_j\}_{\text{DB}} = (C^{-1})_{ij} \qquad \{p_i, p_j\}_{\text{DB}} = -\frac{1}{4}C_{ij} \qquad \{q_i, p_j\}_{\text{DB}} = \frac{1}{2}\delta_{ij} . \tag{2.68}$$

Finally, the quantization itself consists of promoting the phase space variables to operators, $q_i \rightarrow \hat{q}_i$ and $p_i \rightarrow \hat{p}_i$, and replacing the Dirac bracket by the commutator,

$$\{\cdot, \cdot\}_{\text{DB}} \longrightarrow -i[\cdot, \cdot] . \tag{2.69}$$

This leads to the following set of somewhat unconventional commutation relations,

$$[\hat{q}_i, \hat{q}_j] = i(C^{-1})_{ij} \qquad [\hat{p}_i, \hat{p}_j] = -\frac{i}{4}C_{ij} \qquad [\hat{q}_i, \hat{p}_j] = \frac{i}{2}\delta_{ij} . \tag{2.70}$$

In particular, different coordinates do not commute with each other (same for the momenta) and a factor of $\frac{1}{2}$ appeared in the commutator of $q_i$ and $p_i$.

### 2.5.2 Quantization of the chiral boson

With this procedure in hand the quantization of the chiral boson is almost a straightforward process [81, 51, 91, 57]. The main difference is that we are dealing with a continuous system. We write the Lagrangian as

$$L = -\frac{1}{4\pi} \int dx dy \varphi(x) \partial_x \delta(x - y) \partial_t \varphi(y) - H . \tag{2.71}$$

with conjugate momentum $\Pi(x, t) = \frac{1}{4\pi}\partial_x \varphi$. This also applies to a system with a non-vanishing gauge field. The antisymmetric tensor as defined in (2.57) generalizes to a continuous form $C_{ij} \rightarrow C(x, y) = -\frac{1}{2\pi}\partial_x \delta(x - y)$. Quantization of the system requires the inverse $C^{-1}$, which is defined through the Kernel relation $\int dz C(x, z) C^{-1}(z, y) = \delta(x - y)$. The caveat [57, 198] here is that the inverse is not unique and we have for any function $h(t)$

$$C_h^{-1}(x, y) = -\pi \text{sgn}(x - y) + h(t) . \tag{2.72}$$

Here sgn is the sign function. For now we fix $h(t) = 0$ and comment on this issue at the end of this section. The conjugate momentum provides a continuous set of primary constraints,

$$T(x) = \Pi(x) - \frac{1}{4\pi}\partial_x\varphi(x) \approx 0 \,. \tag{2.73}$$

The analysis of determining the Lagrange multipliers and the corresponding Dirac bracket runs along the same lines. In particular the Dirac bracket is given by

$$\{f(x), g(x)\}_{\text{DB}} = \{f, g\} - \int \{f, T(w)\} C^{-1}(w, z)\{T(z), g\} \, dw dz \,. \tag{2.74}$$

With respect to the Dirac bracket the fields obey

$$\{\varphi(x), \varphi(y)\}_{\text{DB}} = C^{-1}(x, y) \qquad\qquad \{\Pi(x), \Pi(y)\}_{\text{DB}} = -\frac{1}{4}C(x, y)$$

$$\{\varphi(x), \Pi(y)\}_{\text{DB}} = \frac{1}{2}\delta(x - y) \,. \tag{2.75}$$

Quantization is now a straightforward process. The equal time commutation relations are

$$[\varphi(x), \varphi(y)] = -i\pi\text{sgn}(x - y) \qquad\qquad [\partial_x\varphi(x), \partial_y\varphi(y)] = i2\pi\partial_x\delta(x - y)$$

$$[\varphi(x), \partial_y\varphi(y)] = i2\pi\delta(x - y) \,. \tag{2.76}$$

In these equations we have performed an additional step: we have replaced the momentum $\Pi(x)$ by its expression in terms of $\varphi(x)$. This is valid since we are only interested in the physics that takes place within the constrained phase space. It's the usage of Dirac's bracket and the corresponding quantization that allows us to apply this reduction of the phase space variables. The commutation relation of $\partial_x\varphi$ with itself is typical of a $u(1)$ Kac-Moody current algebra [207].

From this we can also derive the *chiral constraint* using the Heisenberg equation of motion. A straightforward calculation gives for $\partial_t\varphi = i[K_0, \varphi]$

$$(D_t - v_c D_x)\varphi = 0 \,. \tag{2.77}$$

This equation also holds on the classical level, where it corresponds to Hamilton's equation of motion. As mentioned before, in our approach this equation is not a constraint but an equation of motion. In other approaches [213] it used as a constraint.

The final issue we have left out is the non-uniqueness of the inverse $C^{-1}$, see Eq. (2.72). Different choices of $h(t)$ result in different commutation relations for $\varphi(x)$. As is discussed in Ref. [57, 198] this ambiguity arises because of the continuous nature of the system. A proper treatment requires defining the boundary conditions of the system, which in a non-trivial manner determines the function $h(t)$. Instead of analysing this method in depth we instead switch to a momentum basis, which fixes periodic boundary conditions (on $\partial_x\varphi$) and sets $h(t)$ to be zero.

## 2.6 Mode Expansion and dynamics

In this section we treat the chiral boson using a mode expansion for a finite size system. This serves two goals. The first is that it clears up the remaining issues of quantization. By switching to a momentum basis we implicitly impose boundary conditions on the field $\varphi$, which in turn fix the function $h(t) = 0$ mentioned in Eq. (2.72) as is explained in Ref. [57, 198].

The second goal is that we use the modes to determine the correlation functions of the system. The one-dimensional massless boson is notorious for both its infrared and ultraviolet divergences and these are regularized by using a mode expansion on a finite size system. We follow the conventions of [209]. See also [217, 219] for related treatments.

### 2.6.1 Mode expansion of the chiral boson

The background configuration is a fixed classical solution, and only the homogeneous solution is quantized. The mode expansion is performed only on the homogeneous part. Recall

$$\varphi(x,t) = -\sqrt{\nu}Ut + \int_x^{x_{\text{ref}}} a_x(y)dy + \varphi_h(x,t) . \tag{2.78}$$

We assume a finite system of length $L$ and impose periodic boundary conditions on $\partial_x \varphi_h$. Note that the field $\varphi$ itself is an angular variable and represents the phase of (quasi-)particle operators. It is therefore not periodic, and we clarify below how we interpret the boundary conditions on $\varphi_h$. We impose periodic boundary conditions on $\partial_x \varphi_h$ as it is more convenient for the treatment of the homogeneous part. The bosonic field $\varphi_h(x)$ contains a linear term which accounts for the zero mode structure of $\partial_x \varphi_h$. The expansion is given by

$$\varphi_h(x) = \sqrt{\frac{2\pi}{L}}\varphi_0 + \sqrt{\frac{2\pi}{L}}\rho_0 x - \sqrt{\frac{2\pi}{L}}\sum_{k>0}\frac{1}{\sqrt{k}}\left(e^{-ikx}b_k + e^{ikx}b_k^\dagger\right)e^{-\delta k/2} \tag{2.79}$$

where $k = \frac{2\pi}{L}n, \; n \in \mathbb{Z}$. The positive, infinitesimal constant $\delta$ regulates the UV divergences of the theory while the finite-size $L$ of the system regulates the infrared divergence. The modes $b_k$ are (proportional to) the Fourier modes of $\partial_x \varphi_h$. The mode expansion for the density operator is

$$\partial_x \varphi_h(x) = \sqrt{\frac{2\pi}{L}}\rho_0 + i\sqrt{\frac{2\pi}{L}}\sum_{k>0}\sqrt{k}\left(e^{-ikx}b_k - e^{ikx}b_k^\dagger\right)e^{-\delta k/2} \tag{2.80}$$

The modes $\varphi_0$ and $\rho_0$ are the zero modes of $\varphi_h$ and $\partial_x \varphi_h$ respectively. We refer to both these operators as simply "the zero modes" and it should be clear from context which mode is referred to. The field $\partial_x \varphi_h$ is periodic, meaning the boundary condition imposed on $\varphi_h$ is

$$\varphi_h(L/2) - \varphi_h(-L/2) = \int_{-L/2}^{L/2}\partial_x \varphi_h(x)dx = \sqrt{2\pi L}\rho_0 \tag{2.81}$$

This is also proportional to the total charge operator Eq. (2.38). Put differently, the boundary condition on $\varphi_h$ corresponds to the amount of charge inserted in the system (the edge). The inverse relations are

$$\varphi_0 = \frac{1}{\sqrt{2\pi L}} \int_{-L/2}^{L/2} \varphi_h(x) dx \qquad b_k = \frac{1}{\sqrt{2\pi L}} \frac{-i}{\sqrt{k}} \int_{-L/2}^{L/2} \partial_x \varphi_h(x) e^{ikx} dx \qquad (2.82)$$

$$\rho_0 = \frac{1}{\sqrt{2\pi L}} \int_{-L/2}^{L/2} \partial_x \varphi_h(x) dx \qquad b_k^\dagger = \frac{1}{\sqrt{2\pi L}} \frac{i}{\sqrt{k}} \int_{-L/2}^{L/2} \partial_x \varphi_h(x) e^{-ikx} dx \qquad (2.83)$$

In terms of the (c-number) modes the action is[3]

$$S = \frac{1}{2}\left(\rho_0 \dot\varphi_0 - \varphi_0 \dot\rho_0\right) + \frac{i}{2} \sum_{k>0} (b_k^* \dot b_k - b_k \dot b_k^*) - H \qquad (2.84)$$

with $H$ the Hamiltonian. From this action we can read of the matrix elements of the antisymmetric matrix $C_{ij}$. Its non-vanishing elements are

$$C_{\varphi_0,\rho_0} = -C_{\rho_0,\varphi_0} = 1 \qquad\qquad C_{b_k^\dagger,b_k} = -C_{b_k,b_k^\dagger} = i \qquad (2.85)$$

Furthermore, the zero modes form a conjugate pair meaning $\pi_{\rho_0} = \frac{1}{2}\rho_0$ and $\pi_{\varphi_0} = -\frac{1}{2}\rho_0$. Similarly each pair $b_k$ and $b_k^*$ are also conjugate, $\pi_{b_k} = -\frac{i}{2}b_k^*$, $\pi_{b_k^*} = \frac{i}{2}b_k$. These define the constraints of the system and quantization now follows along the usual route as explained in the previous section. Applying the rules of constrained quantization gives

$$[\varphi_0, \rho_0] = i \qquad\qquad [b_k, b_k^\dagger] = 1 . \qquad (2.86)$$

The operators $b_k$ and $b^\dagger$ satisfy the usual commutation relations of harmonic ladder operators.

## 2.6.2 The Hilbert space

For the Hilbert space we define a vacuum state $|0\rangle = |\text{vac}\rangle$ which has zero charge and is annihilated by all the annihilation operators, i.e.

$$\rho_0|0\rangle = b_k|0\rangle = 0 . \qquad (2.87)$$

We create a tower of momentum states upon this vacuum state using the operators $b_k^\dagger$. All these states carry zero charge, since $\rho_0$ commutes with $b_k^\dagger$. Charged states are created through the coherent-state-like operator $e^{i\alpha\varphi_0}$. This operator acts as a raising operator of the charge eigenstate, as can been seen from the commutation relation

$$[\rho_0, e^{i\alpha\varphi_0}] = \alpha e^{i\alpha\varphi_0} . \qquad (2.88)$$

---

[3]The modes entering the expression for the action are classical. It should be clear from context when we switch to the operator-valued modes.

A charged eigenstate is of the form

$$e^{i\alpha\varphi_0}|0\rangle = |\alpha\rangle . \tag{2.89}$$

On top of this charged state another tower of momentum states arises through the application of the $b_k^\dagger$. With these operation we generate the full Hilbert space. However, we note that not all values of $\alpha$ constitute an operator on the Hilbert space. Only a discrete set of charges $\alpha$ enter the theory. This is due to the compactification of the chiral boson as a result of the $U(1)$ symmetry of the theory. We identify

$$\varphi(x) = \varphi(x) + 2\pi\nu \tag{2.90}$$

The filling fraction $\nu$ is the compactification radius [58, 33]. By demanding that the operator which creates a charge $e^{i\alpha\varphi_0}$ is invariant with respect to this identification, we obtain a discrete spectrum of charges, since

$$e^{2\pi i\alpha\nu} = 1 \tag{2.91}$$

must be satisfied by all charges $\alpha$ appearing in the theory. This is the charged part of the Hilbert space. The full Hilbert space is also determined by the neutral part of the edge theory, see e.g. Ref. [85].

### 2.6.3  The Hamiltonian and time evolution

Having quantized the system we now explore its dynamics. Here we analyse the left moving edge. We set $a_t(t, x) = U$ constant and take $a_x(x)$ time independent and a vanishing zero mode. We recall the grand canonical Hamiltonian, Eq. 2.31, for a chiral boson coupled to a DC voltage

$$K_0[\varphi] = \int_{-L/2}^{L/2} \left[ \frac{v_c}{4\pi}(\partial_x\varphi)^2 - \frac{\sqrt{\nu}}{2\pi}(U - v_c a_x)\partial_x\varphi - \frac{\nu}{4\pi}a_x(U - v_c a_x) \right] dx \tag{2.92}$$

This Hamiltonian applies to the full chiral boson which includes the background configuration. We now switch to the decomposition Eq. (2.78). The Hamiltonian is given by

$$K_0[\bar{\varphi}, \varphi_h] = H_0 - \frac{\nu}{2\pi}\int_{-L/2}^{L/2}(U - v_c a_x)a_x dx \tag{2.93}$$

$$H_0 = \frac{v_c}{4\pi}\int_{-L/2}^{L/2}(\partial_x\varphi)^2 .$$

The Hamiltonian $H_0$ describes the decoupled chiral boson $\varphi_h$. Note that the Hamiltonian $K_0[\bar{\varphi}, \varphi_h]$ does *not* follow from simply replacing $\varphi$ by $\bar{\varphi} + \varphi_h$ in Eq. (2.92). Instead, the substitution of $\varphi$ is performed in the action after which the Hamiltonian follows.

In terms of the mode expansion the Hamiltonian $H_0$ is given by

$$H_0 = \frac{v_c}{2} \rho_0^2 + \frac{v_c}{2} \sum_{k>0} e^{-\delta k} k (b_k^\dagger b_k + b_k b_k^\dagger) \tag{2.94}$$

This expression needs to be normal ordered. In this context this comes down to moving all annihilation operators to the right and regularizing the corresponding divergences. In the last term we replace $b_k b_k^\dagger = b_k^\dagger b_k + 1$, and obtain an infinite sum over integers $n$ ($k = \frac{2\pi}{L} n$) regularized by $e^{-\delta k}$. Using a Laurent series we find

$$\sum_{n=1}^\infty n e^{-\delta n} = \frac{1}{4} \frac{1}{\sinh(\delta/2)^2} = \frac{1}{\delta^2} - \frac{1}{12} + \frac{\delta^2}{240} + \mathcal{O}(\delta^4) . \tag{2.95}$$

valid for $\mathrm{Re}[\delta] > 0$. The sum is divergent in the $\delta \downarrow 0$ limit which is the UV divergence of the theory. Regularization effectively comes down to removing the singular behaviour and taking $\delta \downarrow 0$. This procedure gives

$$\sum_{n=1}^\infty n = -\frac{1}{12} \qquad \text{(regularized)} . \tag{2.96}$$

The normal ordered canonical Hamiltonian is

$$H_0 = \frac{v_c}{2} \rho_0^2 + v_c \sum_{k>0} k b_k^\dagger b_k - \frac{\pi v_c}{12L} . \tag{2.97}$$

**Dynamics**

The free field $\varphi_h(x,t)$ obeys the chiral half of the wave equation, $(\partial_t - v_c \partial_x) \varphi_h(x,t) = 0$. This is solved by $\varphi_h(x,t) = \varphi_h(x + v_c t)$. When we apply this to to the mode expansion (2.79) we simply replace $x \to x + v_c t$ at each occurrence of $x$. Alternatively, we can solve the equations of motion for each mode separately. For instance, the zero mode $\varphi_0$ obeys

$$\partial_t \varphi_0 = i[H_0, \varphi_0] = v_c \rho_0 \implies \varphi_0(t) = \varphi_0(0) + \rho_0 v_c t . \tag{2.98}$$

The other zero mode $\rho_0$ is conserved. From now on we set $\varphi_0 = \varphi_0(0)$. Similarly the momentum modes evolve as plane waves

$$b_k(t) = b_k e^{-i v_c k t} \qquad\qquad b_k^\dagger(t) = b_k^\dagger e^{i v_c k t} . \tag{2.99}$$

This gives for the chiral boson

$$\varphi(x,t) = -\sqrt{\nu} U t + \int_x^{x_{\mathrm{ref}}} a_x(y) dy$$

$$+ \sqrt{\frac{2\pi}{L}} \varphi_0 + \sqrt{\frac{2\pi}{L}} (x + v_c t) \rho_0 + \varphi_+(x + v_c t) + \varphi_-(x + v_c t) \tag{2.100}$$

where the positive and negative frequencies are collectively written by

$$\varphi_+(x) = -\sqrt{\frac{2\pi}{L}} \sum_{k>0} \frac{1}{\sqrt{k}} e^{ikx} b_k^\dagger e^{-\delta k/2} \qquad\qquad \varphi_-(x) = -\sqrt{\frac{2\pi}{L}} \sum_{k>0} \frac{1}{\sqrt{k}} e^{-ikx} b_k e^{-\delta k/2} .$$

48

### 2.6.4  Non-equal time commutation relations

The chiral boson obeys the commutation relations of Eq. (2.76). Here we show that the modes reproduces these commutation relations in the limit of a vanishing IR regulator $\delta \to 0$. To compute the commutator of the chiral boson with itself we can ignore the gauge potential and focus on the (operator-valued) homogeneous solution $\varphi_h$. The mode expansion (2.100) gives

$$[\varphi(x,t),\varphi(0,0)] = \frac{2\pi}{L}[\rho_0,\varphi_0](x+v_ct) + \frac{2\pi}{L}\sum_{k>0}\frac{1}{k}\big(e^{-ik(x+v_ct)}[b_k,b_k^\dagger] + e^{ik(x+v_ct)}[b_k^\dagger,b_k]\big)e^{-\delta k}$$

$$= -\frac{2\pi}{L}(x+v_ct)i + \log\left[\frac{1-e^{-\frac{2\pi}{L}(\delta+i(x+v_ct))}}{1-e^{-\frac{2\pi}{L}(\delta-i(x+v_ct))}}\right] \tag{2.101}$$

In the limit of $\delta \downarrow 0$ the complex logarithm reduces to $\log\big(-e^{i\frac{2\pi}{L}(x+v_ct)}\big) = i\frac{2\pi}{L}(x+v_ct) - i\pi\,\mathrm{sgn}(x+v_ct)$, with the step function due to the branch cut. The non-equal time commutation relation is

$$[\varphi(x,t),\varphi(0,0)] = -i\pi\,\mathrm{sgn}(x+v_ct) \tag{2.102}$$

This expression holds for finite $L$ on the restricted domain $(x+v_ct) \in [-L/2, L/2]$. It corresponds to the commutation relation found in Section 2.5 with $x$ replaced by $x+v_ct$. A similar calculation applies to

$$[\partial_x\varphi(x,t),\varphi(0,0)] = \frac{2\pi}{L}[\rho_0,\varphi_0] - i\frac{2\pi}{L}\sum_{k>0}e^{-\delta k}\big(e^{-ik(x+v_ct)}[b_k,b_k^\dagger] - e^{ik(x+v_ct)}[b_k^\dagger,b_k]\big)$$

$$\approx -2i\frac{\delta}{\frac{L}{\pi}\big(1-\cos\big(\frac{2\pi}{L}(x+v_ct)\big)\big)+\delta^2}\,. \tag{2.103}$$

The function $\frac{L}{\pi}\big(1-\cos\big(\frac{2\pi}{L}(x+v_ct)\big)\big)$ is approximated by $(x+v_ct)$ around the points $x+v_ct = nL$ with $n$ integer. In the limit of $\delta \downarrow 0$ we obtain the Dirac comb, i.e. a periodic delta function. On the restricted domain $[-L/2, L/2]$ we have

$$[\partial_x\varphi(x,t),\varphi(0,0)] = -2\pi i\delta(x+v_ct)\,. \tag{2.104}$$

We have recovered two of the three commutators of expression (2.76) and the last one follows using a similar calculation. In particular the commutation relations all depend on the combination $(x+v_ct)$, regardless of finite-size effects, the presence of a regulator and the coupling to the external gauge field. The resulting relations apply to both the full chiral boson and the homogeneous part, since the latter corresponds to the operator-valued part of the former.

## 2.6.5 Vertex operators

Quasiparticles and electron operators are constructed using vertex operators. Vertex operators are normalized, coherent-state operators which create charged eigenstates as localized wave packets. We first define the normal ordered exponentiated operator as

$$: e^{i\alpha\varphi(x,t)} : \equiv e^{-i\alpha\sqrt{\nu}Ut} e^{i\alpha\sqrt{\nu}\int_x^{x_{\text{ref}}} a_x(y)dy} e^{i\alpha\sqrt{\frac{2\pi}{L}}\varphi_0} e^{i\alpha\sqrt{\frac{2\pi}{L}}\rho_0(x+v_ct)} e^{i\alpha\varphi_+(x,t)} e^{i\alpha\varphi_-(x,t)} \quad (2.105)$$

The exponentiated operator $e^{i\alpha\varphi_0}$ creates a charged eigenstate and therefore it appears to the left of the zero mode $\rho_0$. The total operator has a non-vanishing vacuum expectation value. A vertex operator with label $\alpha$ is a normalized exponential operator

$$\psi_\alpha(x,t) = \left(\frac{2\pi}{L}\right)^{\alpha^2/2} : e^{i\alpha\varphi(x,t)} : \quad (2.106)$$

This operator has vanishing expectation value $\langle\psi_\alpha(x)\rangle$ in the large $L$ limit. The operator carries an electric charge $\sqrt{\nu}\alpha$ as follows from its commutation relation with the charge operator $Q$

$$[Q, \psi_\alpha(x)] = \frac{\sqrt{\nu}}{\pi}\alpha\psi_\alpha(x') \int_{-\infty}^\infty \frac{\delta}{(x-x')^2 + \delta^2} dx = \sqrt{\nu}\alpha\psi_\alpha(x) . \quad (2.107)$$

These relations also hold for finite $\delta$ and $L$. We conclude that the vertex operator carries an electric charge of $Q = \sqrt{\nu}\alpha$. The conjugate operator $\psi^\dagger$ carries the opposite charge and is defined as

$$\psi_\alpha^\dagger = \psi_{-\alpha}(x,t) . \quad (2.108)$$

This operator provides us with the first realization of an anyonic quasiparticle operator. It carries a charge $\sqrt{\nu}\alpha$ which can take on fractional values, and it has a fractional spin given by

$$h_\alpha = \frac{\alpha^2}{2} . \quad (2.109)$$

This last result is motivated through conformal field theory [8, 58] and arises from covariant transformation properties of the operator $\psi_\alpha$ with respect to (conformal) coordinate transformations. The quantity $h_\alpha$ is called the fractional spin or conformal dimension of the operator $\psi_\alpha^\dagger$. To clarify, the homogeneous part of the operator only depends on the holomorphic combination $z = x + v_c t$. Upon a coordinate transformation $z = x + v_c t \to w(z)$ the homogeneous part transforms covariantly as

$$\psi_\alpha(w) = \left(\frac{dw}{dz}\right)^{-h_\alpha} \psi_\alpha(z) . \quad (2.110)$$

This transformation law is typical for conformal primary operators, see e.g. Ref [8, 58]. The fractional spin of quasiparticle operators is closely related to statistics of the quasiparticle.

Bosons and fermions carry integer and half-integer spins respectively. A fractional spin different from half-integer implies the particle is an anyon and obeys a generalized form of statistics.

For the commutator of two vertex operators we employ the identity

$$e^A e^B = e^B e^A e^{[A,B]} \qquad (2.111)$$

which is valid provided the commutator $[A, B]$ is commutes with $A$ and $B$. We have

$$\psi_\alpha(x,t)\psi_\beta(0,0) = \psi_\beta(0,0)\psi_\alpha(x,t)e^{-i\alpha\beta\pi\,\mathrm{sgn}(x+v_c t)} \,. \qquad (2.112)$$

For anyons the product $\alpha\beta$ is typically a fraction and the commutation relation involves a complex phase. This is a reminiscent of the fractional exchange statistics of anyons in $(2+1)D$ dimension. There the exchange of two Abelian anyons results in a phase factor of $e^{i\alpha\beta\pi}$. The difference in $(1+1)D$ is that there is no notion of braiding, so Eq. (2.112) by itself cannot be interpreted as a phase arising from exchange statistics.

In the presence of a neutral channel the quasiparticle operators take on the form

$$\mathcal{W}_n \otimes \psi_\alpha(x,t) \,. \qquad (2.113)$$

The exchange of two operators then depends on the neutral operator $\mathcal{W}_n$ as well.

Finally, we recall the idea of the bulk-edge correspondence [85]. For each $(1+1)D$ edge quasiparticle operator there exists a $(0+2)D$ operator that acts on the bulk. These edge and bulk operators satisfy the same operator product expansion, and so the spectrum of edge "anyons" is the same as that of the bulk.

### 2.6.6 The density operator from point splitting

Consider the simple case of an edge consisting of a single chiral boson. All quasiparticle operators correspond to vertex operators $\psi_\alpha^\dagger(x,t)$. One requirement for a fractional quantum Hall edge is the existence of an electron operator. This operator carries unit electric charge and has a half-integer spin. A vertex operator $\psi_\alpha$ carries charge $\sqrt{\nu}\alpha$ and spin $\frac{\alpha^2}{2}$. The electron operator is therefore of the form

$$\Psi_{\mathrm{electron}}^\dagger = \psi_{M/2}^\dagger(x,t), \qquad M = 1,3,\dots \qquad (2.114)$$

and the filling fraction is $\nu = \frac{1}{M}$. This is the only possible family of quantum Hall edges which can be constructed using a single chiral boson and the requirement of the existence of an electron operator. The series of filling fractions $\nu = \frac{1}{3}, \frac{1}{5}, \dots$ is the Laughlin series and this construction shows that the single chiral boson model is not sufficient to explain the wide

variety of observed quantum Hall edges. In Section 2.3.2 we discussed possible extensions of the chiral boson model.

We finally note that we can use the electron operator to construct the charge density operator. This amounts to obtaining the normal ordered product : $\Psi^\dagger_{\text{electron}}\Psi_{\text{electron}}$ :, for instance through use of point splitting, see Ref. [209]). Specifically, we can determine

$$\lim_{\epsilon\downarrow 0}\Psi^\dagger_{\text{electron}}(x+\epsilon/2)\Psi^\dagger_{\text{electron}}(x-\epsilon/2)\,. \tag{2.115}$$

The lowest order, non-singular term in this expansion corresponds to the charge density operator $\rho(x,t) = \frac{\sqrt{\nu}}{2\pi}D_x\varphi(x,t)$.

## 2.7 Correlation functions

To compute the correlation functions for the chiral boson, its various derivatives and the vertex operators we use an operator-based approach. The calculations presented here follow closely the steps outlined in Refs. [209, 93]. As before we consider the case of DC voltage $U$ and a static gauge field $a_x(x)$. The correlation function of some functional of the chiral boson $F[\varphi]$ at finite temperature is given by

$$\langle F[\bar\varphi + \varphi_h]\rangle = \frac{1}{Z[H_0[\varphi_h]]}\text{Tr}\left[e^{-H_0[\varphi_h]/T}F[\bar\varphi + \varphi_h]\right] \tag{2.116}$$

$$H_0 = \frac{v_c}{2}\rho_0^2 + v_c\sum_{k>0}kb_k^\dagger b_k, \qquad k = \frac{2\pi}{L}n,\ n\in\mathbb{Z}\,.$$

**Mode expectation values**  The non-zero modes are bosonic ladder operators and their correlations functions are the usual Bose-Einstein occupation numbers

$$\langle b_k^\dagger b_k\rangle = \begin{cases} 0 & T=0 \\ n_B(v_ck) & T>0 \end{cases} \qquad \langle b_k b_k^\dagger\rangle = \langle b_k^\dagger b_k\rangle + 1 = \begin{cases} 1 & T=0 \\ -n_B(-v_ck) & T>0 \end{cases} \tag{2.117}$$

with $n_B(v_ck) = (e^{v_ck/T}-1)^{-1}$. The zero mode $\rho_0$ is proportional to the electric charge operator. The vacuum is charge-neutral and so the zero temperature correlator vanishes. To compute the finite temperature correlator requires knowledge of the full chiral algebra. More concretely the correlator is given by

$$\langle\rho\rangle = \frac{1}{Z}\sum_{n\in A}\langle n|e^{-\frac{1}{T}\frac{v_c}{2}\rho_0^2}|n\rangle = \frac{1}{Z}\sum_{n\in A}ne^{-\frac{1}{T}\frac{v_c}{2}n^2} \tag{2.118}$$

where the sum runs over a complete basis of charge eigenstates, which is specified by the full chiral algebra. However, we always encounter this correlator multiplied by a factor of $\sqrt{1/L}$

or $x\sqrt{1/L}x$. In the limit of $L \to \infty$ the correlator vanishes,

$$\sqrt{\frac{2\pi}{L}}\langle \rho_0 \rangle = 0 \qquad (L \to \infty) \,. \tag{2.119}$$

The correlator $\langle \varphi_0 \rangle$ is constant with no physical implications. We set it to zero

$$\sqrt{\frac{2\pi}{L}}\langle \varphi_0 \rangle = \text{const} \to 0 \,. \tag{2.120}$$

### 2.7.1 One-point correlators

In the large $L$ limit the one point correlator of the homogeneous solution vanishes $\langle \varphi_h \rangle = 0$. What remains for the one-point correlator of $\varphi$ is the particular solution given by

$$\langle \varphi(x,t) \rangle = \bar{\varphi}(x,t) = -\sqrt{\nu}Ut + \sqrt{\nu}\int_x^{x_{\text{ref}}} a_x(x')dx' \,. \tag{2.121}$$

From this we obtain the one-point correlators of the edge charge density $\rho = \frac{\sqrt{\nu}}{2\pi}D_x\varphi$ and edge current density $j = -\partial_t \varphi$. By construction the charge density vanishes

$$\langle \rho(x,t) \rangle = \frac{\sqrt{\nu}}{2\pi}\langle D_x\varphi(x,t) \rangle = 0 \,. \tag{2.122}$$

For the current density we have

$$\langle j(x,t) \rangle = -\frac{\sqrt{\nu}}{2\pi}\langle \partial_t\varphi(x,t) \rangle = \frac{\nu}{2\pi}U \,. \tag{2.123}$$

From this we can also obtain the total current through the system. The current density of the right-mover is $\langle j_R(x,t) \rangle = -\frac{\nu}{2\pi}U_R$, which gives for the total current

$$I_0(x) = \langle j_L(x,t) \rangle + \langle j_R(x,t) \rangle = \frac{\nu}{2\pi}(U_L - U_R) \,. \tag{2.124}$$

We finally recover the full quantum Hall relation of current and voltage from the quantized edge theory.

### 2.7.2 Two-point correlators

We consider the bosonic autocorrelator $\langle \varphi(x,t)\varphi(0,0) \rangle$. Substituting in the particular solution and the mode expansion for the homogeneous solutions gives

$$\langle \varphi(x,t)\varphi(x',t') \rangle = \bar{\varphi}(x,t)\bar{\varphi}(x',t') + \langle \varphi_+(x,t)\varphi_-(x',t') \rangle + \langle \varphi_-(x,t)\varphi_+(x',t') \rangle + \dots \tag{2.125}$$

where $\varphi_+$ and $\varphi_-$ are given by Eq. (2.100).

**At zero temperature** the correlator $\langle \varphi_+\varphi_- \rangle = 0$ vanishes and what remains is

$$\langle \varphi_-(x,t)\varphi_+(0,0) \rangle = \frac{2\pi}{L}\sum_{k>0}\frac{1}{k}e^{-k(\delta+i(x+v_ct))} = -\log\big(1 - e^{-\frac{2\pi}{L}(\delta+i(x+v_ct))}\big)$$

$$= -\log\big(\delta + i(x + v_ct)\big) + \log(\frac{L}{2\pi}) + \dots \tag{2.126}$$

This expression is logarithmically divergent in the large $L$ limit. This is the infrared divergence of the system and is a reflection of the invariance $\varphi \to \varphi + \text{const}$. We have

$$\langle \varphi(x,t)\varphi(0,0)\rangle = \bar{\varphi}(x,t)\bar{\varphi}(x',t') - \log\big(\delta + i(x + v_c t)\big) + \log(\frac{L}{2\pi}) + \dots \tag{2.127}$$

**At finite temperature** we cannot perform the summation directly and we instead evaluate it in the large $L$ limit. The complete expansion of the correlators of $\varphi_{+/-}$ is

$$\langle \varphi_+(x,t)\varphi_-(0,0)\rangle + \langle \varphi_-(x,t)\varphi_+(0,0)\rangle =$$
$$\frac{2\pi}{L} \sum_{k>0} \frac{1}{k} e^{-\delta k}\big(e^{ik(x+v_c t)}n_B(v_c k) - e^{-ik(x+v_c t)}n_B(-v_c k)\big) . \tag{2.128}$$

Here we set $x', t' = 0$, since the homogeneous part is translational invariant. To simplify this expression we note that $n_B(v_c k)$ acts as an effective regulator for large, positive $k$ (this does not apply to $n_B(-v_c k)$). Since $\delta$ is infinitesimal we can switch its sign in the first term thereby obtaining a symmetric expression in $k$,

$$\langle \varphi_+(x,t)\varphi_-(0,0)\rangle + \langle \varphi_-(0,0)\varphi_+(0,0)\rangle \longrightarrow \frac{2\pi}{L} \sum_{k \neq 0} \frac{1}{k} e^{k(\delta + i(x+v_c t))}n_B(v_c k) . \tag{2.129}$$

The next step is to take the $L \to \infty$ limit and approximate the sum by an integral which runs over the real axis. The summation excludes the $k = 0$ term meaning the domain of integration is $\gamma = (-\infty, -\frac{2\pi}{L}] \cup [\frac{2\pi}{L}, \infty)$. The resulting integral is

$$\langle \varphi_+(x,t)\varphi_-(0,0)\rangle + \langle \varphi_-(x,t)\varphi_+(x',t')\rangle = \int_\gamma \frac{1}{y} \frac{e^{y\frac{2\pi T}{v_c}(\delta + i(x+v_c t))}}{e^{2\pi y} - 1}dy . \tag{2.130}$$

In the appendix we compute this integral using a contour integral. This is essentially a sum over residues located at $y = mi$ with $m$ integer. The divergence at the origin requires a more subtle approach. The result is Eq. (A.17) in the appendix where the constant $C$ represents the infrared divergence, which arises in the $L \to \infty$ limit. This constant is fixed by demanding that the finite temperature expression matches with the zero temperature case, Eq. (2.127). This fixes $C = \log(\frac{LT}{v_c})$. We have

$$\langle \varphi(x,t)\varphi(x',t')\rangle = \begin{cases} \bar{\varphi}^2 - \log\big(\delta + i(\Delta x + v_c \Delta t)\big) + \log(\frac{L}{2\pi}) & T = 0 \\ \bar{\varphi}^2 - \log\Big[\frac{v_c}{\pi T}\sin\big(\frac{\pi T}{v_c}(\delta + i(\Delta x + v_c \Delta t))\big)\Big] + \log(\frac{L}{2\pi}) & T > 0 \end{cases} \tag{2.131}$$

where we use the notation $\Delta x = x - x'$ and $\Delta t = t - t'$, and

$$\bar{\varphi}^2 = \bar{\varphi}(x,t)\bar{\varphi}(x',t') = \Big(\sqrt{\nu}Ut + \int_x^{x_{\text{ref}}} a_x(y)dy\Big)\Big(\sqrt{\nu}Ut' + \int_{x'}^{x_{\text{ref}}} a_x(y')dy'\Big) . \tag{2.132}$$

### 2.7.3  Density and edge current autocorrelators

The computation of the density autocorrelator for $\rho(x,t) = \frac{\sqrt{\nu}}{2\pi} D_x \varphi = \frac{\sqrt{\nu}}{2\pi} \partial_x \varphi_h$ is performed using the same techniques. Using the mode expansion we find for the charge density autocorrelator

$$\langle \rho(x,t)\rho(0,0) \rangle = \frac{\nu}{(2\pi)^2} \frac{2\pi}{L} \sum_{k>0} k \left( e^{ik(x+v_ct)} \langle b_k^\dagger b_k \rangle + e^{-ik(x+v_ct)} \langle b_k b_k^\dagger \rangle \right) e^{-\delta k} . \qquad (2.133)$$

At zero temperature the expression reduces to a geometric sum which results in

$$\langle \rho(x,t)\rho(0,0) \rangle = \frac{\nu}{(2\pi)^2} \left(\frac{\pi}{L}\right)^2 \sin\left(\frac{\pi}{L}(\delta + i(x+v_ct))\right)^{-2}$$

$$= \frac{\nu}{(2\pi)^2} \frac{1}{(\delta + i(x+v_ct))^2} + \cdots \qquad \begin{pmatrix} T = 0 \\ L \to \infty \end{pmatrix} . \qquad (2.134)$$

At finite temperature we encounter a similar summation as in the case of $\langle \varphi \varphi \rangle$. After the same manipulations we express the correlator as an integral

$$\langle \rho(x,t)\rho(0,0) \rangle \longrightarrow \frac{\nu}{(2\pi)^2} \left(\frac{2\pi T}{v_c}\right)^2 \int_{-\infty}^{\infty} y \frac{e^{y \frac{2\pi T}{v_c}(\delta + i(x+v_ct))}}{e^{2\pi y} - 1} dy \qquad \begin{pmatrix} T > 0 \\ L \to \infty \end{pmatrix} . \qquad (2.135)$$

Here we again switched the sign of $\delta$ in the summation over $\langle b_k^\dagger b_k \rangle$ and approximated the sum by an integral. In this case the integrand is regular at the origin and the $|k| \downarrow 0$ regime does not produce a divergence. Using the methods of contour integration (see Appendix A) we obtain for the density autocorrelator

$$\langle \rho(x,t)\rho(0,0) \rangle = \begin{cases} \dfrac{\nu}{(2\pi)^2} \dfrac{1}{(\delta + i(x+v_ct))^2} & T = 0 \\[3mm] \dfrac{\nu}{(2\pi)^2} \dfrac{\left(\pi T/v_c\right)^2}{\sin\left(\frac{\pi T}{v_c}(\delta + i(x+v_ct))\right)^2} & T > 0 . \end{cases} \qquad (2.136)$$

To obtain the expression for the edge current $j(x,t)$ density autocorrelator we use the chiral constraint $\partial_t \varphi = v_c D_x \varphi - \sqrt{\nu} U$,

$$\langle j(x,t)j(0,0) \rangle = \begin{cases} \left(\dfrac{\nu U}{2\pi}\right)^2 + \dfrac{\nu}{(2\pi)^2} \dfrac{1}{(\delta + i(x+v_ct))^2} & T = 0 \\[3mm] \left(\dfrac{\nu U}{2\pi}\right)^2 + \dfrac{\nu}{(2\pi)^2} \dfrac{\left(\pi T\right)^2}{\sin\left(\frac{\pi T}{v_c}(\delta + i(x+v_ct))\right)^2} & T > 0 . \end{cases} \qquad (2.137)$$

Alternatively, these correlators are obtained from the correlator $\langle \varphi(x,t)\varphi(0,0) \rangle$ by differentiating with respect to $x$ or $t$.

## 2.7.4 Vertex operator correlators

In this section we derive the two-point correlators of vertex operators and the generalized
$N$-point correlators along the lines of Refs. [209, 93]. To compute the correlators we analyse
each mode separately, and merge them together at a final stage. The correlator we investigate
is

$$\langle \psi_\alpha(x,t)\psi_\beta(x',t') \rangle = e^{-i\sqrt{\nu}U(\alpha t + \beta t')} e^{i\sqrt{\nu}\alpha \int_x^{x_{\text{ref}}} a_x(y)dy + i\sqrt{\nu}\beta \int_{x'}^{x_{\text{ref}}} a_x(y)dy}$$

$$\times \langle e^{i\alpha\sqrt{\frac{2\pi}{L}}\varphi_0} e^{i\alpha\sqrt{\frac{2\pi}{L}}\rho_0(x+v_ct)} e^{i\beta\sqrt{\frac{2\pi}{L}}\varphi_0} e^{i\beta\sqrt{\frac{2\pi}{L}}\rho_0(x'+v_ct')} \rangle$$

$$\times \left(\frac{2\pi}{L}\right)^{\frac{\alpha^2+\beta^2}{2}} \langle e^{i\alpha\varphi_+(x,t)} e^{i\beta\varphi_-(x,t)} e^{i\alpha\varphi_+(x',t')} e^{i\beta\varphi_-(x',t')} \rangle . \tag{2.138}$$

As before the correlator of the zero modes is rather trivial in the large $L$ limit. We have

$$\langle e^{i\alpha\sqrt{\frac{2\pi}{L}}\varphi_0} e^{i\alpha\sqrt{\frac{2\pi}{L}}\rho_0(x+v_ct)} e^{i\beta\sqrt{\frac{2\pi}{L}}\varphi_0} e^{i\beta\sqrt{\frac{2\pi}{L}}\rho_0(x'+v_ct')} \rangle = 1 + \dots \tag{2.139}$$

The correlator of the non-zero modes is handled through use of two identities: (a version
of) the Baker-Campbell-Hausdorff formula and Wick's theorem applied to exponentiated
operators. These identities are

$$e^A e^B = e^{A+B} e^{\frac{1}{2}[A,B]} \tag{2.140}$$

$$\langle e^{fb^\dagger + gb} \rangle = e^{\frac{1}{2}fg(\langle b^\dagger b \rangle + \langle bb^\dagger \rangle)} . \tag{2.141}$$

The first of these is valid as long as $[A, B]$ is central. We combine these rules to each pair of
modes, $b_k^\dagger$ and $b_k$. For complex $f$ and $g$ this results in

$$\langle e^{ifb^\dagger} e^{if^*b} e^{igb^\dagger} e^{ig^*b} \rangle = e^{\frac{1}{2}(|f|^2+|g|^2)} e^{-\frac{|f|^2+|g|^2}{2}(\langle b^\dagger b \rangle + \langle bb^\dagger \rangle)} e^{-(fg^*\langle b^\dagger b \rangle + f^*g\langle bb^\dagger \rangle)} \tag{2.142}$$

For the chiral boson the parameters $f$ and $g$ are those appearing in the expansion of $\varphi_+(x,t)$,
see Eq. (2.100). By taking into account all modes we arrive at the following identity

$$\langle e^{i\alpha\varphi_+(x,t)} e^{i\beta\varphi_-(x,t)} e^{i\alpha\varphi_+(0,0)} e^{i\beta\varphi_-(0,0)} \rangle = \left(\frac{2\pi}{L}\delta\right)^{-\frac{\alpha^2+\beta^2}{2}} \prod_k e^{-\frac{\alpha^2+\beta^2}{2}F_k(0,0)} \prod_k e^{-\alpha\beta F_k(x,t)}$$

$$F_k(x,t) \equiv \frac{2\pi}{L}\frac{1}{k} e^{-\delta k} \left( e^{ik(x+v_ct)}\langle b_k^\dagger b_k \rangle + e^{-ik(x+v_ct)}\langle b_k b_k^\dagger \rangle \right) \tag{2.143}$$

Here we used the summation and approximation

$$\exp\left(\frac{\alpha^2+\beta^2}{2}\frac{2\pi}{L}\sum_{k>0}\frac{1}{k}e^{-k\delta}\right) = \left(1 - e^{-\frac{2\pi}{L}\delta}\right)^{-\frac{\alpha^2+\beta^2}{2}} \longrightarrow \left(\frac{2\pi}{L}\delta\right)^{-\frac{\alpha^2+\beta^2}{2}} \tag{2.144}$$

The sum $\sum_{k>0} F_k$ was computed before. Comparing (2.143) with (2.128) we find

$$\sum_{k>0} F_k(x,t) = \langle \varphi_+(x,t)\varphi_-(0,0) + \varphi_-(x,t)\varphi_+(0,0) \rangle$$

$$= \begin{cases} -\log\left(\delta + i(x+v_ct)\right) + \log\left(\frac{L}{2\pi}\right) & T = 0 \\ -\log\left[\frac{v_c}{\pi T}\sin\left(\frac{\pi T}{v_c}(\delta + i(x+v_ct))\right)\right] + \log\left(\frac{L}{2\pi}\right) & T > 0 \end{cases} \tag{2.145}$$

These are all the ingredients needed to determine the two-point correlator. Putting everything together, which includes the normalization of the vertex operator, results in (for small $\delta$)

$$\langle \psi_\alpha(x,t)\psi_\beta(x',t') = e^{-i\sqrt{\nu}U(\alpha t + \beta t')} \exp\left(i\sqrt{\nu}\alpha \int_x^{x_{\text{ref}}} a_x(y)dy + i\sqrt{\nu}\beta \int_{x'}^{x_{\text{ref}}} a_x(y)dy\right)$$

$$\times \left(\frac{2\pi}{L}\right)^{\frac{(\alpha+\beta)^2}{2}} P_{\alpha\beta}(x - x' + v_c(t - t')) \tag{2.146}$$

where we use

$$P_{\alpha\beta}(x + v_c t) = \begin{cases} \dfrac{1}{(\delta + i(x + v_c t))^{\alpha\beta}} & T = 0 \\[2ex] \left(\dfrac{\pi T/v_c}{\sin\left(\frac{\pi T}{v_c}(\delta + i(x + v_c t))\right)}\right)^{\alpha\beta} & T > 0 \,. \end{cases} \tag{2.147}$$

**The neutrality condition** One important property of the two-point correlator for vertex operators is the normalization $\left(2\pi/L\right)^{\frac{(\alpha+\beta)^2}{2}}$. In the $L \to \infty$ limit this factor, and therefore the entire correlator, vanishes unless we have $\alpha = -\beta$. This is called the neutrality condition referring to the fact that $\alpha$ and $\beta$ are directly proportional to the charge of each vertex operator. The condition is enforced by the infrared divergence and represents invariance of the correlator with respect to the symmetry $\varphi \to \varphi + \text{const}$. Setting $\alpha = -\beta$ gives for the two-point correlator

$$\boxed{\langle \psi_\alpha(x,t)\psi_\beta(x',t') \rangle = e^{-i\sqrt{\nu}\alpha U(t-t')} e^{-i\sqrt{\nu}\alpha \int_{x'}^x a_x(y)dy} P_{\alpha^2}(x + v_c t)} \tag{2.148}$$

The phase factor $e^{-i\sqrt{\nu}\alpha \int_{x'}^x a_x(y)dy}$ is the Berry phase of the external (perturbed) magnetic field. The frequency $\sqrt{\nu}\alpha U$ is called the Josephson frequency for a particle with charge $Qe = \sqrt{\nu}\alpha$. In later chapters this is denoted by $\omega_Q = QeU/\hbar$.

$N$**-point correlator** The $N$ point correlator of vertex operators generalizes from the two-point correlator through repeated application of Wick's theorem. As before the correlator factorizes in terms of its zero and non-zero modes. The contribution of the zero modes results in a time-dependent phase factor, while for the non-zero modes we employ Wick's theorem. The repeated application of the identity Eq. (2.140) followed by applying Eq. (2.141) results in

$$\langle \prod_i e^{\alpha_i \varphi_i} \rangle = e^{\frac{1}{2}\sum_i \alpha_i \langle \varphi_i^2 \rangle} e^{\sum_{i<j} \alpha_i \alpha_j \langle \varphi_i \varphi_j \rangle} \tag{2.149}$$

This gives for the $N$-point correlator

$$\langle \psi_{\alpha_1}(x_1, t_1) \cdots \psi_{\alpha_n}(x_2, t_2) \rangle = e^{-i\sqrt{\nu}U \sum_{i=1}^n \alpha_i t_i} e^{i\sqrt{\nu} \sum_i \alpha_i \int_{x_i}^{x_{\text{ref}}} a_x(y)dy}$$
$$\times \left(\frac{2\pi}{L}\right)^{-\frac{1}{2}\sum_{i=1}^n \alpha_i^2} \left(1 - e^{-\frac{2\pi}{L}\delta}\right)^{-\frac{1}{2}\sum_{i=1}^n \alpha_i^2}$$
$$\times \prod_k e^{-\frac{1}{2}\left(\sum_{i=1}^n \alpha_i\right)F_k(0,0)} \prod_k e^{-\left(\sum_{i<j} \alpha_i\alpha_j\right)F_k(x_i-x_j, t_i-t_j)} \quad (2.150)$$

With use of the expression for $\sum_k F_k(x, t)$ we obtain

$$\langle \psi_{\alpha_1}(x_1, t_1) \cdots \psi_{\alpha_n}(x_2, t_2) \rangle =$$
$$e^{-i\sqrt{\nu}U \sum_{i=1}^n \alpha_i t_i} e^{i\sqrt{\nu} \sum_i \alpha_i \int_{x_i}^{x_{\text{ref}}} a_x(y)dy} \prod_{i<j} P_{\alpha_i\alpha_j}(x_i - x_j + v_c(t_i - t_j)) \quad (2.151)$$

with $P_\alpha(x)$ defined as before. We have also left out the normalization factor proportional to $\frac{2\pi}{L}$, since we assume the neutrality condition holds. The $N$-point correlator version of the neutrality condition is

$$\sum_i \alpha_i = 0 . \quad (2.152)$$

## 2.8 Ward Identity

### 2.8.1 Schwinger-Dyson equations

The combined edge and bulk action are gauge invariant with respect to the combined gauge transformation $\varphi \to \varphi - \sqrt{\nu}f$ and $a_\mu \to a_\mu + \partial_\mu f$. When we fix the gauge the edge action is invariant with respect to the residual symmetry of a shift, $\varphi \to \varphi + \text{const}$. Associated with this symmetry is a conserved current and a set of Schwinger-Dyson equations [175] which we derive here. For this we switch to a path integral representation. For now we restrict ourself to real-time, vacuum expectation values. The path integral representation of a time ordered product of $N$ vertex operators is given by

$$\langle 0|\mathcal{T} \prod_{n=1}^N \psi_{\alpha_i}(t_i, x_i)|0\rangle = \frac{1}{Z} \int \mathcal{D}\varphi e^{iS} \prod_{n=1}^N \psi_{\alpha_i}(t_i, x_i) \quad (2.153)$$

This correlator is not exactly the same as the $N$-point correlator we computed before, the reason being that we are dealing with a time-ordered object. To derive the Schwinger-Dyson equations we consider the transformation

$$\varphi(x) \to \varphi'(x) = \varphi(x) + \varepsilon(x) \quad (2.154)$$

with $\varepsilon(x)$ real-valued and small. We do *not* perform the corresponding transformation on the gauge field. This is essentially a change of variables. The measure is invariant with respect to

this transformation and so we have the identity

$$\frac{1}{Z}\int \mathcal{D}\varphi e^{iS[\varphi]}\prod_{n=1}^{N}\psi_{\alpha_i}[\varphi(t_i,x_i)] = \frac{1}{Z}\int \mathcal{D}\varphi e^{iS[\varphi']}\prod_{n=1}^{N}\psi_{\alpha_i}[\varphi'(t_i,x_i)] \,. \tag{2.155}$$

On the right hand side we expand everything to lowest order in $\varepsilon$. The vertex operators are of the form $\psi_\alpha \sim e^{i\alpha\varphi(x,t)}$ and are therefore approximated as $\psi_\alpha[\varphi'(t,x)] = i\alpha\varepsilon(t,x)\psi_\alpha[\varphi(t,x)]$. The change in action requires a bit more work and through use of integration by parts we obtain

$$\delta S = -\frac{1}{2\pi}\int \varepsilon(x,t)(\partial_t - v_c\partial_x)D_x\varphi(x,t)dxdt + \mathcal{O}(\epsilon^2)\,. \tag{2.156}$$

Plugging this back into the path integral results in

$$\frac{1}{Z}\int \mathcal{D}\varphi e^{iS[\varphi]}\prod_{n=1}^{N}\psi_{\alpha_i}(t_i,x_i)$$
$$\times \int \epsilon(x,t)\Big[-\frac{i}{2\pi}(\partial_t - v_c\partial_x)D_x\varphi(x,t) + i\sum_{i=1}^{n}\alpha_i\delta(t-t_i)\delta(x-x_i)\Big]dxdt \tag{2.157}$$

This holds for all $\epsilon$ and results in the Schwinger-Dyson equation

$$\frac{\sqrt{\nu}}{2\pi}(\partial_t - v_c\partial_x)\langle \mathcal{T}D_x\varphi(x,t)\prod_{n=1}^{N}\psi_{\alpha_i}(t_i,x_i)\rangle =$$
$$\sum_{i=1}^{n}\sqrt{\nu}\alpha_i\delta(t-t_i)\delta(x-x_i)\langle \mathcal{T}\prod_{n=1}^{N}\psi_{\alpha_i}(t_i,x_i)\rangle\,. \tag{2.158}$$

As this is derived in the context of a gauge symmetry this equation is also known as a Ward identity. The two-vector $\mathcal{J}^\mu = \frac{\sqrt{\nu}}{2\pi}(D_x\varphi, -v_cD_x\varphi)$ is the associated current.

## 2.8.2 Operator approach to Ward identities

The Schwinger-Dyson equation provide us with differential equations relating different correlation functions. We are interested in an integrated version of these equations, applicable at finite temperatures. Instead of deriving these from the SD equations directly we pursue a different approach which makes use of the commutation relations and the mode decomposition of the chiral boson. More specifically, we are interested in "reducing" the following correlators containing a mode and a number of vertex operators

$$\langle\rho_0\prod_{i=1}^{n}\psi_{\alpha_i}(x_1,t_1)\rangle \qquad \langle b_k\prod_{i=1}^{n}\psi_{\alpha_i}(x_1,t_1)\rangle \qquad \langle b_k^\dagger\prod_{i=1}^{n}\psi_{\alpha_i}(x_1,t_1)\rangle\,. \tag{2.159}$$

By reducing we mean relating each of these correlators to the $n$-point correlator $\langle\prod_{i=1}^{n}\psi_{\alpha_i}\rangle$. Once we succeed in this we can take different combinations of the modes to construct a Ward identity for e.g. the current or the charge density operator.

By definition the correlator is computed by the trace

$$\langle b_k^\dagger \prod_{i=1}^{n} \psi_{\alpha_i}(x_i, t_i)\rangle = \frac{1}{Z}\text{Tr}\left[e^{-H_0/T} b_k^\dagger \prod_{i=1}^{n} \psi_{\alpha_i}(x_i, t_i)\right]. \tag{2.160}$$

The relevant part of the Hamiltonian is

$$H_0[b_k^\dagger] = v_c k b_k^\dagger b_k \tag{2.161}$$

In the expression on the right hand side in Eq. (2.160) the operator $b_k^\dagger$ can be moved to the the farthest right position of the trace by commuting it with all the $\psi_\alpha$ operators. We have

$$\langle b_k^\dagger \prod_{i=1}^{n} \psi_{\alpha_i}(x_i, t_i)\rangle =$$

$$\langle [b_k^\dagger, \psi_{\alpha_1}] \cdots \psi_{\alpha_n}(x_n, t_n)\rangle + \ldots + \langle \psi_{\alpha_1} \cdots [b_k^\dagger, \psi_{\alpha_n}]\rangle + \langle \left[\prod_{i=1}^{n} \psi_{\alpha_i}(x_i, t_i)\right] b_k^\dagger\rangle. \tag{2.162}$$

The commutator of $b^\dagger$ and a vertex operator follows from the field operator commutation relations, Eq. (2.104). It is the typical form of a commutator with a coherent state operator

$$[b_k^\dagger, \psi_\alpha(t, x)] = i\alpha f_k(x, t)\psi_\alpha(t, x) \tag{2.163}$$

$$f_k(x, t) = \sqrt{\frac{2\pi}{L}}\frac{1}{\sqrt{k}}e^{-ik(x+v_c t)}e^{-\delta|k|/2}$$

The final term in (2.162) is manipulated through use of the cyclicity of the trace and by commuting $b_k^\dagger$ with the density operator. This commutation is accomplished through use of the identity $e^X Y e^{-X} = e^\alpha Y$, valid when $[X, Y] = \alpha Y$. This results in

$$b_k^\dagger e^{-H_0/T} = e^{v_c k/T} e^{-H_0/T} b_k^\dagger \tag{2.164}$$

and therefore

$$\langle \left[\prod_{i=1}^{n} \psi_{\alpha_i}(x_i, t_i)\right] b_k^\dagger\rangle = \frac{1}{Z}\text{Tr}\left[b_k^\dagger e^{-K_0/T} \prod_{i=1}^{n} \psi_{\alpha_i}(x_i, t_i)\right] = e^{v_c k/T}\langle b_k^\dagger \left[\prod_{i=1}^{n} \psi_{\alpha_i}(x_i, t_i)\right]\rangle. \tag{2.165}$$

We plug this back into Eq. (2.162) together with the expression for the commutators (2.163). Some rearrangements result in

$$\langle b_k^\dagger \prod_{i=1}^{n} \psi_{\alpha_i}(x_i, t_i)\rangle = i \sum_{i=1}^{n} \alpha_i \frac{f_k(x_i, t_i)}{1 - e^{v_c k/T}}\langle \prod_{i=1}^{n} \psi_{\alpha_i}(x_i, t_i)\rangle. \tag{2.166}$$

$$\langle b_k \prod_{i=1}^{n} \psi_{\alpha_i}(x_i, t_i)\rangle = -i \sum_{i=1}^{n} \alpha_i \frac{f_k^*(x_i, t_i)}{1 - e^{-v_c k/T}}\langle \prod_{i=1}^{n} \psi_{\alpha_i}(x_i, t_i)\rangle. \tag{2.167}$$

Here we also given the corresponding identity for the $b_k$'s, which is obtained following the same steps. Next we look at the zero mode $\rho_0$. Since $\varphi_0$ does not enter the Hamiltonian the

above steps lead to a different outcome if we apply it directly to $\rho_0$. Instead we consider the correlator containing $\varphi_0$

$$\langle \varphi_0 \prod_{i=1}^{n} \psi_{\alpha_i}(x_i, t_i) \rangle =$$

$$\langle [\varphi_0, \psi_{\alpha_1}(x_1, t_1)] \cdots \rangle + \ldots + \langle \cdots [\varphi_0, \psi_{\alpha_n}(x_n, t_n)] \rangle + \langle \left( \prod_{i=1}^{n} \psi_{\alpha_i}(x_i, t_i) \right) \varphi_0 \rangle \quad (2.168)$$

The commutator with a vertex operator is given by

$$[\varphi_0, \psi_{\alpha}(t, x)] = -\alpha \sqrt{\frac{2\pi}{L}} (x + v_c t) \psi_{\alpha}(t, x) . \quad (2.169)$$

In the final term we again use the cyclicity of the trace and commute $\varphi_0$ with the density operator. The Hamiltonian is given by

$$H_0[\varphi_0] = \frac{v_c}{2} \rho_0^2 \quad (2.170)$$

Note that $\varphi_0$ does not enter the Hamiltonian and so $[H_0, \varphi_0] \not\propto \varphi_0$, which is why the zero modes do not behave as the ladder operators. Instead for the commutation with the density operator we apply the relation $e^X Y e^{-X} = Y + [X, Y] + [X, [X, Y]]/2! + \ldots$. The second and higher order terms all vanish for $X = H_0/T$ and $Y = \varphi_0$. We have

$$\varphi_0 e^{-H_0/T} = e^{-H_0/T} (\varphi_0 - i \frac{v_c}{T} \rho_0) \quad (2.171)$$

When this is plugged into (2.168) the correlators containing $\varphi_0$ cancel and we are left with a relation for $\rho_0$

$$\langle \rho_0 \prod_{i=1}^{n} \psi_{\alpha_i}(x_i, t_i) \rangle = i \frac{T}{v_c} \sqrt{\frac{2\pi}{L}} \sum_{i=1}^{n} \alpha_i (x_i + v_c t_i) \langle \prod_{i=1}^{n} \psi_{\alpha_i}(x_i, t_i) \rangle . \quad (2.172)$$

With these identities for the modes we can construct Ward identities for the charge and current density operators using their mode expansions. For instance, the Ward identity for the charge density operator is given by (up to normalization)

$$\langle D_x \varphi(x, t) \prod_{i=1}^{n} \psi_{\alpha_i}(x_i, t_i) \rangle = \langle \prod_{i=1}^{n} \psi_{\alpha_i}(x_i, t_i) \rangle \left[ i \frac{T}{v_c} \frac{2\pi}{L} \sum_{i=1}^{n} \alpha_i (x_i + v_c t_i) \right.$$

$$\left. + \sum_{i=1}^{n} \alpha_i \sqrt{\frac{2\pi}{L}} \sum_{k>0} \sqrt{k} e^{-\delta k/2} \left( e^{ik(x+v_c t)} \frac{f_k(x_i, t_i)}{1 - e^{v_c k/T}} + e^{-ik(x+v_c t)} \frac{f_k^*(x_i, t_i)}{1 - e^{-v_c k/T}} \right) \right] \quad (2.173)$$

To simplify this expression we take the large $L$ limit. In this limit the term linear in $\frac{2\pi T}{L v_c}$ vanishes, while the summation over $k$ can be approximated by an integral over the domain

$\gamma = (-\infty, -\frac{2\pi}{L}] \cup [\frac{2\pi}{L}, \infty)$ which is treated in Appendix A. We have according to (A.17)

$$K(x - x_i + v_c(t - t_i)) \equiv \sqrt{\frac{2\pi}{L}} \sum_{k>0} \sqrt{k} e^{-\delta \frac{k}{2}} \left( e^{ik(x+v_ct)} \frac{f_k(x_i, t_i)}{1 - e^{v_ck/T}} + e^{-ik(x+v_ct)} \frac{f_k^*(x_i, t_i)}{1 - e^{-v_ck/T}} \right)$$

$$\approx -\frac{2\pi T}{v_c} \int_\gamma \frac{e^{y\frac{2\pi T}{v_c}(\delta + i(x+v_ct))}}{e^{2\pi y} - 1} dy = \frac{\pi T}{v_c} \cot\left( \frac{\pi T}{v_c} (\delta + i(x - x_i + v_c(t - t_i))) \right) \qquad (2.174)$$

Two important Ward identities are those associated with the charge density and edge current operators. These are given by

$$\langle \rho(x,t) \prod_{i=1}^n \psi_{\alpha_i}(x_i, t_i) \rangle = \left[ \sum_{i=1}^n \frac{\sqrt{\nu}\alpha_i}{2\pi} K(x - x_i + v_c(t - t_i)) \right] \langle \prod_{i=1}^n \psi_{\alpha_i}(x_i, t_i) \rangle \qquad (2.175)$$

$$\langle j(x,t) \prod_{i=1}^n \psi_{\alpha_i}(x_i, t_i) \rangle = \left[ \frac{\nu}{2\pi} U + \sum_{i=1}^n \frac{\sqrt{\nu}\alpha_i}{2\pi} v_c K(x - x_i + v_c(t - t_i)) \right] \langle \prod_{i=1}^n \psi_{\alpha_i}(x_i, t_i) \rangle \; .$$

$$(2.176)$$

We are not aware of any earlier work which calculates these identities. This Ward identity plays an important role in Chapter 4.

## 2.9  Discussion

In this Chapter we discussed the chiral boson model in the context of a fractional quantum Hall edge. We showed how the bulk of a FQH fluid necessitates the existence of an anomalous edge current, which can be constructed using the chiral boson model. The chiral boson plays a universal role in the edge theory of generic fractional quantum Hall states, as it accounts for the coupling of the edge to the electromagnetic field, due to its $U(1)$ gauge symmetry.

The important properties of the chiral boson model discussed in this chapter are

- **Decomposition of the chiral boson**. The coupling of the chiral boson model to the EM field can be accounted for using the background field method. This decouples the quantum fluctuations from the background configuration.

- **Constrained quantization**. The chiral boson model is constrained. To quantize the model requires Dirac's quantization procedure, which results in somewhat unconventional commutation relations.

- **Vertex operators**. These coherent-state operators represent the quasiparticle excitations of the theory.

- **Correlation functions**. Using a mode expansion we compute the one- and two-point correlation functions of the edge current and charge density operators. We also com-

puted the $N$-point correlators of vertex operators. We also found restrictions on the correlators through use of Ward identities.

# Chapter 3

# Fractional quantum Hall interferometry

## 3.1   Introduction to the interferometer

One of the main challenges in fractional quantum Hall physics is the identification of the topological order for a given filling fraction $\nu$. The most prolific state is the $\nu = 5/2$ state [226, 174, 232] which could potentially realize a non-Abelian FQH phase. Candidates for the corresponding topological order include the Moore-Read Pfaffian state [162, 99] and its particle-hole conjugate the anti-Pfaffian [151, 148]. Measuring the topological order is difficult since, by definition of the low-energy description, the theory has no local order parameters. Experiments which aim to identify the topological order of a particular fractional quantum Hall phase therefore usually focus on exploring the quasiparticle content of the phase. These experiments aim to measure properties of the anyons, such as the fractional charge, conformal dimension, fusion rules and statistics, which consequently tells us more about the corresponding topological order.

Tunnelling experiments probe the gapless excitations which reside at the edge of the system. Through the virtue of the bulk-edge correspondence the edge contains information on the properties of the bulk. Loosely speaking, for every operator which creates a bulk quasiparticle excitation there exists an operator which creates an identical quasiparticle at the edge. Tunnelling experiments such as interferometry make use of this feature in an effort to explore the topological order of the system.

Experiments have successfully measured the fractional charge of tunnelling quasiparticles [193, 55, 64] for a variety of quantum Hall phases. More recent experiments aim to fully
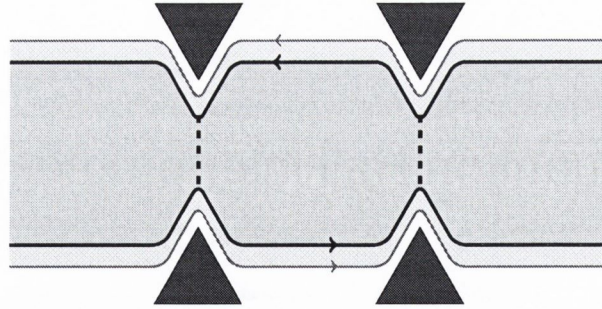
**Figure 3.1:** Figure of an interferometer. Constrictions bring the edges together and causes tunnelling of charge from one edge to the other. Tunnelling occurs only between the inner edge states. The outer edges carry excitations of lower density Hall liquids, such as underlying fully filled Landau levels. We assume these are fully transmitted.

determine the topological order through use of various interferometric devices [126, 32, 228, 229, 1, 230, 231, 227]. The early theory of tunnelling point contacts in the FQH regime focused mostly on the transport properties of a single point contact [215, 130, 161]. In a point contact the edges are forced together which induces a partial overlap of the edge states of opposite edges. This allows for tunnelling of charge. Kane and Fisher showed using the Renormalization Group that in these systems the most relevant operator corresponds to the anyon with smallest charge and smallest conformal dimension. By applying a voltage bias between the edges a net current of charge will flow from one edge to the other through the tunnelling of these anyons. The resulting tunnelling current depends non-linearly on the type of anyon tunnelling and it was conjectured that this can be used to determine e.g. the conformal dimension and fractional charge.

Fractional quantum Hall interferometry takes this one step further and uses two consecutive tunnelling point contacts. The setup is conceptually very similar to optical interference experiments. The edge is chiral, and charge flows in a unidirectional manner. This is the electronic analogue of an optical beam. The tunnelling point contact act as an electronic version of a beam splitter. By combining two tunnelling point contacts we construct an electronic Fabry-Pérot interferometer. This setup is depicted in Figure 3.1. The advantage of an interferometer over a single point contact is simply that it generates a richer signal. The tunnelling current contains a contribution due to interference attributed to the different paths along which anyons tunnel. This interference signal contains information on e.g. dynamical properties of the edge and statistics of the quasiparticles which is not present in the single-point contact case.

## Summary of results

In this chapter we analyse the tunnelling current through a Fabry-Pérot interferometer in linear response theory [40, 82, 18, 80, 17, 153, 16]. In a simple picture we assign $t_1$ and $t_2$ as the complex amplitude of a quasiparticle tunnelling along the corresponding point contact. The tunnelling current follows from the absolute value

$$I_B \sim |t_1 + t_2|^2 = |t_1|^2 + |t_2|^2 + 2\text{Re}[t_1 t_2] \tag{3.1}$$

In linear response theory the form $|t_1|^2$ and $|t_2|^2$ is radically different for the case of a tunnelling anyon as compared to what would be expected for electrons. It is a non-linear function of the applied voltage, the temperature of the system, and the fractional charge and scaling dimension of the tunnelling anyon [215, 44]. The term $2\text{Re}[t_1 t_2]$ is the interference current. Interference arises due to a variety of causes, such as the Aharonov-Bohm effect, the relative phases of the tunnelling coupling constants and the dynamical interference due to the finite velocity of the anyons traversing the interferometer. Perhaps the most interesting contribution to the interference current is due to the statistics of the anyons. Anyons localized in the bulk and inside the interferometer braid with anyons tunnelling between the edges. This braiding of anyons effectively reads out the topological state of the bulk anyons, and this signature manifests itself in the interference current [53, 199, 24, 25]. Further effects arise that go beyond braiding properties which are due to coupling of bulk quasiparticles and edge degrees of freedom [173, 172, 190, 191, 19].

We are primarily interested in the dependence of the interference current on the dynamical properties of the edge, such as the velocity of the edge channels and the applied voltage. Earlier work focused on edge states with a single characteristic velocity [40] or edge states of specific quantum Hall candidates [18, 80] to obtain an expression for the interference current. We present here the more general case of an asymmetric interferometer, a generic number of edge channels with possibly different edge velocities and opposite chiralities, at both zero and finite temperatures.

Our result is an analytic expression for the interference current in terms of a generalized hypergeometric function known as *Carlson's R function* [35]. This scaling function is closely related to the *Lauricella hypergeometric function* [146, 159]. This Lauricella function is a multivariable generalization of the Gauss hypergeometric function [98], which is a function which enters the expression for the interference current for edge states described by a single velocity [40]. Our expression generalizes this result to edge states consisting of an arbitrary number of decoupled channels described in the conformal limit. Each of these channels has its own corresponding velocity. We also find an expression for the interference current at

zero temperature in terms of the *confluent Lauricella hypergeometric function* [159], which is a multivariable generalization of the Bessel function of the first kind. Finally we obtain an expression for the two-point correlator of an anyon situated at the edge in the $(\omega, x)$-representation.

As a function of the voltage between the two edges the interference current behaves as a sum of decaying oscillations. The frequencies of these oscillations are determined by the edge lengths, edge velocities and the quasiparticle charge. For an antisymmetric interferometer this results in four frequencies appearing in the Fourier spectrum of the interference current as a function of the voltage. These four frequencies correspond to the possible combinations of one edge length and one edge velocity. Alternatively, we can fix the voltage and vary the length of one edge. This again results in oscillating behaviour with frequencies determined by the voltage, edge velocities and the quasiparticle charge.

This behaviour of the interference current as a function of varying the edge length is relevant to experiments which measure the Aharonov-Bohm oscillations through application of a plunger gate [231, 227, 1]. The plunger gate effectively deforms the area inside the interferometer through use of the Coulomb interaction. This deformation changes the Aharonov-Bohm phase of the tunnelling quasiparticles, which results in an oscillating interference current as a function of the side-gate voltage. The frequency of these oscillations, which we denote by $\phi_{AB}$, can be used to measure the charge of the tunnelling quasiparticle and the effect of quasiparticle braiding [40, 53, 199, 24, 25].

However, the change in area of the interferometer can also result in a change in the edge length, depending on the specific geometry of the interferometer. We show that for certain assumptions, such as the geometry of the device, this change in edge length results in additional oscillations in the interference current. When the change in edge length is large enough and linear with the side-gate voltage, then the interference current shows multiple oscillations characterized by the frequencies $\phi_{AB}$, $\phi_{AB} + \frac{QeV}{v_c h}$ and $\phi_{AB} + \frac{QeV}{v_n h}$. These shifted frequencies can be used to measure the edge velocity.

**Overview of this chapter**

The chapter is structured as follows. We start in Section 3.2 with a discussion of the edge theory of a fractional quantum Hall phase. We specify the structure of the edge theory and quasiparticle operators, which is based on the decomposition in terms of a charged and neutral channel.

In Section 3.3 we discuss the model Hamiltonian of the Fabry-Pérot interferometer in terms of the quasiparticle operators and the corresponding linear response. This leads to an

expression of the tunnelling current in terms of four-point correlators of the quasiparticle operators, as shown in Section 3.4. Specifically, the tunnelling current is given by evaluating the Fourier transform of these four-point correlators at the value of the Josephson frequency, see expression (3.39).

The four-point correlators depend on the precise nature of the edge state and they do not have a universal form. But as we show in Section 3.5 the correlator has a leading dependence which does have a universal expression, which is a result of the conformal symmetry in the large system-size limit.

This leads to our main result in Section 3.6, which is the Fourier transform of the leading order expression of the four-point correlators at finite temperature, Eq. (3.60). This expression is given in terms of Carlson's $R$ function which acts as a modulating function. Since this function is somewhat obscure we summarize its properties in Appendix B.3 and describe our method of computing the function, which is through its relation to the Lauricella function.

In Section 3.7 the main result is further explored for special cases, such as the zero temperature case. In Section 3.8 we plot the interference current and the $R$ function for a range of experimentally relevant parameters and analyse the result for a number of trial states for the $\nu = 5/2$, $\nu = 7/3$ and $\nu = 12/5$ plateaus. In general the $R$ function has a decaying oscillating behaviour. We show how the frequencies of these oscillations relate to the physical parameters of the system. In Section 3.9 we discuss the relevance of our results to experiments involving the Aharonov-Bohm phase in the interferometer.

## 3.2 Edge Theory

In Chapter 2 we discussed several aspects associated with the edge of a quantum Hall fluid. These mostly revolve around the chiral anomaly and properties of the chiral boson, such as its quantization procedure and correlation functions. However, the chiral boson by itself is insufficient to describe the edge theories of the abundance of quantum Hall state candidates. In particular, many quantum Hall states, which includes the non-Abelian ones, are characterized by the presence of neutral degrees of freedom which do not couple to the electromagnetic field. This section is devoted to developing a general framework of these edge theories containing neutral and charged degrees of freedom.

A quantum Hall fluid is an example of a system described by topological order [218, 219, 165, 221]. The fluid has a mobility gap in the bulk of the system. Simultaneously, gapless states develop at the edge where the confining potential crosses the Fermi level [106, 217]. These gapless edge states are chiral and responsible for the transport properties of the fluid.

The effective edge theory of the fractional quantum Hall effect can be seen as as a consequence of anomaly cancellation [233, 86, 217, 162, 7, 237, 82, 85, 88, 15] described in detail in Section 2.2. The effective bulk theory of the electromagnetic field inside a quantum Hall fluid is a Chern-Simons theory; a topological field theory which develops an anomaly on the boundary where gauge invariance is broken. A dynamical edge theory forms, with the same anomaly, but opposite in sign. The combined bulk plus edge system is gauge invariant and anomaly free.

In the long-wavelength approximation the resulting edge theory is a chiral conformal field theory. The electron and quasiparticles of the theory are represented by local operators in this conformal field theory. The set of all local operators forms the chiral algebra [85]. By specifying the chiral algebra we zoom in on a candidate fractional quantum Hall state at some filling fraction $\nu$. To be a suitable candidate for a quantum Hall state, the chiral algebra needs to fulfil a number of conditions. These conditions include for instance the existence of an electron operator and the presence of a $U(1)$ symmetry. We assume such conditions are always satisfied in our discussion.

The $U(1)$ symmetry arises due to presence of the electric current and it is required to ensure anomaly cancellation. In the case of a Laughlin state the $U(1)$ symmetry is the full gauge symmetry of the edge theory. The corresponding edge theory is the chiral boson treated in Chapter 2. It is also known as a chiral Luttinger liquid or chiral $\hat{u}(1)$ current algebra. [213, 147, 81, 209]. More complicated Abelian edge theories involve the presence of multiple chiral bosons [217, 21, 219, 27]. For non-Abelian quantum Hall states the $U(1)$ symmetry is also present, but only as a subgroup of a larger, more complicated gauge group [162, 184, 21, 82, 26]. Following Ref. [85, 27] we limit ourselves to those states described by a representation of an algebra which is formed by a direct product

$$\mathcal{A} = \mathcal{W}_n \otimes \hat{u}(1) \tag{3.2}$$

Here $\mathcal{W}_n$ is the symmetry of the chiral algebra associated with the neutral degrees of freedom. For non-Abelian states it is $\mathcal{W}_n$ which is responsible for the non-Abelian nature of the system. Quasiparticle operators obey the same decomposition. We refer to the different terms in the product as the neutral and charged channel of the edge theory. Throughout the main text we mostly deal with a single charged and a single neutral channel, although we comment on the more general case of edge states with multiple modes.

Frequently, we deal with quantum Hall states which develop on top of one or multiple completely filled Landau levels, as is the case with candidate states for the filling fraction $\nu = 5/2$. These filled Landau levels form edge states as well, and for simplicity we assume these states completely decouple from the quantum Halls state of interest. In the presence of a

point contact these filled edge states are assumed to fully transmit, meaning charge transfers only between the inner-most edges, see Figure 3.1.

### 3.2.1 Charged channel – the chiral boson

The action of the charged channel is that of the chiral boson [213, 147, 81, 153, 209], and is treated extensively in Chapter 2. Here we summarize the main properties. We consider a single edge with a right-moving chiral boson, held at a voltage bias $U$ in the gauge $a_x = 0$. The action is given by

$$S_c = \int \frac{1}{4\pi} \left[ \partial_t \varphi \partial_x \varphi - v_c (\partial_x \varphi)^2 \right] + \frac{\sqrt{\nu}}{2\pi} eU \left[ \partial_x \varphi \right] \, dt dx \, . \tag{3.3}$$

The field is compactified by the identification $\varphi = \varphi + 2\pi\sqrt{\nu}$ and $v_c$ is the velocity of the channel. The field $\varphi$ represents the charge density along the edge through the relation $\rho(x) = \frac{\sqrt{\nu}}{2\pi} \partial_x \varphi$. Quantization [81] results in the (non-local) equal-time commutation relations

$$[\varphi(x), \varphi(y)] = -i\pi \text{sgn}(x - y) \qquad [\partial_x \varphi(x), \varphi(y)] = -i2\pi \delta(x - y) \tag{3.4}$$

with $\text{sgn}(x) = +1, 0, -1$ for $x > 0$, $x = 0$ and $x < 0$ respectively. Hamilton's equations of motion are given by $(\partial_t - v_c \partial_x)\varphi = -\sqrt{\nu} eU$. The electric charge operator is given by

$$Q = \int \rho(x) dx = \frac{\sqrt{\nu}}{2\pi} \int \partial_x \varphi(x) dx \tag{3.5}$$

The Hamiltonian $K_{L,0,c}$ for a right moving edge held subject to the potential $U$ which follows from the action (3.3) is

$$K_{L,0,c} = H_{L,0,c} - eUQ \, . \tag{3.6}$$

The second term, $eUQ$, is the coupling to the electrostatic potential. The first term corresponds to the Hamiltonian of the system in the absence of an external potential,

$$H_{L,0,c} = \frac{v_c}{4\pi} \int (\partial_x \varphi)^2 \, dx. \tag{3.7}$$

The full Hamiltonian (3.6) is a generalization of the usual grand canonical Hamiltonian of the form $K_0 = H_0 - \mu \hat{N}$, with $\hat{N}$ the number operator. Instead of a number operator we use the charge operator.

### 3.2.2 Neutral channel and quasiparticles

We do not explicitly specify the nature of the neutral channel, but only assume the decomposition (3.2). What matters is that the full chiral algebra fixes the quasiparticle content

of the theory and it comes equipped with consistent rules for fusion and braiding of these quasiparticles [165, 178]. Each quasiparticle is characterized by its conformal dimension and its fusion and braiding rules with respect to the remaining quasiparticles. This specifies its quantum dimension as well.

A general quasiparticle operator factorizes as

$$\psi^\dagger(x,t) \propto \sigma(x,t) \otimes e^{i\frac{Q}{\sqrt{\nu}}\varphi(x,t)} . \tag{3.8}$$

The exponentiated operator $e^{i\frac{Q}{\sqrt{\nu}}\varphi(x,t)}$ represents a vertex operator, see Section 2.6.5. For the sake of notation we do not explicitly write the normalization factor $\left(\frac{2\pi}{L}\right)^{-h_c}$. The operator $\sigma$ represents the neutral channel.

The quasiparticle operator is characterized by its conformal dimension, $h_{\psi^\dagger} = h_\sigma + h_c$. The conformal dimension of the charged channel follows from the charge and the filling fraction, $h_c = \frac{Q^2}{2\nu}$. The commutation relations (3.4) show that the operator obeys

$$[Q, \psi^\dagger(x,t)] = Q\psi^\dagger(x,t) \tag{3.9}$$

and so the corresponding quasiparticle carries an electric charge $Qe$.

For each quasiparticle a conjugate particle exists with opposite charge and the same conformal dimension [178]. We set

$$\psi(x,t) = \bar{\sigma}(x,t) \otimes e^{-i\frac{Q}{\sqrt{\nu}}\varphi(x,t)} . \tag{3.10}$$

The operator $\bar{\sigma}$ is chosen such that the fusion product of $\sigma$ and $\bar{\sigma}$ contains the identity channel,

$$\sigma \times \bar{\sigma} = \mathbf{1} + \dots . \tag{3.11}$$

For non-Abelian quasiparticles we have, in general, multiple fusion channels. We assume that for each operator $\sigma$ there is a unique conjugate operator $\bar{\sigma}$ in the theory which obeys the fusion rule (3.11). This assumption is in fact a condition on the chiral algebra.

The neutral channel comes equipped with some neutral Hamiltonian, $H_n$ for which we assume it follows from a chiral conformal field theory, similar to the charged channel. The channel is also characterized by a neutral velocity $v_n$. However, the neutral channel does not couple to the electromagnetic field, and therefore no analogous coupling of a zero mode to the external electrostatic potential appears. Furthermore we assume the general situation in which $v_n \neq v_c$.
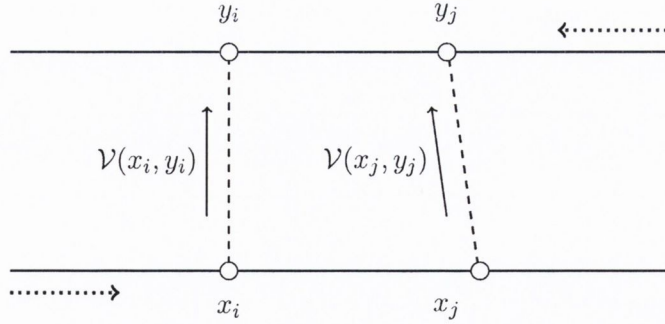
**Figure 3.2:** Figure of an interferometer. Tunnelling of quasiparticles occurs at the point contacts, e.g. from $x_i$ to $y_i$ through the operator $\mathcal{V}_i$. The dotted arrows represent the direction of the edge currents, with a right moving current on the lower edge. In the text we set $a = |y_j - y_i|$ and $b = |x_j - x_i|$.

## 3.3 Model of a Fabry-Pérot interferometer

### 3.3.1 Tunnelling Hamiltonian

In this section we treat the basic idea behind the tunnelling formalism in a system of point contacts [40, 41, 18, 153]. We consider a quantum Hall bar of infinite length at a uniform filling fraction $\nu$. The two edges, denoted as $\Sigma_{R/L}$, are disconnected and multiple constrictions are described by hopping terms allowing for the tunnelling of quasiparticles from one edge to the other. Here the subscript $L$ and $R$ denote the left (upper) and right moving (lower) edge of the system. For each edge we have an electric charge operator

$$\mathcal{Q}_{R/L} = \int_{\Sigma_{R/L}} \rho_{R/L}(x) \, dx. \tag{3.12}$$

We apply a voltage bias between the two edges, which is incorporated by fixing the electrostatic potentials $U_R$ and $U_L$ at the lower and upper edge respectively. The full Hamiltonian $K$ is given by

$$K = K_0 + H_T \,. \tag{3.13}$$

$$K_0 = H_0 - eU_L \mathcal{Q}_L - eU_R \mathcal{Q}_R \tag{3.14}$$

Here $H_T$ is the tunnelling Hamiltonian which is treated perturbatively with respect to $K_0$. The grand-canonical Hamiltonian $K_0$ consists of the terms coupling to the DC voltages through the charge operators and $H_0$. The Hamiltonian $H_0$ decomposes into the Hamiltonians for the decoupled left and right moving edges, $H_L$ and $H_R$. In addition $H_{L/R}$ describes both the charged and neutral channels $H_c$ and $H_n$ of each edge.

The tunnelling Hamiltonian $H_T$ couples the edges through tunnelling of quasiholes and quasiparticles. For this we first introduce the tunnelling operators $\mathcal{V}$. We set $x$ and $y$ as the

coordinates of the lower and upper edge respectively. A generic operator which tunnels a quasiparticle with charge $e^* = Qe$ ($e > 0$) from the lower to the upper edge is then

$$x \longrightarrow y : \qquad \mathcal{V}(x, y) = \psi^\dagger(y)\psi(x) \,. \tag{3.15}$$

The operators $\psi$ and $\psi^\dagger$ are related as explained in Section 3.2.2. Similarly the operator $\mathcal{V}^\dagger(x, y) = \psi^\dagger(x)\psi(y)$ tunnels a quasi-particle from the upper to the lower edge.

We now consider a system of $N$ well-separated point contacts. Each point contact is approximated by a single tunnelling operator $\mathcal{V}(x_i, y_i)$ and a corresponding tunnelling coupling constant $\Gamma_i$. We have in the Schroedinger picture for the tunnelling Hamiltonian

$$H_T = T + T^\dagger \tag{3.16}$$

where the $T$ operator is defined as

$$T = \sum_{i=1}^{N} \Gamma_i \mathcal{V}(x_i, y_i) \,. \tag{3.17}$$

Here the sum runs over the $N$ point contacts and $x_i$ and $y_i$ denote the coordinate of the $i$'th point contact on the lower and upper edge.

### 3.3.2 Tunnelling Current

The quantity of interest is the current running through the point contacts from one edge to the other, the so-called backscattering or tunnelling current $\langle \hat{I}_B \rangle$. It is defined as the rate of change of the difference in electric charge of the edges, $\frac{e}{2}\frac{d}{dt}(Q_R - Q_L)$. Using the equations of motion for operators in the Heisenberg picture we have

$$\hat{I}_B = -i\frac{e}{2}[Q_R - Q_L, T + T^\dagger] \tag{3.18}$$

Here we used that the charge operators commute with the free Hamiltonian $H_0$ as the charge is conserved separately on each edge in the unperturbed system. The commutation relations (3.9) imply $[Q_R, T] = -QT = -[Q_L, T]$, and so we obtain

$$\hat{I}_B = iQe(T - T^\dagger) \,. \tag{3.19}$$

### 3.3.3 Linear Response

Initially, at some reference time $t_0$, the perturbation $H_T$ is absent and the two edges are decoupled. At this initial time $t_0$ both edges are in thermal and (separate) chemical equilibrium with respect to the Hamiltonian $K_0$. The density matrix is given by

$$w_0 \equiv w(t_0) = e^{-\beta K_0}/Z \,. \tag{3.20}$$

Note that the external DC voltage is not treated perturbatively, but directly incorporated into the initial density matrix.

The perturbation $H_T$ is adiabatically switched on at $t > t_0$, slowly driving the system out of equilibrium. The time evolution follows from the usual time evolution operator $U_K(t, t_0)$ which solves the Schroedinger equation with respect to $K$,

$$i\partial_t U_K(t, t_0) = K U_K(t, t_0) . \tag{3.21}$$

Next we factorize [180] the time evolution operator as $U_K(t, t_0) = e^{-iK_0(t-t_0)} U_{H_T(t')}(t, t_0)$. Through (3.21) it follows that $U_{H_T(t')}$ satisfies

$$i\partial_t U_{H_T(t')}(t, t_0) = H_T(t') U_{H_T(t')}(t, t_0)$$
$$H_T(t) \equiv e^{iK_0 t} H_T e^{-iK_0 t} . \tag{3.22}$$

The operator $U_{H_T(t')}$ is expanded as a power series in the tunnelling coupling constants. In a perturbative approach [180] we keep the term lowest order in $\Gamma(x, y)$ which is

$$U_{H_T(t')}(t, t_0) = 1 - i \int_{t_0}^{t} H_T(t') dt' + \dots . \tag{3.23}$$

The expectation value of an operator $\mathcal{O}$ is $\langle \mathcal{O}(t) \rangle = \text{Tr}\left[ w_0 \mathcal{O}_K(t) \right]$ where $\mathcal{O}_K(t)$ is the Heisenberg representation of the operator

$$\mathcal{O}_K(t) = U_K^\dagger(t, t_0) \mathcal{O}_K(t_0) U_K(t, t_0) . \tag{3.24}$$

At the initial time $t_0$ the perturbation $H_T$ is absent, and so $\mathcal{O}_K(t_0) = \mathcal{O}_{K_0}(t_0)$. This identity together with the factorization of $U_K$ and expression (3.24) results in

$$\mathcal{O}_K(t) = U_{H_T(t')}^\dagger(t, t_0) \mathcal{O}_{K_0}(t) U_{H_T(t')}(t, t_0) \tag{3.25}$$

where we have defined

$$\mathcal{O}_{K_0}(t) = e^{iK_0 t} \mathcal{O}_S e^{-iK_0 t} \tag{3.26}$$

and $\mathcal{O}_S$ is the Schroedinger picture of the operator. When $U_{H_T(t')}$ is expanded and we keep only the lowest order term we obtain for the expectation value

$$\langle \mathcal{O}(t) \rangle = \langle \mathcal{O}_{K_0}(t) \rangle_0 - i \int_{-\infty}^{t} \langle [\mathcal{O}_{K_0}(t), H_T(t')] \rangle_0 \, dt' + \dots . \tag{3.27}$$

Here $\langle \cdots \rangle_0 \equiv \text{Tr}\left[ w_0 \cdots \right]$ is the ensemble average with respect to the unperturbed thermal state of the edges, Eq. (3.20), and we have set $t_0 \to -\infty$. We emphasize that this thermal state still includes the nonperturbative effect of the DC voltage. Expression (3.27) is the Kubo formula for the operator $\mathcal{O}$ with respect to the perturbation $H_T$.

### 3.3.4 Time evolution due to applied DC voltage and gauge invariance

In our approach a simplification is possible which elucidates some of the later manipulations. In the interaction picture the time dependence of the operators, (3.26), follows from the edge Hamiltonian $K_0$, which includes the effect of the DC voltage bias. Since the charge operators $Q_{R/L}$ commute with the Hamiltonian $H_0$ we can further factorize the time evolution operator as

$$e^{-iK_0 t} = e^{-iH_0 t} e^{ieU_L Q_L t} e^{ieU_R Q_R t}$$

The time evolution of the tunnelling operators $\mathcal{V}$ due to the applied bias voltage can now be made explicit. We use the commutation relations of the charge operators (3.9) and the form of the tunnelling Hamiltonian (3.16). This gives for the tunnelling operator $\mathcal{V}(x, y)$,

$$\mathcal{V}_{K_0}(x, y, t) = e^{-ie(U_L Q_L + U_R Q_R)t} \mathcal{V}_{H_0}(x, y, t) e^{ie(U_L Q_L + U_R Q_R)t} . \tag{3.28}$$

where $\mathcal{V}_{H_0}(x, y, t) = e^{iH_0 t} \mathcal{V}_S(x, y, t) e^{-iH_0 t}$. This is simplified further by using that when we have two operators $\hat{A}$ and $\hat{B}$ with a commutator of the form $[\hat{A}, \hat{B}] = \alpha \hat{B}$ then we have $e^{-i\beta \hat{A}} \hat{B} e^{i\beta \hat{A}} = \hat{B} e^{i\alpha\beta}$. This gives

$$\mathcal{V}_{K_0}(x, y, t) = e^{i\omega_Q t} \mathcal{V}_{H_0}(x, y, t) . \tag{3.29}$$

Here we have defined $\omega_Q = Qe(U_R - U_L)/\hbar$, which is the Josephson frequency for a particle with charge $Qe$. The value of the charge $Q$ depends on the specific edge and quasiparticle under consideration. Typical experiments are carried out in the $0 - 100$ [$\mu$V] regime, corresponding to a Josephson frequency of $0 - 10^{10}$ [Hz].

We now have for the tunnelling Hamiltonian and current operator in the interaction picture

$$H_T(t) = T(t) + T^\dagger(t) \tag{3.30}$$

$$\hat{I}_B(t) \equiv e^{iK_0 t} \hat{I}_B e^{-iK_0 t} = iQe(T(t) - T^\dagger(t)) \tag{3.31}$$

$$T(t) = \sum_i \Gamma_i e^{i\omega_Q t} \mathcal{V}(x_i, y_i, t) \tag{3.32}$$

$$\mathcal{V}(x, y, t) \equiv \mathcal{V}_{H_0}(x, y, t) = e^{iH_0 t} \mathcal{V}_S(x, y) e^{-iH_0 t} \tag{3.33}$$

The effect of the DC voltage on the time evolution of the tunnelling operators $\mathcal{V}$ is completely captured by the phase factor $e^{i\omega_Q t}$.

What we have performed here is essentially substituted the chiral boson by its decomposition as explained in Section 2.4. This is the background field method, in which $\varphi$ is written as the sum $\bar{\varphi} + \varphi_h$, where $\bar{\varphi} = -\sqrt{\nu}Ut$ is a classical solution to the equations of motion.

Upon this substitution the quasiparticle operator pick ups a phase $e^{i\omega_Q t}$ and the remaining fluctuations $\varphi_h$ decouple from the electromagnetic potential, see Section 2.6.5.

The effective replacement of the tunnelling coupling constant $\Gamma$ by a time dependent one, $\Gamma \to \Gamma e^{i\omega_Q t}$, can also be obtained by performing a suitable gauge transformation; one that gauges the scalar potential of both edges $U$ to zero [147, 40, 219]. Since the quasiparticle operators $\psi$ are charged, the tunnelling operators $T$ pick up a phase term $e^{i\omega_Q t}$ under this gauge transformation [27].

## 3.4 Linear response of the tunnelling current

In the absence of the tunnelling Hamiltonian the tunnelling current vanishes, so $\langle \hat{I}_B \rangle_0 = 0$. The linear response (3.27) for the tunnelling current (3.19) is therefore

$$I_B(\omega_Q) \equiv \langle \hat{I}_B(0) \rangle = -i \int_{-\infty}^{0} \langle [\hat{I}_B(0), H_T(t)] \rangle_0 \, dt.$$

We plug in the expressions for the tunnelling Hamiltonian (3.30) and the tunnelling current (3.19) in terms of the tunnelling operators $T$. This gives

$$I_B(\omega_Q) = Qe \int_{-\infty}^{\infty} \langle [T(t), T^\dagger(0)] \rangle_0 \, dt. \tag{3.34}$$

The correlators of the type $\langle TT \rangle$ and $\langle T^\dagger T^\dagger \rangle$ vanish, as they describe overlaps of states with different electric charge. Furthermore, we also rewrite the correlator of the commutator as $\langle [T^\dagger(t), T(0)] \rangle_0 = -\langle [T(-t), T^\dagger(0)] \rangle_0$ which is a consequence of time translational invariance. A change of integration variable finally results in (3.34).

Next we express Eq. (3.34) in terms of the tunnelling operators $\mathcal{V}(x, y)$ by substituting Eq. (3.32) for $T$. For that we introduce the tunnelling-tunnelling correlators between the $i$'th and $j$'th point contact

$$G_{ij}^>(t) = \langle \mathcal{V}(x_i, y_i, t) \mathcal{V}^\dagger(x_j, y_j, 0) \rangle_0$$
$$G_{ij}^<(t) = \langle \mathcal{V}^\dagger(x_j, y_j, 0) \mathcal{V}(x_i, y_i, t) \rangle_0 . \tag{3.35}$$

This gives

$$\langle [T(t), T^\dagger(0)] \rangle_0 = \sum_{i,j} \Gamma_i \Gamma_j^* e^{i\omega_Q t} \left[ G_{ij}^>(t) - G_{ij}^<(t) \right]$$

where $\Gamma_i$ is the tunnelling coupling constant of the $i$'th point contact. Inserting this into the expression for the tunnelling current, (3.34), the integration over time results in an expression

in terms of the Fourier transform of the $G$-correlators

$$I_B(\omega_Q) = Qe \sum_{i,j} I_{ij}(\omega_Q) \tag{3.36}$$

$$I_{ij}(\omega_Q) = \Gamma_i \Gamma_j^* \left[ G_{ij}^>(\omega_Q) - G_{ij}^<(\omega_Q) \right] .$$

Finally, we make use of complex conjugation, which relates $G_{ij}^>(\omega) = \left[ G_{ji}^>(\omega) \right]^*$, and the Kubo-Martin-Schwinger condition [129]. The KMS condition applies to two-point equilibrium correlators and relates $\langle \hat{A}(t)\hat{B}(0) \rangle_0 = \langle \hat{B}(0)\hat{A}(t + i\beta) \rangle_0$. When applied to the tunnelling-tunnelling correlators $G$ we obtain

$$G_{ij}^>(t) = G_{ij}^<(t + i\beta)$$
$$G_{ij}^>(\omega) = e^{\beta\omega} G_{ij}^<(\omega), \qquad\qquad T \neq 0 \tag{3.37}$$

and so

$$I_{ij}(\omega_Q) + I_{ji}(\omega_Q) = 2|\Gamma_i \Gamma_j^*| \, \mathrm{Re} \left[ e^{i\tilde{\alpha}_{ij}} \left( 1 - e^{-\beta\omega_Q} \right) G_{ij}^>(\omega_Q) \right] . \tag{3.38}$$

Here we introduced $\tilde{\alpha}_{ij}$ as the relative phase between the coupling constants $\Gamma_i \Gamma_j^* = |\Gamma_i \Gamma_j^*| e^{i\tilde{\alpha}_{ij}}$. One contribution to this phase is the Aharonov-Bohm (AB) effect. Quasiparticles traversing along different point contacts enclose a different amount of flux, which causes an AB interference. This interference is independent of the applied voltage, provided the geometry is fixed as a function of this DC voltage [109]; an assumption which does not always apply. We define $\Phi_Q = h/(Qe)$ as the unit flux quantum for a particle with $Q$. The enclosed flux quanta between two point contacts $i$ and $j$ is then given by $\Phi_{ij} = 2\pi(\Phi_i - \Phi_j)/\Phi_Q$, where $\Phi_i$ is the total flux enclosed by the path of quasiparticle tunnelling along the $i$'th point contact. We have for the tunnelling current

$$I_B(\omega_Q) =$$
$$Qe \left( \sum_{i=1}^N |\Gamma_i|^2 \left( 1 - e^{-\beta\omega} \right) G_{ii}^>(\omega_Q) + 2 \sum_{i<j}^N |\Gamma_i \Gamma_j^*| \, \mathrm{Re} \left[ e^{i\Phi_{ij} + i\alpha_{ij}} \left( 1 - e^{-\beta\omega_Q} \right) G_{ij}^>(\omega_Q) \right] \right) \tag{3.39}$$

where we replace $\tilde{\alpha}_{ij} = \Phi_{ij} + \alpha_{ij}$ with $\alpha_{ij}$ the relative phase of the point contacts. The first summation is the sum of the tunnelling current through each point contact in the absence of any interference. All interference effects are encapsulated in the second summation, which we call the interference current.

## 3.5 Correlators

The tunnelling current is completely determined through the $G^>$ correlators. In terms of the quasiparticle operators (3.8) these correlators are given by a product of four-point correlators,

one correlator for each edge channel,

$$G^>_{ij}(t) = \langle \psi^\dagger(y_i, t)\psi(x_i, t)\psi^\dagger(x_j, 0)\psi(y_j, 0)\rangle_0$$

$$= \langle e^{i\frac{Q}{\sqrt{\nu}}\varphi(y_i,t)} e^{-i\frac{Q}{\sqrt{\nu}}\varphi(x_i,t)} e^{i\frac{Q}{\sqrt{\nu}}\varphi(x_j,0)} e^{-i\frac{Q}{\sqrt{\nu}}\varphi(y_j,0)}\rangle_0$$

$$\times \langle \sigma(y_i,t)\bar\sigma(x_i,t)\sigma(x_j,0)\bar\sigma(y_j,0)\rangle_0 . \tag{3.40}$$

### 3.5.1 The neutral mode and conformal blocks

As it stands, the correlator for the neutral channel as stated in Eq. (3.40) is not uniquely defined. Non-Abelian quasiparticles span an internal, non-local Hilbert space. This is the realization of the non-Abelian statistical properties. In the language of conformal field theory [58, 162] this internal space is identified as the space of conformal blocks and the correlator (3.40) is a particular vector in this space. To identify this vector we first need to choose a basis in this space of conformal blocks [69, 70, 24, 18]

The conformal blocks in the correlator correspond to the different, possible fusion channels of the quasiparticles $\sigma$ and $\bar\sigma$. Symbolically the fusion rules of the fields $\sigma$ and $\bar\sigma$ are indicated as

$$\sigma \times \bar\sigma = \sum_\theta N^\theta_{\sigma\bar\sigma}\theta . \tag{3.41}$$

The sum runs over all primary states $\theta$ or quasiparticle types of the corresponding chiral algebra, including the vacuum state. The integers $N^\theta_{\sigma\bar\sigma} \geq 0$ are non-zero whenever a field $\theta$ is present in the fusion channel of $\sigma$ and $\bar\sigma$. This fusion rule signifies the possible outcomes when the two quasiparticles, $\sigma$ and $\bar\sigma$, are brought in close proximity. In this limit the quasiparticles fuse together and either form a new quasiparticle or they annihilate to the vacuum. Generally, a correlator such as Eq. (3.40) represents a superposition of possible fusion outcomes. This superposition is determined by the history of the system.

More concretely, the correlator is a linear combination of conformal blocks, where each conformal block corresponds to an intermediate fusion channel. We write symbolically

$$\langle \sigma\bar\sigma\sigma\bar\sigma\rangle = {\sum_\theta}' a_\theta \mathcal{E}_\theta . \tag{3.42}$$

The sum runs over those primary fields $\theta$ which appear in the fusion channel of $\sigma$ and $\bar\sigma$. With our choice of $\sigma$ and $\bar\sigma$ there is always one channel that corresponds to the identity or vacuum channel. The functions $\mathcal{E}_\theta$ are the conformal blocks and depend on the coordinates of the quasiparticles. The coefficients $a_\theta$ do not follow from the correlator itself but are determined by the history of the quasiparticles.

This summation already assumes a certain order in which the quasiparticles are fused together when the correlator is evaluated. This order is essentially a choice of basis in the space of conformal blocks. A different order in which the quasiparticles are fused together corresponds to a different basis. The corresponding basis transformation that relates the two bases is determined by an object known as the $F$-matrix [178]. To compute a four point correlator, such as $G^>$, we therefore need to choose a suitable basis of the space of conformal blocks for which the coefficients $a_\theta$ are known.

In the case of the $G^>$ correlators the quasiparticles are formed from the vacuum in pairs at a point contact. This means the initial fusion channel is the vacuum channel with respect to this basis. Put differently, the tunnelling operator $\mathcal{V}(x_i, y_i)$ creates a quasiparticle-anti-quasiparticle pair from the vacuum at the $i$'th point contact. It is therefore natural to use this basis, as the correlator is a single conformal block with respect to it,

$$\langle \sigma(y_i, t)\bar{\sigma}(x_i, t)\sigma(x_j, 0)\bar{\sigma}(y_j, 0)\rangle = \mathcal{E}_{\text{vac}} . \tag{3.43}$$

Pictorially we have [70, 18]

$$\mathcal{E}_{\text{vac}} = \sigma(y_i, t)\underset{}{\underline{\quad\underset{\displaystyle\bar{\sigma}(x_i,t)}{|}\quad \text{vac} \quad \underset{\displaystyle\sigma(x_j,0)}{|}\quad}}\bar{\sigma}(y_j, 0) .$$

We now identified the vector in the space of conformal blocks corresponding to the $G^>$ correlator. However, a problem with this basis is that it makes use of fusing quasiparticles on different edges. The conformal block $\mathcal{G}_{\text{vac}}$ has components which corresponds to overlaps between the two edges. We need to project out these overlaps, before explicitly calculating the correlator [70, 18].

To perform this projection, we switch to a basis in which we first fuse together the quasiparticles on the same edge, followed by fusion of the these fusion products. We have

$$\langle \sigma(y_i, t)\bar{\sigma}(x_i, t)\sigma(x_j, 0)\bar{\sigma}(y_j, 0)\rangle = a_{\text{vac}}\mathcal{F}_{\text{vac}} + \sideset{}{'}\sum_\theta a_\theta \mathcal{F}_\theta \tag{3.44}$$

where the basis is now given by

$$\mathcal{F}_\theta = \sigma(y_i, t)\underset{}{\underline{\quad\underset{\displaystyle\bar{\sigma}(y_j,0)}{|}\quad \theta \quad \underset{\displaystyle\sigma(x_i,t)}{|}\quad}}\bar{\sigma}(x_j, 0) .$$

Note that the quasiparticles of each edge are paired together and in particular the vacuum channel is always present. The coefficients $a_{\text{vac}}$ and $a_\theta$ follow from the basis transformation

which relates the blocks $\mathcal{F}$ and $\mathcal{E}$, and they are determined by the components of the $F$-matrix [58]. In particular,

$$a_{\text{vac}} = F \begin{bmatrix} \sigma & \bar{\sigma} \\ \bar{\sigma} & \sigma \end{bmatrix}_{\text{vac,vac}} \tag{3.45}$$

All conformal blocks $\mathcal{F}_\theta$ as appearing in Eq. (3.44) with a fusion channel different from the vacuum ($\theta \neq \text{vac}$) vanish in the large system-size limit. This is the limit in which the size of each edge is taken to infinity, but where the distance between the point contacts is held fixed. The conformal block that remains corresponds to the vacuum channel, and it factorizes into a product of two-point correlators. We have $\mathcal{E}_{\text{vac}} = a_{\text{vac}} \mathcal{F}_{\text{vac}} + \dots$ and so

$$\langle \sigma(y_i,t)\bar{\sigma}(x_i,t)\sigma(x_j,0)\bar{\sigma}(y_j,0)\rangle_0 = a_{\text{vac}}\langle \sigma(y_i,t)\bar{\sigma}(y_j,0)\rangle_0\langle\bar{\sigma}(x_i,t)\sigma(x_j,0)\rangle_0 + \cdots . \tag{3.46}$$

The dots represent finite-size corrections which will be ignored. The two-point correlators are non-zero only when $\sigma$ and $\bar{\sigma}$ fuse to the identity, which is why we started with this assumption. What we have accomplished here is a disentangling of the edges. In this basis the projection onto well-separated edges can be performed.

### 3.5.2 Two-point correlator of a conformal field theory

Two-point correlators in a conformal field theory are strongly constrained due to symmetries of the CFT [8, 58]. Following Ref. [58] we first consider the two-point correlator of some quasiparticle (primary) operator $\mathcal{O}$,

$$\langle \mathcal{O}(z_1)\bar{\mathcal{O}}(z_2)\rangle = \frac{1}{(z_1 - z_2)^g} . \tag{3.47}$$

Here the $z_i$ are complex coordinates of the plane, the parameter $g$ is called the algebraic decay and it is related to the scaling or conformal dimension $h$ of the field $\mathcal{O}$ and $\bar{\mathcal{O}}$ through $g = \frac{1}{2}h$. The fields $\mathcal{O}$ and $\bar{\mathcal{O}}$ must have the same conformal dimension or else the correlator vanishes identically.

A temperature is introduced through the conformal mapping of the plane to the cylinder, given by $z = \exp(2\pi i T w/v)$ where $T$ is the temperature of the system, $v$ is the velocity of the channel and we work in units where $k_B = \hbar = 1$. The fields transform covariantly [8, 58] according to $\mathcal{O}(w) = \left(\frac{dz}{dw}\right)^h \mathcal{O}(z)$, which leads to

$$\langle \mathcal{O}(w_1)\bar{\mathcal{O}}(w_2)\rangle = \frac{(\pi T/v)^g}{\sin(\pi T(w_1 - w_2)/v)^g} . \tag{3.48}$$

This transformation introduces a compactification of the coordinates, which is a geometric realization of the temperature. The Euclidean-time expression is obtained through the relation

$w = v\tau \pm ix$. The sign choice determines the chirality of the CFT, and a minus sign $(-)$ results in a right moving channel. The real-time expression is obtained by performing a Wick rotation. The rotation introduces the infinitesimal regulator [209], which we call $\delta$. We have $w_1 - w_2 = \delta + i(vt_{12} - x_{12})$, where $t_{12} = t_1 - t_2$. This results in

$$\langle \mathcal{O}(x,t)\bar{\mathcal{O}}(0,0)\rangle = \frac{(\pi T/v)^g}{\sin(\pi T(\delta + i(t + x/v)))^g} \tag{3.49}$$

This correlator is sometimes referred to as the greater Green's function. In the end the propagator is neatly summarized as

$$\langle \mathcal{O}(x,t)\bar{\mathcal{O}}(0,0)\rangle = v^{-g}P_g(t - x/v)$$

$$P_g(t) = \begin{cases} \dfrac{1}{(\delta + it)^g} & T = 0 \\[2mm] \dfrac{(\pi T)^g}{\sin(\pi T(\delta + it))^g} & T > 0 \end{cases} \tag{3.50}$$

For completeness, we have included the zero-temperature limit. Putting everything together we obtain for the correlator of the neutral mode

$$\langle \sigma(y_i,t)\bar{\sigma}(x_i,t)\sigma(x_j,0)\bar{\sigma}(y_j,0)\rangle_0 = a_{\text{vac}}\langle\sigma(y_i,t)\bar{\sigma}(y_j,0)\rangle_0\langle\bar{\sigma}(x_i,t)\sigma(x_j,0)\rangle_0 + \cdots$$

$$\approx \frac{a_{\text{vac}}}{v^{2g_n}}P_{g_n}(t + \eta a/v_n)P_{g_n}(t - \eta b/v_n) \tag{3.51}$$

Here $a = |y_i - y_j|$, $b = |x_j - x_i|$, and $v_n$ and $g_n = \frac{1}{2}h_\sigma$ are the velocity and algebraic decay of the neutral channel. The parameter $\eta = \pm 1$ denotes the chirality of the neutral channel relative to the charged mode, with $(\eta = +)$ representing the same chirality.

### 3.5.3  Correlators of the charged mode

The correlators of the charged mode have been calculated in Section 2.7.4. The charged mode is Abelian, meaning all fusion channels are unique and the projection onto disentangled edges can be done without having to perform a change of basis in the space of conformal blocks. The projection onto separate edges is

$$\langle e^{i\frac{Q}{\sqrt{v}}\varphi(y_i,t)}e^{-i\frac{Q}{\sqrt{v}}\varphi(x_i,t)}e^{i\frac{Q}{\sqrt{v}}\varphi(x_j,0)}e^{-i\frac{Q}{\sqrt{v}}\varphi(y_j,0)}\rangle_0$$

$$= \langle e^{i\frac{Q}{\sqrt{v}}\varphi(y_i,t)}e^{-i\frac{Q}{\sqrt{v}}\varphi(y_j,0)}\rangle_0 \times \langle e^{-i\frac{Q}{\sqrt{v}}\varphi(x_i,t)}e^{i\frac{Q}{\sqrt{v}}\varphi(x_j,0)}\rangle_0 + \cdots \tag{3.52}$$

The dots represent finite-size corrections which we ignore.

At this stage we recall the discussion in Section 3.3.4 where we showed that the applied DC voltage resulted in a phase factor $e^{i\omega_Q t}$. This manipulation is the decomposition of the chiral boson as is discussed in Section 2.4. In this method the chiral boson is substituted by a classical field plus fluctuations $\varphi = \bar{\varphi} + \varphi_h$, and in this case $\bar{\varphi} = -\sqrt{\nu}eUt$.

When we perform this substitution an additional change occurs. The Hamiltonian which is used to compute the correlators, $K_0$, is substituted by the Hamiltonian of the remaining fluctuations, $H_0$. The coupling term $UQ$ drops out of the Hamiltonian. Explicitly

$$\frac{\text{Tr}\left[e^{-\beta K_0[\varphi]}F[\varphi]\right]}{\text{Tr}\left[e^{-\beta K_0[\varphi]}\right]} = \frac{\text{Tr}\left[e^{-\beta H_0[\varphi_f]}F[\bar{\varphi}+\varphi_f]\right]}{\text{Tr}\left[e^{-\beta H_0[\varphi_f]}\right]} \tag{3.53}$$

We have already substituted in the decomposition of the chiral boson. The result is that the correlator of the charged mode is given by

$$\langle e^{-i\frac{Q}{\sqrt{\nu}}\varphi(x_i,t)}e^{i\frac{Q}{\sqrt{\nu}}\varphi(x_j,0)}\rangle_0 = \left(\frac{2\pi}{L}\right)^{\frac{2Q^2}{\nu}}\text{Tr}\left[e^{-\beta H_0} : e^{-i\frac{Q}{\sqrt{\nu}}\varphi(x_i,t)} :: e^{i\frac{Q}{\sqrt{\nu}}\varphi(x_j,0)} :\right]. \tag{3.54}$$

Here we also inserted the normalization factors. This correlator is treated in section 2.7.4 see Eq. (2.151). In our case $F[\varphi] \propto : e^{-i\frac{Q}{\sqrt{\nu}}\varphi(x_i,t)} :: e^{i\frac{Q}{\sqrt{\nu}}\varphi(x_j,0)} :$ and since $\bar{\varphi} = \sqrt{\nu}eUt$ we have $F[\bar{\varphi}+\varphi_f] = e^{iQeUt}F[\varphi_f]$. The phase factor corresponds to the Josephson frequency $e^{i\omega_Q t}$. The expression for the relevant correlator is

$$\langle e^{i\frac{Q}{\sqrt{\nu}}\varphi(y_i,t)}e^{-i\frac{Q}{\sqrt{\nu}}\varphi(x_i,t)}e^{i\frac{Q}{\sqrt{\nu}}\varphi(x_j,0)}e^{-i\frac{Q}{\sqrt{\nu}}\varphi(y_j,0)}\rangle_0 = v_c^{-2g_c}P_{g_c}(t+a/v_c)P_{g_c}(t-b/v_c) + \dots \tag{3.55}$$

This form matches with what we obtain by simply replacing the two-point correlators (3.52) by the propagators $P_g$.

## 3.5.4  Quasiparticle braiding and bulk-edge coupling

The correlators of the neutral and charged modes, equations (3.51) and (3.55), encapture part of the dynamical effects of quasiparticles traversing along the edge. The other dynamical contribution is due to the AB phase. In addition, there is also a topological contribution to the tunnelling current due to braiding of bulk and edge quasiparticles [82, 53, 199, 24, 25, 18]. The correlator $G_{ij}^>$ is interpreted as the amplitude of the process in which a pair of quasiparticles $\psi$ and $\psi^\dagger$ are created from the vacuum at the $j$'th point contact and annihilate to the vacuum at the $i$'th point contact. If one or multiple quasiparticles is present between these point contacts, the resulting amplitude contains a contribution coming from the quasiparticle braiding. This so-called matrix element is depicted in Figure 3.3.

More generally, Figure 3.3 represents the expectation value of Wilson lines computed with respect to the full topological quantum field theory and it is fully determined in terms of the $S$-matrix [25]. To fully determine this expectation value we require to specify the exact TQFT and the configuration and state of the bulk quasiparticles. In general the outcome is some complex valued function $\mathcal{A}_{ij}(\chi)$, bounded by $|\mathcal{A}_{ij}(\chi)| \leq 1$, which depends on the topological
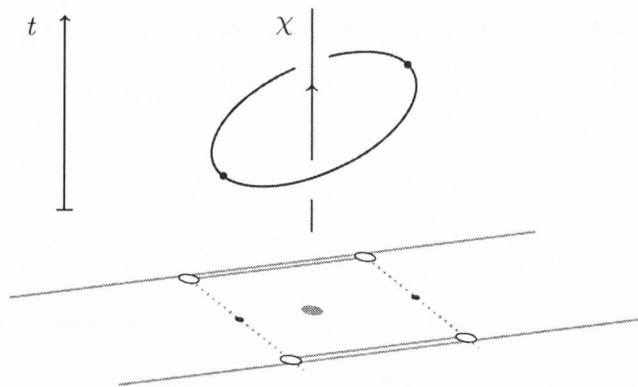
**Figure 3.3:** Quasiparticles inside the interferometer braid with quasiparticles tunnelling along the point contacts. At lowest order the effect of braiding is captured by the corresponding braiding diagram, which is determined from the topological quantum field theory.

quantum number $\chi$ associated with the bulk anyons inside the interferometer. For the $G^>$ correlators we have

$$G_{ij}^> = a_{\text{vac}}\, \mathcal{A}_{ij}(\chi) \times (\text{dynamical contributions}) + \text{finite-size effects} .\tag{3.56}$$

The effect of quasiparticle braiding is a topological effect, due to the statistical properties of the anyons. In the case of the Moore-Read state the effect leads to what is known as the even-odd effect [82, 53, 199, 24, 25, 18]. When there are bulk quasiparticles present inside the interferometer and these quasiparticles are located far from the edge then the interference current due to tunnelling of the $e/4$ quasiparticle vanishes when the number of bulk quasiparticles is odd. When the number is even the interference current re-emerges.

The situation is more complicated when the bulk quasiparticles are close enough to the edge of the system. In that case the coupling between the bulk quasiparticles and edge degrees of freedom needs to be taken into account [173, 172, 190, 191, 19]. This coupling can induce tunnelling of the neutral degrees of freedom associated with the non-Abelian statistics from the bulk quasiparticles to the edge theory. One result is that even in the case of an even number of bulk quasiparticles located inside the interferometer this bulk-edge coupling can effectively flush out the interference current. Averaged over time the tunnelling of neutral degrees of freedom can greatly reduce the strength of the interference current. We do not take into account the effect of bulk-edge coupling, but we do note that this effect can be relevant to recent experiments [1, 231, 227]

### 3.5.5 $G^>$ correlators and its Fourier transform

The expression for the $G^>$ correlator (3.40) follows straightforwardly from combining the correlators for the neutral and charged mode, (3.51) and (3.55).

$$G^>_{ij}(t) = a_{\text{vac}} \langle \psi^\dagger(y_i, t)\psi(y_j, 0)\rangle \langle \psi(x_i, t)\psi^\dagger(x_j, 0)\rangle + \dots$$
$$= A_{ij}(\chi) v_n^{-2g_n} v_c^{-2g_c} P_{g_c}(t + \tfrac{a}{v_c}) P_{g_n}(t + \eta\tfrac{a}{v_n}) P_{g_c}(t - \tfrac{b}{v_c}) P_{g_n}(t - \eta\tfrac{b}{v_n}) . \quad (3.57)$$

Here we have defined $a = |y_i - y_j|$ and $b = |x_i - x_j|$ as the distance between the $i$'th and $j$'th point contact along the upper and lower edge respectively. Recall furthermore that $\eta = \pm$ represents the chirality of the neutral channel relative to the charged channel and $A_{ij}(\chi)$ is due to braiding of quasiparticles.

For the tunnelling current we need the Fourier transform of the $G^>$ correlator. In Appendix A.3 we show how this Fourier transform is obtained. We first treat the contribution due to tunnelling along a single point contact, $G^>_{ii}$. The correlator for $G^>_{ii}(t)$ is independent of position, since $a = b = 0$ in (3.57). We have

$$G^>_{ii}(t) = v_n^{-2g_n} v_c^{-2g_c} P_{2g}(t) . \quad (3.58)$$

with $g = g_n + g_c$ twice the total scaling dimension of the quasiparticle. Using the result of (A.20) gives

$$G^>_{ii}(\omega) = e^{\frac{\omega}{2T}} \frac{(2\pi T)^{2g-1}}{v_n^{2g_n} v_c^{2g_c}} B\left(g + i\frac{\omega}{2\pi T}, g - i\frac{\omega}{2\pi T}\right) \quad (3.59)$$

Here $B(x, y)$ is the Euler beta function and we have set the integral regulator $\delta$ to zero. We treat the zero temperature case later on.

The expression for the more general case $(i \neq j)$ is more complicated. We write the Fourier transform of $G^>_{ij}(\omega)$ $(i \neq j)$ as the integral definition of Carlson's $R$ function [35]. This is a multivariable generalization of the Gauss hypergeometric function. An alternative way of representing Carlson's $R$ function is through the fourth Lauricella hypergeometric function [146, 35, 159], see also the appendix. We have cf. Eq. (A.23) the following expression,

$$G^>_{ij}(\omega_Q) = A_{ij}(\chi) H^{\text{mod}}_{ij}(\omega_Q) G^>_{ii}(\omega_Q) \quad (3.60)$$

where all (trajectory-dependent) interference effects are hidden away in the modulating function $H^{\text{mod}}$ given by

$$H^{\text{mod}}_{ij}(\omega_Q) = e^{\pi T(b-a)\left(\frac{g_c}{v_c} + \eta\frac{g_n}{v_n}\right)}$$
$$\times R\left(g - i\frac{\omega_Q}{2\pi T}; \{g_c, g_c, g_n, g_n\}; e^{-2\pi T\frac{a}{v_c}}, e^{2\pi T\frac{b}{v_c}}, e^{-\eta 2\pi T\frac{a}{v_n}}, e^{\eta 2\pi T\frac{b}{v_n}}\right) . \quad (3.61)$$

The $R$ function is treated extensively in Ref. [35] and we have summarized some of its properties in Appendix B. In particular, the order in which the parameters appear in (3.61) is relevant for its evaluation. Furthermore the $R$ function allows for certain transformations of the arguments, see also the appendix. Computation of the $R$ function is explained in Appendix B.3 using results of Ref. [140]. We mention one transformation in particular which is equation (B.5). Through this transformation we have the equivalent expression of the modulating function (3.61). This transformation effectively switches $a \leftrightarrow b$ in the expression of $H_{ij}^{\mathrm{mod}}$ and simultaneously changes the sign of $\omega_Q$,

$$
\begin{aligned}
H_{ij}^{\mathrm{mod}}(\omega_Q) = {}& e^{\pi T(a-b)\left(\frac{g_c}{v_c} + \eta \frac{g_n}{v_n}\right)} \\
& \times R\left(g + i\frac{\omega_Q}{2\pi T}; \{g_c, g_c, g_n, g_n\}; e^{2\pi T \frac{a}{v_c}}, e^{-2\pi T \frac{b}{v_c}}, e^{\eta 2\pi T \frac{a}{v_n}}, e^{-\eta 2\pi T \frac{b}{v_n}}\right).
\end{aligned} \quad (3.62)
$$

The function $\mathcal{A}_{ij}(\chi)$ describes the effect of possible quasiparticle braiding entering the correlator $G_{ij}$. Finally, in the expression for $G_{ij}^{>}(\omega)$ we recover the expression for the single point contact case, Eq. (3.59). The effect of the spatial separation of the point contacts, and thus all interference effects, is completely captured by the modulating function $H^{\mathrm{mod}}$.

Since the $R$ function is so closely related to the Lauricella function we also mention the form of the Fourier transform in terms of this function. The exact relation is explained in the appendix. Here we assume for simplicity a symmetric interferometer $b = a$. Assuming $\frac{a}{v_n} > \frac{a}{v_c}$ and the expression reduces to

$$
\begin{aligned}
H_{ij}^{\mathrm{mod}}(\omega_Q) = {}& e^{-2\pi T \frac{a}{v_n} g} e^{i\omega_Q \frac{a}{v_n}} \\
& \times F_D^{(3)}\left(g - i\frac{\omega_Q}{2\pi T}; \{g_c, g_c, g_n\}; 2g; 1 - e^{-2\pi T a\left(\frac{1}{v_n} + \frac{1}{v_c}\right)}, 1 - e^{-2\pi T a\left(\frac{1}{v_n} - \frac{1}{v_c}\right)}, 1 - e^{-4\pi T \frac{a}{v_n}}\right).
\end{aligned}
$$
$$(3.63)$$

This expression no longer depends on the chirality parameter $\eta = \pm$. The symmetric interferometer does not distinguish between chiral and anti-chiral edge states.

## 3.6   Expression for the tunnelling current

We combine the expression for the tunnelling current (3.39) with the expression for the Fourier transform of the correlators (3.59) and (3.60) and obtain the following expression

$$
I_B(\omega_Q) = 2Qe\frac{(2\pi T)^{2g-1}}{v_n^{2g_n} v_c^{2g_c}} a_{\mathrm{vac}} |\Gamma_{\mathrm{eff}}(\omega_Q)|^2 \sinh\left(\frac{\omega_Q}{2T}\right) B\left(g + i\frac{\omega_Q}{2\pi T}, g - i\frac{\omega_Q}{2\pi T}\right). \quad (3.64)
$$

In the spirit of Ref. [40] we have combined the effects due to interference into an effective tunnelling coupling amplitude,

$$
|\Gamma_{\mathrm{eff}}(\omega_Q)|^2 = \sum_{i=1}^{N} |\Gamma_i|^2 + 2\sum_{i<j}^{N} |\Gamma_i \Gamma_j| \, \mathrm{Re}[\mathcal{A}_{ij}(\chi) e^{i\Phi_{ij} + i\alpha_{ij}} H_{ij}^{\mathrm{mod}}(\omega_Q)]. \quad (3.65)
$$

The function $H_{ij}^{\text{mod}}(\omega_Q)$ is given by (3.61), which we call the modulating function. The $\Gamma_i$'s are the tunnelling coupling constant of the $i$'th point contact and $\alpha_{ij}$ is the relative phase between $\Gamma_i$ and $\Gamma_j$. We also introduced the Aharonov-Bohm phase $\Phi_{ij}$ and contributions due to quasiparticle braiding are attributed to $\mathcal{A}_{ij}(\chi)$. The disentangling of the conformal blocks results in the factor $a_{\text{vac}}$. Within our setup only $H_{ij}^{\text{mod}}$ depends explicitly on the external voltage bias. The tunnelling constants $\Gamma_i$ depend on the exact geometry of the interferometric device, and so the normalization of the current is not universal.

Expression (3.65) for the tunnelling current is of the form,

$$I_B(\omega_Q) \sim \left( \sum_i |\Gamma_i|^2 + \sum_{i<j}^{N} F_{ij}^{\text{mod}} \right) I_{\text{single pc.}}(\omega_Q) \equiv I_0 + I_{\text{osc}} \tag{3.66}$$

$$F_{ij}^{\text{mod}} = 2|\Gamma_i \Gamma_j| \, \text{Re}[\mathcal{A}_{ij}(\chi) e^{i\Phi_{ij} + i\alpha_{ij}} H_{ij}^{\text{mod}}(\omega_Q)]$$

All interference effects are contained in the function $F_{ij}^{\text{mod}}$, which we call the interference term. We only deal with interference between pairs of point contacts; there are no interference effects involving tunnelling along three or more point contacts. This is due to the linear response approximation, which only takes into account effects up to order $|\Gamma_i \Gamma_j|$.

A measure for the strength of the interference signal of a two-point interferometer is the visibility of the tunnelling current $\text{Vis}(\omega_Q)$. This is defined as

$$\text{Vis}(\omega_Q) = \frac{\max_\Phi(I_B(\omega_Q)) - \min_\Phi(I_B(\omega_Q))}{\max_\Phi(I_B(\omega_Q)) + \min_\Phi(I_B(\omega_Q))} . \tag{3.67}$$

Here $\max_\Phi(I_B(\omega_Q))$ and $\min_\Phi(I_B(\omega_Q))$ are the maximum and minimum values of the tunnelling current as a function of varying the AB phase $\Phi_{ij}$, while keeping all other parameters fixed. In the absence of bulk quasiparticles the maximum and minimum values of the tunnelling current are given by $I_0 \pm \tilde{I}_{\text{osc}}$, with $\tilde{I}_{\text{osc}} = 2|\Gamma_1 \Gamma_2| \, |H_{12}^{\text{mod}}| I_{\text{single pc.}}$ and $|\cdots|$ the absolute value. This gives for the visibility

$$\text{Vis}(\omega_Q) = \frac{2|\Gamma_1 \Gamma_2|}{|\Gamma_1| + |\Gamma_2|} |H_{12}^{\text{mod}}(\omega_Q)| . \tag{3.68}$$

The modulating function $H_{ij}^{\text{mod}}$ is a function of the different energy scales, which are set by the temperature and voltage bias, and the scales associated with the velocity and distance between the point contacts,

$$\left\{ \frac{v_c}{a}, \frac{v_c}{b}, \frac{v_n}{a}, \frac{v_n}{b}, \frac{k_B T}{\hbar}, \omega_Q \right\} . \tag{3.69}$$

These parameters enter the expression for the function $H_{ij}^{\text{mod}}$ through dimensionless combinations, and the function depends on the relative scales. The modulating function is, up to an exponential factor, determined by Carlson's $R$ function which we treat in the appendix.

The $R$ function is a scaling function, which manifests itself through the homogeneous scaling transformation (B.4). It is computed through its relation to the Lauricella function and the corresponding Taylor series as described in Appendix B.3.

The expression for the interference current is very general, and the price we pay for this is a limited intuition when it comes to the behaviour of the corresponding modulating function, $H^{\mathrm{mod}}$. We can still summarize the general behaviour of the function as a function of the physical parameters. As a function of increasing voltage $\omega_Q$ the modulating function is the sum of multiple, decaying oscillations. The frequencies of the oscillations are determined by the edge lengths and edge velocities. The temperature and algebraic decay determines the relative amplitudes of the oscillations. In addition, for large temperatures $H^{\mathrm{mod}}$ decays exponentially. Some of these features are proven analytically, while others follow empirically from numerical analyses.

## 3.7 Special cases and generalizations

The main result of our work is the expression for the interference term (3.65) for the tunnelling current (3.64) in terms of the $R$ function (3.61). Here we consider several limits and generalizations, such as the zero temperature limit and other cases in which the expression for the modulating function $H^{\mathrm{mod}}$ simplifies. This relates our results to earlier work [40, 18, 80, 16, 17]. We consider the generalization to more than two modes and discuss a relation to the two-point quasiparticle propagator.

Recall that we use $g_c$ and $g_n$ to denote the algebraic decay of the charged and neutral channel, and $v_c$ and $v_n$ the corresponding edge velocities and $\eta = \pm$ as the chirality of the neutral mode. In the case of three or more point contacts we obtain a modulating function for each unique pair of point contacts, $H_{ij}^{\mathrm{mod}}$. We use $a$ and $b$ to denote the length between the $i$'th and $j$'th point contact along the upper and lower edge respectively. In principle, these lengths depends on $i$ and $j$, so $a = a_{ij}$ and $b = b_{ij}$. However, we omit these subscripts for the sake of brevity.

Finally, we set $g = g_c + g_n$ as the total algebraic decay and work in units where $k_B = \hbar = 1$.

### 3.7.1 Zero temperature limit

The zero temperature limit can be obtained in two ways. The first is to start with the expression for the propagator at zero temperature, (3.50), and follow the same steps as in the finite-temperature case by computing the Fourier transform of $G^>$ and $G^<$. Alternatively, we can start with the expression for the tunnelling current at finite temperature, and from here take

the zero temperature limit. Both routes should produces the same result.

However, the first route leads to an obstruction. When we attempt to determine the interference current we encounter the following integral (see also Appendix C)

$$G^>_{ij}(\omega) - G^<_{ji}(\omega) \sim$$

$$\int_{-\infty}^{\infty} e^{i\omega t} \left[ P_{g_c}(t + \frac{a}{v_c}) P_{g_n}(t + \eta \frac{a}{v_n}) P_{g_c}(t - \frac{b}{v_c}) P_{g_n}(t - \eta \frac{b}{v_n}) - (t \longleftrightarrow -t) \right] dt . \quad (3.70)$$

We do not know how to solve this integral with these general parameters and we are not aware of a reference in which it is treated. Therefore we proceed with the other route, in which we start with the finite temperature expression, Eq. (3.64), and take the zero temperature limit. For the current we find the usual power-law behaviour times an effective coupling amplitude

$$I_B(\omega_Q) = 2Qe \frac{2\pi}{v_n^{2g_n} v_c^{2g_c}} a_{\text{vac}} |\Gamma_{\text{eff}}(\omega_Q)|^2 |\omega_Q|^{2g-1} \text{sgn}(\omega_Q) . \quad (3.71)$$

The expression for $|\Gamma_{\text{eff}}(\omega_Q)|^2$ is the same as in the finite temperature case, Eq. (3.65), but with a different expression for the modulating function $H^{\text{mod}}_{ij}$. We have worked out the zero temperature limit of $H^{\text{mod}}_{ij}$ in Appendix C. The result is

$$H^{\text{mod}}_{ij}(\omega) =$$

$$e^{i\omega \frac{a}{v_n}} \Phi_2^{(3)} \left( \{g_c, g_c, g_n\}; 2g; -i\omega(\frac{a}{v_n} + \eta \frac{a}{v_c}), -i\omega(\frac{a}{v_n} - \eta \frac{b}{v_c}), -i\omega(\frac{a}{v_n} - \frac{b}{v_n}) \right) \quad (3.72)$$

The function $\Phi_2^{(3)}$ is the *confluent Lauricella hypergeometric function* of 3 variables [159] and its series representation is given by Eq. (C.17). It can be extended to include more than two modes per edge. This expression for $H^{\text{mod}}_{ij}$ should also be obtained by direct computation of the integral (3.70).

In the symmetric case where $a = b$ the modulating function reduces to

$$H^{\text{mod}}_{ij}(\omega) = e^{i\omega \frac{a}{v_n}} \Phi_2^{(2)} \left( \{g_c, g_c\}; 2g; -i\omega a(\frac{1}{v_n} + \frac{1}{v_c}), -i\omega a(\frac{1}{v_n} - \frac{1}{v_n}) \right) .$$

The function $\Phi_2^{(2)}$ is known as a Humbert confluent hypergeometric function of two variables [68, 98]. For the symmetric interferometer the chirality of the neutral mode has no effect on the current.

### 3.7.2 Equal velocities and chiralities

For equal velocities and equal chiralities between the two channels we set $v = v_n = v_c$ and $\eta = +1$. This is effectively an edge with a single channel. The modulating function $H^{\text{mod}}_{ij}(\omega)$ reduces to the Gauss hypergeometric function.

$$H^{\text{mod}}_{ij}(\omega) \longrightarrow e^{\pi T g \frac{(b-a)}{v}} R\left(g - i\frac{\omega}{2\pi T}; g, g; e^{-2\pi T \frac{a}{v}}, e^{2\pi T \frac{b}{v}}\right)$$

$$= e^{-\pi T \frac{(a+b)}{v}} e^{i\omega \frac{b}{v}} {}_2F_1\left(g - i\frac{\omega}{2\pi T}; g; 2g; 1 - e^{-2\pi T \frac{(a+b)}{v}}\right) \quad (3.73)$$

The function $_2F_1$ is the Gauss hypergeometric function. For equal distances between the tunnelling points on both edges ($a = b$) the expression coincides with that found in Ref. [40], although to arrive at this expression we require some manipulations of the Gauss function. These can be found at e.g. [p. 1009] in Ref. [98]. Thus

$$\text{eq. (3.73)} = 2\pi \frac{\Gamma(2g)}{\Gamma(g)} \frac{e^{-2\pi g T \frac{a}{v}}}{\sinh(\frac{\omega}{2T})} \text{Im} \left[ \frac{e^{i\omega \frac{a}{v}} {}_2F_1\left(g; g - i\frac{\omega}{2\pi T}; 1 - i\frac{\omega}{2\pi T}; e^{-4\pi T \frac{a}{v}}\right)}{\Gamma(g + i\frac{\omega}{2\pi T})\Gamma(1 - i\frac{\omega}{2\pi T})} \right] . \tag{3.74}$$

Expression (3.74) seems obscure and overly complicated in comparison with (3.73). However, the representation (3.74) is an expansion in terms of the parameter $e^{-4\pi T \frac{a}{v}}$, which tends to zero for large temperature. In contrast, the expansion appearing in (3.73) is in terms of $1 - e^{-2\pi T \frac{(a+b)}{v}}$, meaning the argument of the Gauss function tends to one for high temperatures. The exact behaviour of the Gauss function around unit argument is problematic, and leads to slow convergence of its Taylor series or even singular behaviour. In fact, the standard way of analysing the behaviour of $_2F_1(a, b; c; 1 - z)$ for $z \to 0$ is by first transforming it into a function of the form $_2F_1(a', b'; c'; z)$.

The zero temperature limit can again be obtained in two ways: by directly computing the Fourier transform or by taking the zero temperature limit of the finite temperature expression. In this case it is possible to determine the Fourier transform directly, which we have done in Appendix C.1. We also show that this Fourier transform matches with the zero-temperature limit, demonstrating the equivalence of both routes. We find

$$H_{ij}^{\text{mod}}(\omega) = \Gamma\left(g + \frac{1}{2}\right) \left(\frac{a+b}{4v} |\omega|\right)^{\frac{1}{2} - g} e^{-i\frac{a-b}{2v}\omega} J_{g-\frac{1}{2}}\left(\frac{a+b}{2v} |\omega|\right) . \tag{3.75}$$

Here $J_{g-\frac{1}{2}}(x)$ is the Bessel function of the first kind and this expression matches with what was found in Ref. [40] when we set $a = b$.

### 3.7.3 Fast charged channel

We consider the limit where the energy scales associated with the charged mode are far greater than the remaining energy scales,

$$\frac{v_c}{a}, \frac{v_c}{b} \gg \frac{v_n}{a}, \frac{v_n}{b}, \frac{k_B T}{\hbar}, \omega_Q . \tag{3.76}$$

The scales on the right hand side are that of the neutral mode, the temperature scale and the applied voltage bias. In this limit the modulating function is

$$H_{ij}^{\text{mod}}(\omega) = e^{\pi T(b-a)\frac{g_n}{v_n}} \times R\left(g - i\frac{\omega}{2\pi T}; \{2g_c, g_n, g_n\}; 1, e^{-2\pi T \frac{a}{v_n}}, e^{2\pi T \frac{b}{v_n}}\right) .$$

$$= e^{-\pi T(a+b)\frac{g_n}{v_n}} e^{-2\pi T \frac{b}{v_n} g_c} e^{i\omega \frac{b}{v_n}}$$

$$\times F_1\left(g - i\frac{\omega}{2\pi T}; \{2g_c, g_n\}; 2g; 1 - e^{-2\pi T \frac{b}{v_n}}, 1 - e^{-2\pi T \frac{a+b}{v_n}}\right) \tag{3.77}$$

On the final line we obtain the first Appell hypergeometric function of two variables [98], $F_1(\alpha; \beta, \gamma; z_1, z_2)$. When $g_c = 0$ this function reduces to the case of a single edge mode Eq. (3.73), as expected.

### 3.7.4 Large interferometer and high temperature limit

For well separated contacts we consider large $a + b$. In Appendix B.2 we show how this behaviour can be extracted from the integral. This limit suppresses the interference current exponentially according to

$$H_{ij}^{\text{mod}} \longrightarrow \exp\left(-\pi T(a+b)\sum_i \frac{g_i}{v_i}\right) \tag{3.78}$$

This is interpreted as an effective dephasing length

$$L_T = \frac{\hbar}{\pi k_B T}\left[\sum_i \frac{g_i}{v_i}\right]^{-1}. \tag{3.79}$$

Beyond this scale the interference current is suppressed as $I \propto e^{-(a+b)/L_T}$ with $a + b$ the total circumference of the interferometer. A similar analysis applies for high temperatures. Setting

$$k_B T_L = \frac{1}{\pi(a+b)}\left[\sum_i \frac{g_i}{v_i}\right]^{-1} \tag{3.80}$$

and the interference signal vanishes as $I \propto e^{-T/T_L}$. In general the decoherence effects are reduced by decreasing the temperature. See Ref. [17] for further discussion on energy scales and visibility of the interference signal.

### 3.7.5 Asymmetric interferometer

We now consider the limit where the length of one edge approaches zero. We set $a = 0$ which effectively merges the point contacts on one edge. We obtain

$$H_{ij}^{\text{mod}}(\omega) = e^{-\pi T a\left(\frac{g_c}{v_c}+\eta\frac{g_n}{v_n}\right)} R\left(g - i\frac{\omega}{2\pi T}; \{g, g_c, g_n\}; 1, e^{-2\pi T\frac{a}{v_c}}, e^{-\eta 2\pi T\frac{a}{v_n}}\right) \tag{3.81}$$

The reduction of this expression to the corresponding hypergeometric form depends on the sign of $\eta$. For $\eta = +1$ we have

$$H_{ij}^{\text{mod}}(\omega) = e^{-\pi T a\left(\frac{g_c}{v_c}+\frac{g_n}{v_n}\right)} F_1\left(g - i\frac{\omega}{2\pi T}; g_c, g_n; 2g; 1 - e^{-2\pi T\frac{a}{v_c}}, 1 - e^{-2\pi T\frac{a}{v_n}}\right)$$

while for $\eta = -1$ we obtain

$$H_{ij}^{\text{mod}}(\omega) = e^{-\pi T a\left(\frac{g_c}{v_c}+\frac{g_n}{v_n}\right)} e^{-2\pi T\frac{a}{v_n}g_c} e^{i\omega\frac{a}{v_n}}$$
$$\times F_1\left(g - i\frac{\omega}{2\pi T}; g, g_c; 2g; 1 - e^{-2\pi T\frac{a}{v_n}}, 1 - e^{-2\pi T a\left(\frac{1}{v_c}+\frac{a}{v_n}\right)}\right).$$

Here $F_1$ is the Appell hypergeometric function of two variables [98]. Using transformation properties of the Appell function, which can be found in e.g. [p. 1020] in Ref. [98], for the case of $\eta = -1$ we can obtain a single expression for the $H_{ij}^{\text{mod}}(\omega)$ function given by

$$H_{ij}^{\text{mod}}(\omega) = e^{-\pi T a \left( \frac{g_c}{v_c} + \eta \frac{g_n}{v_n} \right)} F_1 \left( g - i \frac{\omega}{2\pi T}; g_c, g_n; 2g; 1 - e^{-2\pi T \frac{a}{v_c}}, 1 - e^{-2\pi T \eta \frac{a}{v_n}} \right). \quad (3.82)$$

### 3.7.6 More than two channels

Our result for the interference current generalizes to edges which consists of more than one mode, all with different velocities. We can also include the possibility of different edge velocities for each edge. The edge velocity is not a topologically protected property of the edge mode, and its value(s) can depend on the exact geometric details of the corresponding device.

The generalized result is obtained if we assume the modes decouple in a similar fashion as in the two-channel case or that the propagator factorizes along the lines of (3.57). In these cases the correlator $G^>$ generalizes to

$$G_{ij}^>(t) = a_{\text{vac}} \mathcal{A}_{ij}(\chi) \prod_{i=1}^{m} v_{i,L}^{-g_i} v_{i,R}^{-g_i} P_{g_i}(t + \eta_i a / v_{i,L}) P_{g_i}(t - \eta_i b / v_{i,R}) \quad (3.83)$$

Here $g_i$ and $\eta_i$ are the algebraic decay and chirality of the $i$'th edge channel and $v_{i,R}$ and $v_{i,L}$ the velocity of the $i$'th edge mode on the lower and upper edge. The function $\mathcal{A}_{ij}(\chi)$ accounts for possible braiding of quasiparticles and $a_{\text{vac}}$ arises due to disentangling of the edges. The current is still determined by the Fourier transform, and the only change arises in the modulating function and the normalization of the tunnelling current which now involves all of the velocities, see (3.64). We have

$$H_{ij}^{\text{mod}}(\omega) = e^{\pi T \sum_{i=1}^{m} \eta_i g_i \left( \frac{b}{v_{i,R}} - \frac{a}{v_{i,L}} \right)} R \left( g - i \frac{\omega}{2\pi T}; \{g_i, g_i\}_{i=1}^{m}; \{e^{-2\pi T \eta_i \frac{a}{v_{i,L}}}, e^{2\pi T \eta_i \frac{b}{v_{i,R}}}\}_{i=1}^{m} \right)$$

$$(3.84)$$

Here the arguments are ordered sets consisting of the algebraic decay and energy scales,

$$\{g_i, g_i\}_{i=1}^{m} = \{g_1, g_1, g_2, g_2, \cdots, g_m, g_m\}$$

$$\{e^{-\eta_i 2\pi T \frac{a}{v_{i,L}}}, e^{\eta_i 2\pi T \frac{b}{v_{i,R}}}\}_{i=1}^{m} = \{e^{-\eta_i 2\pi T \frac{a}{v_{1,L}}}, e^{\eta_i 2\pi T \frac{b}{v_{n,R}}}, \cdots, e^{-\eta_i 2\pi T \frac{a}{v_{n,L}}}, e^{\eta_i 2\pi T \frac{b}{v_{n,R}}}\}.$$

and $g = \sum_i g_i$. Computation of this function is similar to the two-channel case and covered in Appendix B.3.

### 3.7.7 Two-point correlators and the $R$ function

The tunnelling correlator $G_{ij}^>$ is constructed through projection onto decoupled edges, which results in a decomposition in terms of a product of two-point correlators. A simpler expression

arises when we consider the the two-point propagator of a non-Abelian anyon on a single edge. We have in the conformal limit

$$X^>_{\{v_i\}}(t,x) \equiv \langle \psi^\dagger(x,t)\psi(0,0)\rangle = \prod_{i=1}^{m} |v_i|^{-g_i} P_{g_i}(t - x/v_i) \, . \tag{3.85}$$

Here we absorb the chirality of each mode into the velocity $v_i$, which can therefore take on negative values. The corresponding Fourier transform with respect to time is

$$X^>_{\{v_i\}}(\omega,x) = (2\pi T)^{g-1} H_{\{v_i\}}(\omega,x) \left[ \prod_{i=1}^{m} |v_i|^{-g_i} \right] e^{\frac{\omega}{2T} - \omega\delta} B\left(\frac{g}{2} + i\frac{\omega}{2\pi T}, \frac{g}{2} - i\frac{\omega}{2\pi T}\right) \tag{3.86}$$

where $g = \sum_i g_i$ and all spatial dependence is captured by the function

$$H_{\{v_i\}}(\omega,x) = e^{-\pi T x \sum_i \frac{g_i}{v_i}} R\left(\frac{g}{2} - i\frac{\omega}{2\pi T}; \{g_i\}_{i=1}^{m}; \{e^{-2\pi T \frac{x}{v_i}}\}_{i=1}^{m}\right) \, . \tag{3.87}$$

This is the equilibrium two-point quasiparticle propagator in a frequency-coordinate representation.

From this we also have an expression for the $R$ function in terms of a convolution integral. For instance, we can write for a product of four propagators

$$X^>_{\{v_1,v_2,v_3,v_4\}}(t,x) = X^>_{\{v_1,v_2\}}(t,x) X^>_{\{v_3,v_4\}}(t,x) \tag{3.88}$$

$$X^>_{\{v_1,v_2,v_3,v_4\}}(\omega,x) = \int X^>_{\{v_1,v_2\}}(\omega',x) X^>_{\{v_3,v_4\}}(\omega - \omega',x) d\omega' \, .$$

The two-point propagators reduce to the Gauss hypergeometric function, see Eq. (3.73). In turn this expression can be rewritten into Eq. (3.74), through use of identities of the Gauss function. The advantage of this final expression is that it is a series expansion in terms of $e^{-4\pi \frac{a}{v}T}$, in contrast to the old expansion in terms of $1 - e^{-2\pi \frac{a}{v}T}$. This expansion in terms of $e^{-4\pi \frac{a}{v}T}$ behaves better in the high temperature limit since it avoids the singularity of the Gauss function.

For the $R$ function we only have the series expansion to our disposal, which converges very poorly in the large temperature limit. Perhaps through use of the convolution integral (3.88) and the transformation identities of the Gauss hypergeometric function this high temperature can be better regulated, although we have not investigated this further.

## 3.8 Plots of the modulating function and interference current

In this section we plot the modulating function and the corresponding interference current. Based on experiments [228, 229, 230, 231, 227] we take the distance between two point contacts to be around 2 [$\mu$m]. For the velocity no experimental data is available, but numerics

[118] suggests a much faster velocity for the charged mode compared to the neutral mode on the order of $v_c/v_n \sim 10$ and $v_c \sim 10^4$ [m/s]. The applied voltage bias lies typically in the range of 10 to 50 [$\mu$V] and temperature ranges in the order of $10 - 25$ [mK]. We assume a lower temperature of $\sim 1$ [mK] as this significantly improves the rate of convergence of the series used to compute the expression for the tunnelling current, see Appendix B.3.

In this section we are mainly interested in the behaviour of the $R$ function. In the expression for the modulating function the factor $\mathcal{A}_{ij}(\chi)e^{i\Phi_{ij}+i\alpha_{ij}}$ is due to quasiparticle braiding, the AB phase and the relative phase between the tunnelling amplitudes of the point contacts. They are assumed to be independent of the applied voltage bias and we set the total factor to unity. We comment on the AB effect in the next section.

The final parameters that need to be fixed are model-dependent, and correspond to the filling fraction $\nu$, the algebraic decay of the quasiparticle propagators $g_n$ and $g_c$, and the quasiparticle charge $Qe$. For a given edge state a renormalization group analysis predicts the quasiparticle with the lowest algebraic decay, $g_n + g_c$, to be the most relevant perturbation [130, 161, 70]. Quasiparticles with a larger algebraic decay are less relevant in the language of the renormalization group and we ignore their contributions in the plots. A second effect is that the effective magnetic length, $l_B^2 = \hbar/(QeB)$, is larger for quasiparticles with a smaller charge. The bare tunnelling matrix element depends on this length scale, and it is expected that a smaller charge correspond to larger matrix elements. Some trial states predict multiple quasiparticles with the same algebraic decay. In these cases the contributions to the tunnelling current is expected to arise from the quasiparticles with the smaller charge.

Computation of Carlson's $R$ function is not completely straightforward. The function is related to the Lauricella hypergeometric function which has a known multivariable Taylor expansion or one can resort to numerical integration of the Fourier transform $G^>$. Using combinatoric results of Ref. [140] the Taylor expansion is cast into a single summation, which we explain in Appendix B.3. We use this expansion for computing the $R$ function. For physically relevant values of the input parameters both the series expansion and numerical integration schemes converge very slowly. In particular a higher temperature scale reduces the convergence rate significantly. We apply a series acceleration using the CNCT method [125] to partially remedy this problem, see also the appendix. However, even the CNCT method is not practical for high temperatures and to our knowledge an efficient numerical scheme is still lacking.

Due to these convergence problems we are not able to compute the $R$ function for all ranges of the physical parameters. For instance, we mostly assume temperatures of 1 or even 0 [mK] for the sake of convergence of the modulating function. We also plot the modulating

function over a range of the source-drain voltage which lies outside of what is reached in experiments. We have chosen for this range as we want to demonstrate the non-trivial behaviour of the $R$ function over a greater voltage range. Finally, we point out that currently the edge velocities have not been measured and it is possible that the values used in the plots are inaccurate.

### 3.8.1  The tunnelling current without interference

Before we provide some plots of the modulating function and the interference current we first discuss the general behaviour of the tunnelling current in the absence of interference [213]. This expression also enters the result for the total interference current. It is given by Eq. (3.64) in terms of the Euler beta and the hyperbolic sine function, with the tunnelling amplitude held constant. The tunnelling current is characterized by the total algebraic decay, and we discuss two particular values of $g$ for which the function simplifies. These follow from the properties of the gamma function [68]

$$
I_B(\omega_Q) \propto
\begin{cases}
\tanh\left(\dfrac{\omega_Q}{2T}\right) & g = \dfrac{1}{2} \\[2ex]
T\omega_Q & g = 1
\end{cases}
\tag{3.89}
$$

In the limit of $\omega_Q \to \infty$ and $g = \frac{1}{2}$ the expression for the tunnelling current approaches a constant value, while $g = 1$ grows linearly with $\omega_Q$. For the remaining cases the current decays to zero for $g < \frac{1}{2}$, grows sub-linearly for $\frac{1}{2} < g < 1$, and grows super-linearly for $g > 1$. Finally, at zero temperature the expression for the current follows the power law behaviour

$$
I_B \propto |\omega_Q|^{2g-1} \mathrm{sgn}(\omega_Q)
\tag{3.90}
$$

while for high temperatures the function follows

$$
I_B \propto \omega_Q T^{2g-2} .
\tag{3.91}
$$

### 3.8.2  The tunnelling current with interference

The upper panel of Figure 3.4 is a plot of the total tunnelling current (eq. (3.64)) with and without interference for the case of the Moore-Read / Pfaffian quantum Hall trial state [162, 99] for the $\nu = 5/2$ plateau. The lower panel of Figure 3.4 is a plot of the corresponding modulating function $\mathrm{Re}[H_{ij}^{\mathrm{mod}}]$, given by equations (3.65) and (3.61). The parameters for the set $g_c = g_n = 1/8$ and $Qe = e/4$. This result is also analysed in Ref. [18]. See the figure caption for the exact values of all parameters.
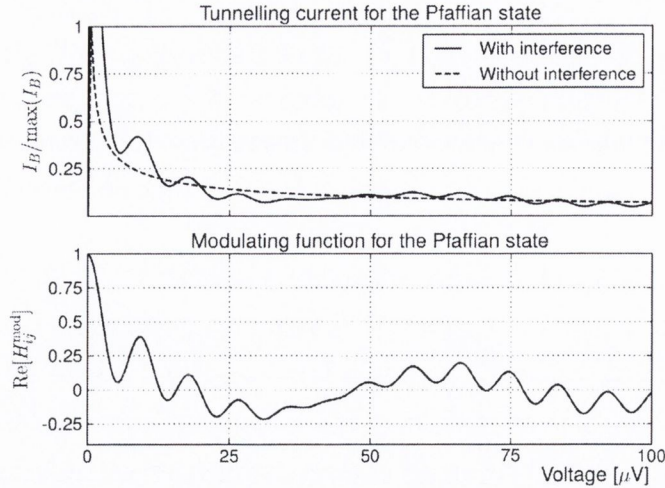
**Figure 3.4:** The tunnelling current through an interferometer with and without the modulating function. The current is normalized by the maximal value of the tunnelling current without interference ($\max(I_B(H^{\mathrm{mod}} = 0))$). The quasiparticle is the $Qe = e/4$ QP of the Pfaffian state which has $g_n = g_c = \frac{1}{8}$. The remaining parameters are $v_c = 7 \cdot 10^3$ [m/s], $v_n = 1 \cdot 10^3$ [m/s], $T = 1$ [mK], $a = 2.0$ [$\mu$m] and $b = 1.8$ [$\mu$m]. All coupling constants are equal. Interference effects due to braiding with bulk quasiparticles is absent, i.e. we set $\mathcal{A}_{ij}(\chi) = 1$.

The normalization of the current, which is the prefactor appearing in expression (3.64), contains the tunnelling coupling constants $\Gamma_i$. These factors are non-universal, meaning the normalization of the current is non-universal as well. In Figure 3.4 the current without interference is normalized by its maximum value. The normalization of the current with interference is chosen such that when the two currents cross in Figure 3.4 the modulating function vanishes $H^{\mathrm{mod}} = 0$.

### 3.8.3 Voltage and geometry dependent oscillations and frequencies
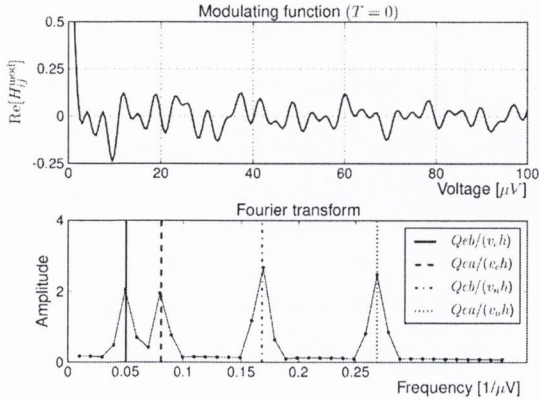


**Figure 3.5:** Fourier analysis of the modulating function when the **voltage** is varied. Upper panel: the modulating transform. Lower panel: the corresponding Fourier transform. The vertical lines represent the predicted frequency components. Parameters are $g_c = 1/8$ and $g_n = 1/6$ at $T = 0$ [K], $Qe = e/4$, $v_c = 3 \cdot 10^3$ [m/s], $v_n = 9 \cdot 10^2$ [m/s], $a = 4.0$ [$\mu$m] and $b = 2.5$ [$\mu$m].
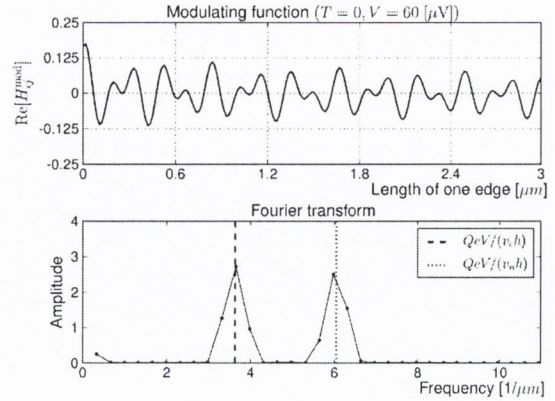
**Figure 3.6:** Fourier analysis of the modulating function when the **length of one edge** is varied. The parameters used are $g_c = g_n = 1/8$ at $T = 0$ [K] and $V = 60$ [$\mu$V]. Furthermore $Qe = e/4$, $v_c = 1 \cdot 10^3$ [m/s], $v_n = 6 \cdot 10^2$ [m/s] and $b = 2.5$ [$\mu$m].

The modulating function $\text{Re}[H_{ij}^{\text{mod}}]$ shows multiple oscillations and decays when $V \to \infty$, see the lower panel of Figure 3.4 and the upper panel of Figure 3.5. A numerical analysis (Figure 3.5) shows that for an asymmetric interferometer ($a \neq b$) and two different edge velocities the modulating function consists of four oscillating signals with frequencies

$$f_{x_j, v_i} = \frac{Qe x_j}{v_i h} \tag{3.92}$$

where $x_j = a, b$ and $v_j = v_c, v_n$. These frequencies can be extracted from the $(x, t)$ representation of the tunnelling-tunnelling correlators $G_{ij}^>(t)$, see Eq. (3.57). The peak values appearing in this correlator correspond to the frequencies (3.92). We also find that the frequencies are independent of the temperature and algebraic decay – these parameters only influence the total and relative amplitudes of the oscillations. In the limit of a symmetric interferometer ($a \approx b$) the number of contributing oscillating frequencies drops from four to two, since $f_{a, v_i} \approx f_{b, v_i}$. In this regime the two oscillations form a modulating signal with 'fast' and 'slow' frequencies $\frac{Qea}{2h}(\frac{1}{v_n} \pm \frac{1}{v_c})$, which was also found in Ref. [18]. It is also possible that the edge velocity for each channel is different on opposite edges. In that case we still have four different frequencies in the Fourier spectrum, even in the case of a symmetric interferometer.

The second analysis we perform looks at the oscillating behaviour of the modulating

function as a function of the length of one edge, while keeping all other parameters fixed. These are the oscillations in $H_{ij}^{\mathrm{mod}}$ when $a$ is varied. The frequencies of these oscillations are obtained through a numerical Fourier transform, see Figure 3.6. The modulating function shows a similar decaying, oscillating behaviour as in the case of varying the voltage, with frequencies given by

$$f_{v_i} = \frac{QeV}{v_i h} \, . \tag{3.93}$$

Since the other edge length $b$ is kept constant we observe only two contributing frequencies. For the case of a single edge velocity these frequencies can be extracted from the expression of the current at zero temperature, (3.75), by making use of properties of the Bessel function. However, we are not able to extract the frequencies in expression (3.93) analytically for the more general case. We suspect that such a result can be obtained from the $R$ function through an asymptotic expansion, which we leave as an open problem. We expect that these results carry over to the more general case of several edge channels and different velocities, see Section 3.7.6.

### 3.8.4  Temperature dependence

In Figure 3.7 the modulating function is plotted for the temperatures 0 [mK], 10 [mK] and 18 [mK]. The $T = 0$ case is computed using the confluent Lauricella hypergeometric function, as explained in Appendix C. Computation of the confluent Lauricella function is very similar to the finite temperature case.

The convergence of the series representation used to compute $R$ function becomes progressively worse for temperature scales larger compared to the remaining energy scales. Computing the $R$ function using the series expansion in this regime becomes impracticable, even when we employ a series acceleration. This type of slow convergence is similar to that exhibited by the Gauss function $_2F_1(a, b; z)$ when $|z| \to 1$. For the Gauss function a set of linear transformations exist which allow one to avoid this $|z| = 1$ singularity [98], see also Eq. (3.74) and the corresponding discussion. We are not aware of a generalized type of transformations applicable to the $R$ function. Due to this slow converge for high temperatures we frequently put $T = 0$ or $T = 1$ [mK] throughout this work.

From Figure 3.7 we observe that the oscillations are independent of the temperature. Other numerical analyses suggest that this remains valid for other physical parameters as well. Instead the temperature appears to be responsible for the relative and absolute amplitudes of the oscillations which were studied in the previous section. In particular, higher temperatures cause an exponential suppression of the function as was found in Section 3.7.4. Lower temperature increases the visibility of the interference signal.
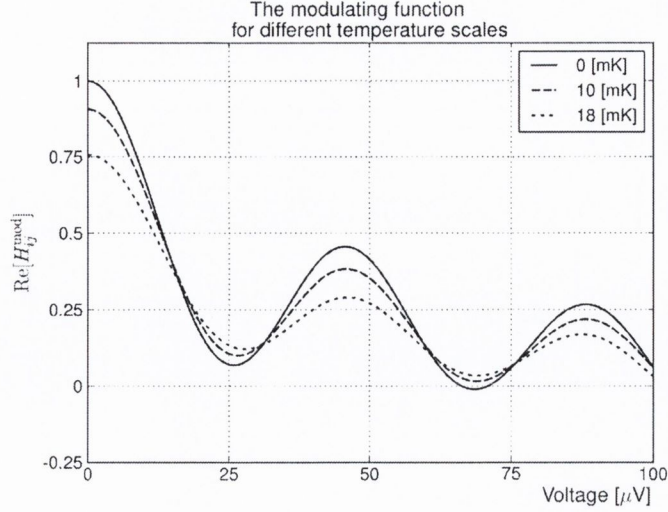
**Figure 3.7:** The modulating function at three different temperatures, keeping all other parameters fixed. The tunnelling quasiparticle is the $e/4$ quasiparticle of the Pfaffian state with $g_c = g_n = \frac{1}{8}$. The remaining parameters are $v_c = 9 \cdot 10^4$ [m/s], $v_n = 9 \cdot 10^3$ [m/s], $a = 3.5$ [$\mu$m] and $b = 3.5$ [$\mu$m].

The experiments are typically performed at temperatures of $T = 25$ [mK] or lower. Numerically, we have not been able to reach temperatures higher than $T = 20$ [mK]. We expect that the behaviour of the modulating function as predicted by our results remains valid in this regime. In particular we expect that the frequencies of the oscillations (3.92) and (3.93) are independent of the temperature, although we have not proven this analytically.

### 3.8.5  $\nu = 5/2$ **state**



Modulating function for $\nu = 5/2$ candidates
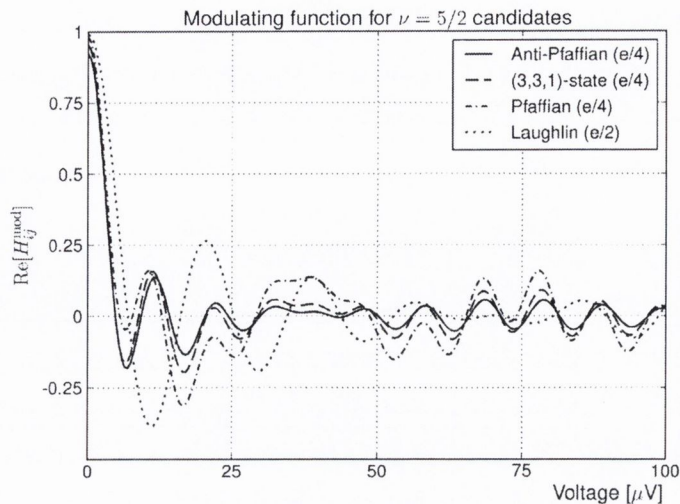
| Model | $Qe$ | $g_c$ | $g_n$ | $g$ | $\eta$ |
|-------|------|-------|-------|-----|--------|
| MR | $e/4$ | $\frac{1}{8}$ | $\frac{1}{8}$ | $\frac{1}{4}$ | $+$ |
| APF | $e/4$ | $\frac{1}{8}$ | $\frac{3}{8}$ | $\frac{1}{2}$ | $-$ |
| (331) | $e/4$ | $\frac{1}{8}$ | $\frac{1}{4}$ | $\frac{3}{8}$ | $+$ |
| L$_{1/2}$ | $e/2$ | $\frac{1}{2}$ | $0$ | $\frac{1}{2}$ | |

**Table 3.1**

**Figure 3.8:** The modulating function of four candidate states for the $\nu = 5/2$ state. The proposed states and corresponding quasiparticles are listed in table 3.1 with L$_{1/3}$ standing for the Laughlin quasiparticle. Data obtained from Ref. [17]. The $e/2$ Laughlin quasiparticle is present in all three states. The parameters used for this plot are $v_c = 5 \cdot 10^3$ [m/s], $v_n = 1.4 \cdot 10^3$ [m/s], $T = 1$ [mK], $a = 2.4$ [$\mu$m] and $b = 2.1$ [$\mu$m].

The most prominent state for which the corresponding topological phase is conjectured to be non-Abelian is the $\nu = 5/2$ state [226, 174]. In table 3.1 we list some of the proposed edge states for the $\nu = \frac{5}{2}$ state and their quasiparticle properties. The edge states we consider are the Moore-Read state [162, 99] also known as the Pfaffian, its particle-hole conjugate the Anti-Pfaffian [148, 151] and the (331)-state [105]. See also Ref. [17]. Of these the (331)-state is an Abelian theory. The proposed edge theories consist in all cases of a decoupled neutral and charged channel as described in Section 3.2. In the case of the Anti-Pfaffian the neutral and charged channels have opposite chiralities. All of these edge theories predict a charge of $Qe = e/4$ associated with the quasiparticle with the lowest algebraic decay. Furthermore, the quasiparticle with second-smallest algebraic decay is for all cases a Laughlin-type anyon with a charge of $e^* = e/2$ and algebraic decays of $g_c = 1/2$ and $g_n = 0$. Figure 3.8 is a plot of the corresponding modulating functions for the different edge theories, including the $e/2$ quasiparticles.

As we mentioned before, in the language of the renormalization group the most relevant tunnelling operator correspond to quasiparticles with the lowest algebraic decay. In the case of the Anti-Pfaffian the lowest algebraic decay is given by $\frac{1}{2}$ and it corresponds to two quasiparticles, the $e/4$ and $e/2$ anyon. In this case we also need to take into account that quasiparticles

with a smaller charge have a larger magnetic length, and therefore a larger bare tunnelling amplitude. So also in the case of the Anti-Pfaffian it is expected that the interference current is due to tunnelling of the $e/4$ quasiparticle.

### 3.8.6 $\nu = 7/3$ **state**



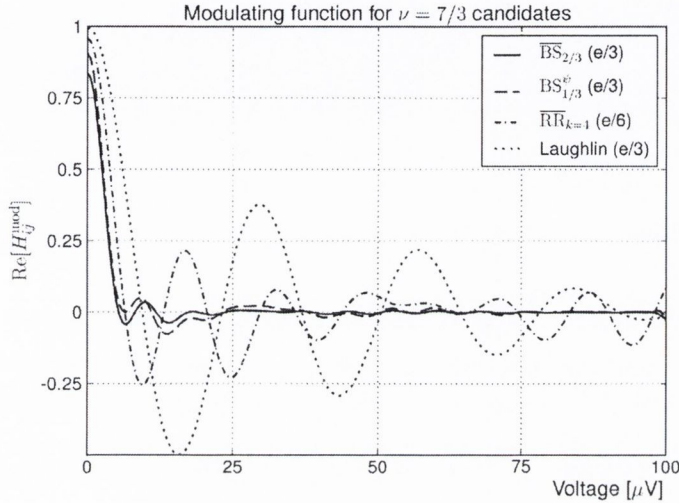| Model | $Qe$ | $g_c$ | $g_n$ | $g$ | $\eta$ |
|---|---|---|---|---|---|
| $\overline{\text{BS}}_{2/3}$ | $e/3$ | $\frac{1}{3}$ | $\frac{5}{8}$ | $\frac{23}{24}$ | $-$ |
| $\text{BS}^{\psi}_{1/3}$ | $e/3$ | $\frac{1}{3}$ | $\frac{3}{8}$ | $\frac{17}{24}$ | $+$ |
| $\overline{\text{RR}}_{k=4}$ | $e/6$ | $\frac{1}{12}$ | $\frac{1}{4}$ | $\frac{1}{3}$ | $-$ |
| $\text{L}_{1/3}$ | $e/3$ | $\frac{1}{3}$ | $0$ | $\frac{1}{3}$ | |

**Table 3.2**

**Figure 3.9:** The modulating function of four candidate states for the $\nu = 7/3$ state. The proposed states and corresponding quasiparticles are listed in table 3.2 with $\text{L}_{1/3}$ representing the Laughlin quasiparticle. Data obtained from Ref. [17]. The $e/3$ Laughlin quasiparticle is present in the Laughlin $\nu = 2 + 1/3$ state and all other non-Abelian states. The parameters used for this plot are $v_c = 5 \cdot 10^3$ [m/s], $v_n = 1.4 \cdot 10^3$ [m/s], $T = 1$ [mK], $a = 2.4$ [$\mu$m] and $b = 2.1$ [$\mu$m].

The next state we look at is the $\nu = 7/3$ plateau [226, 174]. The trial states and the corresponding quasiparticles with lowest algebraic decay are listed in table 3.2. These trial states are the Abelian Laughlin [145] state at $\nu = 2 + 1/3$, the particle-hole conjugate of the Read-Rezayi [184] state at $k = 4$, and two Bonderson-Slingerland states [26]. The BS states are formed through a hierarchical construction of a non-Abelian candidate state, in this case the Pfaffian and Anti-Pfaffian state. Figure 3.9 shows the modulating function for the proposed states.

In addition to plotting the tunnelling current for a number trial states, Figures 3.8 and 3.9 show the effect of different values of $g_n$ and $g_c$ on the $R$ function. The general rule is that a larger value of $g_i$ corresponds to a larger damping on the contributing frequency. In particular, a larger sum of $g_n + g_c$ corresponds to an $R$ function which decays more rapidly for increasing $V$.

### 3.8.7 $\nu = 12/5$ state



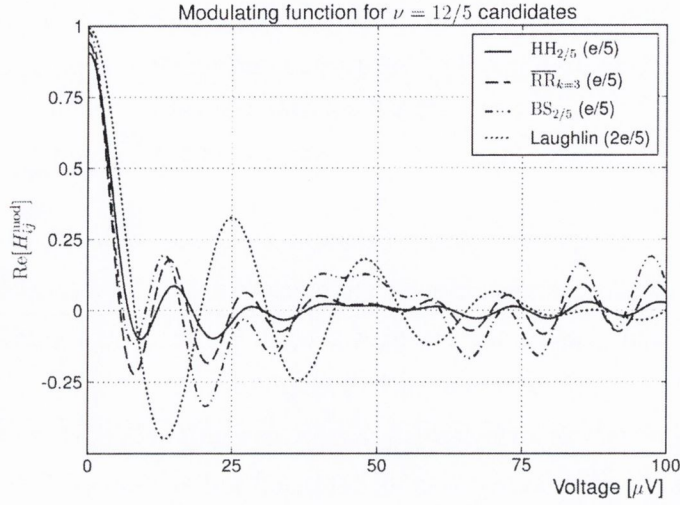| Model | $Qe$ | $g_c$ | $g_n$ | $g$ | $\eta$ |
|---|---|---|---|---|---|
| $\mathrm{HH}_{2/5}$ | e/5 | $\frac{1}{5}$ | $\frac{2}{5}$ | $\frac{3}{5}$ | $+$ |
| $\overline{\mathrm{RR}}_{k=3}$ | e/5 | $\frac{1}{10}$ | $\frac{3}{10}$ | $\frac{2}{5}$ | $-$ |
| $\mathrm{BS}_{2/5}$ | e/5 | $\frac{1}{10}$ | $\frac{1}{8}$ | $\frac{9}{40}$ | $+$ |
| $\mathrm{L}_{2/5}$ | 2e/5 | $\frac{2}{5}$ | $0$ | $\frac{2}{5}$ | |

Table 3.3

**Figure 3.10:** The modulating function of four candidate states for the $\nu = 12/5$ state. The proposed states and corresponding quasiparticles are listed in table 3.3 with $\mathrm{L}_{1/3}$ standing for the Laughlin quasiparticle. Data obtained from Ref. [17]. The $2e/5$ Laughlin quasiparticle is present in all the listed states. The parameters used for this plot are $v_c = 5 \cdot 10^3$ [m/s], $v_n = 1.4 \cdot 10^3$ [m/s], $T = 1$ [mK], $a = 2.4$ [$\mu$m] and $b = 2.1$ [$\mu$m].

The last plateau we discuss is [234] at $\nu = 12/5$. There are numerical studies [186, 197, 23] each of which suggest a different quantum Hall trial state for the $\nu = 12/5$ plateau. The edge states we discuss here are the particle-hole conjugate of the Read-Rezayi state [184, 186] at $k = 3$, a Haldane-Halperin edge [102, 107, 197], and a Bonderson-Slingerland state [26, 23]. The corresponding quasiparticles with lowest algebraic decay are listed in table 3.3. The modulating functions for these states are plotted in 3.10.

From the plots on the $\nu = 5/2$, $\nu = 7/3$ and $\nu = 12/5$ we find empirically that the parameters $g_i$ control the amplitudes of the different oscillations present in the $R$ function. These are the oscillations discussed in Section 3.8.3. We find that a larger $g_i$ causes a relatively smaller amplitude of the corresponding oscillation. This empirical rule is supported by the discussion on dephasing in Section 3.7.4. Here it was found that for a typical length or temperature scale the $R$ function is exponentially suppressed as a function of increasing temperature or increasing circumference of the interferometer. These scales are partially determined by $\left[\sum_i \frac{g_i}{v_i}\right]^{-1}$. Here we find empirically that also the relative amplitude of each oscillation is inversely related to the corresponding algebraic decay.

## 3.9 The Aharonov-Bohm effect and the interference current

### 3.9.1 The Aharanov-Bohm phase revisited

The AB-phase is determined by the magnetic field strength $B$, the area of the interferometer and the quasiparticle charge. The phase is given by

$$e^{i\Phi/\Phi_Q}, \qquad \text{where} \quad \begin{cases} \Phi = 2\pi B \times \text{Area} \\ \Phi_Q = \frac{h}{Qe} \end{cases} . \tag{3.94}$$

Here $\Phi$ is $2\pi$ times the total number of flux quanta through the interferometer and $\Phi_Q$ is a unit flux quantum for a quasiparticle with charge $Qe$. So far the appearance of the AB phase has been rather ad-hoc. Here we examine its origin in more detail.

Consider the tunnelling operators $\mathcal{V}$. These operators tunnel a quasiparticle from the lower to the upper edge. It picks up an AB phase determined by the line integral along the tunnelling path $e^{iQe \int A \cdot dl}$. If we include this phase explicitly then the tunnelling Hamiltonian is given by

$$H_T = \sum_i \Gamma_i e^{iQe \int_i A \cdot dl} \mathcal{V}(x_i, y_i) + \Gamma_i e^{-iQe \int_i A \cdot dl} \mathcal{V}^\dagger(x_i, y_i) \tag{3.95}$$

where $\int_i dl$ integrates along a path from the lower to the upper edge along the $i$'th point contact.

In addition, the quasiparticle propagators $\langle \psi^\dagger \psi \rangle$ also pick up an AB phase. This is explicitly determined in Section 2.7.4. The final result for the two-point propagator is Eq. (2.148) and it includes the phase factors $e^{-i\sqrt{\nu}\alpha U(t-t')} e^{-i\sqrt{\nu}\alpha \int_{x_i}^{x_j} a_x(y)dy}$. The first is the Josephson frequency $e^{i\omega_Q t}$, whereas the second is a line integral from the $i$'th to the $j$'th point contact along either the upper or lower edge. Since the interference current is determined by the product of two-point propagators of the lower and upper edge we end up with a total phase factor of

$$e^{iQe \oint_{\gamma_{ij}} A \cdot dl} . \tag{3.96}$$

This includes the phase coming from the tunnelling Hamiltonian (3.95). The line integral is along a closed contour which encircles the area between the $i$'th and $j$'th point contact. This is precisely the AB phase factor $e^{i\Phi/\Phi_Q}$.

### 3.9.2 Weak tunnelling and the AB phase

The expression for the AB phase applies only in the weak tunnelling limit, where quasiparticles with the smallest algebraic decay are the most relevant operators in the language of the Renormalization Group. In this limit the interferometer is said to be in the Aharonov-Bohm regime and throughout this work we assume this always applies.
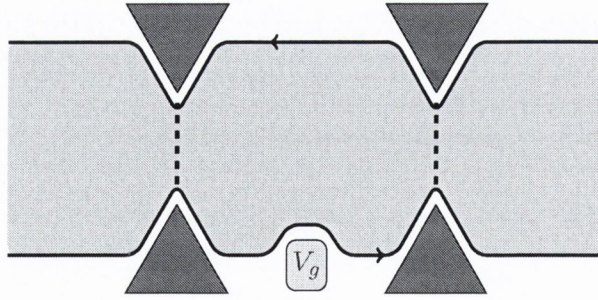
**Figure 3.11:** Idea of the setup of an interferometer with a side gate. By applying a voltage on the side gate the electrons are repelled thereby deforming the edge of the quantum Hall liquid. As a function of the side-gate voltage the effective area of the interferometer and the length of the lower edge grow or shrink. This changes both the AB phase and the $R$ function.

In contrast, in the strong tunnelling limit the tunnelling current effectively pinches off the area within the interferometer, thereby forming a quantum dot. This is called Coulomb blockade [189, 109]. In this limit electrons tunnelling between the quantum dot and the fluid outside the interferometer form the most relevant operators. The AB phase is no longer determined by expression (3.94), see e.g. Ref. [239] for the case of the integer QHE.

### 3.9.3 Manipulating the AB phase through a side gate

The AB phase is manipulated by either varying the magnetic field strength or deforming the effective area of the interferometer. We are interested in the latter case. In practice [1, 228] the area is changed through a side-gate voltage. This setup is depicted in Figure 3.11 with the side-gate voltage given by $V_g$ (not to be confused with the voltage bias between the two edges, $\omega_Q$). By charging the side gate the Coulomb interaction repels electrons inside the interferometer, effectively deforming the area of the quantum Hall fluid. If we ignore the interference effects due to the $R$ function or quasiparticle braiding, then the current shows the following oscillating behaviour due to the AB phase

$$I_B = I_0 + I_{\text{osc}} \times \cos\left(\Phi_{AB}(V_g)/\Phi_Q + \delta\right) \qquad (3.97)$$

$$\Phi_{AB}(V_g) = 2\pi \frac{B}{h/Qe} \times \text{Area}(V_g) .$$

This oscillating signal arises in the weak tunnelling limit. One typically assumes the change in area is linear with respect to the side-gate voltage, meaning $\text{Area}(V_g) \propto V_g$. The Coulomb interaction and localization effects can alter this behaviour and cause small, non-linear fluctuations as a function of the side-gate voltage [109]. This is called the Coulomb dominated regime (not to be confused with Coulomb blockade). In this regime the edge and the area inside the interferometer readjust to keep the dot neutral. Quasiparticles still tunnel along

the point contacts and the interference current is still visible, but the corresponding AB phase does not follow expression (3.97). We assume the interferometer is not Coulomb dominated and the change in area is linear with respect to the side-gate voltage.

Recent experiments [231, 227, 1] observe on the order of $\lesssim 5$ full oscillations when the side-gate voltage is varied. This applies to the $\nu = 5/2$ state, with a magnetic field strength of $B \sim 5.5$ [T]. The area of the interferometer is estimated in the range of 0.1 - 0.4 [$\mu$m$^2$], depending on the exact geometry of the device. For an interferometry area of 0.15 [$\mu$m$^2$] and a quasiparticle with charge $Qe = e/4$ this corresponds to a total of roughly 50 unit flux quanta. If we assume the interferometer is in the AB dominated regime, then a generous estimate of the change in area is about $\leq 10\%$ when five full oscillations are observed.

### 3.9.4 The interference current: combining the AB phase and the $H^{\text{mod}}$ function

When the side-gate is used to change the area of the interferometer, then almost inevitably the length of the edge between the two point contacts changes as well. This change in length causes interference effects through the modulating function $H_{ij}^{\text{mod}}$. Including this in the expression for the interference current gives

$$I_B = I_0 + I_{\text{osc}} \times \text{Re} \left[ e^{i\Phi_{AB}(V_g)/\Phi_Q + i\delta} H_{ij}^{\text{mod}}(\omega_Q; V_g) \right] . \tag{3.98}$$

The function $H_{ij}^{\text{mod}}$ implicitly depends on the side-gate voltage $V_g$ through the length of the lower edge, $a(V_g)$. Whether the change in $H_{ij}^{\text{mod}}$ as a function of $V_g$ is significant is determined by the change in the length of the edge, the velocity of the edge modes and the voltage bias between the two edges $\omega_Q$.

For instance, in the experiment of Ref. [231] the quantum Hall fluid inside the interferometer is cigar-shaped with the ends of the cigar corresponding to the point contacts. We can picture the scenario in which the side-gate voltage deforms the lower edge uniformly, such that a 5% change in the area of the interferometer is accompanied with relatively negligible change in the length of the edge. In this scenario the function $H_{ij}^{\text{mod}}(\omega_Q; V_g)$ is approximately constant as a function of $V_g$.

The other possibility is that the change in $a(V_g)$ is not small. The device used in the experiment of Ref. [1] has a circular shape, and it is possible that the change in edge length is relatively larger than that of Ref. [231]. It then depends on the remaining parameters, the velocity and voltage bias, if the change in $H_{ij}^{\text{mod}}(\omega_Q; V_g)$ is large enough to be observable.

In Figure 3.12 and 3.13 we have plotted these two scenarios. Figure 3.12 is the "weak" case in which the function $H_{ij}^{\text{mod}}$ remains largely constant while $V_g$ is varied. In the lower panel
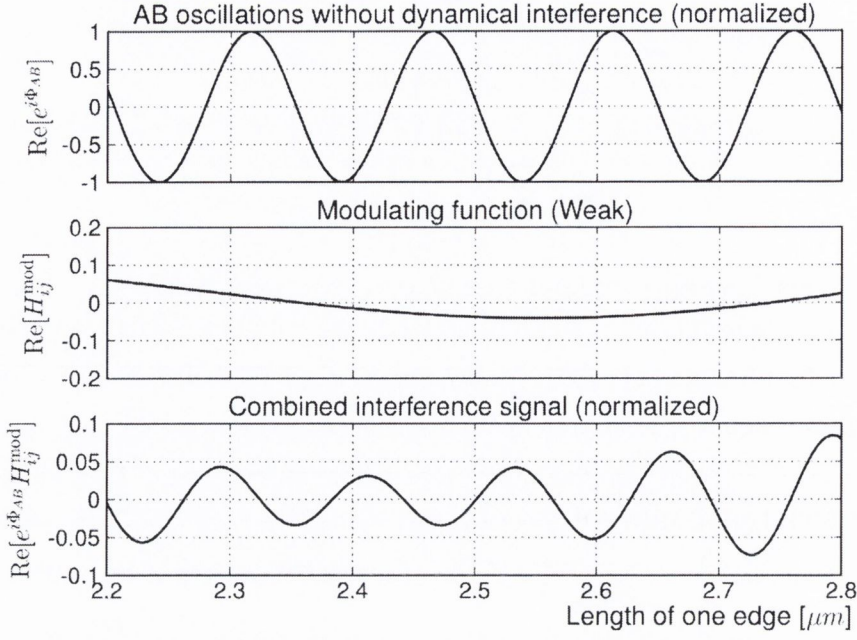
**Figure 3.12:** Plot of estimated AB oscillations as a function of the varying edge length. This variation is caused by the side-gate voltage and we assume a linear relation between the area of the interferometer, the side-gate voltage and the length of the edge. The parameters used are $Q = e/4$, $g_c = \frac{1}{10}$, $g_n = \frac{1}{8}$, $v_c = 8 \cdot 10^3$ [m/s], $v_n = 3 \cdot 10^3$ [m/s], $b = 2.5$ [$\mu$m], $a = 2.25$–$2.75$ [$\mu$m], $V = 50$ [$\mu$V], $T = 0$ [K]. The plot is "weak" in the sense that the modulating function does not change much over the plotted range.

of this figure the function $H_{ij}^{\mathrm{mod}}$ causes a small modulation of the total interference signal. The interference due to a varying edge length is difficult to observe through measurement of this signal. Figure 3.13 shows the "strong" case where the change in $H_{ij}^{\mathrm{mod}}$ is much larger. These plots differ in the values used for the velocities and edge lengths, keeping all other parameters fixed. The frequencies of the oscillations at which $H_{ij}^{\mathrm{mod}}$ varies are given by Eq. (3.93).

### 3.9.5 Frequency analysis of interference current

In plotting the figures 3.12 and 3.13 we assume a linear relation between the area and the side gate voltage, Area $\propto V_g$, and the length of the edge and side-gate voltage, $a(V_g) \propto V_g$. Under this assumption the interference due to the AB effect oscillates at some frequency with respect to the varying edge length $a(V_g)$. We denote this frequency by $\phi_{AB}$,

$$e^{i\Phi/\Phi_Q} = e^{2\pi i\phi_{AB} \cdot a(V_g)} \tag{3.99}$$

In other words, $\phi_{AB}$ corresponds to the frequency of the oscillations appearing in the upper panels of figures 3.12 and 3.13. Fixing the proportionality constant between the change in
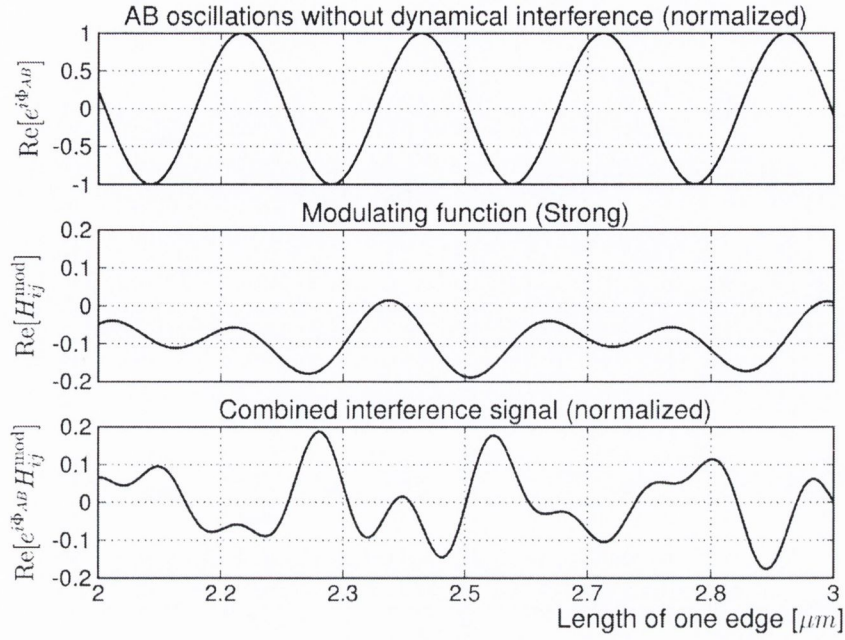
**Figure 3.13:** The same plot as in Figure 3.12, but with different velocities, namely $v_c = 9 \cdot 10^2$ [m/s], $v_n = 6 \cdot 10^2$ [m/s] and the range over which the edge length is varied is larger, $a = 2.0\text{--}3.0$ [$\mu$m]. These slower velocities and larger range lead to a $H_{ij}^{\text{mod}}$ function which varies significantly more than that of Figure 3.12.

area and the change in edge length equal to $C_1$, i.e. $\Delta\text{Area}(V_g) = C_1 \times \Delta a(V_g)$, then $\phi_{AB} = C_1 \times \frac{B}{h/Qe}$. The proportionality constant depends on the exact details of the interferometric device, and the change of both area and edge length is performed through the side-gate voltage $V_g$. The charge of the quasiparticle in the fractional regime can then obtained by looking at the ratio of this frequency compared to that in the integer regime where $Q = 1$,

$$\frac{\phi_{AB}(\nu = \text{fractional})}{\phi_{AB}(\nu = \text{integer})} = Q \tag{3.100}$$

In Figure 3.6 we showed that the as a function of a varying edge length the modulating function $H_{ij}^{\text{mod}}$ oscillates with frequencies $\frac{QeV}{v_i h}$. A similar analysis shows that the combined signal of the AB oscillations and the modulating function oscillates at three frequencies, given by

$$\text{frequency peaks} = \left\{ \phi_{AB}, \phi_{AB} + \frac{QeV}{v_n h}, \phi_{AB} + \frac{QeV}{v_c h} \right\}. \tag{3.101}$$

These frequencies correspond to the signals appearing in the lower panels of figures 3.12 and 3.13. In particular the "pure" AB oscillations corresponding to $\phi_{AB}$ remain present and the quasiparticle charge can be measured through formula (3.100) even if the oscillations in $H_{ij}^{\text{mod}}$ are strong. The shifted peaks $\phi_{AB} + \frac{QeV}{v_i h}$ provide an experimental probe of the velocity
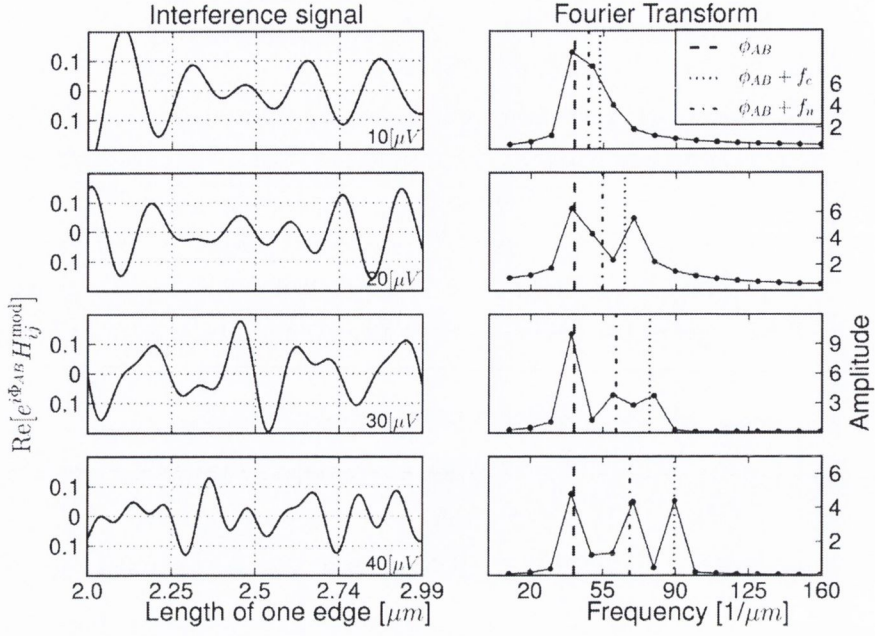
**Figure 3.14:** The four figures on the left plot the interference current $\mathrm{Re}[e^{i\phi_{AB}\cdot a}H_{ij}^{\mathrm{mod}}]$ as a function of varying the edge length $a = [2.0 - 3.0]$ $[\mu\mathrm{m}]$ for an applied voltage bias of $V_{\mathrm{bias}} = 10, 20, 30$ and $40$ $[\mu\mathrm{V}]$. The voltage bias $V_{\mathrm{bias}}$ should not be confused with the side-gate voltage. The figures on the right are the corresponding Fourier transforms. The peaks correspond to Eq. (3.101). The remaining parameters are $g_c = g_n = 1/8$, $T = 0$ [K], $Qe = e/$, $b = 2.5$ $[\mu\mathrm{m}]$, $v_n = 5 \cdot 10^2$ [m/s], $v_c = 9 \cdot 10^2$ [m/s]. Finally, $\phi_{AB} = C_1 \times \frac{B}{\hbar/Qe} = 4.11$ $[\mu\mathrm{m}^{-1}]$ with $C_1 = 1.0 \cdot 10^{-2}$ $[\mu\mathrm{m}]$ and $B = 6.8$ [T].

of the edge modes. Numerical estimates [118] indicate that $v_c > v_n$, meaning the largest frequency corresponds to the velocity of the neutral mode.

If the terms $\frac{QeV}{v_i h}$ in (3.101) are small compared to $\phi_{AB}$, then the frequency peaks overlap in a Fourier analysis and become indiscernible. To enhance the visibility of the different peaks we can either reduce $\phi_{AB}$, increase the range over which the edge length is changed or increase $\frac{QeV}{v_i h}$. The frequency $\phi_{AB}$ and the variation in edge length are both determined by the geometric properties of the interferometric device and the side-gate voltage.

Increasing $\frac{QeV}{v_i h}$ can be accomplished by injecting a larger current into the system which is equivalent to increasing the voltage bias $\omega_Q$. The effect of a larger current on the frequency spectrum is demonstrated in Figure (3.14), where the applied voltage bias is increased from 10 $[\mu\mathrm{V}]$ to 40 $[\mu\mathrm{V}]$ in steps of 10 $[\mu\mathrm{V}]$, while keeping all other parameters fixed. For a voltage bias of 10 $[\mu\mathrm{V}]$ the frequency peaks merge and are indistinguishable. This is due to the relative magnitude of $\frac{QeV}{v_i h}$ and $\phi_{AB}$. At a voltage bias of 40 $[\mu\mathrm{V}]$ three frequency peaks emerge corresponding to the frequencies (3.101).

## 3.10 Summary

We have calculated the tunnelling current through a Fabry-Pérot fractional quantum Hall interferometer in linear response theory for a broad class of edge theories. Our main result is an expression for the tunnelling current in terms of Carlson's $R$ function at finite temperatures and in terms of the confluent Lauricella hypergeometric function at zero temperature. This expression arises as the tunnelling current is related to the Fourier transform of the quasiparticle propagators. In the conformal limit these propagators have a universal form, which is the reason behind the generality of our result.

Our result applies to both Abelian and non-Abelian edge theories with an arbitrary number of edge modes – the neutral and charged degrees of freedom – each of which is characterized by its own edge velocity and chirality. In addition our result is applicable to interferometers with different edge lengths between the point contacts and our result can be straightforwardly extended to include more than two point contacts as explained in Section 3.4.

We have implemented a numerical scheme to calculate Carlson's $R$ function and the confluent Lauricella hypergeometric function, and the corresponding interference current using a series representation. This numerical scheme is written in NumPy and Fortran and publicly available [196]. We have also made available the code that reproduce the plots in this work.

The interference in the tunnelling current is attributed to the Aharonov-Bohm phase, the dynamical interference induced by the voltage bias between the edges and the statistical properties of the quasiparticles. Recent experiments [231, 1] measure the Aharonov-Bohm phase by deforming the area inside the interferometer through a plunger gate. This setup also changes the edge length between the point contacts which induces interference effects through the dynamical interference. We show that the total interference results in oscillations in the tunnelling current as a function of the edge length. We have determined the frequency of these oscillations in terms of the edge velocities and the source-drain voltage, i.e. Eq. (3.101). These frequencies can be used to measure the edge velocities.

The visibility of the frequency peaks depends among other things on the geometry of the interferometer and the range over which the length of the edge is varied. If there are many AB oscillations, while the change in edge length is small then the dynamical interference effects are hardly discernible from the AB oscillations. It is possible that the change in edge length of current interferometric devices is negligible and the interference effects we describe are indeed not measurable. In this case our proposed experiment requires an alteration of the interferometer, using for instance a different geometry.

Another way to increase the visibility of the frequency peaks is to increase the strength of

the injected current. The frequencies are directly proportional to the source-drain voltage bias. The frequency of the AB oscillations is independent of the source-drain voltage, while the frequencies of the oscillations due to dynamical interference increase with larger source-drain voltages.

Alternatively, this dependency can be used to check if the dynamical oscillations play a role in experiments which focus on the AB interference. If the effect of dynamical oscillations play a role in experiments which measure AB oscillations, then our results predict that this becomes apparent by running the experiment multiple times at different source-drain voltages.

# Chapter 4

# Non-equilibrium noise in a point contact

---

This chapter is based on and overlaps with the pre-print:

O. Smits, J. K. Slingerland, S. H. Simon, *Non-equilibrium noise in the (non-)Abelian fractional quantum Hall effect*. ArXiv e-prints `arXiv:1401.4581`

## 4.1 Introduction

In the previous chapter we analysed the linear response theory of a fractional quantum Hall interferometer. Our main result is a general expression for the tunnelling current and we provided an analysis of interference due to dynamical effects. In this Chapter we (1) consider a simpler setup that consists of a single tunnelling point contact and (2) analyse non-perturbative aspects of transport properties of the system. In particular we look at the noise generated by the tunnelling and edge currents of a fractional quantum Hall point contact, and our main result is a non-equilibrium fluctuation-dissipation theorem.

The tunnelling current through a point contact probes the edge theory and underlying topological order of the fractional quantum Hall plateau. The tunnelling is a stochastic process, and the tunnelling is a time-averaged measure of these processes. The intrinsic randomness of the current is characterized by the fluctuations around the mean. This is called, somewhat unfortunately, the noise of the signal. It is unfortunate, because the fluctuations around the mean explore the state space of the system and is therefore sensitive to e.g. the electric charge and statistics of the tunnelling anyon. The noise is therefore another important probe of the edge theory and the topological order [20, 157, 48].

The expression for the noise and in particular its relation to the tunnelling current (or, equivalently, the transmission) has been studied perturbatively for general and specific quantum Hall states [131, 41, 42, 44, 157, 9, 10, 192, 77, 36, 120]. For special cases such as the integer quantum Hall effect [143, 30, 158] and the Laughlin series [72, 74, 206] there are

---
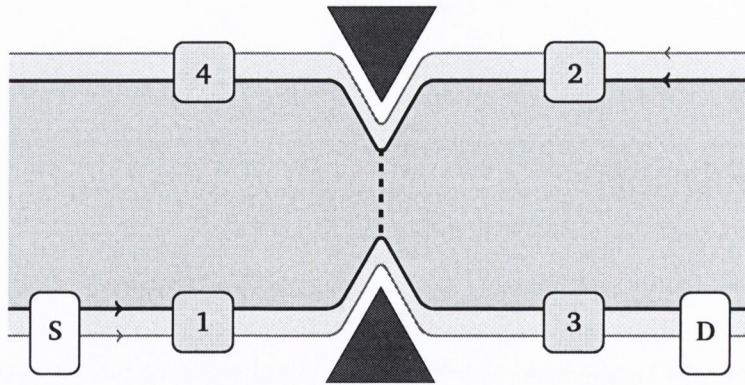
**Figure 4.1:** Sketch of a point contact. A current is injected at the source (S), flows along the edge and is collected by the drain (D). At the point contact quasiparticles tunnel between the edges and a backscattering current forms flowing from the lower to the upper edge. The probes 1 through 4 can be used to measure the local edge current and the corresponding noise.

also non-perturbative results. The simplest example of a perturbative approach is the Schottky relation [194], which arises in the low temperature and weak tunnelling limit. It relates the shot noise and tunnelling current through $S_{I_B}(0) = e^* I_B$ which can be used to measure the quasiparticle charge. However, a universal expression relating the noise and the current non-perturbatively is still an open question.

Experiments that measure shot noise [193, 55, 95, 187, 94, 100, 114, 49, 46, 47, 115, 116, 64, 45, 13, 60, 62, 61, 63] do not actually measure the noise in the tunnelling current directly, but instead look at the noise in the outgoing edge currents. To clarify, consider Figure 4.1 which shows a schematic of the experimental setup of a tunnelling point contact. A current is injected at the source (S). It flows along the edge and is partially reflected at the point contact. The dotted line represents the tunnelling current. This tunnelling current $I_B$ and the corresponding noise $S_{I_B}$ are not measured directly, but instead end up in the outgoing branches of the edge currents. A probe located at position 3 or 4 then measures the local edge current and corresponding fluctuations (this probe can also be incorporated with the drain – here we use a simplistic picture).

This setup then begs the question: how is the noise at, say, probe number 3 related to the noise in the tunnelling current? In this work we derive such a relation based on general grounds: the conservation of electric charge combined with the chiral structure of the edge. Any charge tunnelling from the upper to the lower edge will end up at probe number 3 due to the chiral structure. In this work we study the *non-perturbative* expression relating the noise in the outgoing current to the noise in the tunnelling current. This question has been studied several times before, both non-perturbatively [30, 131, 72, 10, 211] and perturbatively

[42, 210, 120].

We will give a summary of our approach and our results in the next section. What is important to keep in mind is that the expression which relates the noise in the edge current to the noise in the tunnelling current is *not* linear. The fluctuations of the tunnelling current do not simply add to the fluctuations in the edge current. The relation between the noise in the edge current and the noise in the tunnelling current is also known as a *non-equilibrium fluctuation-dissipation theorem*.

Where does the term "non-equilibrium fluctuation-dissipation theorem" come from? First, there is a close relation of a fractional quantum Hall point contact system to quantum dissipative systems [133], such as the Caldeira-Leggett model [31]. Second, the theorem resembles the form of the fluctuation-dissipation theorem for equilibrium systems [180]. Finally, the theorem is an expression in terms of symmetric and anti-symmetric combinations of certain two-point correlators. For equilibrium systems in general such symmetric and anti-symmetric combinations are related to the dissipative properties and (auto-)correlations of the system.

### 4.1.1 Summary and overview of this chapter

Let us present an intuitive picture of the derivation in this Chapter which relates the noise in the outgoing edge current to the noise in the tunnelling current. We start with the simplified Figure 4.2. A current is injected at $S$ into the lower edge carried by the (right moving) edge current $j_R$. This chiral current is partially reflected by the point contact, where a tunnelling current $I_B$ tunnels to the upper edge and ends up in the left moving edge current. On the basis of charge conservation the edge current that is measured by probe 3 equals

$$j_3 = j_R - I_B . \tag{4.1}$$

Suppose we now measure the noise of the edge current at probe 3. This noise is roughly given by the square of the operator or

$$S_3 \sim (j_R - I_B)^2 = j_R^2 + I_B^2 - (j_R I_B + I_B j_R)$$

$$\sim S_{\text{bg}} + S_{I_B} - \Delta S . \tag{4.2}$$

In the second line we identify $I_B^2$ with the noise in the tunnelling current $S_{I_B}$ and $S_{\text{bg}}$ a type of background noise (the noise of the edge current in the absence of a point contact). There also appears a third term $\Delta S$, which represents the coupling of the tunnelling current with the equilibrium edge current. This extra term quantifies the "backreaction" and shows that the noise of the tunnelling does not add linearly to the noise in the edge current.

In this work we reproduce this argument *at the operator level to all orders of perturbation theory*, which is also what distinguishes our approach from previous work [131, 10, 210]. We
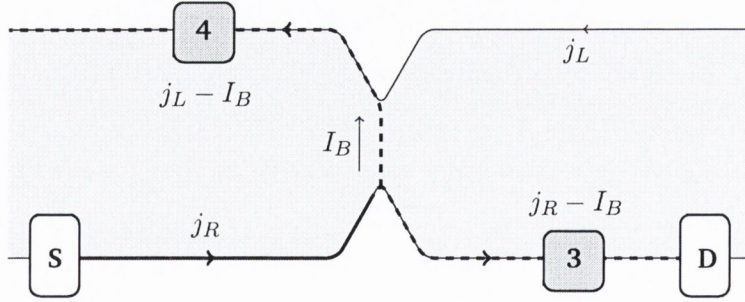
**Figure 4.2:** Sketch of a point contact. An edge current $j_R$ is injected at the source $S$, and is partially reflected by the point contact resulting in a tunnelling current $I_B$. The edge current after the point contact is therefore $j_R - I_B$ (on the basis of charge conservation and the chiral structure of the edge). The noise measured at probe 3 corresponds to Eq. (4.2). In this work this relations are derived at the operator level.

analyse the non-symmetrized noise in the outgoing edge current $S_3$ for generic quantum Hall systems. For that we use two new tools which we have developed in this work. The first is the *non-equilibrium Kubo formula*. This NE-Kubo formula formally extends the expression for linear response theory to all orders of perturbation theory, and from it we obtain the current equation (Kirchoff's law) Eq. (4.1) at the operator level. Using the same logic we obtain a formula of the form Eq. (4.2).

The second tool we develop is a *non-equilibrium Ward identity*. A Ward identity is an identity imposed on correlation functions, due to the presence of a symmetry in the theory. In this work the symmetry is associated with charge conservation (and $j_R$ is the associated conserved current), which leads to a well-known equilibrium Ward identity [139]. We have extended this identity to correlation functions evaluated in the non-equilibrium system. The non-equilibrium Ward identity is used to simplify the expression for the correction term $\Delta S \sim (j_R I_B + I_B j_R)$. This results in the anti-symmetrized noise of $I_B$, i.e. this correction term is proportional to $\Delta S \sim (S_{I_B}(\omega) - S_{I_B}(-\omega))$.

The final result is an expression for the noise in the edge current related to the noise in the tunnelling current, see Eq. (4.78). Therefore to compute the noise in the edge current, we only need to determine the expression for the noise in the tunnelling current which is often easier to obtain and for which more work has been performed. Related to this is an expression for the excess noise Eq. (4.82), a non-equilibrium fluctuation-dissipation theorem Eq. (4.89) and an expression for the shot-noise limit Eq. (4.90). Our main work focuses on an edge with a single charged channel (described by a chiral boson) and possibly one or multiple neutral channels. In addition we show how the results extend to quantum Hall edges with multiple charged modes, possibly counter propagating. Finally, we also look at similar expressions for

the noise at the remaining probes of Figure 4.1, and the noise of combinations of these probes (i.e. cross-correlations of different probes). All results are valid to all orders of perturbation theory.

An important simplification that we assume is that away from the point contact the edge is described by a collection of free and decoupled channels, each described by a chiral conformal field theory in the long wavelength limit. Interaction effects and disorder [43, 133], which can for instance cause equilibration of the edge currents after the point contact, are beyond the scope of this work. We also note that this chapter looks at the (non-equilibrium) relation between the noise of the edge currents and the tunnelling current. We do not determine the expression for the noise or its relation to the tunnelling current. We will comment on this in the next Chapter, which treats the linear response theory of the noise and tunnelling current.

In Section 4.2 we recall the structure of a generic quantum Hall edge. We focus on the definition of the edge current operator in the chiral boson model and the non-equal time commutation relations of the theory, and extend this construction to edges with multiple charged channels.

In Section 4.3 we discuss the model of a point contact and in Section 4.4 we summarize the non-equilibrium formalism. This discussion is very similar to that of Chapter 3, although we need to go beyond the linear approximation. In Section 4.5 we discuss the non-equilibrium Kubo formula and in Section 4.6 we apply the NE-Kubo formula to the edge current operator which results in an operator-version of Kirchoff's law.

The main results regarding the noise are obtained in Section 4.7. This makes use of the non-equilibrium Ward identity to simplify the expression for the correction term $\Delta S$. We obtain expressions for the non-symmetrized noise, the excess noise and the shot noise (all of the noise in the edge current) and generalize these expression to the multichannel case. Finally, Section 4.8 discusses expressions for the noise in related quantities. We discuss our findings in the Section 4.9

## 4.2 The edge theory revisited

In this section we discuss the edge theory of a generic fractional quantum Hall state. Before we come to this we emphasize that our main analysis is quite general and does not require all technical details associated with the edge theory. The required input for the treatment on the noise is (1) the edge current operator $j_R$ (2) the quasiparticle operator $\psi^\dagger$ which is used to represent quasiparticle tunnelling, and (3) the non-equal time commutation relations of the edge current and quasiparticle operator, Eq. (4.15). These relations combined with some

basic assumptions, such as translational invariance and chirality, are enough input for our main work which is treated in Section 4.3 and beyond.

The treatment of the edge theory builds upon that of Chapter 3.2, and we refer to this chapter for a more involved treatment. In the long wavelength limit the effective edge theory is a chiral conformal field theory and it comes equipped with a set of quasiparticle operators and fusion rules [213, 85]. The edge contains a $U(1)$ symmetry due to the coupling with the electromagnetic field, which is accounted for by the chiral boson. In this chapter we also consider the possibility of multiple chiral bosons which couple to the electromagnetic field. We assume the quasiparticle operators at the edge obey the following decomposition [85]

$$\mathcal{A}_{\text{edge}} = \mathcal{W}_n \otimes \hat{u}(1) \otimes \cdots \otimes \hat{u}(1) \,. \tag{4.3}$$

Here the $\hat{u}(1)$'s correspond to the different charged channels of the edge. Since we are interested mostly in the properties of the charged channels we describe all neutral degrees of freedom collectively through $\mathcal{W}_n$. We first discuss the case of a single charged channel, and expand this to the multichannel case at the end of this section.

### 4.2.1 The charged and neutral channels in the absence of tunnelling

We consider the chiral boson [81, 213] from Chapter 2 coupled to a DC voltage bias. We do not consider a perturbed magnetic field. The action is given by

$$S_R = \frac{1}{4\pi} \int_{\Sigma_R} \left[ -\eta_R \partial_t \varphi_R \partial_x \varphi_R - v_c (\partial_x \varphi_R)^2 \right] dt dx + \frac{\sqrt{\nu}}{2\pi} U_R \int_{\Sigma_R} [\partial_x \varphi_R] dt dx \,. \tag{4.4}$$

Throughout this work we mostly focus on a single right moving chiral boson defined on the lower edge $\Sigma_R$ with velocity $v_c$ and coupled to the potential $U_R$. The chirality $\eta_R = 1$ is written explicitly, such that we can easily switch to a left moving boson by replacing $R \rightarrow L$ (and $\eta_L = -1$). The quantization [81] is performed in Chapter 2.5 and results in

$$[\varphi_R(x), \varphi_R(x')] = i\eta_R \pi \text{sgn}(x - x') \tag{4.5}$$

with $\text{sgn}(x) = +1, 0, 1$ for the regions $x > 0$, $x = 0$ and $x < 0$. Using the equations of motion $(-\eta_R \partial_t - v_c \partial_x)\varphi_R = -\sqrt{\nu} U_R$ we can extend the commutation relations to non-equal time (see Chapter 2)

$$[\varphi_R(x, t), \varphi_R(0, 0)] = i\eta_R \pi \text{sgn}(x - \eta_R v_c t)$$

$$[\partial_x \varphi_R(x, t), \varphi_R(0, 0)] = i\eta_R 2\pi \delta(x - \eta_R v_c t)) \,. \tag{4.6}$$

The left and right moving bosons commute. The dependency on the combination $x \pm v_c t$ reflects the chiral nature of the system and we assume the system is translational invariant.

The non-equal time commutation relations play an important role in the derivation of the NE-FDT. The charge density and total charge operators along the edge are identified with the operator

$$\rho_R(x) = \frac{\sqrt{\nu}}{2\pi}\partial_x\varphi_R(x) . \qquad\qquad \mathcal{Q}_R = \frac{\sqrt{\nu}}{2\pi}\int_{\Sigma_R}\partial_x\varphi_R(x)\,dx . \qquad (4.7)$$

The neutral channel describes edge degrees of freedom which do not couple to the external voltage bias. In this work we are primarily interested in properties of the electric edge current. This current completely decouples from the neutral channel. So although the neutral channel plays an import role in specifying the topological we do not specify its exact nature and only demand that the decomposition (4.3) holds.

The neutral channel is described in the long wavelength limit by some chiral CFT which comes equipped with a consistent set of fusion rules [163, 178], a neutral velocity $v_n$ and some Hamiltonian $H_n$. A general quasiparticle operator is of the form

$$\psi_R^\dagger(x,t) \propto \sigma_R(x,t)\, e^{-i\eta_R\frac{Q}{\sqrt{\nu}}\varphi_R(x,t)} . \qquad (4.8)$$

It has a charge $Q$ (we work in units of $e = 1$) and conformal dimensions $h_n$ and $h_c$ corresponding to the neutral and charged part. In particular, $h_c = \frac{Q^2}{2\nu}$ and $h = h_n + h_c$ is the total conformal dimension. In addition there exists a conjugate operator $\psi(x,t) = \bar{\sigma}_R(x,t)\, e^{i\eta_R\frac{Q}{\sqrt{\nu}}\varphi_R(x,t)}$ with charge $-Q$, where the fusion product of $\bar{\sigma}_R$ and $\sigma_R$ contains the identity channel (see Chapter 3.2).

The total edge Hamiltonian is constructed using the Hamiltonians $H_{0,c}$ and $H_{0,n}$ of the neutral and charged channels, and the electric charge operators. The grand canonical Hamiltonian $K_0$ of the total system is given by

$$K_0 = H_{0,c} + H_{0,n} - U_R\mathcal{Q}_R - U_L\mathcal{Q}_L \qquad (4.9)$$

The combination $H_{0,c,R} - U_R\mathcal{Q}_R$ follows from the action Eq. (4.4), and we set $H_{0,c} = H_{0,c,L} + H_{0,c,R}$. Eq. (4.9) is of the form of a grand canonical Hamiltonian $K_0 = H_0 - \mu\hat{N}$, with $\mathcal{Q}$ a generalization of the number operator $\hat{N}$. Although the edges are held at different chemical potentials we still refer to this system and the corresponding Hamiltonian as the equilibrium system. When we include the point contact we refer to the system as out of equilibrium.

### 4.2.2 Edge current operator

The main object under investigation in this Chapter is the edge current operator. This operator is derived in Chapter 2.3.4 using the complete bulk plus edge theory, see also Ref. [132]. It was found that the edge current operator is given by

$$j_R(x) = -\frac{\sqrt{\nu}}{2\pi}\partial_t\varphi_R(x) . \qquad (4.10)$$

Together with the charge density operator Eq. (4.7) it satisfies the continuity equation $\partial_t \rho_R(x) + \partial_x j_R(x) = 0$. Using the equations of motion we have the alternative form in terms of the charge density operator

$$j_R(x) = \eta_R v_c \rho_R(x) - \eta_R \frac{\nu}{2\pi} U_R \qquad (4.11)$$

Here we recall that by replacing $R \to L$ we obtain the left moving chiral boson. The total current running through the system is given by

$$\hat{I}_0(x) = j_R(x) + j_L(x) . \qquad (4.12)$$

We have defined the vacuum such that it is charge neutral. This implies the vanishing of the one-point correlator $\langle \rho_R(x) \rangle = \langle \partial_x \varphi_R(x) \rangle = 0$ and we find for the current densities on the edge

$$\langle j_R(x, t) \rangle = -\eta_R \frac{\nu}{2\pi} U_R \qquad (4.13)$$

This one-point correlator is also treated in Chapter 2.7. The expectation values are with respect to the equilibrium Hamiltonian at finite temperature, i.e. $\langle \cdots \rangle = \text{Tr}\left[e^{-\beta K_0} \cdots \right]$. For the total current we obtain the familiar Hall relation between voltage and current in the absence of backscattering

$$I_{\max} = \langle \hat{I}_0 \rangle = \langle j_L \rangle + \langle j_R \rangle = \frac{\nu}{2\pi}(U_L - U_R) . \qquad (4.14)$$

in units where $\hbar = e = 1$. Throughout this work $I_{\max}$ is called the equilibrium current which refers to the current running through the system in the absence of tunnelling between edges. We define $V_{\text{SD}} = U_L - U_R$ as the source-drain voltage. Finally, there is also the commutation relation between the edge current and the quasiparticle operator at non-equal times. Using Eq. (4.6) we obtain

$$[j_R(x, t), \psi_R^\dagger(0, 0)] = \eta_R v_c Q \psi_R^\dagger(0, 0) \delta(x - \eta_R v_c t) . \qquad (4.15)$$

### 4.2.3 Generalization to multiple charged channels

The single chiral boson model is only sufficient to explain the Laughlin series at filling fraction $\nu = 1/(2M + 1)$ with $M$ a positive integer. This construction can be extended through use of neutral channels, which allows for a diverse range of filling fractions. An alternative method is to consider multiple copies of chiral bosons, each of which couples to the electromagnetic field. Both constructions are needed to account for the wide variety of observed filling fractions.

We follow here the treatment of Ref. [153] and Ref. [217]. We assume the bosons are decoupled from each other. The action of the right moving edge is given by

$$S_R = \frac{1}{4\pi} \sum_i \int_{\Sigma_R} \left[ -\eta_i \partial_t \varphi_i \partial_x \varphi_i - v_i (\partial_x \varphi_i)^2 \right] dt dx + \frac{1}{4\pi} U_R \sum_i \kappa_i \int \partial_x \varphi_i \, dt dx . \qquad (4.16)$$

Each chiral boson $\varphi_i$ has its own edge velocity $v_i$, a chirality $\eta_i$ and a coupling parameter $\kappa_i > 0$. The index $i$ refers to the $i$'th chiral boson of the right-moving edge. The left moving edge consists of a similar set of bosons, but with opposite chiralities i.e. $\eta_i^L = -\eta_i^R$, etc. We will always work with the right moving current unless explicitly stated otherwise. It is possible to have $\kappa_i = 0$, which corresponds to a chiral boson which does not couple to the electromagnetic field. Such a boson already falls into the category of neutral channels, so we assume $\kappa_i > 0$.

It is possible to formulate the edge theory in terms of coupled chiral bosons, which is usually done through use of a $K$-matrix [215, 219]. Starting from this formulation we can always switch to a different basis of fields through a linear transformation, which results in an action of the form Eq. (4.16). Therefore there is no loss of generality by assuming decoupled chiral bosons.

For each boson we have the equation of motion

$$(-\eta_i \partial_t - v_c \partial_x) \varphi_i = -\kappa_i U_R . \qquad (4.17)$$

Since the channels are decoupled we can apply the same argument as before to obtain the edge current operator for each channel separately. The charge density, its corresponding conserved charge and the edge current density operator of the $i$'th channel are

$$\rho_i = \frac{\kappa_i}{2\pi} \partial_x \varphi_i , \qquad Q_i = \frac{\kappa_i}{2\pi} \int_{\Sigma_R} \partial_x \varphi_i \, dx , \qquad (4.18)$$

$$j_i = -\frac{\kappa_i}{2\pi} \partial_t \varphi_i = \eta_i v_i \rho_i - \eta_i \frac{\kappa_i^2}{2\pi} U_R . \qquad (4.19)$$

Likewise, the commutation relations also decouple

$$[\partial_x \varphi_i(x,t), \varphi_j(0,0)] = i\eta_i 2\pi \delta(x - \eta_i v_i t) \delta_{ij} . \qquad (4.20)$$

The total charge density, electric charge and edge current of the right moving edge is the sum of these operators

$$\rho_R = \sum_i \rho_i , \qquad Q_R = \sum_i Q_i , \qquad j_R = \sum_i j_i . \qquad (4.21)$$

A similar definition applies to the left moving edge.

The total current operator is again the sum $j_R(x) + j_L(x)$, Eq. (4.12). To obtain the current-voltage relation (4.14) we assume that each channel is in chemical equilibrium, meaning the

density matrix is of the form $e^{-\beta K_0}/Z$ and the charge density of each channel vanishes $\langle \rho_i \rangle = 0$. The expectation value of the right-moving edge current is

$$\langle j_R(x,t) \rangle = -\frac{1}{2\pi} U_R \sum_i \eta_i \kappa_i^2 \qquad (4.22)$$

and similarly for the left-moving edge current. For a right moving edge we require $\left( \sum_i \eta_i \kappa_i^2 \right) > 0$, while for a left moving edge it is negative. The usual conductivity relation Eq. (4.14) is obtained provided we have

$$\sum_i \eta_i \kappa_i^2 = \nu . \qquad (4.23)$$

This restriction is in fact a consequence of anomaly cancellation [15], so we assume that it holds. Unlike the single-channel case the conductivity does not uniquely specify the couplings $\kappa_i$ (recall that in single channel case we simply have $\kappa_1 = \sqrt{\nu}$). To fully specify the topological order we also need to define the electron operators of the theory, which in turn determines the quasiparticle content. We refer to the literature for further discussions on this classification scheme.

A generic quasiparticle operator is of the form

$$\psi_R^\dagger(x,t) \propto \sigma_R(x,t) e^{-i \sum_i \eta_i q_i \varphi_i(x,t)} \qquad (4.24)$$

which is defined by the $q_i$'s. The electric charge $Q$ of the quasiparticle is determined using the commutation relation with the charge operator

$$Q\psi_R^\dagger = [Q_R, \psi_R^\dagger] = \frac{1}{2\pi} \sum_i \kappa_i \int [\partial_x \varphi_i(x), \psi_R^\dagger]\, dx . \qquad (4.25)$$

It follows that the charge is given by

$$Q = \sum_i \kappa_i q_i . \qquad (4.26)$$

In addition the conformal dimension for the $i$'th channel is $h_i = \frac{q_i^2}{2}$ and so the total conformal dimension equals $h = h_n + h_c$ with

$$h_c = \sum_i \frac{q_i^2}{2} . \qquad (4.27)$$

Finally, the non-equal time commutation relations between the current and the quasiparticle is given by

$$[j_R(x,t), \psi_R^\dagger(y,t')] = \left( \sum_i \eta_i v_i \kappa_i q_i \delta(x - y - \eta_i v_i(t - t')) \right) \psi_R^\dagger(y,t') . \qquad (4.28)$$

The generic form of the quasiparticle operator (4.24) involves all the channels of the edge theory, although this mixing does not always occur.

An example of a state which is described by multiple charged chiral bosons is the Moore-Read trial state [162, 99, 160] of the $\nu = \frac{5}{2}$ plateau [226, 174]. Here we deal with a half-filled Landau level on top of two fully filled Landau levels. The edge theory consists of two chiral bosons with couplings $\kappa_1 = \kappa_2 = 1$, a third chiral boson with $\kappa_3 = \frac{1}{\sqrt{2}}$ and a neutral channel described by the chiral Ising model. This corresponds to a conductivity of $\nu = \frac{5}{2}$. All channels are completely decoupled and have the same chirality. The quasiparticle operators do not mix different chiral bosons, so for each quasiparticle the sum appearing in Eq. (4.24) consists of only one term.

A second example is a hierarchial trial state [102, 107] of the $\nu = \frac{2}{5}$ plateau. The trial state is formed through condensation of quasiparticles in the $\nu = \frac{1}{3}$ state. The corresponding edge [217] consists of two (co-propagating) chiral bosons with couplings $\kappa_1 = \frac{1}{\sqrt{3}}$ and $\kappa_2 = \frac{1}{\sqrt{15}}$, which brings the conductivity to $\nu = \frac{2}{5}$. A simplified description assumes the distance between the two charged channels is large and the chiral bosons can be treated as completely decoupled. Each quasiparticle operator is then associated with strictly one chiral boson.

In practice the distance between the channels is small, the Coulomb interaction needs to be taken into account [217] and the channels no longer decouple (although the currents still commute). In this case it is possible to diagonalize the interaction term through a linear transformation of the fields. The new fields are, again, completely decoupled. In this new basis the quasiparticle and electron operators are constructed from multiple fields, and in particular the sum appearing in (4.24) contains both chiral bosons of the new basis.

We finalize this discussion by noting that it is currently not completely clear if the case of counter propagating charge modes arises in the quantum Hall effect, as they have never been experimentally verified. One explanation for this is that counter propagating modes are unstable in the presence of disorder. In Ref. [133] it was found that for the $\nu = 2/3$ state disorder induces tunnelling of charge between the counter propagating modes. This results in a different effective edge theory that consists of a single charged mode and a counter propagating *neutral* mode. In this work we do not consider such dynamical effects which alter the edge theory away from the point contact. We simply assume the different channels completely decouple, and allow for the possibility of counter propagating modes. A recent experiment [14] suggests that counter propagating neutral modes are in fact present in multiple states, including the $\nu = 5/2$ state. However, we do expect that our results can be generalized to include for instance the $K$-matrix formalism.
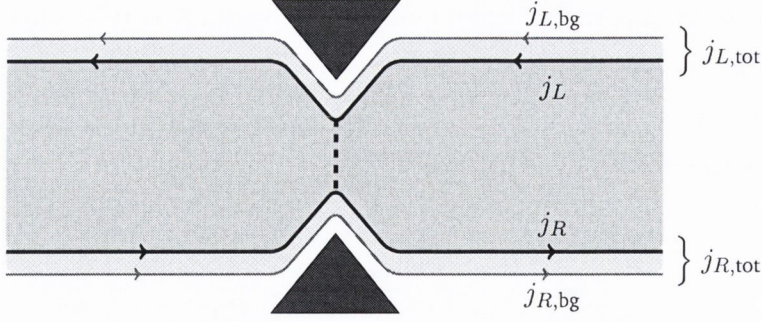
**Figure 4.3:** The point contact induces tunnelling between the two edges. Tunnelling occurs between the inner channels of the edges. We decompose the total edge current ($j_{R/L,\text{tot}}$) into channels which are partially reflected ($j_{R/L}$), and which are fully transmitted ($j_{R/L,\text{bg}}$).

## 4.3 Tunnelling point contact

### 4.3.1 Tunnelling Hamiltonian and tunnelling current

We consider a quantum Hall bar at filling fraction $\nu$ with two disconnected edges [41, 42, 70], see also Chapter 3.3 and Figure 4.3. The tunnelling operator tunnels a quasiparticle $\psi$ between the edges and is defined as

$$\mathcal{V} = \psi_L^\dagger(x=0)\psi_R(x=0) \,. \tag{4.29}$$

The quasiparticle is characterized by its quasiparticle charge $Q$ and conformal dimensions $h_n$ and $h_c$. In the multichannel case we assume the couplings $\kappa_i$ and individual charges $q_i$ are known. The tunnelling Hamiltonian is the tunnelling operator together with a tunnelling coupling constant

$$H_T = \Gamma\mathcal{V} + \Gamma^*\mathcal{V}^\dagger \,. \tag{4.30}$$

It is treated as a perturbation to the grand canonical Hamiltonian $K_0$, Eq. (4.9). The tunnelling operator follows from the rate of change of charge

$$\hat{I}_B \equiv \frac{e}{2}\frac{d}{dt}(\mathcal{Q}_L - \mathcal{Q}_R) = -i\frac{e}{2}[\mathcal{Q}_L - \mathcal{Q}_R, K_0 + H_T]$$
$$= -iQe\left(\Gamma\mathcal{V} - \Gamma^*\mathcal{V}^\dagger\right) \,. \tag{4.31}$$

Charge is conserved in the equilibrium system, so $[K_0, \mathcal{Q}_{R/L}] = 0$, and since the quasiparticles carry a charge $Q$ we have $[\mathcal{Q}_L, \mathcal{V}] = -[\mathcal{Q}_R, \mathcal{V}] = Q\mathcal{V}$. This also applies to the case of multiple charged channels.

### 4.3.2 Background current and multichannel case

The point contact induces tunnelling of quasiparticles between the innermost channels of the left- and right moving edge. In particular it does not always involve all edge channels. An example is the Moore-Read state for the $\nu_{\text{tot}} = 5/2$ plateau. In this case the outer channels correspond to the fully filled Landau levels which are fully transmitted. Tunnelling occurs only between the inner channels described by the chiral Ising model times a chiral boson.

We therefore decompose the edge current into two pieces: the channels which are fully transmitted and not involved in the tunnelling process (called the background current), and the channels which are partially reflected (called the reflected current). This decomposition is sketched in Figure 4.3. The corresponding current operators are denoted $j_{R,\text{bg}}$ for the background current and $j_R$ for the reflected current. The total edge current operator is written as

$$j_{R,\text{tot}} = j_R + j_{R,\text{bg}} \tag{4.32}$$

In addition the reflected current and background current can also consist of multiple channels. Note also that the conductivity splits accordingly

$$\nu_{\text{tot}} = \nu + \nu_{\text{bg}} . \tag{4.33}$$

The decomposition (4.32) is reflected in the definition of the tunnelling Hamiltonian and the tunnelling current. The perturbation $H_T$ commutes with the current operators of the channels not involved in the tunnelling, i.e. $[\mathcal{Q}_{R,\text{bg}}, H_T] = 0$ and so

$$[\mathcal{Q}_{R,\text{tot}}, H_T] = [\mathcal{Q}_R, H_T] . \tag{4.34}$$

We can therefore treat the background current as an equilibrium system unaffected by the perturbation.

## 4.4 Non-equilibrium formalism

The non-equilibrium formalism is partially treated in Chapter 3.3.3. There we developed the linear response theory of a system of tunnelling point contacts. The approach used in this Chapter is more general, as we keep track of all orders in perturbation theory. We therefore keep the discussion self-contained.

The tunnelling Hamiltonian is treated as a perturbation of the grand canonical Hamiltonian $K_0$. Initially at some time $t < t_0$ the perturbation is absent and the system is described by an equilibrium density matrix of the form

$$w_0 \equiv w(t_0) = e^{-K_0/k_B T}/Z . \tag{4.35}$$

We also denote $\langle\cdots\rangle$ as the expectation value with respect to $w_0$,

$$\langle\cdot\rangle \equiv \mathrm{Tr}\big[w_0\cdots\big] . \tag{4.36}$$

This density matrix further factorizes as a product of density matrices – one for each channel of the system. At some time $t_0$ the perturbation is switched on adiabatically and the system is slowly driven away from equilibrium. Eventually, after the perturbation is fully switched on ($t \gg t_0$) the system is described by a steady state. In our approach we make use of the fact that (1) the initial state is an equilibrium state and (2) the unitary time evolution of the system is completely described by the (known) perturbed Hamiltonian $K = K_0 + H_T$.

Concretely, when the system reaches a steady state the expectation value of an operator $\mathcal{O}$ is given by $\langle\mathcal{O}(t)\rangle = \mathrm{Tr}\big[w_0\mathcal{O}_K(t)\big]$ where $\mathcal{O}_K(t)$ is the Heisenberg representation of the operator $\mathcal{O}$ with respect to the grand canonical Hamiltonian $K$,

$$\mathcal{O}_K(t) = \mathcal{S}_K^\dagger(t,t_0)\mathcal{O}_K(t_0)\mathcal{S}_K(t,t_0) . \tag{4.37}$$

The unitary time evolution operator $\mathcal{S}_K(t,t_0)$ solves the Schrödinger equation,

$$i\partial_t\mathcal{S}_K(t,t_0) = K\mathcal{S}_K(t,t_0) \tag{4.38}$$

and $\mathcal{S}_K(t,t) = 1$. Next, we follow Ref. [180] and factorize the time evolution operator according to $\mathcal{S}_K(t,t_0) = e^{-iK_0(t-t_0)}\mathcal{U}(t,t_0)$. From Eq. (4.38) it follows that the unitary operator $\mathcal{U}(t,t_0)$ satisfies the equation of motion

$$i\partial_t\mathcal{U}(t,t_0) = H_T(t)\mathcal{U}(t,t_0) \tag{4.39}$$

$$H_T(t) \equiv e^{iK_0t}H_Te^{-iK_0t} . \tag{4.40}$$

Here $H_T(t)$ is in an interaction-like picture with its time evolution dictated by the unperturbed Hamiltonian $K_0$. The time evolution operator $\mathcal{U}$ is also known as the S-matrix operator and it is given by Dyson's series

$$\mathcal{U}(t,t_0) = \mathcal{T}\exp\Big(-i\int_{t_0}^t H_T(t')\,dt'\Big) = 1 + \sum_{n=1}^\infty \frac{(-i)^n}{n!}\Big[\prod_{i=1}^n \int_{t_0}^t dt_i\Big]\mathcal{T}\prod_{j=1}^n H_T(t_j) \tag{4.41}$$

Here $\mathcal{T}$ is the time-ordering operator and the exponentiated form is an abbreviation for the corresponding expansion. Similarly, we set for an operator $\mathcal{O}$

$$\mathcal{O}_{K_0}(t) = e^{iK_0(t-t_0)}\mathcal{O}(t_0)e^{-iK_0(t-t_0)} = e^{iK_0t}\mathcal{O}(0)e^{-iK_0t} . \tag{4.42}$$

By using the factorization of the unitary time evolution operator in (4.37) and taking the limit $t_0 \to -\infty$ we obtain for an operator $\mathcal{O}$ its expectation value

$$\mathcal{O}^I(t) \equiv \mathcal{U}^\dagger(t,-\infty)\mathcal{O}_{K_0}(t)\mathcal{U}(t,-\infty) \tag{4.43}$$

$$\langle\mathcal{O}^I(t)\rangle = \mathrm{Tr}\big[w_0\mathcal{O}^I(t)\big] = \mathrm{Tr}\big[w_0\mathcal{U}^\dagger(t,-\infty)\mathcal{O}_{K_0}(t)\mathcal{U}(t,-\infty)\big] . \tag{4.44}$$

Here $\mathcal{O}^I(t)$ is still the Heisenberg representation $\mathcal{O}_K(t)$, but with the time evolution operators factorized. The superscript $^I$ denotes that the tunnelling Hamiltonian is switched on and the operator is taken in the Heisenberg representation. The effect of the perturbation $H_T$ is completely captured by the time evolution operator $\mathcal{U}$. All correlators are evaluated with respect to the equilibrium density matrix $w_0$.

As an example the expectation value of the tunnelling current is given by

$$I_B = \langle \hat{I}_B^I(t) \rangle \tag{4.45}$$

$$\hat{I}_B^I(t) = \mathcal{U}^\dagger(t, -\infty)\hat{I}_B(t)\mathcal{U}(t, -\infty) \,. \tag{4.46}$$

If we want to explicitly determine this correlator we need a different approach such as perturbation theory.

## 4.5 A Kubo formula and Ward identity for non-equilibrium systems

The effect of the tunnelling perturbation is fully captured by the time evolution operator $\mathcal{U}(t, t_0)$. In linear response theory the time evolution operator Eq. (4.41) is expanded to lowest order in the tunnelling coupling constant, which leads to the Kubo formula,

$$\mathcal{O}^I(t) \cong \mathcal{O}_{K_0}(t) - i \int_{-\infty}^{t} [\mathcal{O}_{K_0}(t), H_T(t')] \, dt' + \dots \,. \tag{4.47}$$

The dots represent higher order contributions. We present here an extension of the Kubo formula, which includes the higher order contributions. It is based on Ref. [87]. This non-equilibrium Kubo formula is given by

$$\boxed{\mathcal{O}^I(t) = \mathcal{O}_{K_0}(t) - i \int_{-\infty}^{t} \mathcal{U}^\dagger(t', -\infty)[\mathcal{O}_{K_0}(t), H_T(t')]\mathcal{U}(t', -\infty) \, dt'} \tag{4.48}$$

We emphasize that this expression is an operator identity. Ref. [87] obtains this formula for the class of operators which commute with the equilibrium Hamiltonian $K_0$ and can be considered a conserved charge in the equilibrium system. The second term is the difference of the operator in a system in equilibrium and a system out of equilibrium,

$$\delta\mathcal{O}^I(t) \equiv \mathcal{O}^I(t) - \mathcal{O}_{K_0}(t) = -i \int_{-\infty}^{t} \mathcal{U}^\dagger(t', -\infty)[\mathcal{O}_{K_0}(t), H_T(t')]\mathcal{U}(t', -\infty) \, dt' \tag{4.49}$$

This equation separates the effect of the perturbation on the operator $\mathcal{O}$ when the perturbation is turned on and the system is forced out of equilibrium.

### 4.5.1 Proof of the non-equilibrium Kubo formula

In the this subsection we prove the non-equilibrium Kubo formula Eq. (4.48) to all orders of perturbation theory. The proof combines the series expansion for the time evolution operator with some combinatorial manipulations.

We define the Hamiltonian as $K(t) = K_0 + \lambda(t)H_T$ with $H_T$ some perturbation that is adiabatically switched on through the function $\lambda(t)$. This function starts off as $\lambda(t < t_0) = 0$. Then at $t = t_0$ the function slowly increases until $\lambda(t \geq t_a) = 1$ at some time $t_a$. This process adiabatically turns on the interaction. Measurement of e.g. the current and noise are performed at a much later time $t \gg t_a$. In the main text we take $t_a, t_0 \to -\infty$ and set $\lambda(t) = 1$. We assume that the final expression for the Kubo formula of this section obtained (Eq. (4.48)) converges to Eq. (4.59) when this limit is taken.

We write Dyson's series expansion of the S matrix operator $\mathcal{U}$ as

$$\mathcal{U}(t, t_0) = 1 + \sum_{n=1}^{\infty} \frac{(-i)^n}{n!} \int_{t_0}^{t} \mathcal{D}t_n \, \mathcal{T} \prod_{j=1}^{n} \lambda(t_j) H_T(t_j) \qquad (4.50)$$

Here we use the notation $\int_{t_0}^{t} \mathcal{D}t_n \equiv \prod_{i=1}^{n} \int_{t_0}^{t} dt_i$. To prove the NE-Kubo formula we start with the following expansion of the left-hand side of Eq. (4.48) which follows automatically from the Dyson's series of $\mathcal{U}$,

$$\mathcal{O}^I(t) = \mathcal{U}^\dagger(t, t_0)\mathcal{O}_{K_0}(t)\mathcal{U}(t, t_0) = \mathcal{O}_{K_0}(t) + \sum_{n=1}^{\infty} \frac{(-i)^n}{n!} A^{(n)}, \qquad (4.51)$$

where $\mathcal{O}_{K_0}(t) = e^{iK_0(t-t_0)}\mathcal{O}(t_0)e^{-iK_0(t-t_0)}$ and

$$A^{(n)} = \sum_{m=0}^{n} (-1)^m \binom{n}{m} \int_{-t_0}^{t} \mathcal{D}t_n \, \bar{\mathcal{T}}\Big[\prod_{j=1}^{m} \lambda(t_j)H_T(t_j)\Big]\mathcal{O}_{K_0}(t)\mathcal{T}\Big[\prod_{j=m+1}^{n} \lambda(t_j)H_T(t_j)\Big] . \quad (4.52)$$

Here $\mathcal{T}$ and $\bar{\mathcal{T}}$ are time and anti-time ordering symbols, respectively, and they only act on the operators within the brackets. Empty products are equal to one, i.e. $\prod_{j=n+1}^{n} \lambda(t_j)H_T(t_j) \equiv 1$.

Each summation $A^{(n)}$ can be written as a sum over commutators $\lambda(t_j) [\mathcal{O}(t), iH_T(t_i)]$. First notice that if we exclude the effect of the remaining (anti-)time ordering but include the multiplicity due to the binomial $\binom{n}{m}$, the sum $A^{(n)}$ contains $2^n$ terms. This sum can be written as a sum over $2^{n-1}$ commutators. To illustrate this we fix the time ordering. The $m = 0$ and $m = 1$ terms combine as (for the sake of notation we momentarily absorb $\lambda(t)$ into the definition of $H_T(t)$)

$$\binom{n}{0} H_T(t_1) \prod_{j=2}^{n} H_T(t_j) - \binom{n}{1} H_T(t_1)\mathcal{O}(t) \prod_{j=2}^{n} H_T(t_j) =$$

$$\binom{n-1}{0} [\mathcal{O}(t), H_T(t_1)] \prod_{j=2}^{n} H_T(t_j) - \binom{n-1}{1} H_T(t_1)\mathcal{O}(t) \prod_{j=2}^{n} H_T(t_j) . \quad (4.53)$$

The first term contains the desired commutator. The second term can be combined with the $m = 2$ contribution in (4.52). The remainder of this can be combined with the $m = 3$ term, etc. The process is iterated until all terms are combined into commutators. The multiplicity of the $k$'th term in this sum over commutators is

$$\sum_{m=0}^{k}(-1)^m \binom{n}{m} = (-1)^k \binom{n-1}{k}. \tag{4.54}$$

To write down an expression of $A^{(n)}$ we need to incorporate the effect of time ordering. For that we fix the dummy indices such that $\{t_1, \ldots, t_{m-1}\} > t_m > \{t_{m+1}, \ldots, t_n\}$, and relabel $t_m \to t'$ and $\{t_{m+1}, \ldots, t_n\} \to \{t_m, \ldots, t_{n-1}\}$. This can always be accomplished through relabelling of the integration variables for any given time ordering. The resulting expression is plugged back into the integration over all dummy variables $t_m$. Since we have a time-ordered (and anti-time ordered) set of integrals the integration limits need to be adjusted accordingly. The result is,

$$A^{(n)} = n \int_{-t_0}^{t} dt' \sum_{m=0}^{n-1}(-1)^m \binom{n-1}{m} \int_{-t_0}^{t'} \mathcal{D}t_n$$
$$\bar{\mathcal{T}}\Big[\prod_{j=1}^{m} \lambda(t_j)H_T(t_j)\Big] [\mathcal{O}(t), \lambda(t')H_T(t')] \mathcal{T}\Big[\prod_{j=m+1}^{n-1} \lambda(t_j)H_T(t_j)\Big] \tag{4.55}$$

The upper limit of the integration variables $t_m$ is $t'$, which is the label of $H_T$ appearing in the commutator. An extra factor of $n$ appears because we are summing over all possible (anti-)time orderings. Plugging this expression back into the original expansion (4.51) results in

$$\sum_{n=1}^{\infty} \frac{(-i)^n}{n!} A^{(n)} = -i \int_{t_0}^{t} \sum_{n=0}^{\infty} \frac{(-i)^n}{n!} B^{(n)}(t') \, dt' \tag{4.56}$$

where $B^{(0)}(t') = [\mathcal{O}(t), H_T(t')]$ and for $n > 0$

$$B^{(n)}(t') =$$
$$\sum_{m=0}^{n}(-1)^m \binom{n}{m} \int_{-t_0}^{t'} \mathcal{D}t_n \, \bar{\mathcal{T}}\Big[\prod_{j=1}^{m} \lambda(t_j)H_T(t_j)\Big] [\mathcal{O}(t), \lambda(t')H_T(t')] \mathcal{T}\Big[\prod_{j=m+1}^{n-1} \lambda(t_j)H_T(t_j)\Big].$$
$$\tag{4.57}$$

The summation over $B^{(n)}$ matches that of Eq. (4.51), but with $\mathcal{O}(t)$ replaced by $[\mathcal{O}(t), H_T(t')]$. The right hand side of Eq. (4.56) is therefore equal to

$$-i \int_{t_0}^{t} \sum_{n=0}^{\infty} \frac{(-i)^n}{n!} B^{(n)}(t') \, dt' = -i \int_{t_0}^{t} \mathcal{U}^\dagger(t, t_0)[\mathcal{O}(t), \lambda(t')H_T(t')]\mathcal{U}(t, t_0) \, dt' \tag{4.58}$$

Putting everything together results in the non-equilibrium Kubo formula

$$\mathcal{O}^I(t) = \mathcal{O}_{K_0}(t) - i \int_{t_0}^t \mathcal{U}^\dagger(t, t_0)[\mathcal{O}(t), \lambda(t')H_T(t')]\mathcal{U}(t, t_0)\, dt' \,. \tag{4.59}$$

For the non-equilibrium Kubo formula used in the main text (Eq. (4.49)) we take the limit $t_0 \to -\infty$, and set $t = 0$ and $\lambda(t) = 1$. We assume that the resulting integral converges in this limit.

## 4.6 Edge current operator in the non-equilibrium formalism

In the absence of the point contact, the current through the system is given by the usual quantum Hall relation $I_{\max} = \frac{\nu}{2\pi}(U_L - U_R)$. In the presence of a point contact this Hall relation no longer holds. The point contact induces a tunnelling current $I_B$, which is effectively a form of backscattering, since the edge currents of the system are chiral. On the basis of charge conservation we expect the current in the presence of a point contact to be

$$I_0 = I_{\max} - I_B \,. \tag{4.60}$$

We now show that this relation is also satisfied at the level of the operators. For this we make use of the non-equilibrium Kubo formula. Recall that in the interaction representation the total current operator is

$$\hat{I}_0^I(x, t) = j_R^I(x, t) + j_L^I(y, t) \,. \tag{4.61}$$

Here $j_R^I$ and $j_L^I$ are the edge currents in the interaction picture, Eq. (4.43). We focus initially on an edge with a single charged channel and comment on the multichannel case at the end of the section.

We now apply the non-equilibrium Kubo formula Eq. (4.48). For this we need the commutator of the edge current and the tunnelling Hamiltonian. We use the commutation relations of the edge current with the quasiparticle operator, Eq. (4.15), and the expression of the tunnelling Hamiltonian in terms of the quasiparticles, $H_T = \Gamma \psi_L^\dagger \psi_R + \text{c.c.}$. This gives

$$[j_R(x, t), H_T(t')] = -i\eta_R v_c \hat{I}_B(t')\delta(x - \eta_R v_c(t - t'))$$
$$[j_L(x, t), H_T(t')] = i\eta_L v_c \hat{I}_B(t')\delta(x - \eta_L v_c(t - t')) \tag{4.62}$$

with $\eta_R = +1$ and $\eta_L = -1$. Plugging this into (4.48) for $j_{R/L}^I$ and performing the integration over $t'$ results in

$$j_R^I(x, t) = j_R(x, t) - \theta(x)\hat{I}_B^I(t - x/v_c) \,. \tag{4.63}$$
$$j_L^I(x, t) = j_L(x, t) - \theta(-x)\hat{I}_B^I(t + x/v_c) \tag{4.64}$$

Here $\theta(x)$ is the unit step function, and $j^I(x,t)$ and $\hat{I}_B^I$ are the edge current and the tunnelling current operator in the interaction representation, see Eq. (4.46).

This operator has an intuitive meaning. It is a reflection of both charge conservation and the chiral structure of the edge current. Consider Eq. (4.63) for the rightmoving current. For the region $x < 0$ the operator reduces to $j_R^I(x,t) = j_R(x,t)$, meaning the current operator in this region is not affected by the presence of the tunnelling point contact. This is as expected, since the region $x < 0$ is "upstream" of the point contact. For the region $x > 0$ the backscattering current $I_B$ at a retarded time $(t - x/v_c)$ is subtracted. The backscattering current is the charge transferred from the lower to the upper edge and is therefore subtracted from the current past the point contact (it is also subtracted from the left moving current because of the direction of total current). The identity resembles Kirchoff's law as charge is conserved along the point contact.

The fact that we subtract the operator $\hat{I}_B^I$ from $j_R$ at a retarded time $t - x/v_c$ is a manifestation of the chiral and causal structure. Chirality and translational symmetry enforces all observables to be functions of the combination $t - x/v_c$. A similar argument is used in Ref. [210] as a derivation of the edge current operator for the system out of equilibrium. The chiral structure takes into account the position of the point contact (at $x_R = 0$, hence the step function), the chirality of the edge (right-moving) and the finite velocity of the charged channel.

The total current operator in the interacting regime is now

$$\hat{I}_0^I(x,t) = j_R(x,t) + j_L(x,t) - \hat{I}_B^I(t - |x|/v_c) . \tag{4.65}$$

This indeed reproduces the current relation Eq. (4.60)

$$I_0 = \langle j_R(x,t) + j_L(x,t)\rangle - \langle \hat{I}_B^I(t - |x|/v_c)\rangle = I_{\max} - I_B . \tag{4.66}$$

A similar relation applies to the charge density operators. When we apply the non-equilibrium Kubo formula to these operators we find

$$\rho_R^I(x,t) = \rho_R(x,t) - \frac{1}{v_c}\hat{I}_B^I(t - x/v_c)\theta(x)$$
$$\rho_L^I(x,t) = \rho_L(x,t) + \frac{1}{v_c}\hat{I}_B^I(t + x/v_c)\theta(-x) \tag{4.67}$$

Note that the sign of $I_B$ in the equations are merely a consequence of our conventions (direction of the current and backscattering current, charge of the tunnelling quasiparticle, etc.)

Let us remark on the more general case of multiple charged channels. First note that the inclusion of background currents (see Section 4.3.2) does not modify the relation, since the

background currents commute with the tunnelling Hamiltonian. This is intuitively clear, since the background currents are fully transmitted.

In the more general case the additional charged channels do not commute with the tunnelling Hamiltonian. The total edge current is a sum of the background currents plus the reflected edge currents

$$j_{R,\text{tot}} = j_R + j_{R,\text{bg}} \,, \qquad\qquad j_R = \sum_i j_i \,. \qquad (4.68)$$

Each channel is characterised by its own edge velocity $v_i$ and chirality $\eta_i$. The commutator of the edge current operator with the tunnelling Hamiltonian becomes

$$[j_{R,\text{tot}}(x,t), H_T(t')] = [j_R(x,t), H_T(t')] = -i\hat{I}_B(t') \sum_i \frac{\kappa_i q_i}{Q} \eta_i v_i \delta(x - \eta_i v_c(t - t')) \,. \qquad (4.69)$$

and for completeness we also note the left moving edge (with chiralities $\eta_i^L$)

$$[j_{L,\text{tot}}(x,t), H_T(t')] = [j_L(x,t), H_T(t')] = i\hat{I}_B(t') \sum_i \frac{\kappa_i q_i}{Q} \eta_i^L v_i \delta(x + \eta_i^L v_c(t - t')) \,. \qquad (4.70)$$

The charge of the quasiparticle in this case is given by $Q = \sum_i \kappa_i q_i$. The edge current operator in the interaction picture is given by

$$j_{R,\text{tot}}^I(x,t) = j_{R,\text{tot}}(x,t) - \sum_i \left(\frac{\kappa_i q_i}{Q}\right) \eta_i \theta(\eta_i x) \hat{I}_B^I(t - \eta_i x/v_i) \,. \qquad (4.71)$$

The summation reflects the chiral structure of each channel separately and the current relation Eq. (4.60) is again obtained.

## 4.7  Non-equilibrium noise

The main result of the previous section is the operator identity Eq. (4.65) which captures the effect of the tunnelling Hamiltonian on the edge current. In this section we analyse the noise in the edge current in the non-equilibrium system. Using the identity Eq. (4.65) we can relate the noise in the edge current out of equilibrium to the noise in the tunnelling current. This results in a non-equilibrium fluctuation-dissipation theorem [131] and an expression for the excess noise in the edge current. Put differently, we are studying the effects of the non-equilibrium Kubo formula on autocorrelators and their Fourier transform.

Let us first recall some definitions [20, 157, 48]. Given an operator $\mathcal{O}$ we set $\Delta\mathcal{O}(t) = \hat{\mathcal{O}}(t) - \langle\hat{\mathcal{O}}\rangle$ and define the autocorrelator $S_{\mathcal{O}}(t)$ as

$$S_{\mathcal{O}}(t) = \langle\Delta\mathcal{O}(t)\Delta\mathcal{O}(0)\rangle = \langle\mathcal{O}(t)\mathcal{O}(0)\rangle - \langle\mathcal{O}\rangle^2 \,. \qquad (4.72)$$
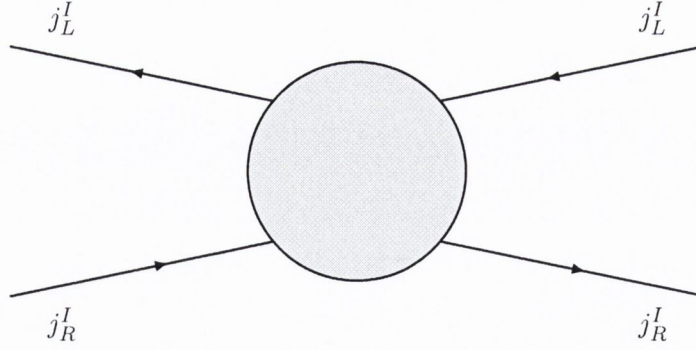
**Figure 4.4:** The point contact viewed as a scattering source at $x_R = x_L = 0$ with the edges depicted as incoming and outgoing edge currents. The arrows denote the direction of the local electric current. The edge currents are taken in the interaction picture.

The non-symmetrized noise is the corresponding Fourier transform

$$S_\mathcal{O}(\omega) = \int e^{i\omega t} S_\mathcal{O}(t)\, dt\,. \tag{4.73}$$

The symmetric and antisymmetric combinations of the noise are denoted by

$$C_\mathcal{O}(\omega) = \frac{1}{2}\left(S_\mathcal{O}(\omega) + S_\mathcal{O}(-\omega)\right) \tag{4.74}$$

$$R_\mathcal{O}(\omega) = \frac{1}{2}\left(S_\mathcal{O}(\omega) - S_\mathcal{O}(-\omega)\right)\,. \tag{4.75}$$

The same notation is used in Ref. [131].

### 4.7.1 Noise in the outgoing edge current

In the spirit of Ref. [42] we think of the point contact as a scattering source with the edges as two incoming and two outgoing branches, see Figure 4.4. We focus on the noise in the outgoing branch of the right-moving edge, which corresponds to the noise in $j^I_{R,\text{tot}}(x,t)$ for $x > 0$. We first consider the case of a single reflected charged channel plus any number of background currents which are fully transmitted. The edge current operator is

$$\Delta j^I_{R,\text{out}}(x,t) = j^I_R(x,t) + j_{R,\text{bg}}(x,t) - \langle j^I_R(x,t) + j_{R,\text{bg}}(x,t)\rangle \tag{4.76}$$

with $j^I_R$ given by (4.63) and $x > 0$. The noise in this outgoing edge current is defined as

$$
\begin{aligned}
S_{\text{out}}(t) &= \langle \Delta j^I_{R,\text{out}}(x,t)\Delta j^I_{R,\text{out}}(x,0)\rangle \\
&= \langle \Delta j^I_R(x,t)\Delta j^I_R(x,0)\rangle + \langle \Delta j_{R,\text{bg}}(x,t)\Delta j_{R,\text{bg}}(x,0)\rangle, \qquad x > 0\,.
\end{aligned} \tag{4.77}
$$

We now show that this non-equilibrium noise is completely determined in terms the noise of the tunnelling current and the equilibrium noise of the edge current. For this we substitute

for $j_R^I$ the operator equation (4.63) and expand to obtain (momentarily suppressing the $x$-dependency of the edge current operator)

$$S_{\text{out}}(t) = \langle \Delta j_R(t) \Delta j_R(0) \rangle + \langle \Delta j_{R,\text{bg}}(t) \Delta j_{R,\text{bg}}(0) \rangle + \langle \Delta I_B^I(t - x/v_c) \Delta I_B^I(-x/v_c) \rangle$$
$$- \langle \Delta j_R(t + x/v_c) I_B^I(0) + I_B^I(t - x/v_c) \Delta j_R(0) \rangle$$

The term $\langle \Delta j_{R,\text{bg}}(t) \Delta I_B^I(-x/v_c) \rangle$ vanishes and the term $\langle \Delta j_R(t) \Delta I_B^I(-x/v_c) \rangle$ simplifies to $\langle \Delta j_R(t + x/v_c) I_B^I(0) \rangle$. This expression is an expansion of $(j_R + j_{R,\text{bg}} - I_B)^2$. Note that we assume all edge currents operators completely decouple, and so there are no cross-correlations between different channels appearing in this expansion. The Fourier transform of the autocorrelator is the noise of in the outgoing current. We have

$$S_{\text{out}}(\omega) = S_{\text{bg}}(\omega) + S_{I_B}(\omega) - \Delta S(\omega) \,. \tag{4.78}$$

These contributions correspond to the equilibrium noise $\langle j_R j_R \rangle + \langle j_{R,\text{bg}} j_{R,\text{bg}} \rangle$, the noise in the tunnelling current $\langle I_B I_B \rangle$ and the cross terms $\langle j_R I_B \rangle + \langle I_B j_R \rangle$.

To be more precise, the first term in Eq. (4.78) is given by

$$S_{\text{bg}}(\omega) = \int e^{i\omega t} \langle \Delta j_{R,\text{tot}}(x,t) \Delta j_{R,\text{tot}}(x,0) \rangle \, dt = \omega N(\omega) G \,. \tag{4.79}$$

which represents the noise of the edge in the absence of a point contact. Here $G = \frac{\nu_{\text{tot}}}{4\pi}$ is half the total conductivity and $N(\omega) = \coth\left(\frac{w}{2k_B T}\right) + 1$. This was determined in Section 4.2. This expression is known as the (non-symmetrized) Nyquist-Johnson noise.

The second term in Eq. (4.78) is

$$S_{I_B}(\omega) = \int e^{i\omega t} \langle \Delta \hat{I}_B^I(t) \Delta \hat{I}_B^I(0) \rangle \, dt \tag{4.80}$$

which is the noise of the tunnelling current. It is a type of non-equilibrium noise meaning it is not described in terms of the Nyquist-Johnson relation.

The final term is a cross-term between the tunnelling and edge current

$$\Delta S(\omega) = \int e^{i\omega t} \Big( \langle \Delta j_R(x, t + x/v_c) I_B^I(0) \rangle + \langle I_B^I(0) \Delta j_R(x, -t + x/v_c) \rangle \Big) dt$$
$$= N(\omega) R_{I_B}(\omega) \,. \tag{4.81}$$

This contribution arises due to the correlation between the (equilibrium) edge current and the tunnelling current. It is completely determined by the anti-symmetrized noise of the tunnelling current.

The final expression for $\Delta S(\omega)$ in Eq. (4.81) requires some justification. We make use of a *non-equilibrium Ward identity* to simplify the expression for the correlators $\langle \Delta j_R I_B^I \rangle$ and $\langle I_B^I \Delta j_R \rangle$. This is explained in Appendix D. Ward identities are identities imposed on

correlations functions due to symmetries of the theory. In this case this is due to the $u(1)$ symmetry associated with conservation of electric charge. The Ward identity allows us to incorporate the effect of the inserted current operator $j_R$ in the correlator $\langle \Delta j_R I_B^I \rangle$, without explicitly determining these correlators. In particular, we do not need to specify the structure of the neutral mode since it decouples from the current operator.

The expression for the noise in the outgoing current Eq. (4.78) combined with the expression for the cross term Eq. (4.81) is our first main result. It is, up to a an equilibrium contribution, completely determined by the noise in the tunnelling current $S_{I_B}$. This is not surprising, since fluctuations that arise in the tunnelling current $I_B$ end up in the edge current. However, $S_{\text{out}}(\omega) \neq S_{\text{bg}}(\omega) + S_{I_B}(\omega)$. A correction term $\Delta S$ arises due to the correlation between the edge current and the tunnelling current.

An alternative way of writing the noise in the outgoing current, Eq. (4.78), is by replacing $S_{I_B}(\omega) = C_{I_B}(\omega) + R_{I_B}(\omega)$. This gives

$$S_{\text{out}}^{xc}(\omega) = C_{I_B}(\omega) - \coth(\tfrac{w}{2k_BT})R_{I_B}(\omega) \tag{4.82}$$

where we have also replaced the left-hand side by the *excess noise* in the outgoing current

$$S_{\text{out}}^{xc}(\omega) \equiv S_{\text{out}}(\omega) - S_{\text{out}}(\omega, V = 0) = S_{\text{out}}(\omega) - S_{\text{bg}}(\omega) . \tag{4.83}$$

By definition the excess noise is obtained by subtracting the $V = 0$ contribution from the noise. In Eq. (4.82) the right hand side vanishes at $V = 0$ due to the equilibrium fluctuation-dissipation theorem. We show this in the next section. Keep in mind that $S_{I_B}(\omega, V = 0)$ does not vanish, but the combination appearing on the right hand side in Eq. (4.82) at $V = 0$ does. The noise in the edge current at zero voltage is therefore simply the equilibrium noise $S_{\text{out}}(\omega, V = 0) = S_{\text{bg}}(\omega)$.

Finally, we note that the excess noise $S_{\text{out}}^{xc}(\omega)$ is symmetric as follows from the right hand side of Eq. (4.82)

$$S_{\text{out}}^{xc}(\omega) = C_{\text{out}}^{xc}(\omega) . \tag{4.84}$$

Since $R_{out}^{xc}(\omega) = 0$ we also obtain

$$R_{out}(\omega) = R_{\text{bg}}(\omega) . \tag{4.85}$$

### 4.7.2 Non-equilibrium fluctuation-dissipation theorem

Equations (4.78) and (4.82) are non-equilibrium relations between the noise in the outgoing and tunnelling current. In equilibrium both sides of Eq. (4.82) are zero due to the equilibrium

fluctuation-dissipation theorem (FDT). To analyse this further we recall the FDT for a system in equilibrium and some operator $\mathcal{O}$,

$$C_{\mathcal{O}}^{eq}(\omega) - \coth(\tfrac{\omega}{2k_BT})R_{\mathcal{O}}^{eq}(\omega) = 0 \ . \tag{4.86}$$

The fact that the left hand side of Eq. (4.82) does not vanish signals the non-equilibrium nature of the excess noise in the outgoing current.

The equilibrium FDT is a direct consequence of the Kubo-Martin-Schwinger condition[180] satisfied by the autocorrelator $S_{\mathcal{O}}^{eq}(t)$. This condition states that a two-point correlator computed with respect to a thermal state satisfies

$$\langle \hat{A}(t)\hat{B}(0)\rangle_{eq} = \langle \hat{B}(0)\hat{A}(t+i/k_BT)\rangle_{eq} \ . \tag{4.87}$$

For an autocorrelator evaluated at equilibrium $S_{\mathcal{O}}^{eq}(t)$ this gives

$$S_{\mathcal{O}}^{eq}(-t) = S_{\mathcal{O}}^{eq}(t - i/k_BT)$$

$$S_{\mathcal{O}}^{eq}(-\omega) = e^{-\omega/k_BT}S_{\mathcal{O}}^{eq}(\omega) \ . \tag{4.88}$$

This equation and Eq. (4.86) are both known as the equilibrium fluctuation-dissipation theorem.

The noise in the outgoing current $S_{\text{out}}(\omega)$ does not satisfy the equilibrium FDT and is therefore a type of non-equilibrium noise. However, some terms appearing in its expansion Eq. (4.78) do. In particular the noise in the background current $S_{\text{bg}}$ and the correction term $\Delta S$ both satisfy the FDT. For $\Delta S(\omega)$ this follows from simply inserting Eq. (4.81) into Eq. (4.86).

With these results we apply the equilibrium FDT to the first main result (4.78) (the expansion of the noise in the outgoing edge current) and arrive at a *non-equilibrium fluctuation-dissipation theorem* (NE-FDT), satisfied by the noise in the tunnelling and outgoing currents,

$$\boxed{C_{\text{out}}(\omega) - \coth\left(\frac{\omega}{2k_BT}\right)R_{\text{out}}(\omega) = C_{I_B}(\omega) - \coth\left(\frac{\omega}{2k_BT}\right)R_{I_B}(\omega) \ .} \tag{4.89}$$

This relation was derived by Kane and Fisher [131] for a system of a chiral Luttinger liquid. In the case of Ref [131] the noise in the tunnelling current is identified with the noise in the voltage drop over the point contact through $\hat{V}_B = \nu \frac{e^2}{h} \hat{I}_B$. As Kane and Fisher put it, this equation shows that the fluctuations in the edge and tunnelling currents are locked together. Here we have shown how this naturally follows from analysing the edge current operator in the non-equilibrium system.

This NE-FDT relation is our second main result. Here we have generalized the proof to general fractional quantum Hall states, including non-Abelian states. The result also applies

to the multichannel case, as we show in Section 4.7.4. The relation is a direct consequence of conservation of charge and the chirality of the edges. We emphasize though that the main result of this work is the expansion for the noise in the outgoing current Eq. (4.78) and the excess noise Eq. (4.82), and these results do not follow from the NE-FDT.

### 4.7.3  Zero frequency limit

The zero frequency limit for the excess noise is given by[131, 73, 210, 192]

$$S_{\text{out}}^{\text{xc}}(0) = S_{I_B}(0) - 2k_B T \frac{dI_B}{dV} \,. \tag{4.90}$$

To obtain this we use the relation

$$\lim_{\omega \downarrow 0} \coth(\tfrac{\omega}{2k_B T}) R_{I_B}(\omega) = 2k_B T \frac{dI_B}{dV} \,. \tag{4.91}$$

Here $\frac{dI_B}{dV} = \frac{d}{dV}\langle \hat{I}_B^I \rangle$ is the differential conductance of the tunnelling current. To prove (4.91) requires more work. First note that

$$\lim_{\omega \downarrow 0} \coth(\tfrac{\omega}{2k_B T}) R_{I_B}(\omega) = 2k_B T \frac{dS_{I_B}(\omega)}{d\omega}\bigg|_{\omega=0} \tag{4.92}$$

Next we show how you can prove that $\frac{d}{dV}\langle \hat{I}_B^I \rangle$ equals $\frac{dS_{I_B}(\omega)}{d\omega}\big|_{\omega=0}$. For this we use the expression for $\hat{I}_B^I$ in terms of the time evolution operator $\mathcal{U}$, Eq. (4.46), and the expansion of $\mathcal{U}$, Eq. (4.41). Acting with $\frac{d}{dV}$ on $\mathcal{U}$ results in

$$\frac{d}{dV}\mathcal{U}(0, -\infty) = -i \int_{-\infty}^{0} \mathcal{T}\left(\frac{d}{dV} H_T(t) e^{-i \int_{-\infty}^{0} H_T(t')dt'}\right) dt$$
$$= -\frac{d}{d\omega} \int_{-\infty}^{0} e^{i\omega t} \mathcal{U}(0, -\infty) \hat{I}_B^I(t) dt\bigg|_{\omega=0} \,. \tag{4.93}$$

Here we made use of

$$\frac{d}{dV} H_T(t) = -\frac{it}{2}[\mathcal{Q}_L - \mathcal{Q}_R, H_T(t)] = -i \frac{d}{d\omega} e^{i\omega t} \hat{I}_B(t)\bigg|_{\omega=0} \,. \tag{4.94}$$

By applying this relation to $\frac{dI_B}{dV} = \frac{d}{dV}\langle \mathcal{U}^\dagger \hat{I}_B \mathcal{U} \rangle$ we can relate the differential conductance to the noise

$$\frac{dI_B}{dV} = \frac{d}{d\omega} \int_{-\infty}^{0} e^{i\omega t}\langle \hat{I}_B^I(t)\hat{I}_B^I(0) - \hat{I}_B^I(0)\hat{I}_B^I(t)\rangle\bigg|_{\omega=0} = \frac{dS_{I_B}(\omega)}{d\omega}\bigg|_{\omega=0} \,. \tag{4.95}$$

Putting everything together results in the shot noise relation Eq. (4.90).

### 4.7.4 The multichannel case

In the interaction representation the edge current operator in the multichannel case is given by (Eq. (4.71))

$$
j_{R,\text{total}}^I = j_{R,\text{bg}} + \sum_i \hat{j}_i - \sum_i \left(\frac{\kappa_i q_i}{Q}\right)\eta_i \theta(\eta_i x)\hat{I}_B^I(t - \eta_i x/v_i) \tag{4.96}
$$

The autocorrelator of the total edge current is this operator squared. Since all channels decouple the autocorrelator is also a sum over the individual channels. Using the current relation Eq. (4.96) we expand this autocorrelator to

$$
S_{\text{out}}(t) = S_{\text{bg}}(t) + S_{I_B}(t)\left(\sum_i \theta(\eta_i x)\frac{\kappa_i q_i}{Q}\right)^2 - \sum_{i,j}\theta(\eta_j x)\frac{\kappa_j q_j}{Q}\Delta S_{ij}(t) \tag{4.97}
$$

where $S_{\text{bg}}(t)$ is the autocorrelator of the total edge current in equilibrium $j_{R,\text{tot}}$, $S_{I_B}(t)$ is the autocorrelator of the tunnelling current, and

$$
\Delta S_{ij}(t) = \langle\Delta j_i(x, t + \eta_j x/v_j)\hat{I}_B^I(0)\rangle + \langle\hat{I}_B^I(0)\Delta j_i(x, -(t + \eta_j x/v_j))\rangle . \tag{4.98}
$$

The expression $\Delta S_{ij}(t)$ can be simplified using a non-equilibrium Ward identity which holds for each edge channel separately, see Appendix D. For the diagonal components ($\Delta S_{ii}$) we obtain the same result as in the single-channel case, Eq. (4.81). For the off-diagonal components ($\Delta S_{ij}$ with $i \neq j$) some care is required since the velocities are assumed to be different. We find

$$
S_{\text{out}}(\omega) = S_{\text{bg}}(\omega) + S_{I_B}(\omega)\left(\sum_i \theta(\eta_i x)\frac{\kappa_i q_i}{Q}\right)^2
$$
$$
- \Delta S(\omega)\left(\sum_{i,j}\theta(\eta_i x)\frac{\kappa_i q_i}{Q}\frac{\kappa_j q_j}{Q}e^{i\omega x(\frac{\eta_i}{v_i} - \frac{\eta_j}{v_j})}\right) \tag{4.99}
$$

The functions $S_{\text{bg}}$, $S_{I_B}$ and $\Delta S(\omega)$ are the same as for the single channel case, see Section 4.7.1. The tunnelling current mixes different channels, which manifests itself in expression (4.99) through the oscillating contributions. This mixing enters the expression through an oscillating contribution which oscillates at a frequency $x(\frac{\eta_i}{v_i} - \frac{\eta_j}{v_j})$ for each pair of channels as a function of varying $\omega$. For frequencies smaller compared to $v_i/x$ these phase factors are unity. The noise relation Eq. (4.99) automatically takes into account the chirality of the edges and the effect of counter propagating modes.

The nonequilibrium FDT that follows from Eq. (4.99) is given by

$$
C_{out}(\omega) - \coth(\tfrac{\omega}{2k_BT})R_{out}(\omega) =
$$
$$
\left(C_{I_B}(\omega) - \coth(\tfrac{\omega}{2k_BT})R_{I_B}(\omega)\right)\left(\sum_i \theta(\eta_i x)\frac{\kappa_i q_i}{Q}\right)^2 . \tag{4.100}
$$

When all edge currents are co-propagating we have $\sum_i \frac{\kappa_i q_i}{Q} = 1$. The extra factor in Eq. (4.100) compared to Eq. (4.89) only arises when we deal with counter propagating charged channels. The reason for this discrepancy is that the distinction of incoming and outgoing edge currents is not applicable for a system with counter propagating charged edge modes. If the left moving edge is taken into account we recover the usual NE-FDT.

The shot noise limit is given by

$$
\begin{aligned}
S_{\text{out}}(0) = S_{\text{bg}}(0) + S_{I_B}(0) \left( \sum_i \theta(\eta_i x) \frac{\kappa_i q_i}{Q} \right)^2 \\
+ 2k_B T \frac{dI_B}{dV} \left( \sum_{i,j} \theta(\eta_i x) \frac{\kappa_i q_i}{Q} \frac{\kappa_j q_j}{Q} \right) .
\end{aligned}
\tag{4.101}
$$

## 4.8 Cross- and autocorrelators of edge currents

### 4.8.1 Edge current correlations

In this section we expand on our previous results and investigate the finite frequency noise between the different branches of a quantum point contact. Following Ref. [42] the starting point is the definition of the different branches of a quantum Hall point contact, as given by Figure 4.4. We label these as $j_k(t) \equiv j_{R/L}(x_k, t)$ with $k = 1, 2, 3, 4$. These correspond to the different in- and outgoing edge currents. When we apply the non-equilibrium Kubo formula we obtain

$$
\begin{aligned}
j_1^I(t) &= j_{R,\text{tot}}(x_1, t) & x_1 < 0 \\
j_2^I(t) &= j_{L,\text{tot}}(x_2, t) & x_2 > 0 \\
j_3^I(t) &= j_{R,\text{tot}}(x_3, t) - \hat{I}_B^I(t - x_3/v_c) & x_3 > 0 \\
j_4^I(t) &= j_{L,\text{tot}}(x_4, t) - \hat{I}_B^I(t + x_4/v_c) & x_4 < 0
\end{aligned}
\tag{4.102}
$$

We define the correlation between the $n$'th and $m$'th branch as

$$
\mathcal{S}_{nm}(\omega) = \int e^{i\omega t} \langle \Delta j_n^I(t) \Delta j_m^I(0) \rangle \, dt .
\tag{4.103}
$$

It is now a straightforward process of determining all relations by inserting the current operators and simplifying all the terms. All autocorrelators decompose into terms already encountered in the main part of this Chapter and Appendix D. Here we list them once more (we use

$\eta = \pm$ to denote the right ($\eta = -$) and left moving ($\eta = +$) current),

$$S_{\text{bg}}(\omega) = \int e^{i\omega t} \langle \Delta j_{\eta,\text{tot}}(x,t) \Delta j_{\eta,\text{tot}}(x,0) \rangle \, dt = \omega N(\omega) G_{\text{tot}} \tag{4.104}$$

$$S_{I_B}(\omega) = \int e^{i\omega t} \langle \hat{I}_B^I(t) \hat{I}_B^I(0) \rangle \, dt \tag{4.105}$$

$$\mathcal{F}(\omega) = \int e^{i\omega t} \langle \Delta j_{\eta}(x,t) \hat{I}_B^I(\eta x/v_c) \rangle \, dt \qquad = \frac{1}{2} N(\omega) \left( R_{I_B}(\omega) + iQ^2 \langle H_T^I \rangle \right) \tag{4.106}$$

$$\Delta S(\omega) = \mathcal{F}(\omega) + e^{\omega/T} \mathcal{F}(-\omega) \qquad = N(\omega) R_{I_B}(\omega) \, . \tag{4.107}$$

with $R_{\mathcal{O}}(\omega)$ the antisymmetric part of $S_{I_B}(\omega)$. Note also the relations

$$\mathcal{F}(\omega)^* = e^{\omega/T} \mathcal{F}(-\omega) \qquad 2\text{Re}\,[\mathcal{F}(\omega)] = \Delta S(\omega) \qquad 2\text{Im}\,[\mathcal{F}(\omega)] = Q^2 N(\omega) \langle H_T^I \rangle \, . \tag{4.108}$$

The correlator $\langle H_T^I(0) \rangle$ arises as a consequence of the non-equilibrium Ward identity. Furthermore, we also have

$$S_{I_B}(\omega) - \Delta S(\omega) = C_{I_B}(\omega) - \coth\left(\frac{\omega}{2k_B T}\right) R_{I_B}(\omega) \, . \tag{4.109}$$

The diagonal terms of the correlation matrix $S$ are

$$\mathcal{S}_{11}(\omega) = \mathcal{S}_{22}(\omega) = S_{\text{bg}}(\omega) \tag{4.110}$$

$$\mathcal{S}_{33}(\omega) = \mathcal{S}_{44}(\omega) = S_{\text{bg}}(\omega) + S_{I_B}(\omega) - \Delta S(\omega) \tag{4.111}$$

These autcorrelators are the noise of the edge currents. $\mathcal{S}_{33}$ and $\mathcal{S}_{44}$ are treated extensively in Section 4.7 and correspond to the noise in the outgoing branches. The correlations in the incoming branches, $\mathcal{S}_{33}$ and $\mathcal{S}_{44}$, are equilibrium noise due to the chirality of edge.

The remaining correlators $\mathcal{S}_{nm}$ ($n \neq m$) cannot be interpreted as noise. Since $\mathcal{S}_{nm} = \mathcal{S}_{mn}^*$ we only look at the cases where $m > n$. We obtain

$$\mathcal{S}_{12}(\omega) = 0$$

$$\mathcal{S}_{34}(\omega) = e^{i\omega(x_3+x_4)/v_c} \left( S_{I_B}(\omega) - \Delta S(\omega) \right)$$

$$\mathcal{S}_{13}(\omega) = e^{i\omega(x_1-x_3)/v_c} \left( S_{\text{bg}}(\omega) - \mathcal{F}(\omega) \right)$$

$$\mathcal{S}_{24}(\omega) = e^{i\omega(x_2-x_4)/v_c} \left( S_{\text{bg}}(\omega) - \mathcal{F}(\omega) \right)$$

$$\mathcal{S}_{14}(\omega) = -e^{i\omega(x_1+x_4)/v_c} \mathcal{F}(\omega)$$

$$\mathcal{S}_{23}(\omega) = -e^{-i\omega(x_2+x_3)/v_c} \mathcal{F}(\omega) \, . \tag{4.112}$$

Naturally the incoming edge currents are not correlated, hence $\mathcal{S}_{12} = \mathcal{S}_{21} = 0$. The remaining correlators all contain phase factors which depend on the relative distance of the points of measurements to the point contact.
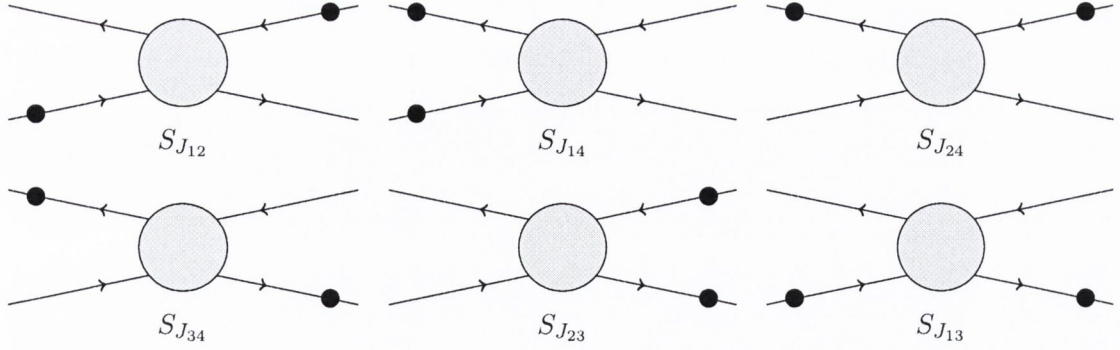
**Figure 4.5:** The noise $S_{J_{nm}}$ represented pictorially. The operator $J_{nm}$ corresponds to the sum $j_n + j_m$ of edge current operators, and $S_{J_{nm}}$ is the corresponding noise. The figures represents the possible combinations of $j_n$ and $j_m$ (with $n \neq m$).

### 4.8.2 Edge currents noise and FDT's

The cross correlations $\mathcal{S}_{nm}$ do not correspond to a type of noise when $n \neq m$. They do enter the expressions for the noise in operators which compare different edge currents. Such an operator is defined as

$$J_{nm}(t) = j_n(t) + j_m(t), \quad n \neq m . \tag{4.113}$$

The corresponding noise is given by

$$S_{J_{nm}} = \mathcal{S}_{nn} + \mathcal{S}_{mm} + \mathcal{S}_{nm} + \mathcal{S}_{mn} \tag{4.114}$$

We note the symmetry $J_{nm} = J_{mn}$ and set $m > n$. This gives rise to six different autocorrelators, which are depicted in Figure 4.5. We also assume the frequency $\omega$ at which the noise is measured is small compared to the combinations $v_c/x_{ij} = v_c/(x_i \pm x_j)$ as they appear in Eq. (4.112), and the noise is measured relatively close to the point contacts. In this limit there are four different cases for the cross-correlator noise. We first have $S_{J_{12}}$ and $S_{J_{34}}$,

$$S_{J_{12}}(\omega) = 2S_{\text{bg}}(\omega) \tag{4.115}$$

$$S_{J_{34}}(\omega) = 2S_{\text{bg}}(\omega) + 4S_{I_B}(\omega) - 4\Delta S(\omega) .$$

Next we have $S_{J_{14}} = S_{J_{24}}$, where

$$S_{J_{14}}(\omega) = 2S_{\text{bg}}(\omega) + S_{I_B}(\omega) - 2\Delta S(\omega) \tag{4.116}$$

And finally $S_{J_{24}} = S_{J_{13}}$ with

$$S_{J_{13}}(\omega) = 4S_{\text{bg}}(\omega) + S_{I_B}(\omega) - 2\Delta S(\omega) \tag{4.117}$$

All cross correlations are expressed in terms of the equilibrium noise of the background current $S_{\text{bg}}$ and the noise in the tunnelling current $S_{I_B}$ (since $\Delta S$ is also determined by $S_{I_B}$). In addition all these autocorrelators satisfy the same nonequilibrium FDT

$$C_{J_{nm}}(\omega) - \coth(\tfrac{\omega}{2k_BT})R_{J_{nm}}(\omega) = C_{I_B}(\omega) - \coth(\tfrac{\omega}{2k_BT})R_{I_B}(\omega) \,. \tag{4.118}$$

In the shot noise limit we replace $S_{bg} \to 2k_BTG$ (with $G = G_{\text{tot}}$) and

$$\lim_{\omega \downarrow 0} \Delta S(\omega) = 2k_BT\frac{dI_B}{dV}$$

This results in

$$S_{J_{12}}(0) = 4k_BTG \tag{4.119}$$
$$S_{J_{34}}(0) = 4k_BTG + 4S_{I_B}(0) - 8k_BT\tfrac{dI_B}{dV}$$
$$S_{J_{14}}(0) = S_{J_{23}}(0) = 4k_BTG + S_{I_B}(0) - 4k_BT\tfrac{dI_B}{dV}$$
$$S_{J_{13}}(0) = S_{J_{24}}(0) = 8k_BTG + S_{I_B}(0) - 4k_BT\tfrac{dI_B}{dV}$$

## 4.9 Conclusion

In this Chapter we investigated the relation between the noise in the outgoing edge current and the noise in the tunnelling current. We found an expression for the finite frequency (non-symmetrized) noise of the outgoing edge current, in terms of the noise in the tunnelling current and the equilibrium Nyquist-Johnson noise (Eq. (4.78)). From this we also obtained an expression for the excess noise in the edge current (Eq. (4.82)). This excess noise is symmetric and completely determined by the noise in the tunnelling current. Finally, we also obtained a relation for the zero frequency limit of these expressions (Eq. (4.90)). The resulting expressions are called non-equilibrium fluctuation-dissipation theorems as they relate different types of noise in the system.

Our approach made use of two new tools, which are also derived in this work. The first is the non-equilibrium Kubo formula. This operator equation separates the effect of time evolution due to a perturbation from the time evolution due to the free Hamiltonian, and is a non-equilibrium extension of the Kubo formula. More specifically, in our context we obtain an equation relating the edge current operator for the system out of equilibrium, to the edge current operator for the system in equilibrium minus the tunnelling current (Eq. (4.63)). This is an operator-version of Kirchoff's law and reflects charge conservation and the chiral structure of the edge theory.

The second tool we made use of is a non-equilibrium Ward identity, which is treated in the appendix. This identity extends the equilibrium Ward identity to hold for certain correlators evaluated out-of-equilibrium.

The treatment in this Chapter applies to generic quantum Hall edges consisting of a single chiral channel and any number of neutral channels. We have also extended the relation to apply to edges with multiple charged channels, possibly counter-propagating. In the next Chapter we relate our results to recent experimental work.

# Chapter 5

# Linear response and relation to experiments

In the previous Chapter we analysed the noise in the edge current of a tunnelling point contact system. One of the main results is that the excess noise in the edge currents is completely determined by the noise in the tunnelling current through the relation

$$S_{\text{out}}^{\text{xc}}(\omega) = C_{I_B}(\omega) - \coth\left(\frac{\omega_Q}{2\pi k_B T}\right) R_{I_B}(\omega)$$

$$\rightarrow S_{I_B}(0) - 2k_B T \frac{dI_B}{dV_{\text{SD}}} \tag{5.1}$$

The second line is the zero frequency limit. These results are non-perturbative, and essentially a manifestation of charge conservation, and the symmetries and chirality of the edges. They are examples of non-equilibrium fluctuation-dissipation theorems as they relate different kinds of non-equilibrium noise.

Related to these NE-FDT's are so-called non-equilibrium Nyquist-Johnson relations. The equilibrium Nyquist-Johnson relation expresses the noise of a system in equilibrium in terms of its conductivity, $S_{\text{edge}}^{\text{eq}} = 2k_B T G$. The non-equilibrium generalization of this is to express the non-equilibrium noise (i.e. $S_{I_B}$ or $S_{\text{out}}^{\text{xc}}$) in terms of the non-equilibrium current (i.e. $I_B$). The biggest challenge here is to formulate this relation non-perturbatively, which is beyond the scope of this thesis. There are some results for this which make use of integrability properties of the Laughlin state [71, 73, 72, 74, 206]. However, these results are obtained in the context of the Laughlin state. In this Chapter we use linear response theory to compute the tunnelling current[1] this $I_B$, the noise in the tunnelling current $S_{I_B}$ and the excess noise in the edge current $S_{\text{out}}^{\text{xc}}$. This also formulates the NE-Nyquist-Johnson noise in the linear approximation of the tunnelling coupling constant. We then focus on the zero-frequency limit of the noise in the tunnelling and edge current.
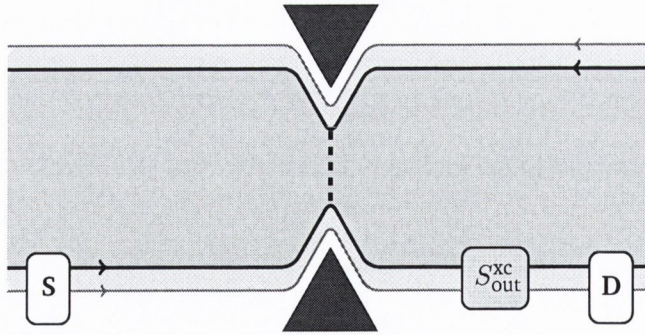
**Figure 5.1:** Figure of the point contact setup. A current is injected at the source $S$, flows chirally along the edge and is partially reflected at the point contact. A drain collects the current at $D$. The noise is measured at the probe $S_{out}^{xc}$, which is the noise of the edge current.

### Which noise is measured in the experiments?

Many theoretical efforts [41, 44, 157, 9, 36, 37] describe the (modification of) noise in the tunnelling current $S_{I_B}$. However, here we want to emphasize that this is not the noise which is measured in experiments such as Refs. [193, 55] (see below for a larger list of references to experimental papers). Figure 5.1 shows the experimental setup used to in these experiments. In particular, the probe which measures the noise is situated at the edge of the system. There is no probe which measures the tunnelling current or its noise directly.

The NE-FDT (5.1) does show that the measured noise is very closely related to the noise in the tunnelling current. The difference is due to the differential conductance. It has been shown [131] that in certain limits this differential conductance vanishes, and in this limit the excess noise reduces to the noise in the tunnelling current.

We emphasize that the analyses in experimental papers do not mistake the measured noise for the noise in the tunnelling current. However, as we describe below, experimental analyses use an expression for the noise which is based on non-interacting electrons.

### Generalized Nyquist-Johnson noise

Many experiments [193, 55, 95, 187, 94, 100, 114, 49, 46, 47, 115, 116, 64, 45, 13, 60, 62, 61, 63] measure the zero frequency noise and obtain the fractional charge of the tunnelling quasiparticle by making use of the shot noise limit. In this limit the tunnelling current can be viewed a series of independent, random tunnelling events where the probability of a quasiparticle tunnelling is constant. The corresponding noise $S_{I_B}$ is called Poissonian and it

---

[1]The tunnelling current is already computed in Chapter 2. However, many quantities are expressed in terms of the tunnelling current, so we briefly recall the main results of that chapter.

is related to the tunnelling current through the Schottky relation [194, 20]

$$S_{I_B} = QeI_B \, . \tag{5.2}$$

The fractional charge is determined by measuring the ratio $S_{I_B}/I_B$. The Schottky relation is the simplest approximation of a non-equilibrium Nyquist-Johnson expression.

However, all of the experiments referenced above also measure noise that goes beyond the shot noise limit and the Schottky relation does not apply. In this regime interaction effects become important and, consequently, the statistics of the anyons become important. To describe this regime requires a non-perturbative, non-equilibrium Nyquist-Johnson relation, which does not exist for anyons. Such a relation does exist for non-interacting electrons [150, 158, 30]. To circumvent this discrepancy Refs. [55, 187, 100, 114, 49, 46, 47, 115, 116, 64, 45, 13, 60, 62, 61, 63] make an educated guess and generalize the expression for the non-interacting electrons to anyons. We call this the "substitution approach". Starting with the expression for non-interacting electrons [150, 158, 30] the charge and conductivity are replaced by their fractional counterparts $e \to Qe$, $\frac{e^2}{2\pi} \to \nu\frac{e^2}{2\pi} = G_{\bar{\nu}}$. This results in the following formula for the excess noise in the edge current

$$S^{\text{xc}}_{\text{out}} = QeG_\nu V_{\text{SD}}\mathbb{T}(1 - \mathbb{T})\left(\coth\left(\frac{QeV_{\text{SD}}}{2\pi k_B T}\right) + \frac{2k_B T}{QeV_{\text{SD}}}\right) \tag{5.3}$$

where $QeV_{\text{SD}} = \omega_Q$ is the Josephson frequency and $V_{\text{SD}}$ is the source-drain voltage and we use units of $\hbar = 1$. Furthermore, $\mathbb{T}$ is the transmission and $G_{\bar{\nu}}$ the conductivity of the channel involved in the tunnelling (we define all these parameters in this Chapter).

**Overview of this chapter**

In this Section 5.1 we analyze the linear response theory of the tunnelling point contact. We compute the tunnelling current, noise and related quantities such as the transmission and Fano factors. In Section 5.2 we discuss the origin of the formula Eq. (5.3). We then compare the results of linear response theory to the linear approximation of Eq. (5.3). We show that Eq. (5.3) does *not* reproduce the results from linear response theory, as it fails to take into account the contributions due to the differential conductance. In particular, Eq. (5.3) does not take into account the statistics of the anyons (or, equivalently, the interaction effects of the edge). We propose a modification to Eq. (5.3) to resolve this discrepancy.

## 5.1 Linear response approximation

### 5.1.1 Tunnelling current

The linear response theory of the tunnelling current is treated in Chapter 2. For the upcoming discussion we provide here a short, concise summary based on Chapter 3.3, 3.4 and 3.5. The tunnelling operator is defined as $\mathcal{V} = \psi_L^\dagger \psi_R$, and from this we obtain the tunnelling Hamiltonian $H_T = \Gamma\mathcal{V} + \Gamma^*\mathcal{V}^\dagger$ and tunnelling current operator $\hat{I}_B = -iQe(\Gamma\mathcal{V} - \Gamma^*\mathcal{V}^\dagger)$. We use units of $\hbar = 1$. The effect of a voltage bias between the two edge is accounted for by the Josephson frequency phase factor $\mathcal{V} \longrightarrow e^{i\omega_Q t}\mathcal{V}(t)$, where $\omega_Q = QeV_{SD}$. In linear response we only keep the terms up to order $|\Gamma|^2$ in the tunneling coupling constant. After some manipulations (see Chapter 3.4) we obtain for the tunnelling current

$$I_B\left(\omega_Q\right) = = Qe|\Gamma|^2(1 - e^{-\omega/k_BT})G^>(\omega_Q) . \tag{5.4}$$

Here we use the tunneling-tunneling correlator $G^>(t) = \langle\mathcal{V}(t)\mathcal{V}^\dagger(0)\rangle$ and the KMS relation. These correlators are determined in Chapter 3.5. It was found that the correlators factorize into a product of two-point correlators; one for each edge.

$$G^>(t) = a_I\langle\psi_L^\dagger(t)\psi_L(0)\rangle\langle\psi_R(t)\psi_R^\dagger(0)\rangle + \ldots = a_I \prod_i v_i^{-2g_i} P_{2g_i}(t) + \ldots \tag{5.5}$$

where $i$ runs over the different channels, $g_i = 2h_i$ is twice the conformal dimension of each channel and $g = \sum_i g_i$. The dots represent finite-size corrections to the propagator. The universal form of its Fourier transform is given by (see Appendix (A.3.1) for a derivation)

$$P_{g_i}(\omega) = e^{\omega/(2k_BT)} (2\pi k_BT)^{g_i-1} B\left(\frac{g_i}{2} + i\frac{\omega}{2\pi k_BT}, \frac{g_i}{2} - i\frac{\omega}{2\pi k_BT}\right) . \tag{5.6}$$

This gives for the backscattering current at lowest order [215]

$$\boxed{I_B\left(\omega_Q\right) = |\tilde{\Gamma}(T)|^2 \sinh\left(\frac{\omega_Q}{2k_BT}\right) B\left(g + i\frac{\omega_Q}{2\pi k_BT}, g - i\frac{\omega_Q}{2\pi k_BT}\right) .} \tag{5.7}$$

Here we have combined all factors that are independent of the applied voltage into the non-universal normalisation $|\tilde{\Gamma}(T)|^2$

$$|\tilde{\Gamma}(T)|^2 = 2a_I Qe|\Gamma|^2 (2\pi k_BT)^{2g-1} \prod_i v_i^{-2g_i} . \tag{5.8}$$

In our analysis of experiments the temperature is kept fixed. The non-universality is due to the tunnelling coupling constant $\Gamma$ which depends on the experimental setup. A final quantity of interest is the transmission $\mathbb{T}$ of a channel. It reflects the amount of the electric current in an edge channel which flows from the source to the drain. The quantity $\mathbb{R} = 1 - \mathbb{T}$ is
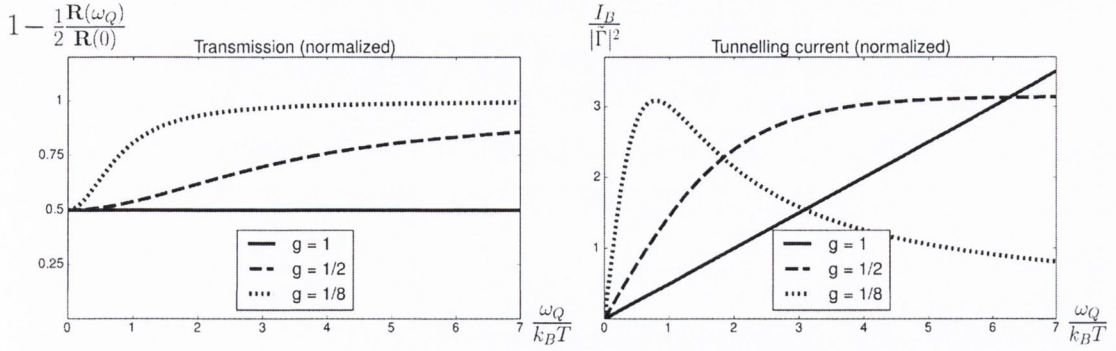
**Figure 5.2:** Plots of the "transmission" (left) and tunnelling current (right) for three values of $g$ as a function of $\frac{\omega_Q}{k_B T}$. The tunnelling current is normalized by $|\tilde{\Gamma}(T)|^2$. The left plot does not represent the true transmission, since its absolute value is non-universal. Instead, we plot $1 - \mathsf{C} \times \mathbb{R}(\omega_Q)$ with $\mathbb{R}$ the reflection and set the non-universal constant $\mathsf{C} = 1/(2\mathbb{R}(\omega_Q = 0))$. The true transmission is determined by linear response theory up to the non-universal constant $C$.

the reflection, which represents the amount of current reflected (backscattered) by the point contact. We have

$$\mathbb{T}(\omega_Q) = 1 - \frac{I_B(\omega_Q)}{G_{\bar{\nu}} V_{\mathrm{SD}}} \qquad (= 1 - \mathbb{R}(\omega_Q)) \tag{5.9}$$

$$G_{\bar{\nu}} = \bar{\nu} \frac{e^2}{2\pi} \tag{5.10}$$

where $\bar{\nu} = \nu - \nu_{\mathrm{bg}}$ is the filling fraction of the channel(s) involved in the tunnelling process, i.e. we subtract the conductivity from the background channels, which are fully transmitted. The quantity $G_{\bar{\nu}}$ is the conductivity of the channels involved in the tunnelling process. If there are no background channels then $\bar{\nu} = \nu$ and $I_0 = G_{\bar{\nu}} V_{\mathrm{SD}}$ equals the current through the system in the absence of a point contact (the equilibrium current). It is more common to work with the transmission than the reflection.

Figure 5.2 shows plots of the tunnelling current and the transmission for three cases of $g$. These three cases capture the qualitative dependency of the current on the conformal dimensions. For $g < \frac{1}{2}$ the tunnelling current vanishes as $\omega_Q \to \infty$ and the current is fully transmitted (transmission approaches one). In addition, there is a maximum in the tunnelling current. For $\frac{1}{2} \leq g < 1$ the transmission still approaches one as $\omega_Q \to \infty$, but the tunnelling current keeps increasing and the function does not have a maximum. For $g = 1$ the tunnelling current is linear in the source-drain voltage and the transmission is constant. Finally, the current always vanishes at $\omega_Q = 0$.

Given a fractional quantum Hall edge we can construct a tunnelling point contact model for each quasiparticle present in the theory. Renormalization group arguments [130] predict that the quasiparticle with the lowest conformal dimension ($g$) is the most relevant operator in

the RG sense. Therefore it is usually assumed that there is only one quasiparticle contributing to the tunnelling current (which is the quasiparticle with lowest conformal dimension). In the case of multiple quasiparticles with an equal conformal dimension the quasiparticle with the lowest electric charge should make the dominant contribution. The reason is that this particle has the largest effective magnetic length, as this length scales with $1/\sqrt{Q}$, i.e. $l_B = \sqrt{\frac{hc}{QeB}}$. The magnetic length is a measure for the size of a quasiparticle wavepacket along the edge.

### 5.1.2  Noise in the tunnelling and edge currents

**Finite frequency noise**

The noise the backscattered current at lowest order in $|\Gamma|^2$ is the Fourier transform of the autocorrelator[2]

$$\int e^{i\omega t} S_{I_B}(t) dt \cong \int e^{i\omega t} \langle \hat{I}_B(t) \hat{I}_B(0) \rangle dt$$
$$= (Qe)^2 |\Gamma|^2 \left[ G^>(\omega + \omega_Q) + e^{(\omega - \omega_Q)/k_B T} G^>(-(\omega - \omega_Q)) \right] \quad (5.11)$$

The tunneling current $I_B$ is given in terms of $G^>$ through (5.4). Using this expression we can relate the noise to the tunnelling current [41]

$$\boxed{S_{I_B}(\omega) = \frac{Qe}{2} \sum_{p=\pm} I_B\left(\omega + p\omega_Q\right) \left( \coth\left( \frac{\omega + p\omega_Q}{2k_B T} \right) + 1 \right).} \quad (5.12)$$

This relation is sometimes called a generalized or non-equilibrium Nyquist-Johnson relation [30], as it expresses the noise in terms of the tunnelling current. The symmetric and anti-symmetric noise are given by

$$C_{I_B}(\omega) = \frac{Qe}{2} \sum_{p=\pm} I_B\left(\omega + p\omega_Q\right) \coth\left( \frac{\omega + p\omega_Q}{2k_B T} \right) \quad (5.13)$$

$$R_{I_B}(\omega) = \frac{Qe}{2} \sum_{p=\pm} I_B\left(\omega + p\omega_Q\right). \quad (5.14)$$

The excess noise of the outgoing edge current is given by Eq. (5.1). At linear response this results in [42, 10]

$$\boxed{S_{\text{out}}^{\text{xc}}(\omega) = \frac{Qe}{2} \sum_{p=\pm} I_B\left(\omega + p\omega_Q\right) \left( \coth\left( \frac{\omega + p\omega_Q}{2k_B T} \right) - \coth\left( \frac{\omega}{2k_B T} \right) \right)} \quad (5.15)$$

This noise is already symmetric, i.e. $S_{\text{out}}^{\text{xc}}(\omega) = C_{\text{out}}^{\text{xc}}(\omega)$. Finite (i.e. non-zero) frequency noise could be used as an experimental probe to determine properties of the tunnelling quasiparticle

---

[2]The standard definition of power noise, which is also used in the experiments, refers to the cosine transformation of the symmetric combination of the current $\int dt \cos(\omega t) \langle \{ I_B(t), I_B(0) \} \rangle$. This noise equals the symmetric noise of the definition used here times a factor of 2.
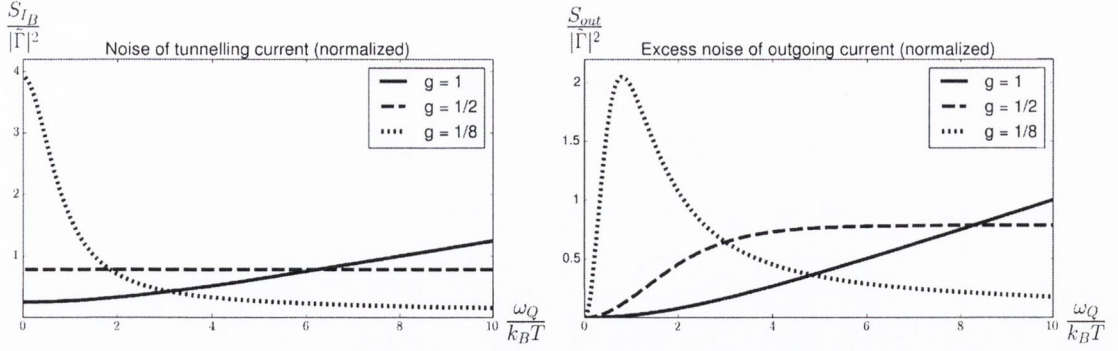
**Figure 5.3:** Plots of noise in the tunnelling current $S_{I_B}$ (left) and the excess noise in the edge current (right) for three values of $g$. The noise is normalized by dividing it by $|\tilde{\Gamma}(T)|^2$. We use units of $e = 1$ and we set $Q = 1/4$.

[42, 10, 37]. However, current experiments focus on the zero frequency limit which we treat in the remainder of this Chapter. We will not explore the properties of finite frequency noise in greater detail, although this is certainly an interesting topic to investigate further. A possible topic is the finite frequency noise of a fractional quantum Hall interferometer, which would unite the results from Chapter 3 and 4.

### Zero frequency limit

In the zero frequency limit we take $\omega \downarrow 0$. This gives

$$S_{I_B}(0) = C_{I_B}(0) = Qe \coth\left(\frac{\omega_Q}{2k_BT}\right) I_B(\omega_Q) \tag{5.16}$$

$$R_{I_B}(0) = Qe I_B(\omega_Q) \tag{5.17}$$

In the zero temperature limit ($k_BT \ll \omega_Q$) we recover the Schottky relation [194], as $\coth(x) \to 1$ for $x \to \infty$, and so $S_{I_B} = Qe I_B$. This is the shot noise regime. In this limit statistical effects do not play a role and the tunnelling can be viewed as a Poisson process, hence the noise is called Poissonian. For the differential conductance we obtain

$$\frac{dI_B}{dV_{\text{SD}}} = \frac{Qe}{2k_BT} I_B(\omega_Q)\left(\coth\left(\frac{\omega_Q}{2k_BT}\right) - \frac{2}{\pi}\text{Im}\left[\psi\left(g + i\frac{\omega_Q}{2\pi k_BT}\right)\right]\right). \tag{5.18}$$

which gives for the excess noise (using Eq. (5.1) or taking the $\omega \downarrow 0$ limit of Eq. (5.15))

$$S_{\text{out}}^{\text{xc}}(0) = \frac{2Qe}{\pi} I_B(\omega_Q)\text{Im}\left[\psi\left(g + i\frac{\omega_Q}{2\pi k_BT}\right)\right]. \tag{5.19}$$

Here $\psi(x) = \frac{\Gamma'[x]}{\Gamma[x]}$ is the digamma function and we are taking the imaginary part (note that $\overline{\psi(z)} = \psi(\bar{z})$). For large $\frac{\omega_Q}{2k_BT}$ (shot noise limit) we have the limit [68]

$$\lim_{x \to \infty}\left\{\coth(\pi x) - \frac{2}{\pi}\text{Im}\left[\psi(g + ix)\right]\right\} = 0 \tag{5.20}$$
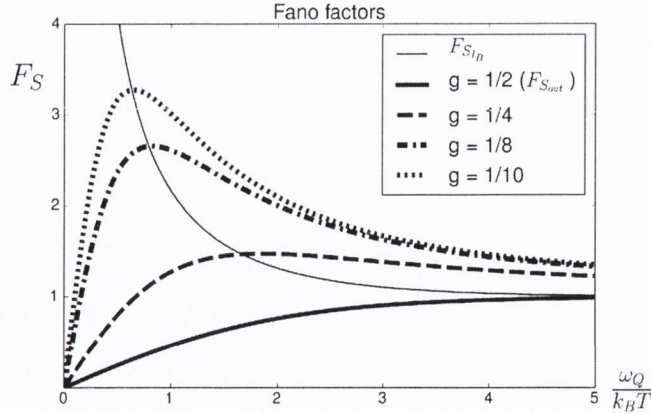
**Figure 5.4:** Plots of the Fano factor $F_{S_{\text{out}}}$ for multiple values of $g$. The case of $g = \frac{1}{2}$ is a boundary case, as for $g < \frac{1}{2}$ the function $F_{S_{\text{out}}}(\omega_Q)$ always has a maximum. The gray line represents the Fano factor $F_{S_{I_B}}$, which is independent of $g$. All functions converge to a value of 1, which is the shot noise limit. The noise in the edge current changes from sub- to super-Poissonian behaviour as a function of $\frac{\omega_Q}{k_B T}$ for $g < \frac{1}{2}$. For $g \geq \frac{1}{2}$ the noise is always sub-Poissonian.

Therefore the differential conductance vanishes in the shot noise limit, and $S_{\text{out}}^{\text{xc}} = S_{I_B}$ [131]. Put differently, in the shot noise limit fluctuations in the tunnelling current carry over to the edge current and there is no additional backreaction between the tunnelling and edge current. The backreaction (differential conductance) is thermally activated, meaning this contribution vanishes when $k_B T \ll \omega_Q$. We have

$$S_{I_B}(0) \cong S_{\text{out}}^{\text{xc}}(0) \quad \text{and} \quad \frac{dI_B}{dV} \to 0 \qquad \text{when} \quad \frac{\omega_Q}{2k_B T} \to \infty. \tag{5.21}$$

Figure 5.3 shows plots of the zero frequency noise in the tunnelling current and the excess noise in the edge current for three cases of $g$ (same cases appear in Figure 5.2). We emphasize some important qualitative behaviour. The two types of noise show different behaviour at the origin. By definition, the excess noise always vanishes when $\omega_Q = 0$. This is not the case for $S_{I_B}$ (for $g < \frac{1}{2}$), where the maximum value is located at $\omega_Q = 0$. Asymptotically (large $\frac{\omega_Q}{2k_B T}$, which is the shot noise limit) the two types of noise become equal.

Alternatively, we can write the zero frequency relations in terms of the transmission Eq. (5.9), source-drain voltage ($\omega_Q = QeV_{\text{SD}}$) and the conductivity of the channel

$$S_{I_B}(0) = (1 - \mathbb{T})G_{\bar{\nu}}QeV_{\text{SD}} \coth\left(\frac{QeV_{\text{SD}}}{2k_B T}\right) \tag{5.22}$$

$$S_{\text{out}}^{\text{xc}}(0) = \frac{2}{\pi}(1 - \mathbb{T})G_{\bar{\nu}}QeV_{\text{SD}}\text{Im}\left[\psi\left(g + i\frac{QeV_{\text{SD}}}{2\pi k_B T}\right)\right] \tag{5.23}$$

This notation is commonly used in the Landauer-Büttiker approach to which we will return.

**Fano factors**

A Fano factor is a measure of the fluctuations compared to the "mean" (average current). Ref. [20] defines it as the ratio of the noise over the noise in the shot noise limit. The Fano factor is a measure for sub- ($F < 1$) or super-Poissonian ($F > 1$) noise. A Fano factor different from one means that effects due to the anyon's statistics become important. We define $F_{S_{I_B}}$ as the Fano factor of the noise $S_{I_B}$. The shot noise limit corresponds to $QeI_B$ and so

$$F_{S_{I_B}} = \frac{S_{I_B}(0)}{QeI_B} = \coth\left(\frac{\omega_Q}{2k_BT}\right) . \tag{5.24}$$

The function on the right hand side converges to one for large argument where the shot noise limit is reached. The function $\coth(x) > 1$ for all $x > 0$, therefore the noise is strictly super-Poissonian ($F > 1$). The Fano factor is independent of the statistics of the tunnelling anyon and the super-Poissonian characteristic is due to thermal effects.

Another Fano factor is that of the excess noise of the edge current. This current has the same shot noise limit as the noise in the tunnelling current, and so

$$F_{S_{\text{out}}} = \frac{S_{\text{out}}^{\text{xc}}(0)}{QeI_B} = \frac{2}{\pi}\text{Im}\left[\psi\left(g + i\frac{\omega_Q}{2\pi k_BT}\right)\right] . \tag{5.25}$$

This expression also appears in [120]. This Fano factor depends explicitly on the conformal dimension, which is not the case with the other Fano factor Eq. (5.24) (although implicitly $Q$ is determined by the conformal dimension of the charged channel). The statistical properties of the anyons determine the properties of this Fano factor. However, the Fano factor does not distinguish between Abelian and non-Abelian anyons.

Figure 5.4 shows plots for the Fano factors for multiple values of $g$. The Fano factor of the edge current shows both sub- ($F < 1$) and super-Poissonian ($F > 1$) behaviour when $g < \frac{1}{2}$. For $g > \frac{1}{2}$ the noise is strictly sub-Poissonian. This non-Poissonian characteristic depends on the conformal dimension of the anyon (with $g = 2h$). Ref. [120] attributes properties of this Fano factor to "thermal bunching" as the noise is enhanced due to a combination of thermal fluctuations and the anyon's statistics. Even at linear response the statistics already plays an important in the properties of the Fano factor of the excess noise of the edge current. This is not the case for the Fano factor of the tunnelling current.

### 5.1.3 Simplifications for special cases of $g$

For two values of $g$ ($g = \frac{1}{2}$ and $g = 1$) the expressions for the tunnelling current and noise simplify. The case of $g = \frac{1}{2}$ is, for instance, realized by an $e/4$ quasiparticle of the Anti-Pfaffian state [151, 148]. The case of $g = 1$ corresponds to a fermion, and is realized for instance by electrons of an integer QH edge state. Note that the interactions of a *fractional* QH edge cause

the electrons to have a $g > 1$, so the case of $g = 1$ does not apply to the electrons of fractional edges (interacting electrons have half-integer $h$ greater than $\frac{1}{2}$). The simplifications are due to a reflection formula of the gamma function which relates $\Gamma(1-x)\Gamma(x) = \frac{\pi}{\sin(\pi x)}$ (see Ref. [68] and the appendix). This gives for the tunnelling current and differential conductance

$$I_B(\omega_Q) = |\tilde{\Gamma}(T)|^2 \times \begin{cases} \sqrt{\pi}\tanh\left(\frac{\omega_Q}{2k_BT}\right) & g = \frac{1}{2} \\ \pi\dfrac{\omega_Q}{2k_BT} & g = 1 \end{cases} \tag{5.26}$$

$$\frac{dI_B}{dV_{\rm SD}} = \frac{Qe}{2k_BT}|\tilde{\Gamma}(T)|^2 \times \begin{cases} \sqrt{\pi}\cosh\left(\frac{\omega_Q}{2k_BT}\right)^{-2} & g = \frac{1}{2} \\ \pi & g = 1 \end{cases} \tag{5.27}$$

The tunnelling current becomes constant ($g = \frac{1}{2}$) or grows linear with $V_{\rm SD}$ ($g = 1$). In addition $|\tilde{\Gamma}(T)|^2$ is independent of $T$ for $g = \frac{1}{2}$ and $|\tilde{\Gamma}(T)|^2 \propto T$ for $g = 1$. The transmission $\mathbb{T}$ is constant for non-interacting electrons ($g = 1$), and will tend to zero for $g = \frac{1}{2}$ and $\omega_Q \to \infty$. For the zero frequency limit the expressions for the noise become

$$S_{I_B}(0) = Qe|\tilde{\Gamma}(T)|^2 \times \begin{cases} \sqrt{\pi} & g = \frac{1}{2} \\ \pi\dfrac{\omega_Q}{2k_BT}\coth\left(\frac{\omega_Q}{2k_BT}\right) & g = 1 \end{cases} \tag{5.28}$$

$$S_{\rm out}^{\rm xc}(0) = Qe|\tilde{\Gamma}(T)|^2 \times \begin{cases} \sqrt{\pi}\tanh\left(\frac{\omega_Q}{2k_BT}\right)^2 & g = \frac{1}{2} \\ \pi\left(\dfrac{\omega_Q}{2k_BT}\coth\left(\frac{\omega_Q}{2k_BT}\right) - 1\right) & g = 1 \end{cases} \tag{5.29}$$

Finally, we also have the Fano factor $F_{S_{\rm out}}$ (the other Fano factor is independent of $g$)

$$F_{S_{\rm out}} = Qe \times \begin{cases} \tanh\left(\frac{\omega_Q}{2k_BT}\right) & g = \frac{1}{2} \\ \left(\coth\left(\frac{\omega_Q}{2k_BT}\right) - \dfrac{2k_BT}{\omega_Q}\right) & g = 1 \end{cases} \tag{5.30}$$

## 5.2 Landauer-Büttiker formalism

### 5.2.1 Non-interacting electrons in the Landauer-Büttiker formalism

In the Landauer-Büttiker formalism [29, 20, 167] the tunnelling point contact is approached through a transmission formalism. The electrons reside in reservoirs held at a chemical potential $\mu_L$ and $\mu_R$. These reservoirs are connected through some transmission channels, and to each channel we associate a transmission amplitude or coefficient which represents the probability of an electron tunnelling through this channel. The total current is determined by (1) the sum or integral over all transmission probabilities and (2) the Fermi-Dirac distribution of both reservoirs (since electrons can only tunnel from a filled to an empty state).

To be exact, we consider tunnelling of non-interacting electrons through one channel and allow for an *energy-dependent transmission coefficient* $t(\omega)$. This quantity is not the same as the (total) transmission $\mathbb{T}$ defined in Eq. (5.9). In particular, we formulate the problem here is a transmission problem between the edges, with $t(\omega)$ representing the probability that a wave packet of energy $\omega$ tunnels from the lower to the upper edge. The Fermi-Dirac distributions of the two reservoirs are given by $f_i(\omega) = (e^{(\omega - \mu_i)/k_B T} + 1)^{-1}$ with $i = L, R$ and $\mu_L - \mu_R = eV_{SD}$ the Josephson frequency ($\omega_Q = eV_{SD}$ for $Q = 1$). In this formalism the total current flowing from one reservoir to the other is given by [167]

$$ I = \frac{e}{2\pi} \int_{-\infty}^{\infty} (f_L(\omega) - f_R(\omega)) t(\omega) d\omega \tag{5.31} $$

In general, $t(\omega)$ is some geometric-dependent function. The advantage of this approach is that it is not restricted by the particular model used for the point contact. All information regarding the tunnelling probability is attributed to the (unknown) transmission coefficient $t(\omega)$. In particular, the resulting expressions for the noise also hold for small modifications of the point contact model.

In our simple model we compute the tunnelling perturbatively in $|\Gamma|^2$, which is equivalent to a linear approximation in $t(\omega)$ in the Landauer-Büttiker formalism. Using this formalism the noise in tunnelling point contacts of *non-interacting electrons* is analysed non-perturbatively in Refs. [150, 158, 30]. In these references the expression for the zero frequency noise is found to be

$$ S_{I_B} = G \int_{-\infty}^{\infty} t(\omega)\big(f_L(1 - f_R) + f_R(1 - f_L)\big) - t(\omega)^2 (f_L - f_R)^2 d\omega . \tag{5.32} $$

Here $G = \frac{e^2}{2\pi}$ is the unit of conductance. This expression is a generalized or non-equilibrium Nyquist-Johnson relation. From the expression for the current we can also obtain a Landauer-like expression for the differential conductance

$$ \frac{dI}{dV_{SD}} = G \int_{-\infty}^{\infty} \frac{t(\omega)}{2k_B T}(f_L(1 - f_L) + f_R(1 - f_R)) + (f_L - f_R)\frac{dt(\omega)}{d(eV_{SD})} d\omega . \tag{5.33} $$

Here we used $2k_B T \frac{d}{dV} f_{L,R} = \pm f_{L/R}(1 - f_{L,R})$. Finally, using our general formula we also obtain a Landauer-like expression for the excess noise of the edge current

$$ S_{out}^{xc} = G \int_{-\infty}^{\infty} t(\omega)(f_L - f_R)^2 - t(\omega)^2 (f_L - f_R)^2 + 2k_B T(f_L - f_R)\frac{dt(\omega)}{d(eV_{SD})} d\omega . \tag{5.34} $$

This expression is obtained in Refs. [158, 30] using a scattering ($S$-matrix) formalism of electron wave packets. However, in these references the final term involving the derivative of the transmission is absent, as it is assumed that the transmission is independent of the applied voltage bias. The formalism presented in this subsection has not been developed for strongly interacting systems or tunnelling anyons.

**Energy independent transmission**

The expressions appearing in the preceding discussion apply to systems of non-interacting electrons. Therefore it is perhaps uprising to see that many experiments [55, 187, 100, 114, 49, 46, 47, 115, 116, 64, 45, 13, 60, 62, 61, 63] determine the fractional charge using a modified non-equilibrium Nyquist-Johnson relation based on the non-interacting case. This formula, Eq. (5.39) below, is obtained by assuming an energy independent transmission $t(\omega) = t$, replacing the charge by the fractional charge $e \to Qe$ and the conductivity by the conductivity of the FQH channel involved in the tunnelling $G \to G_{\bar{\nu}}$.

To obtain this expression we start with the tunnelling current and a $t(\omega)$ which is energy-independent. Then the tunnelling current becomes linear in $V_{\text{SD}}$ as can be seen by performing the integral over $\omega$

$$I_B = \frac{e}{2\pi} t \int_{-\infty}^{\infty} (f_1(\omega) - f_2(\omega)) d\omega = G t V_{\text{SD}} . \tag{5.35}$$

Since by definition $\mathbb{T} = 1 - I_B/(G V_{\text{SD}})$ we have $\mathbb{T} = 1 - t$ in this special case. With a constant transmission the integrals appearing in the expression for the noise Eq. (5.32) and Eq. (5.34) can be performed. This results in

$$S_{I_B} = \mathbb{T}(1 - \mathbb{T}) G e V_{\text{SD}} \coth\left(\frac{e V_{\text{SD}}}{2k_B T}\right) + 2k_B T G (1 - \mathbb{T})^2 \tag{5.36}$$

$$S_{\text{out}}^{\text{xc}} = \mathbb{T}(1 - \mathbb{T}) G \left(e V_{\text{SD}} \coth\left(\frac{e V_{\text{SD}}}{2k_B T}\right) - 2k_B T\right) \tag{5.37}$$

and $\frac{dI}{dV_{\text{SD}}} = G$. Finally, the formula used to determine the fractional charge is obtained by replacing the charge and conductance by their fractional counterparts

Substitution approach (non-perturbative)

$$\boxed{S_{I_B} = \mathbb{T}(1 - \mathbb{T}) G_{\bar{\nu}} Q e V_{\text{SD}} \coth\left(\frac{Q e V_{\text{SD}}}{2k_B T}\right) + 2k_B T G_{\bar{\nu}} (1 - \mathbb{T})^2} \tag{5.38}$$

$$\boxed{S_{\text{out}}^{\text{xc}} = \mathbb{T}(1 - \mathbb{T}) G_{\bar{\nu}} \left(Q e V_{\text{SD}} \coth\left(\frac{Q e V_{\text{SD}}}{2k_B T}\right) - 2k_B T\right) .} \tag{5.39}$$

For completeness we also provided the equivalent generalization of the noise in the tunnelling current, although this expression is not used in experiments to determine the fractional charge. In the next subsection we compare these expressions to the results from linear response theory. However, it is already apparent that one assumption cannot hold: the transmission is not constant in the case of tunnelling anyons. Therefore the manipulations leading up to Eq. (5.38) and Eq. (5.39) cannot be correct when we consider anyons. We therefore assume Eq. (5.38) and Eq. (5.39) also hold when the transmission is a function of the source-drain voltage, $\mathbb{T} \to \mathbb{T}(\omega_Q)$.

## 5.2.2 Comparison between two approaches

To summarize, in the "substitution approach" outlined in the previous subsection we start with an expression for the noise of tunnelling, non-interacting electrons which is based on a constant transmission. We then replace the charge and conductivity by the equivalent quantities of the fractional quantum Hall edge, and we assume the transmission is energy-dependent. We now compare the linear approximation of this "substitution approach" to the results from the linear response theory of a FQH tunnelling point contact.

Let us recall and compare the results from linear response theory (L.R.) of the model of a point contact (Eq. (5.22) and Eq. (5.23)) to the linear approximation of Eq. (5.38) and Eq. (5.39))

Model of point contact (L.R.)          Substitution approach (L.R.)

$$S_{I_B} = (1 - \mathbb{T})G_{\bar{\nu}}QeV_{\text{SD}}\coth\left(\frac{QeV_{\text{SD}}}{2k_BT}\right) \qquad S_{I_B} = (1 - \mathbb{T})G_{\bar{\nu}}QeV_{\text{SD}}\coth\left(\frac{QeV_{\text{SD}}}{2k_BT}\right)$$

$$S_{\text{out}}^{\text{xc}} = (1 - \mathbb{T})G_{\bar{\nu}}QeV_{\text{SD}}\frac{2}{\pi}\text{Im}\left[\psi\left(g + i\frac{\omega_Q}{2\pi k_BT}\right)\right] \quad S_{\text{out}}^{\text{xc}} = (1 - \mathbb{T})G_{\bar{\nu}}\left(QeV_{\text{SD}}\coth\left(\frac{QeV_{\text{SD}}}{2k_BT}\right) - 2k_BT\right)$$

Linear response theory shows that the "substitution approach" fails for the excess noise, but is consistent for the noise in the tunnelling current. This is related to the properties of the Fano factor which we explored in Section 5.1.2. The Fano factor associated with $S_{I_B}$ does not depend on the statistical properties of the anyon. It is therefore *not* unreasonable to simply replace the charge, conductivity and transmission by their fractional values in the expression for $S_{I_B}$, provided we allow for an energy-dependent transmission. This is not the case for the excess noise Eq. (5.38), which fails to reproduce the results from linear response theory. This is attributed to the incorrect assumption of a transmission independent of the voltage bias and energy.

### An ansatz for the non-perturbative expression of the noise

We provide an alternative "educated guess" which assumes the expression for $S_{I_B}$ from the substitution approach (Eq. (5.38)) holds. This is our first of two ansatzes. The expression for the excess noise in the edge current is obtained using the fluctuation-dissipation theorem from the previous chapter, Eq. (5.1). First, we can write the differential conductance as

$$\frac{dI_B}{dV_{\text{SD}}} = \frac{d((1 - \mathbb{T})G_{\bar{\nu}}V_{\text{SD}})}{dV_{\text{SD}}} = G_{\bar{\nu}}(1 - \mathbb{T}) - G_{\bar{\nu}}V_{\text{SD}}\frac{d\mathbb{T}}{dV_{\text{SD}}} \tag{5.40}$$

Using Eq. (5.1) and replacing $S_{I_B}$ by Eq. (5.38) and the transmission by Eq. (5.40) gives

First ansatz

$$S_{I_B} = \mathbb{T}(1-\mathbb{T})G_{\bar{\nu}}QeV_{\text{SD}}\coth\left(\frac{QeV_{\text{SD}}}{2k_BT}\right) + 2k_BTG_{\bar{\nu}}(1-\mathbb{T})^2$$

$$S_{\text{out}}^{\text{xc}} = \mathbb{T}(1-\mathbb{T})G_{\bar{\nu}}\left(QeV_{\text{SD}}\coth\left(\frac{QeV_{\text{SD}}}{2k_BT}\right)\right) - 2k_BT\right) + \delta S_{\text{out}}^{\text{xc}}. \qquad (5.41)$$

where

$$\delta S_{\text{out}}^{\text{xc}} = 2k_BTG_{\bar{\nu}}V_{\text{SD}}\frac{d\mathbb{T}}{dV_{\text{SD}}} \qquad (5.42)$$

is the term which is absent in the substitution approach. For completeness we have repeated the expression for $S_{I_B}$. We stress that in this expression the transmission $\mathbb{T} = 1 - I_B/(G_{\bar{\nu}}V_{\text{SD}})$ and conductivity $G_{\bar{\nu}} = \bar{\nu}\frac{e^2}{2\pi\hbar}$ are associated with the channel involved in the tunnelling process. The background currents (fully transmitted) do not enter the definition of the transmission $\mathbb{T}$. The extra term vanishes when $\frac{d\mathbb{T}}{dV_{\text{SD}}} = 0$, which is valid for non-interacting electrons but not for strongly interacting systems.

## A second ansatz

Results from Ref. [39] show that the symmetric, finite frequency noise of the tunnelling current due to a chiral boson has the following limit near zero frequency

$$\lim_{\omega\downarrow0}\frac{C_{I_B}(\omega) - C_{I_B}(0)}{\omega} = 2\frac{1}{G_{\bar{\nu}}}\left(\frac{dI_B}{dV_{\text{SD}}}\right)^2. \qquad (5.43)$$

This limit is quadratic in $I_B$ and therefore does not appear at linear response. The expression for the noise $S_{I_B}$ from the substitution approach does not reproduce this limit, which brings the validity of Eq. (5.41) into question. It is not unreasonable to make a second ansatz which incorporates this limit. This is also done in Ref. [206]. Ref. [206] uses a non-perturbative approach towards the $e/3$ quasiparticle in the $\nu = 1/3$ Laughlin state. In particular, in Eq. (5.41) for $S_{I_B}$ we replace

$$(1-\mathbb{T})^2 = \left(\frac{I_B}{G_{\bar{\nu}}V_{\text{SD}}}\right)^2 \longrightarrow \left(\frac{1}{G_{\bar{\nu}}}\frac{dI_B}{dV_{\text{SD}}}\right)^2 \qquad (5.44)$$

$$\mathbb{T}(1-\mathbb{T})G_{\bar{\nu}}V_{\text{SD}} = \left(1 - \frac{I_B}{G_{\bar{\nu}}V_{\text{SD}}}\right)I_B \longrightarrow \left(1 - \frac{1}{G_{\bar{\nu}}}\frac{dI_B}{dV_{\text{SD}}}\right)I_B \qquad (5.45)$$

which gives (using the NE-FDT for the excess noise)

$$S_{I_B} = QeI_B\left(1 - \frac{1}{G_{\bar{\nu}}}\frac{dI_B}{dV_{\text{SD}}}\right)\coth\left(\frac{QeV_{\text{SD}}}{2k_BT}\right) + 2k_BT\frac{1}{G_{\bar{\nu}}}\left(\frac{dI_B}{dV_{\text{SD}}}\right)^2 \qquad (5.46)$$

$$S_{\text{out}}^{\text{xc}} = QeI_B\left(1 - \frac{1}{G_{\bar{\nu}}}\frac{dI_B}{dV_{\text{SD}}}\right)\coth\left(\frac{QeV_{\text{SD}}}{2k_BT}\right) - 2k_BT\left(\frac{dI_B}{dV_{\text{SD}}}\right)\left(1 - \frac{1}{G_{\bar{\nu}}}\frac{dI_B}{dV_{\text{SD}}}\right) \qquad (5.47)$$

This ansatz for $S_{I_B}$ was numerically compared to results from the non-perturbative approach and showed excellent agreement [206]. These expressions are also again consistent with the results from linear response theory (keeping only terms linear in $I_B$). In terms of the transmission (using Eq. (5.40)) these expressions are given by

Second ansatz

$$\boxed{S_{I_B} = Qe\mathbb{T}(1 - \mathbb{T})G_{\tilde{\nu}}V_{\text{SD}}\coth\Big(\frac{QeV_{\text{SD}}}{2k_BT}\Big) + 2k_BTG_{\tilde{\nu}}(1 - \mathbb{T})^2 + \delta S_{I_B}}$$

$$\boxed{S_{\text{out}}^{\text{xc}} = \mathbb{T}(1 - \mathbb{T})G_{\tilde{\nu}}\Big[QeV_{\text{SD}}\coth\Big(\frac{QeV_{\text{SD}}}{2k_BT}\Big) - 2k_BT\Big] + \delta S_{\text{out}}^{\text{xc}}} \tag{5.48}$$

where

$$\delta S_{I_B} = V_{\text{SD}}\frac{d\mathbb{T}}{dV_{\text{SD}}}(1 - \mathbb{T})G_{\tilde{\nu}}\Big[QeG_{\tilde{\nu}}V_{\text{SD}}\coth\Big(\frac{QeV_{\text{SD}}}{2k_BT}\Big) - 4k_BT\Big] + 2k_BTG_{\tilde{\nu}}\Big(V_{\text{SD}}\frac{d\mathbb{T}}{dV_{\text{SD}}}\Big)^2 \tag{5.49}$$

$$\delta S_{\text{out}}^{\text{xc}} = \delta S_{I_B} + 2k_BTG_{\tilde{\nu}}V_{\text{SD}}\frac{d\mathbb{T}}{dV_{\text{SD}}} \tag{5.50}$$

This ansatz might be too ambitious considering its complexity. However, it does have a feature (the squared term $\big(\frac{d\mathbb{T}}{dV_{\text{SD}}}\big)^2$) which qualitatively explains discrepancies observed in recent experiments.

The second ansatz adds more complexity compared to the first. The most important feature that both ansatzes posses is that they depend on the differential transmission. Such a term does not appear in the non-interacting case on which the substitution approach is based.

Why do we care about this differential term? One reason, which we explore further in the next section, is that it might account for recent experimental work which shows that the results from the substitution approach do not always explain the measured shot noise. In these experiments a large variation in the transmission is observed, which could explain why the substitution approach breaks down: it fails to take into account the slope of the transmission.

A second reason is that it is quite reasonable to include such a term in the noise for strongly interacting system. The Landauer approach for non-interacting electrons treats the single-electron states at energy $\omega$ as completely decoupled [158, 30]. In a strongly interacting system the quasiparticles are collective excitations of the system. The tunnelling of a quasiparticle cannot be decomposed into the simple picture where each wavepacket of energy $\omega$ tunnels independently through the point contact. Instead, correlation effects need to be taken into account.

## 5.3 Relation to experiments

We now consider some experiments which measure noise outside the pure shot noise regime. We do not at this point have a detailed analysis of the experimental data of these experiments, but we do identify some problems that are associated with the analyses of the zero frequency noise. We suggest that our analysis hints at least at a qualitative solution to these problems.

### Shot noise results from $\nu = 1/3$

Zero frequency noise has been very successfully employed in measuring the $e/3$ charge in tunnelling experiments conducted at the $\nu = 1/3$ state [193, 55]. To measure the charge Glattli, et al. (the authors of Ref. [193] and later experiments [95, 94] ) employ the following formula (based on the work of Ref. [131] which provide a linear approximation of the NE-FDT for the $\nu = 1/3$ state)

$$S_{\text{out}}^{\text{xc}} = QeI_B \coth\left(\frac{QeV_{\text{SD}}}{2k_BT}\right) - 2k_BT\frac{dI_B}{dV_{\text{SD}}} \ . \tag{5.51}$$

This expression also follows from linear response theory, see Eq. (5.23), but without an explicit expression for the differential conductance $\frac{dI_B}{dV_{\text{SD}}}$. Consequently, the analyses performed here match with the linear response theory, and therefore also with the linear approximation of the proposed expressions Eq. (5.41) and Eq. (5.48).

Ref. [55], which is experimental work performed by a different group of Heiblum et al., does not make use of this expression but instead applies the results from the substitution approach, Eq. (5.39). They measure the same charge of $e/3$ at the $\nu = 1/3$ plateau. A possible explanation for the fact that both approaches measure the same fractional charge is that Ref. [55] also reports a constant transmission $\mathbb{T}$ for each of their measurements, which means $\frac{d\mathbb{T}}{dV_{\text{SD}}} = 0$. In that case the proposed expressions reduce to the result of the substitution approach.

### Shot noise experiments involving other states

The success of measuring the $e/3$ quasiparticle at the $\nu = 1/3$ plateau has not been replicated for all other filling fractions. In fact, more recently the shot noise technique as a tool to measure the quasiparticle charge has been questioned [60, 61].

Experimental work that followed after the $e/3$-discovery looked at different plateaux and considered the low transmission regime. These included $\nu = 2/5, 3/7$ and $2/3$ in the lowest Landau level and $\nu = 5/2, 8/3, 7/3$ in the second Landau level [187, 100, 114, 49, 46, 47, 115, 116, 64, 45, 13, 60, 62, 61, 63]. In all these references the noise is fitted using the results from
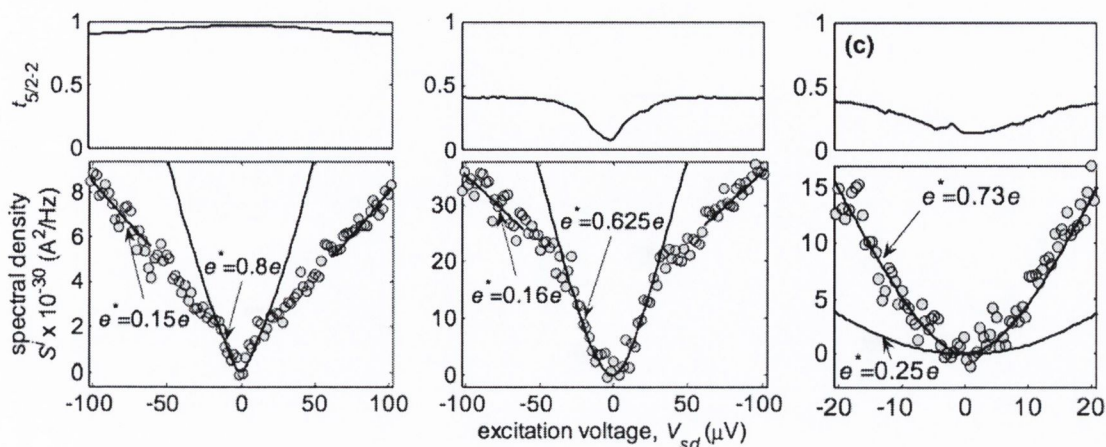
**Figure 5.5:** These plots of zero frequency noise measurements are taken from Ref. [61]. They show multiple measurements of the noise and transmission for filling fraction $\nu = 5/2$. The upper plots represent the measured transmission and the lower plots the corresponding measurements of the zero frequency noise. The noise is fitted to the expression from the substitution approach and these fits performs poorly when the entire range of the voltage is taken into account. A clear correlation is present between a non-constant transmission and the appearence of a dip in the noise. Note that the voltage range on the right figure is much smaller compared to the other two figures.

the substitution approach. We do not go through all these papers, but do note that especially in experiments which measure shot noise in the $\nu = 5/2$ plateau, the noise measurements do not provide consistent predictions of the quasiparticle charge [60, 61] (similar behaviour is found at other plateaux). In particular, the measurement of an $e/4$ charge in the $\nu = 5/2$ state was already announced in 2008 (see Ref. [64]) on the basis of shot noise measurements, but more recent work showed that the noise predicted by the substitution approach does not fit the measured noise well nor is it consistent with a charge of $e/4$. This is especially the case at lower voltages and low temperature.

Figures 5.5 and 5.6 show plots taken from Ref. [60, 61]. The fits shown in these plots are generated using the formula for the noise from the substitution approach. These fits perform poorly if the entire range of source-drain voltage is considered, and it is not clear what region should be used to determine the quasiparticle charge. In particular, near low voltages there is a sudden dip in the the measured noise. This occurs simultaneously with a sudden increase or decrease in the transmission. The slope of the transmission is non-zero. This is especially clear in Figure 5.6, which shows shot noise experiments of the $\nu = 1/3$ plateau. The left figure shows a clear dip in the shot noise which is associated with a clear mound in the transmission.

We conjecture that this explains the failure of the fits, at least at a qualitative level. Even at
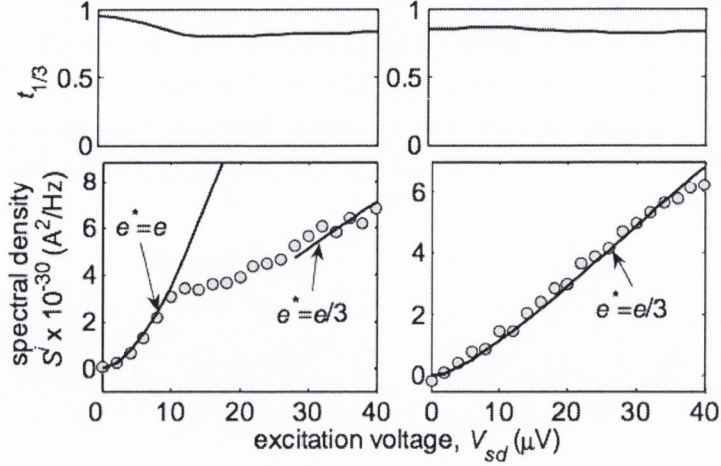
**Figure 5.6:** Same type of plots and fits as Figure 5.5, taken from Ref. [61] but now for measurements of $\nu = 1/3$. Upper plots are the measured transmission, and lower plots are the corresponding measured zero frequency noise. In the right plot the transmission is almost flat and the noise shows a good fit according the substitution approach. In the left plot the transmission is not flat, and the noise is poorly fitted using the the substitution approach. To account for these discrepancies we conjecture that the slope of the transmission $\frac{d\mathbb{T}}{dV_{SD}}$ needs to be taken into consideration.

linear response our proposed expressions for the noise Eq. (5.41) and Eq. (5.48) predict that the derivative $\frac{d\mathbb{T}}{dV_{SD}}$ needs to be taken into account when the noise is fitted. The discrepancy is accounted for by $\delta S_{\text{out}}^{\text{xc}} = S_{\text{out}}^{\text{xc}}(\text{measured}) - S_{\text{out}}^{\text{xc}}(\text{substitution approach})$ which we conjecture depends explicitly on the differential transmission. Eq. (5.42) and Eq. (5.50) are "educated guesses" of $\delta S_{\text{out}}^{\text{xc}}$.

The most important difference between our two conjectured expressions for the noise is that the second ansatz depends on the squared differential transmission. In figures 5.5 and 5.6 a dip in the excess noise occurs at low voltage for both increasing and decreasing transmission. Therefore an expression for $\delta S$ which is independent of the sign of the differential transmission is favourable, which suggests that the second ansatz better accounts (at least qualitatively) for the observed noise.

## Possible obstructions

Although we feel that our conjectured expressions are a step into the right direction it is quite possible that neither of them can fully explain the measured noise. A possibly way to falsify or support our ansatzes is to look at the next order in perturbation theory. There exists some numerical work for this [9] and it would be interesting to see if an analytic expression can obtained as well. Ref. [9] also reports that the next order in perturbation theory explicitly

depends on the (non-)Abelian nature of the tunnelling quasiparticle. This is not the case at linear response, and our conjectured expressions also do not take this into account (although the transmission could possibly account for this).

Other scenarios which modify the properties of the noise and tunnelling current in a point contact are also possible. The system could be in the strong coupling regime and linear response theory does not apply. In fact, Figure 5.5 shows a transmission of $\sim \frac{1}{2}$ which is well beyond the linear regime. Another possibility is that there could be multiple types of tunnelling quasiparticles contributing to the current [69, 70, 78, 36]. Renormalization Group arguments normally predict a unique quasiparticle to be the most relevant operator, but this does not prohibit the tunnelling of other quasiparticles. Other possibilities are interactions with the environment of the point contact [188, 28], finite-size effects [76, 75] and edge reconstruction [43, 235].

## 5.4 Conclusion

In this chapter we determined the linear response theory of a tunnelling point contact. We computed the tunnelling current, the transmission and the noise in the tunnelling current. These results are combined with the non-equilibrium fluctuation-dissipation theorem from the previous chapter to determine the excess noise in the edge current. From these we determine the Fano factors which measure the sub-Poissonian and super-Poissonian characteristics of the noise. In addition we obtain the linear approximation of a non-equilibrium Nyquist-Johnson relation between the noise (in either the tunnelling or edge current) and the tunnelling current.

The noise in the edge current is the noise which is measured in the experiment. We compared our results against the expression which is frequently used to determine the fractional charge in experiments. This so-called substitution approach is based on the expression for the noise of the current due to tunnelling of non-interacting electrons. As such it fails to take into account the statistics of the quasiparticles (caused by the interactions of the electrons). In particular, it does not take into account the dependency of the noise (for tunnelling quasiparticles) on the differential transmission. This may provide an explanation for the discrepancy measured in recent shot noise experiments [60, 61].

# Summary and outlook

In this thesis we study theoretical aspects of tunnelling point contacts in the fractional quantum Hall regime. We employ both perturbative and non-perturbative techniques in researching the transport properties of these systems. The original research presented in this thesis is captured in Chapter 3, 4 and 5. A compendium of essential background material is presented in Chapter 2.

## The chiral boson

The transport properties of a quantum Hall system are to a great extent determined by the properties of the edge of the system. Although there is no single action which describes all quantum Hall edge theories, there are universal features which are shared among the different edge models. One of these features is the coupling to the electromagnetic field which in the low energy limit is accounted for through the chiral boson model. This $(1+1)D$ model and its relation to the quantum Hall effect is the subject of Chapter 2. In this chapter we provide an overview of the chiral boson in the context of the quantum Hall effect. We discuss in detail the quantization of the theory and the computation of the correlation functions. We also show how the model recovers the quantum Hall transport equations and obtain a real-time Ward identity associated with the electric current.

## Fractional quantum Hall interferometry

In Chapter 3 we study the linear response theory of the tunnelling current through a fractional quantum Hall Fabry-Pérot interferometer. We assume the edge theory decomposes into a neutral and charged channel, both of which are described by a conformal field theory in the long-wavelength limit. The charged channel corresponds to the chiral boson and is responsible for the coupling to the electromagnetic field. Through linear response theory we obtain an expression for the tunnelling current in terms of the Fourier transform of the edge quasiparticle propagator. Using the conformal nature of the edge we find an expression for the tunnelling current in terms of a multivariable hypergeometric function known as Carlson's $R$ function. The expression (see Eq. (3.64) and Eq. (3.61)) is a function of the quasiparticle's conformal dimension and the various energy scales of the system, which are in turn determined by the

source-drain voltage, the distance between the point contacts, the velocities of the neutral and charged channels and the temperature of the system. Our result is novel in the sense that it is an analytical expression which applies to edge theories with different velocities for the neutral and charged channels, and different distances between the point contacts on the left- and right-moving edge. We provide an extensive analysis of the interference current and a numerical scheme to compute Carlson's $R$ function.

Finally, we propose an experimental scheme which may be used to measure the edge velocity of the neutral or charged channel traversing the edge of the system. In this setup the tunnelling current is measured as a function of the distance between the point contacts on one edge. The velocities can be extracted from the Fourier spectrum of the tunnelling current.

## Non-equilibrium noise

Noise experiments in quantum Hall tunnelling point contacts are used to identify characteristics of the tunnelling quasiparticles. For instance, in the weak tunnelling regime the Schottky relation can be used to measure the quasiparticle charge using the noise and the tunnelling current. This relation has been successfully employed to measure a fractional charge of $e/3$ at the $\nu = 1/3$ plateau. More recent experiments involve tunnelling experiments that go beyond the shot noise regime, and consequently these require a model which takes into account the strongly interacting nature of the edge.

The tunnelling point contact is by itself not a closed system. The tunnelling current flows through the contact and ends up in the edge of the system. Therefore fluctuations that arise in the tunnelling current end up in the edge current, which reflects the non-equilibrium nature of the system. In Chapter 4 we study the noise in the edge current of the system in a non-perturbative setting. We find that the excess noise in the edge current is completely determined by the noise in the tunnelling current. However, the noise in the tunnelling current and the noise in the edge current do not simply add. The process is non-linear and a correction term arises which is proportional to the anti-symmetrized noise of the tunnelling current. We find a non-equilibrium fluctuation-dissipation theorem (NE-FDT), see Eq. (4.78), Eq. (4.82) and Eq. (4.90). This theorem relates the noise in the edge current to the noise in the tunnelling current, without explicitly determining them. In the zero-frequency limit the correction term becomes the differential conductance of the tunnelling current.

To prove the NE-FDT we have developed a new tool, called the non-equilibrium Kubo formula, Eq. (4.48). This formula is a non-perturbative generalization of the Kubo formula used in linear response theory. With this formula we show that the edge current operator after the point contact in the system out of equilibrium equals the same edge current in equilibrium

(i.e. in the absence of a point contact) minus the tunnelling operator evaluated at a retarded time. Note that this is an operator identity. It is a consequence of charge conservation combined with the chiral nature of the edge. With this explicit expression for the edge current operator in the system out of equilibrium we determine the noise in the edge current which results in the NE-FDT.

The NE-FDT has important consequences with regard to shot noise experiments. These experiments measure the noise in the edge current and therefore any analysis of the measurements needs to take into account this NE-FDT. In Chapter 5 we determine explicit expressions for the noise in the tunnelling and edge current using linear response theory. We then compare these results to the analyses performed in recent experimental work. We find that these analyses do not properly take into account the strongly correlated nature of the system. We provide a qualitative explanation for recent experimental work involving zero frequency noise. In these experiments the theoretical prediction is a poor fit for the measured noise, the reason being that this fit is based on a model for non-interacting particles. It does not properly take into account the strongly interacting nature of the system and we believe that this discrepancy can be understood using our model.

**Future work**

We mentioned some experimental opportunities suggested by our work. For the interferometer we already described an experiment which can be used to measure the velocities of the edge channels. The results from Chapter 5 should be tested against data from recent experimental work involving shot noise. In particular, we predict that the measured shot noise should be a function of the derivative of the transmission with respect to the source-drain voltage. Even at linear response theory this dependency needs to be taken into account. It would be interesting to see if recent measurements such as Ref. [60] can be understood using this modified noise.

On the theoretical side there are multiple possibilities for future study. Although we obtained expressions for the finite frequency noise, we did not fully analyze the properties of this noise. This coloured noise (as opposed to white noise) again contains information on the properties of the edge theory that potentially cannot be measured using the zero frequency regime. Another possibility is to study higher moments of (shot) noise, i.e. multi-point auto-correlators, of the edge current. The goal would again be an NE-FDT which relates the higher moments (multi-point correlators) of shot noise in the tunnelling and edge current.

An important open problem is a non-equilibrium Nyquist-Johnson relation for the noise in the tunnelling current. Such a relation exists for non-interacting electrons and expresses the noise in terms of the tunnelling current, or a related quantity such as the transmission

coefficient. In Chapter 5 we derive such an expression in linear response theory. Although a non-perturbative expression is difficult if not impossible to obtain, it should at least be possible to study the next order contribution in perturbation theory. This could either support or falsify our ansatzes for the NE-Nyquist-Johnson relation. Related to this is to compare our ansatzes to non-pertubative results of the $\nu = 1/3$ state.

Finally, there is the opportunity to combine the results from both projects. The tools developed in the noise project are directly applicable to the fractional quantum Hall interferometer, or other types of point contact systems. This should lead to a geometry-dependent non-equilibrium fluctuation-dissipation theorems, which take into account the presence of multiple point contacts. In particular the properties of finite-frequency noise need to be studied here, as most likely the shot noise limit is not sensitive to the presence of multiple point contacts.

# Chapter A
# Mathematical supplement

This section is dedicated to an overview of mathematical results used in the main text. References used include Refs. [68, 98].

## A.1   Series and special functions

Some series which occur are

$$\sum_{n=1}^{\infty} \frac{1}{n} x^n = -\log(1-x) \qquad \sum_{n=0}^{\infty} x^n = \frac{x}{1-x} \qquad \sum_{n=1}^{\infty} n x^n = \frac{1}{(x^{1/2} - x^{-1/2})^2} \qquad (A.1)$$

for $|x| < 1$. These series are usually encountered with $x = e^{-(\delta + it)}$.

The gamma function is defined by its integral representation

$$\Gamma(z) = \int_0^{\infty} t^{z-1} e^{-t} dt \qquad (A.2)$$

and obeys $\Gamma(x+1) = x\Gamma(x)$ and reduces to $\Gamma(n+1) = n!$ for $n \geq 0$ and integer. Furthermore, $\Gamma(\frac{1}{2}) = \sqrt{\pi}$. Related to the gamma function is the Euler beta function. We frequently encounter the expression

$$B(x+iy, x-iy) = \frac{|\Gamma(x+iy)|^2}{\Gamma(2x)} . \qquad (A.3)$$

Some important relations are the doubling formula

$$\Gamma(2x) = \frac{2^{2x-1}}{\sqrt{\pi}} \Gamma(x)\Gamma(x+1) \qquad (A.4)$$

and the reflection formulas

$$\Gamma(1-x)\Gamma(x) = \frac{\pi}{\sin(\pi x)} \qquad \Gamma(\tfrac{1}{2} - x)\Gamma(\tfrac{1}{2} + x) = \frac{\pi}{\cos(\pi x)} . \qquad (A.5)$$

These expression extend to the complex plane. In particular, it leads to the relations

$$B(\tfrac{1}{2} + iy, \tfrac{1}{2} - iy) = \frac{\sqrt{\pi}}{\cosh(\pi x)} \qquad B(1+iy, 1-iy) = \frac{\pi x}{\sinh(\pi x)} . \qquad (A.6)$$

Another special function is the Gauss hypergeometric function $_2F_1(a, b; c; x)$. It has the integral representation ($\text{Re}[c] > \text{Re}[a] > 0$)

$$_2F_1(a, b; c; x) = \frac{1}{B(a, c - a)} \int_0^1 t^{a-1}(1 - t)^{c-a-1}(1 - zt)^{-b}dt . \tag{A.7}$$

It also has a series representation

$$_2F_1(a, b; c; x) = \frac{\Gamma(c)}{\Gamma(a)\Gamma(b)} \sum_{n=0}^{\infty} \frac{\Gamma(a + n)\Gamma(b + n)}{\Gamma(c + n)} \frac{x^n}{n!} \tag{A.8}$$

See Refs. [68, 98] for many more properties and identities of this function.

## A.2  Integrals from Chapter 2 – Integration over momenta

In Chapter 2 we encounter summations of the form

$$\mathcal{I}_f = \frac{2\pi}{L} \sum_{k \neq 0} f(k)e^{k(\delta + i(x + v_c t))}n_B(z), \qquad k = \frac{2\pi}{L}n, \quad n \in \mathbb{Z} . \tag{A.9}$$

Here $f(k)$ is a function of the form $k^m$. The relevant cases are $m = -1$, $m = 0$ and $m = 1$. In the large $L$ limit the summation is approximated by an integral over the domain $\gamma = (-\infty, -\frac{2\pi}{L}] \cup [\frac{2\pi}{L}, \infty)$, i.e.

$$\mathcal{I}_f \longrightarrow \int_\gamma f(y)\frac{e^{yz}}{e^{2\pi y} - 1} \, dy \tag{A.10}$$

where $z = \frac{2\pi T}{v_c}(\delta + i(x + v_c t))$. We assume $\text{Im}[z] < 0$, although the final results also holds for $\text{Im}[z] > 0$ (but requires a different proof). In the $L \to \infty$ limit the integral approaches the origin at $y = 0$. If $f(y)$ is regular than this is no problem, and we can include the origin into the domain of integration. For the case of $f(y) = 1/y$ the function is singular at the origin, and the integral is formally divergent. This divergence needs to be regularized.

For now we assume a domain of integration equal to $\gamma_L = [-R, -\epsilon] \cup [\epsilon, R]$, which excludes the origin and has an upper and lower bound given by $R$ (which we will take to $\infty$). We extend this domain with two contours, $\gamma_R$ and $\gamma_\epsilon$, thereby closing the contour. See Figure A.1. The resulting integral is computed using the residue theorem.

The domain $\gamma_R$ is a semi-circle of radius $R$ in the upper-half plane of complex $y$. The integral over this contour vanishes in the large $R$ limit. The contour $\gamma_\epsilon$ is a semicircle of radius $\epsilon$. For $f(y)$ regular this contribution also vanishes in the limit of $\epsilon \downarrow 0$. For finite $R$ and $\epsilon$ the integral $\mathcal{I}_f$ equals the difference

$$\mathcal{I}_f = \lim_{\epsilon \downarrow 0} \lim_{R \to \infty} \left[ \int_{\gamma'} - \int_{\gamma_\epsilon} \right] f(y)\frac{e^{yz}}{e^{2\pi y} - 1} \, dy \tag{A.11}$$
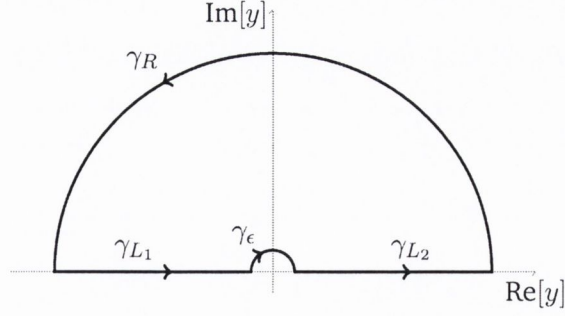
**Figure A.1:** The contour along the integral is determined using the residue theorem. The function $f(y)\frac{e^{yz}}{e^{2\pi y}-1}$ has poles at $y=ni$ with $n$ integer. For $f(y)=1/y$ the limit of $\epsilon\downarrow 0$ is divergent and needs to be regularized.

where $\gamma'=\gamma_L\cup\gamma_\epsilon\cup\gamma_R$.

**The first integral** is along a closed contour $\gamma'$ and is handled using the residue theorem. The residues are situated at $y=ni$ for $n>0$ and integer. We have

$$2\pi i \operatorname*{Res}_{y=ni}\left[f(y)\frac{e^{yz}}{e^{2\pi y}-1}\right]=if(ni)e^{inz} \tag{A.12}$$

valid since $f(y)=y^m$ is regular at the the points $y=ni$. The contour integral is determined by taking the sum over $n$ and take the limit of $R\to\infty$. For three cases of interest this gives

$$\lim_{\epsilon\downarrow 0}\lim_{R\to\infty}\int_{\gamma'}f(y)\frac{e^{yz}}{e^{2\pi y}-1}\,dy=i\sum_{n=1}^{\infty}f(ni)e^{inz}=\begin{cases}-\log(1-e^{iz}) & f(y)=\dfrac{1}{y};\ \ n=-1\\[2mm] i\dfrac{e^{iz}}{1-e^{iz}} & f(y)=1\\[2mm] \dfrac{1}{4}\dfrac{1}{\sin(z/2)^2} & f(y)=y;\ \ n=1\end{cases} \tag{A.13}$$

**The remaining integral** is over the semi-circle corresponding to $\epsilon$. The contour is described by $\gamma_\epsilon=\epsilon e^{i\theta}$ with $\theta\in[\pi,0]$. We have

$$-\lim_{\epsilon\downarrow 0}\int_{\gamma_\epsilon}f(y)\frac{e^{yz}}{e^{2\pi y}-1}\,dy=\lim_{\epsilon\downarrow 0}\int_0^{\pi}f(\epsilon e^{i\theta})\frac{e^{\epsilon e^{i\theta}z}}{e^{2\pi\epsilon e^{i\theta}}-1}i\epsilon e^{i\theta}\,d\theta\ . \tag{A.14}$$

For the case of $f(k)=k^m$ with $m>0$ the integral vanishes when we take $\epsilon\downarrow 0$. For $m=0$ the integral is finite, while for $m<0$ it diverges. We approximate the integrand by a Laurent series in $\epsilon$ for the cases of $m=-1$ and $m=0$ gives

$$f(\epsilon e^{i\theta})\frac{e^{\epsilon e^{i\theta}z}}{e^{2\pi\epsilon e^{i\theta}}-1}i\epsilon e^{i\theta}=\begin{cases}\dfrac{i}{2\pi}e^{-i\theta}\dfrac{1}{\epsilon}+\dfrac{i}{2\pi}(z-\pi)+\dots & f(y)=\dfrac{1}{y}\\[2mm] \dfrac{i}{2\pi}+\dots & f(y)=1\end{cases} \tag{A.15}$$

The dots represent terms linear or higher order in $\epsilon$ which vanish in the $\epsilon \downarrow 0$ limit. For the case of $f(y) = \frac{1}{y}$ the $\frac{1}{\epsilon}$ term captures the divergence of the integral. We denote this divergence by $C$ and integrate the remaining term. Plugging the Laurent series back into the integral gives

$$- \lim_{\epsilon \downarrow 0} \int_{\gamma_\epsilon} f(y) \frac{e^{yz}}{e^{2\pi y} - 1} \, dy = \begin{cases} C - \log(ie^{-iz/2}) & f(y) = \frac{1}{y} \\[2ex] \dfrac{i}{2} & f(y) = 1 \\[2ex] 0 & f(y) = y \, . \end{cases} \tag{A.16}$$

The final expression for the desired integral is obtained by summing (A.13) and (A.16). We have

$$\boxed{\mathcal{I}_f = \int_{\gamma_L} f(y) \frac{e^{yz}}{e^{2\pi y} - 1} \, dy = \begin{cases} -\log(\sin(z/2)) + C & f(y) = \frac{1}{y} \\[2ex] -\dfrac{1}{2} \cot\left(z/2\right) & f(y) = 1 \\[2ex] \dfrac{1}{4} \dfrac{1}{\sin(z/2)^2} & f(y) = y \, . \end{cases}} \tag{A.17}$$

where $z = \frac{2\pi T}{v_c}(\delta + i(x + v_c t))$. This was proven for $\text{Im}[z] < 0$. The proof for $\text{Im}[z] > 0$ is almost the same, with the exception that the contour is closed along the lower half plane. The constant $C$ represents the (regularized) divergence of the integral and its divergence is determined in the main text.

## A.3   Integrals from Section 3.5.5 – Propagators

In Chapter the interference current is written in terms of a Fourier transform of a product of propagators. Here we discuss how these transforms are determined and show that the interference current is given in terms of Carlson's $R$ function.

### A.3.1   Single channel propagator

We require the Fourier transform of the two-point propagator. We start with the finite-temperature case and no spatial dependence,

$$P_g(t) = (\pi T)^g \sin\left[\pi T(\delta + it)\right]^{-g} \, . \tag{A.18}$$

Here $\delta > 0$ is an infinitesimal integral regulator which is taken to zero in the end. To compute its Fourier transform $P_g(\omega) = \int e^{i\omega t} P_g(t) dt$ we follow Ref. [157] and substitute $\delta + it =$

$i\frac{x}{2\pi T} + \frac{1}{2T}$. This leads to

$$P_g(t) = (\pi T)^g \cosh\left(\frac{x}{2}\right)^{-g} = (2\pi T)^g e^{-gx/2} \left(1 + e^{-x}\right)^{-g} . \tag{A.19}$$

With this substitution the limits of the contour are $\pm\infty + i(\pi - \delta)$. The contour is deformed so that it runs over the real line of $x$, which can be done provided there are no singularities that prevent this deformation. The function $\cosh(x/2)$ is zero at the points $x_n = (2n + 1)\pi i$, for $n$ integer. It is therefore the presence of the integral regulator $\delta$, which allows for the deformation.

After substitution the resulting integral is an integral representation of the Euler beta function [98]. We have

$$\begin{aligned}
P_g(\omega) &= \frac{e^{\frac{\omega}{2T}}}{(2\pi T)^{1-g}} \int_{-\infty}^{\infty} e^{-\left(\frac{g}{2} - i\frac{\omega}{2\pi T}\right)x} \left(1 + e^{-x}\right)^{-g} dx \\
&= \frac{e^{\frac{\omega}{2T}}}{(2\pi T)^{1-g}} B\left(\frac{g}{2} + i\frac{\omega}{2\pi T}, \frac{g}{2} - i\frac{\omega}{2\pi T}\right). 
\end{aligned} \tag{A.20}$$

Here we have taken $\delta \to 0$ in the final result.

### A.3.2 Multichannel propagators

Through a similar manipulation the Fourier transforms of products of two-point propagators with unequal arguments can be obtained. This results in the Fourier transform for $G_{ij}^>$, Eq. (3.57). The propagators entering this expression for $G_{ij}^>$ are given by $P_g(t + \xi)$ with $\xi$ of the form $\xi = \pm\frac{a}{v}$. We first note that with the substitution $\delta + it = i\frac{x}{2\pi T} + \frac{1}{2T}$ we have

$$P_g(t + \xi) = (2\pi T)^g\, e^{-\pi T\xi g} e^{-\frac{g}{2}x} A_g(\xi) \tag{A.21}$$

$$\text{where} \quad A_g(\xi) = \left(1 + e^{-2\pi T\xi} e^{-x}\right)^{-g} .$$

When applying this substitution to the Fourier transform of the product of four propagators (setting $g = g_n + g_c$) we obtain

$$G_{ij}^>(\omega) \propto \int_{-\infty}^{\infty} \left[e^{i\omega t} P_{g_c}(t + \tfrac{a}{v_c}) P_{g_c}(t - \tfrac{b}{v_c}) P_{g_n}(t + \eta\tfrac{a}{v_n}) P_{g_n}(t - \eta\tfrac{b}{v_n})\right] dt = e^{\frac{\omega}{2T}} (2\pi T)^{2g-1}$$

$$\times\, e^{\pi T(b-a)\left(\frac{g_c}{v_c} + \eta\frac{g_n}{v_n}\right)} \int_{-\infty}^{\infty} \left[e^{-(g - i\frac{\omega}{2\pi T})x} A_{g_c}(\tfrac{a}{v_c}) A_{g_c}(-\tfrac{b}{v_c}) A_{g_n}(\eta\tfrac{a}{v_n}) A_{g_n}(-\eta\tfrac{b}{v_n})\right] dx . \tag{A.22}$$

The resulting integral is an integral definition of Carlson's $R$ function [35], see Eq. (B.3). This function is discussed in detail in Appendix B. It is a scaling function and it is closely related to the Lauricella hypergeometric function[146, 159] $F_D^{(n)}$ . This Lauricella function is a multivariable generalization of the Gauss hypergeometric function of one variable and the Appell hypergeometric function of two variables [98]. For our purposes it is convenient

---

to use the $R$ function to represent our main result, although the two representations are interchangeable, see Eq. (B.9).

Applying the integral representation (B.3) gives for the integral

$$
\begin{aligned}
\text{(A.22)} = {} & e^{\pi T(b-a)\left(\frac{g_c}{v_c}+\eta\frac{g_n}{v_n}\right)} P_{2g}(\omega) \\
& \times R\left(g - i\frac{\omega}{2\pi T}; \{g_c, g_c, g_n, g_n\}; e^{-2\pi T\frac{a}{v_c}}, e^{2\pi T\frac{b}{v_c}}, e^{-\eta 2\pi T\frac{a}{v_n}}, e^{\eta 2\pi T\frac{b}{v_n}}\right) \quad \text{(A.23)}
\end{aligned}
$$

where $P_g(\omega)$ is given by (A.20). The resulting $R$ function is Carlson's $R$ function. Note that the order in which the parameters appear is important.

# Chapter B
# Carlson's $R$ function

The interference current for a fractional quantum Hall state through a Fabry-Përot interferometer is given in terms of Carlson's $R$ function. In this chapter we discuss its main features, such as its integral and series representation, and how the function is computed numerically.

## B.1 Main properties of the $R$ function

We first introduce a notation. We define $\mathcal{G}_n$ as the ordered set with $n$ elements given by

$$\mathcal{G}_n = \{g_1, \ldots, g_n\} \tag{B.1}$$

and we set

$$\gamma = \sum_{i=1}^{n} g_i \; . \tag{B.2}$$

In the main text we usually work with the case where $n = 4$, the ordered set corresponds to $\mathcal{G}_n = \{g_c, g_c, g_n, g_n\}$, and $\gamma = 2(g_h + g_n) = 2g$. Carlson's $R$ function is treated in Ref. [35] and is defined through the integral representation

$$R\left(\alpha; \mathcal{G}_n; \{z_i\}\right) = \frac{1}{B\left(\alpha, \gamma - \alpha\right)} \int_{-\infty}^{\infty} e^{-\alpha x} \left[ \prod_{i=1}^{n} (1 + z_i e^{-x})^{-g_i} \right] dx \; . \tag{B.3}$$

Here, $B(x, y)$ is the Euler beta function, and $\{z_i\}$ is the ordered set $\{z_i\}_{i=1}^{n} = \{z_1, \ldots z_n\}$. We require $\mathrm{Re}\,[\alpha] > 0$ and $\mathrm{Re}\,[\gamma - \alpha] > 0$ for convergence of the integral. Furthermore, we take the $z_i$'s to be real and positive. The $R$ function is symmetric under the simultaneous interchange of $g_i \leftrightarrow g_j$ and $z_i \leftrightarrow z_j$. In the main text the $z_i$ correspond to the exponentials $e^{\pm 2\pi T \eta_i \frac{a}{v_i}}$.

The $R$ function is a scaling function, i.e. it is homogeneous. This follows directly from the integral definition (B.3)

$$R\left(\alpha; \mathcal{G}_n; \{z_1, \ldots z_n\}\right) = \lambda^{\alpha} R\left(\alpha; \mathcal{G}_n; \{\lambda z_1, \ldots, \lambda z_n\}\right) \; . \tag{B.4}$$

We also have the Euler-type transformation

$$R\left(\alpha; \mathcal{G}_n; z_1, \ldots z_n\right) = \left[ \prod_{i=1}^{n} z_i^{-g_i} \right] R\left(\gamma - \alpha; \mathcal{G}_n; z_1^{-1}, \ldots z_n^{-1}\right) \; . \tag{B.5}$$

For some special values the $R$ function with $n$ arguments reduces to one with $m < n$ arguments. For instance

$$R\left(\alpha; \mathcal{G}_n; \{z_1, \dots z_k, z, \dots, z\}\right) = R\left(\alpha; \{g_1, \dots, g_k, \tilde{g}\}; \{z_1, \dots z_k, z\}\right) \tag{B.6}$$

where $\tilde{g} = g_{k+1} + \cdots + g_n$. We also have the case

$$B(\alpha, \gamma - \alpha)R\left(\alpha; \mathcal{G}_n; \{z_1, \dots z_k, 0, \dots, 0\}\right) = B(\alpha, \gamma - \alpha - \tilde{g})R\left(\alpha; \mathcal{G}_k; \{z_1, \dots z_k\}\right) \ . \tag{B.7}$$

The $R$ function is closely related to the Lauricella hypergeometric function [146, 35, 159]. We define the Lauricella function through its series representation

$$F_D^{(n)}\left(\alpha; \mathcal{G}_n; \gamma; \{1 - w_1, \dots 1 - w_n\}\right) = \sum_{m_1=0}^{\infty} \cdots \sum_{m_n=0}^{\infty} \frac{(\alpha)_{\sum_i m_i}}{(\gamma)_{\sum_i m_i}} \left[\prod_{i=1}^{n} \frac{(g_i)_{m_i}}{m_i!}(1 - w_i)^{m_i}\right] \tag{B.8}$$

where $(\alpha)_m = \Gamma[\alpha + m]/\Gamma[\alpha]$ is the Pochhammer symbol and we require $|1 - w_i| < 1$ and $\arg(1 - w_i) > 0$ for convergence of the series.

To demonstrate the relation between the two functions we define $z_n \equiv \max(z_1, \dots, z_n)$ as the largest parameter of the $z_i$'s. Because of the identity (B.3) we can always set this parameter to be the last argument of the $R$ function. Furthermore, we will demand $z_i \neq z_j$ for $i \neq j$, which can always be accomplished through the reduction property (B.6). The relation between $R$ and $F_D$ is given by

$$R\left(\alpha; \mathcal{G}_n; \{z_1, \dots z_n\}\right) = z_n^{-\alpha} F_D^{(n-1)}\left(\alpha; \mathcal{G}_{n-1}; \gamma; \{1 - \frac{z_1}{z_n}, \dots 1 - \frac{z_{n-1}}{z_n}\}\right) \tag{B.9}$$

The arguments of the Lauricella function all satisfy $|1 - z_i/z_n| < 1$ and $\arg(1 - z_i/z_n) = 0$ meaning we have convergence of the series (B.8). We do not prove this relation explicitly, but it follows from manipulating the integral (B.3) and makes use of the binomial series.

The Lauricella hypergeometric function is a generalization of the single-variable Gauss hypergeometric function, denoted by $_2F_1$, and the two-variable Appell hypergeometric function, $F_1$. We have

$$R\left(\alpha; \{g_1\}; \{z_1\}\right) = z_1^{-\alpha} \tag{B.10}$$

$$R\left(\alpha; \{g_1, g_2\}; \{z_1, z_2\}\right) = z_2^{-\alpha} \, _2F_1(\alpha; \{g_1\}; g_1 + g_2; \{1 - \tfrac{z_1}{z_2}\})$$

$$R\left(\alpha; \{g_1, g_2, g_3\}; \{z_1, z_2, z_3\}\right) = z_3^{-\alpha} \, F_1(\alpha; \{g_1, g_2\}; g_1 + g_2 + g_3; \{1 - \tfrac{z_1}{z_3}, 1 - \tfrac{z_2}{z_3}\}).$$

Here we assume $z_3 > z_2 > z_1$.

## B.2 High temperature behaviour

Consider again the expression for $G_{ij}^>(\omega)$, Eq. (3.57). We are interested in its behaviour at large $T$. The expression $G_{ij}^>(\omega)$ is proportional to the integral

$$\mathcal{I} \equiv \int_{-\infty}^{\infty} e^{i\omega t} \prod_{i=1}^{m} P_{g_i}(t + \xi_i)\, dt \tag{B.11}$$

where the $\xi_i$ correspond to the energy scales set by the velocity and edge lengths, $\xi \sim \pm\eta_i \frac{a}{v_i}$ and $P_g(t)$ is the propagator given by Eq. (A.18). We are interested in the behaviour for this function when $T$ grows large. For this we substitute $\delta + it \to ix + \frac{1}{2T}$, which gives

$$P_{g_i}(t + \xi_i) = (\pi T)^{g_i} \cosh\left(\pi T (x + \xi_i)\right)^{-g_i} \tag{B.12}$$

and the integral becomes

$$\mathcal{I} = (\pi T)^{2g}\, e^{\frac{\omega}{2T}} \int_{-\infty}^{\infty} e^{i\omega x} \prod_i \cosh\left(\pi T (x + \xi_i)\right)^{-g_i}\, dx$$

To be consistent with the main text we set $\sum_i g_i = 2g$. We split the integral into two domains, and pull out an exponential from the cosh function. This gives

$$e^{-\frac{\omega}{2T}} \frac{\mathcal{I}}{(2\pi T)^{2g}} = \int_0^{\infty} e^{-(2\pi Tg - i\omega)x} \prod_i (e^{\pi T\xi_i} + e^{-2\pi T(x + \frac{\xi_i}{2})})^{-g_i}\, dx$$
$$+ \int_{-\infty}^0 e^{(2\pi Tg + i\omega)x} \prod_i (e^{2\pi T\left(x + \frac{\xi_i}{2}\right)} + e^{-\pi T\xi_i})^{-g_i}\, dx \tag{B.13}$$

Consider the first integral. We perform an integration by parts, and obtain a boundary term and a remainder,

$$\int_0^{\infty} e^{-(2\pi Tg - i\omega)x} \prod_i (e^{\pi T\xi_i} + e^{-2\pi T(x + \frac{\xi_i}{2})})^{-g_i}\, dx$$
$$= \frac{1}{2\pi Tg - i\omega}\left[ \prod_i (e^{\pi T\xi_i} + e^{-\pi T\xi_i})^{-g_i} + \int_0^{\infty} e^{-(2\pi Tg - i\omega)x} f(x) \right]\, dx \tag{B.14}$$

where

$$f(x) = 2\pi T \prod_i (e^{\pi T\xi_i} + e^{-2\pi T(x + \frac{\xi_i}{2})})^{-g_i} \sum_j g_j \frac{e^{-2\pi T(x + \frac{\xi_j}{2})}}{e^{\pi T\xi_j} + e^{-2\pi T(x + \frac{\xi_j}{2})}} \tag{B.15}$$

We can estimate an upper bound for the remainder term. For this we note that $f(x)$ is positive on the integration domain and bounded by

$$f(x) \le 4\pi Tg \prod_i (e^{\pi T\xi_i} + e^{-\pi T\xi_i})^{-g_i}, \quad x \in [0, \infty)$$

This gives an upper bound on the remainder given by (up to a factor of $(2\pi Tg - i\omega)^{-1}$)

$$\left| \int_0^\infty e^{-(2\pi Tg - i\omega)x} f(x)\, dx \right| \leq 4\pi Tg \prod_i (e^{\pi T\xi_i} + e^{-\pi T\xi_i})^{-g_i} \int_0^\infty e^{-(2\pi Tg - i\omega)x}\, dx$$

$$= \frac{4\pi Tg}{2\pi Tg - i\omega} \prod_i (e^{\pi T\xi_i} + e^{-\pi T\xi_i})^{-g_i} \tag{B.16}$$

The product also appears in the expression for the boundary term in Eq. (B.14). This product therefore determines the asymptotic behaviour of the boundary term in the high temperature limit, and acts as an upper bound on the remainder term. A similar analysis can be applied to the second integral in Eq. (B.13). It follows that the asymptotic behaviour of the integral $\mathcal{I}$ in the high temperature limit is given by

$$\mathcal{I} \sim (2\pi T)^{2g-2} e^{-\pi T \sum_i |\xi_i| g_i} \tag{B.17}$$

The factor $(2\pi T)^{2g-2}$ is the high temperature behaviour of expression (A.20). This shows that the high temperature behaviour of the modulating function is given by the exponential $\exp(-\pi T \sum_i |\xi_i| g_i)$.

## B.3  Computing the $R$ function

For $n = 1$ and $n = 2$ the $R$ function reduces to the Gauss and Appell hypergeometric functions respectively for which various efficient numerical implementations exist. For $n > 3$ no numerical implementation is available and we can either perform numerical integration or compute the expansion (B.8) to some finite order. Numerical integration of the integral (B.3) takes into account the Beta function as well, which is why we use the series expansion instead. We will follow Ref. [140] to cast this series expansion into a more tractable form suitable for a numerical implementation.

The main result of Ref. [140] is that the multivariate Taylor expansion (B.8) can be written as the single summation

$$F_D^{(n)}\left(\alpha; \mathcal{G}_n; \gamma; \{1 - w_1, \ldots 1 - w_n\}\right) = 1 + \sum_{m=1}^\infty \frac{(\alpha)_m}{(\gamma)_m} \Lambda_m(t_1, \ldots, t_m). \tag{B.18}$$

Here $(\alpha)_n = \Gamma[\alpha + n]/\Gamma[\alpha]$ is the Pochhammer symbol and $\Lambda_m$ is the *cycle index* (of the symmetric group $S_m$) of the variables $t_j$. Defining the variables $t_j$ $(j = 1, \ldots, m)$

$$t_j = \sum_{i=1}^n g_i (1 - w_i)^j \tag{B.19}$$

then the cycle index $\Lambda_m$ of this set $\{t_j\}_{j=1}^m$ is given by

$$\Lambda_m(t_1, \ldots, t_m) = \sum_{\substack{k_1, \ldots, k_m \\ k_1 + 2k_2 \cdots + mk_m = m}} \left[ \prod_{j=1}^m \frac{1}{k_j!} \left( \frac{t_j}{j} \right)^{k_j} \right]. \tag{B.20}$$

The summation over the $k_i$'s (B.20) is constrained by $\sum_{j=1}^{m} jk_j = m$, which makes its computation for large $m$ rather involved. It's more efficient to use an iterative approach, as $\Lambda_m$ can be expressed in terms of $\{\Lambda_n\}_{n<m}$. Defining $\Lambda_0 = 1$ we have for $m \geq 1$

$$\Lambda_m(t_1, \ldots, t_m) = \frac{1}{m} \sum_{j=1}^{m} t_j \Lambda_{m-j}(t_1, \ldots, t_{m-j}) \tag{B.21}$$

Let us also give the corresponding expansion for the $R$-function. For that we again assume $z_n$ is the largest argument of the function. Then

$$R\left(\alpha; \{g_1, \ldots, g_n\}; \{z_1, \ldots, z_n\}\right) = z_n^{-\alpha} \sum_{m=0}^{\infty} \frac{(\alpha)_m}{(\gamma)_m} \Lambda_m(\tau_1, \ldots, \tau_m) \tag{B.22}$$

where $\gamma = \sum_{i=1}^{n} g_i$ and $z_n = \max(z_1, \ldots, z_n)$ as before. The $\tau_j$ $(i = 1, \ldots, n-1)$ are given by

$$\tau_j = \sum_{i=1}^{n-1} g_i(1 - z_i/z_n)^j . \tag{B.23}$$

This algorithm is due to Laarhoven and Kalker [140].

In the main text the $R$ function which enters the expression for the interference term is a multivariate expansion in terms of the scales $1 - \frac{z_i}{z_n} = 1 - \exp(-2\pi T(\frac{a_i}{v_i} - \frac{a_j}{v_j})) < 1$. For large temperature scales ($\geq 15$ mK) the arguments approach the radius of convergence, $(1 - z_i/z_n) \lesssim 1$, and the rate of convergence of the series becomes extremely slow, especially when the frequency $\omega_Q$ becomes large as well. This requires a very large number of terms in the expansion, which becomes problematic since the algorithm for $\Lambda_m$ scales as order $\mathcal{O}(N^2)$ with $N$ the number of terms in the series. In this regime numerical integration does not seem to be an alternative, as the standard integration schemes suffer from slow convergence as well.

The situation is somewhat improved by using a series acceleration. We have chosen a series acceleration via the *Combined Nonlinear-Condensation Transformation* (CNCT) as outlined in Ref. [125]. The algorithm works in two steps. First, the (largely monotone) series (B.18) is transformed into an alternating series via a Van Wijngaarden transformation. Alternating series are known to converge better using a series acceleration. Second, this alternating series is accelerated via a nonlinear sequence transformation. For our purposes we have chosen Levin's $u$ transformation [125], although other choices yield similar results.

The advantage of the CNCT method is that only a handful of terms of the original series are needed to obtain a high precision estimate of the series. This method significantly improves the rate of convergence of many series [125]. However, the method requires the capability to compute "random" terms in the series (B.22). To be specific, to perform the Van Wijngaarden transformation we require the terms $\frac{(a)_M}{(c)_M} \Lambda_M$ with $M = 2^k(j+1) - 1$ and $j$ and $k$ integers,

see Ref. [125]. Typically we need all terms with $j, k < 30$ for a decent precision in the final answer. But note that the index $M$ grows exponentially. This is problematic, because our algorithm is designed to determine $\Lambda_m$ iteratively and this iteration process grows as $\mathcal{O}(N^2)$. The CNCT method and similar acceleration methods therefore do not fully resolve the issue of slow convergence. To avoid this problem our plots are performed at low temperature ($T = 1$ [mK] or $T = 0$ [mK]).

A second problem that arises is a lack of precision in the terms computed. We found that the typical double floating point accuracy can lead to problems when evaluating the series for large $\omega_Q$ ($> 100$ [mK]) and values of the velocities and distance scales as mentioned in Section 3.8. This issue is resolved by making use of high-precision floating point accuracy [127]. The downside to this is that the computation of a large number of terms is extremely slow. In particular, we cannot simultaneously make use of the CNCT algorithm and high-precision floating point accuracy.

We have implemented this algorithm through a combination of `NumPy` [170] and `Fortran`, making use of `F2PY` [176]. In some cases we also made use of the high-precision floating-point arithmetic package `mpmath` [127]. All plots are generated using `matplotlib` [119].

# Chapter C

# The interference current at zero temperature

In the zero temperature case the KMS relation of the $G$ correlators, see Eq. (3.37), no longer applies. Within our approximation we do have the relation $G_{ij}^>(t) = G_{ji}^<(-t)$. The expression of the tunnelling current at zero temperature is therefore given by

$$I_B(\omega_Q) =$$
$$Qe\Big( \sum_{i=1}^N |\Gamma_i|^2 \left[ G_{ii}^>(\omega_Q) - G_{ii}^<(\omega_Q) \right] + 2\sum_{i<j}^N |\Gamma_i \Gamma_j^*| \mathrm{Re} \left[ e^{i\Phi_{ij}+i\alpha_{ij}} \left[ G_{ij}^>(\omega_Q) - G_{ij}^<(\omega_Q) \right] \right] \Big) .$$

$$(C.1)$$

The analysis of the $G^>$ correlator is the same as in the finite temperature case, with the exception that we use the zero temperature expression of the propagator $P_g(t)$. In particular (3.57) still applies, but with the propagator given by

$$P_g(t) = \frac{1}{(\delta + it)^g} .$$

$$(C.2)$$

The expression for $G^>$ and $G^<$ then boils down to

$$G_{ij}^>(\omega) - G_{ji}^<(\omega) =$$
$$a_{\mathrm{vac}} \mathcal{A}_{ij}(\chi) v_c^{-2g_c} v_n^{-2g_n} \int_{-\infty}^\infty e^{i\omega t} \Big[ P_{g_c}(t+\frac{a}{v_c}) P_{g_c}(t-\frac{b}{v_c}) P_{g_n}(t+\eta\frac{a}{v_n}) P_{g_n}(t-\eta\frac{b}{v_n})$$
$$- P_{g_c}(-t+\frac{a}{v_c}) P_{g_c}(-t-\frac{b}{v_c}) P_{g_n}(-t+\eta\frac{a}{v_n}) P_{g_n}(-t-\eta\frac{b}{v_n}) \Big] \, dt \quad (C.3)$$

We have not found a reference or method to treat this Fourier transform directly. It can be treated for the special case of a symmetric interferometer and a single edge mode, where $v_c = v_n$ and $a = b$. This special case is treated in Appendix C.1. Alternatively, we can start with the expression for the tunnelling current of the finite temperature case and take the zero temperature limit. This approach allows for more general values of the physical parameters and is performed in Section C.2. Finally, we suggest in Section C.3 a solution to the integral (C.3), obtained by taking the zero temperature limit from the finite temperature expression.

As in the finite temperature case we find for the tunnelling current

$$I_B(\omega_Q) = \frac{Qe}{v_c^{2g_c} v_n^{2g_n}} a_{\mathrm{vac}} |\Gamma(\omega_Q)|^2 I_{2g}(\omega_Q) \mathrm{sgn}(\omega_Q)$$

$$(C.4)$$

with $I_{2g}$ given by (C.6) and the effective tunnelling amplitude equals

$$|\Gamma|^2 = \sum_{i=1}^{N} |\Gamma_i|^2 + 2 \sum_{i<j}^{N} |\Gamma_i \Gamma_j^*| \mathrm{Re} \left[ \mathcal{A}_{ij}(\chi) e^{i\Phi_{ij} + i\alpha_{ij}} H_{ij}^{\mathrm{mod}}(\omega_Q) \right] \tag{C.5}$$

The modulating function $H_{ij}^{\mathrm{mod}}(\omega_Q)$ is given by (C.12) in the symmetric interferometer case with a single mode, and by (C.18) in the more general case.

## C.1   Interference current – single channel case

We start with the Fourier transform of the correlator $G_{ii}(\omega)$. This corresponds to the tunnelling current through a single point contact, see Eq. (C.1). We require the Fourier transform of the propagator $P_g(t)$, which is given by [98]

$$P_g(\omega) = I_g(\omega) \Theta(\omega) \tag{C.6}$$

$$\text{where} \quad I_g(\omega) \equiv \frac{2\pi}{\Gamma(g)} |\omega|^{g-1}$$

and $\Theta(\omega)$ is the step function. Then

$$G_{ii}^>(\omega) - G_{ii}^<(\omega) = a_{\mathrm{vac}} v_c^{-2g_c} v_n^{-2g_n} I_{2g}(\omega) \mathrm{sgn}(\omega) . \tag{C.7}$$

For the expression of the interference term we set $v = v_c = v_n$ and $a = b$. The required integral is (see Eq. (C.3))

$$K_g(\omega) = \int_{-\infty}^{\infty} e^{i\omega t} \left[ P_g(t + \frac{a}{v}) P_g(t - \frac{a}{v}) - P_g(-t - \frac{a}{v})) P_g(-t + \frac{a}{v}) \right] dt . \tag{C.8}$$

We consider the separate cases where $g < 1$ and $g > \frac{1}{2}$. The two cases overlap, and we find a single expression applicable for all values of $g$. For $g < 1$ the integral regulator is not required, so we set $\delta = 0$. With some careful manipulations of the fractional powers of $i$ we obtain

$$K_{g<\frac{1}{2}}(\omega) = 4 \sin(\pi g) \mathrm{sgn}(\omega) \int_{\frac{a}{v}}^{\infty} \frac{\sin(|\omega| t)}{(t^2 - (\frac{a}{v})^2)^g} \, dt$$

$$= \Gamma\left(g + \frac{1}{2}\right) \left(\frac{|\omega| a}{2v}\right)^{\frac{1}{2} - g} J_{g-\frac{1}{2}}\left(\frac{a|\omega|}{v}\right) I_{2g}(\omega) \mathrm{sgn}(\omega) . \tag{C.9}$$

The function $J_g(x)$ is the Bessel function of the first kind. The integral is found in Ref. [98]. For the case of $g > \frac{1}{2}$ we need an integral representation of the confluent hypergeometric function $_1F_1$

$$\int_{-\infty}^{\infty} (\beta + it)^{-g} (\gamma + it)^{-g} e^{i\omega t} dt = e^{-\gamma \omega} {}_1F_1(g; 2g; (\gamma - \beta)\omega) I_{2g}(\omega) \Theta(\omega) . \tag{C.10}$$

This applies when $\mathrm{Re}[\beta], \mathrm{Re}[\gamma] > 0$ and $\mathrm{Re}[g] > \frac{1}{2}$. With this integral representation we find

$$K_{g>\frac{1}{2}}(\omega) = e^{-\delta|\omega|} e^{i\frac{|\omega| a}{v}} {}_1F_1\left(g; 2g; -2i\frac{|\omega| a}{v}\right) I_{2g}(\omega) \mathrm{sgn}(\omega) . \tag{C.11}$$

For these specific parameters the confluent hypergeometric function ${}_1F_1$ reduces to the Bessel function of the first kind [98]

$$e^{i\frac{|\omega|a}{v}} {}_1F_1\left(g; 2g; -2i\frac{|\omega|a}{v}\right) = \Gamma\left(g + \frac{1}{2}\right)\left(\frac{|\omega|a}{2v}\right)^{\frac{1}{2}-g} J_{g-\frac{1}{2}}\left(\frac{|\omega|a}{v}\right).$$

Therefore both cases ($g > \frac{1}{2}$ and $g < 1$) match in the limit of $\delta \to 0$ and expression (C.9) extends to all values of $g > 0$. Finally, we have for the zero temperature expression of the modulating function of a symmetric interferometer

$$H_{ij}^{\text{mod}}(\omega) = \Gamma\left(g + \frac{1}{2}\right)\left(\frac{|\omega|a}{2v}\right)^{\frac{1}{2}-g} J_{g-\frac{1}{2}}\left(\frac{|\omega|a}{v}\right). \tag{C.12}$$

## C.2 Zero temperature limit from the finite temperature expression

The more general case in which we consider multiple modes with different edge velocities involves a more complicated Fourier transform which we are not able to determine directly. Instead, we use the result for finite temperatures and take the limit of $T \downarrow 0$.

We require the zero temperature limit of the modulating function, $H_{ij}^{\text{mod}}$ see Eq (3.61). To perform this limit we make use of the series representation of the $R$ function, Eq. (B.8). This gives

$$\lim_{T\downarrow 0} R\left(\alpha - i\frac{\omega}{2\pi T}; \mathcal{G}_n; e^{2\pi T x_1}, \ldots, e^{2\pi T x_n}\right) =$$

$$\lim_{T\downarrow 0} e^{-(2\pi T\alpha - i\omega)x_n} \sum_{m_1=0}^{\infty} \cdots \sum_{m_{n-1}=0}^{\infty} \frac{(\alpha - i\frac{\omega}{2\pi T})_{\sum_{i=1}^{n-1} m_i}}{(\gamma)_{\sum_{i=1}^{n-1} m_i}} \left[\prod_{i=1}^{n-1} \frac{(g_i)_{m_i}}{m_i!}\left(1 - e^{-2\pi T x_{n,i}}\right)^{m_i}\right]. \tag{C.13}$$

The $x_i$'s correspond to the (real valued) energy scales associated with the edge modes, i.e. $\pm\frac{a}{v_c}$ and so on. We assume $x_n \geq x_i$ for all $i$ and we write $x_n - x_i = x_{n,i} \geq 0$. The limit is determined term-by-term. We first note the approximation

$$\left(1 - e^{-2\pi T x_{n,i}}\right)^{m_i} = (2\pi T)^{m_i} x_{n,i}^{m_i} + \ldots. \tag{C.14}$$

The dots are of higher order in $T$. Combining this with the $(a - i\frac{\omega}{2\pi T})_m$ term, where we have set $m = \sum_{i=1}^{n-1} m_i$, we obtain for the zero temperature limit

$$\lim_{T\downarrow 0} \prod_{j=1}^{n-1}\left(2\pi T x_{n,j}\right)^{m_j} \prod_{k=0}^{m-1}\left(\alpha - i\frac{\omega}{2\pi T} + k\right) = \prod_{j=1}^{n-1}(-i\omega x_{n,j})^{m_j} + \ldots. \tag{C.15}$$

181

The higher order corrections of (C.14) vanish in this limit. Plugging this back into (C.13) gives

$$\lim_{T\downarrow 0} R\big(\alpha - i\tfrac{\omega}{2\pi T}; \mathcal{G}_n; \{e^{2\pi T x_1}, \ldots, e^{2\pi T x_n}\}\big)$$

$$= e^{i\omega x_n} \sum_{m_1=0}^{\infty} \cdots \sum_{m_{n-1}=0}^{\infty} \frac{1}{(\gamma)_{\tilde{m}}} \left[\prod_{i=1}^{n-1} \frac{(g_i)_{m_i}}{m_i!} (-i\omega x_{n,j})^{m_i}\right]$$

$$= e^{i\omega x_n} \Phi_2^{(n-1)}(\mathcal{G}_{n-1}; \gamma; \{-i\omega x_{n,1}, \ldots, -i\omega x_{n,n-1}\}) \qquad (C.16)$$

with $\tilde{m} = \sum_{i=1}^{n-1} m_i$. The resulting series is called the *confluent Lauricella hypergeometric function* [159]

$$\Phi_2^{(n)}(\mathcal{G}_n; \gamma; \{w_1, \ldots, w_n\}) = \sum_{m_1=0}^{\infty} \cdots \sum_{m_n=0}^{\infty} \frac{1}{(\gamma)_{\sum_i m_i}} \left[\prod_{i=1}^{n} \frac{(g_i)_{m_i}}{m_i!} w_i^{m_i}\right] . \qquad (C.17)$$

This series is a multivariable generalization of the confluent hypergeometric $\Phi_2^{(n=2)}$ function [98]. The expression for the modulating function is

$$H_{ij}^{\mathrm{mod}}(\omega) = e^{i\omega x_n} \Phi_2^{(n-1)}(\mathcal{G}_{n-1}; \gamma; \{-i\omega x_{n,1}, \ldots, -i\omega x_{n,n-1}\}) . \qquad (C.18)$$

Here we recall that the $x_i$ correspond to all combinations of $\eta_i \frac{a}{v_i}$ and $-\eta_i \frac{b}{v_i}$, the parameter $x_n$ satisfies $x_n > x_i$ for $i < n$ and $x_{n,i} \equiv x_n - x_i > 0$. As a sanity check we look at the case treated in Appendix C.1, which corresponds to the symmetric interferometer and a single channel. The confluent Lauricella function reduces to the confluent hypergeometric function, $\Phi_2^{(1)}(b, c; x) = {}_1F_1(b, c; x)$, which follows from the series representation. And so

$$\lim_{T\downarrow 0} R\left(g - i\frac{\omega}{2\pi T}; \{g, g\}; \{e^{2\pi T \frac{a}{v}}, e^{-T\frac{a}{v}}\}\right) = e^{i\omega \frac{a}{v}} {}_1F_1\left(g; 2g; -2i\omega\frac{a}{v}\right) . \qquad (C.19)$$

This matches with the result (C.9).

The series expansion of the confluent Lauricella function (C.17) is of the same form as the non-confluent Lauricella function, (B.8). The same combinatoric trick as explained in Appendix B.3 can be used to rewrite this multivariable series as a single expansion in terms of cycle indices, see Section B.3. For this expansion we find that the convergence of the confluent series is much better than the non-confluent (finite temperature) case. In general, we do not require as many terms in the series. However, for the physical values of the velocity, distance and voltage used in the main text we find that double floating precision is still not sufficient and we require high-precision floating point numbers [127].

## C.3  Interference current – general case

We have obtained the general expression for the zero temperature case by taking the zero temperature limit of the finite temperature expression. The same result can also be obtained

by taking the Fourier transform of the zero-temperature expression for the $G^>$ correlators. Since these calculations must produce the same answer we obtain the following integral representation of the confluent Lauricella hypergeometric function. With $P_g(t) = (\delta + it)^{-g}$ we have

$$\int_{-\infty}^{\infty} e^{i\omega t} \Big[ \prod_j P_{g_j}(t + x_j) - \prod_k P_{g_k}(-t + x_k) \Big] \, dt =$$
$$I_{2g}(\omega)\text{sgn}(\omega) e^{i\omega z_n} \Phi_2^{(n-1)}\big( \mathcal{G}_{n-1}; \gamma; -i\omega x_{n,1}, \cdots, -i\omega x_{n,n-1} \big) . \quad \text{(C.20)}$$

Here $x_{n,i} = x_n - x_i > 0$ for all $i < n$, all $g_i > 0$ and $\delta$ is taken to zero in the end. The function $I_g$ is given by (C.6) and $\Phi_2^{(n-1)}$ is the confluent Lauricella hypergeometric function, which has the series representation (C.17).

# Chapter D

# Non-equilibrium Ward identity and cross correlations

In Chapter 4 we encounter a correlator $\Delta S$, which appears in the expression for the finite frequency noise of the edge current (Eq. (4.78)). We recall the expression for this correlator

$$\Delta S(\omega) = \int_{-\infty}^{\infty} e^{i\omega t} \Big( \langle \Delta j_R(x, t + x/v_c) I_B^I(0) \rangle + \langle I_B^I(0) \Delta j_R(x, -t + x/v_c) \rangle \Big) dt \,. \tag{D.1}$$

In this appendix we derive a non-equilibrium Ward identity. Such an identity arises because the correlator contains a conserved current $j_R$. In general, Ward identities arise in a QFT due to constraints imposed on correlation functions associated with symmetries of the theory.

**Cross correlation**

The two correlators appearing in Eq. (D.1) are determined with respect to a thermal density matrix. As a consequence the two correlators are related through the Kubo-Martin-Schwinger relation [180]. This relation is explained in Section 4.7.2 and states that $\langle I_B^I(0) \Delta j_R(x,t) \rangle_0 = \langle \Delta j_R(x, t - i/T) I_B^I(0) \rangle_0$. We therefore write $\Delta S(t)$ as

$$\Delta S(t) = \mathcal{F}(t) + \mathcal{F}(-t - i/T)$$
$$\mathcal{F}(t) = \langle \Delta j_R(x, t + x/v_c) \hat{I}_B^I(0) \rangle \,. \tag{D.2}$$

In Fourier space the KMS relations results in

$$\Delta S(\omega) = \mathcal{F}(\omega) + e^{\omega/T} \mathcal{F}(-\omega) \tag{D.3}$$

Making the time evolution operators $\mathcal{U}$ explicit we have for $\mathcal{F}(\omega) = \int e^{i\omega t} \mathcal{F}(t) dt$,

$$\mathcal{F}(t) = \langle \Delta j_R(x, t + x/v_c) \mathcal{U}^\dagger(0, -\infty) \hat{I}_B(0) \mathcal{U}(0, -\infty) \rangle \tag{D.4}$$

Here $\Delta j_R(t) = j_R(x, t + x/v_c) - \langle j_R \rangle = -v_c \frac{\sqrt{\nu}}{2\pi} \partial_x \varphi_R$. Our goal is to simplify the expression for $\mathcal{F}(\omega)$. This accomplished by making use of the Ward identity associated with the current $j$.

**The equilibrium Ward identity**

Ward identities are restrictions imposed on correlation functions in a theory as a consequence of symmetries of the theory. In our case the insert operator $\Delta j_R$ is a conserved current as-

sociated with the $U(1)$ symmetry. We derived the equilibrium Ward identity in Chapter 2. Specifically, we obtained Eq. (2.176)

$$\langle \Delta j_R(x,t) \prod_{i=1}^{n} \psi_{\alpha_i}(x_i,t_i) \rangle = \Big[ \sum_{i=1}^{n} Q_i K(x-x_i-v_c(t-t_i)) \Big] \langle \prod_{i=1}^{n} \psi_{\alpha_i}(x_i,t_i) \rangle \tag{D.5}$$

where the propagator[1] is given by

$$K(x+v_c t) = \frac{T}{2} \cot\Big( \frac{\pi T}{v_c}(\delta + i(x+v_c t)) \Big) . \tag{D.6}$$

Here $Q_i \equiv \frac{\sqrt{\nu}}{2\pi}\alpha_i$ is the normalized charge carried by the quasiparticle operators $\psi_{\alpha_i}$. In Eq. (D.5) we do not require an expression for the $N$-quasiparticle correlator appearing on the right hand side. The Ward identity follows from the commutation relations of the current operator $j_R$ and the quasiparticle operators $\psi_{\alpha_i}$ and these relations are independent from the specific structure of the neutral channel. The Ward identity therefore applies to general edge theories, provided the edge contains a single chiral boson that decouples from the remaining channels. We comment on the multichannel case below.

**Non-equilibrium Ward identity**

The Ward identity (D.6) applies to correlators in which the time evolution of the operators is due to the equilibrium Hamiltonian. The operators that enter the expression of $\mathcal{F}$, see Eq. (D.4), are in the interaction representation. We therefore need to extend the Ward identity to this interaction picture. To accomplish this we expand the correlators using the series expansion of the time evolution operators $\mathcal{U}$ and apply the Ward identity term-by-term. The final result of these manipulations is Eq. (D.18). We recall the series expansion for $\mathcal{U}$

$$\mathcal{U}(t,-\infty) = \sum_{n=0}^{\infty} \frac{(-i)^n}{n!} \prod_{i=1}^{n} \int_{-\infty}^{t} dt_i \, \mathcal{T}\Big[ \prod_{i=1}^{n} H_T(t_i) \Big] . \tag{D.7}$$

Both the tunnelling Hamiltonian and tunnelling current $H_T$ and $\hat{I}_B^I$ are given in terms of $V$ and $V^\dagger$. Furthermore, $V \propto \psi_L^\dagger \psi_R$ and so the operator $V$ ($V^\dagger$) carries a charge of $-Q$ ($Q$) with respect to $j_R$. Therefore, whenever the correlator contains a tunneling Hamiltonian $H_T$ we have

$$\langle \Delta j_R(t) \cdots H_T(t') \cdots \rangle = iK(t-t')\langle \cdots \hat{I}_B(t') \cdots \rangle + \dots \tag{D.8}$$

Here the dots represent the remaining contractions. A similar expression holds for the tunnelling operator $\hat{I}_B(t)$ in which case $\hat{I}_B^I$ is replaced by $-iQ^2 H_T(t)$. We now apply this result

---

[1]We use a slightly different definition of $K(t)$ compared to Chapter 2.8.

to (D.4). First we expand the operators $\mathcal{U}$ and $\mathcal{U}^\dagger$. This results in

$$\mathcal{F}(t) = \sum_{n,m=0}^{\infty} \frac{(i)^n}{n!} \frac{(-i)^m}{m!} \prod_{i=1}^{n} \int_{-\infty}^{0} dt_i \prod_{j=1}^{m} \int_{-\infty}^{0} dt'_j \left\{ \langle \Delta j(t) \bar{\mathcal{T}} \Big[ \prod_{i=1}^{n} H_T(t_i) \Big] \hat{I}_B(0) \mathcal{T} \Big[ \prod_{j=1}^{m} H_T(t'_j) \Big] \rangle \right\}$$

(D.9)

with $\mathcal{T}[\cdot]$ and $\bar{\mathcal{T}}[\cdot]$ time and reversed-time ordering operators. Applying the Ward identity results in

$$\langle \Delta j(t) \bar{\mathcal{T}} \Big[ \prod_{i=1}^{n} H_T(t_i) \Big] \hat{I}_B(0) \mathcal{T} \Big[ \prod_{j=1}^{m} H_T(t'_j) \Big] \rangle =$$

$$- iQ^2 K(t) \langle \bar{\mathcal{T}} \Big[ \prod_{i=1}^{n} H_T(t_i) \Big] H_T(0) \mathcal{T} \Big[ \prod_{j=1}^{m} H_T(t'_j) \Big] \rangle$$

$$+ i \sum_{k=1}^{n} K(t - t_k) \langle \bar{\mathcal{T}} \Big[ I_B(t_k) \prod_{\substack{i=1 \\ i \neq k}}^{n} H_T(t_i) \Big] \hat{I}_B(0) \mathcal{T} \Big[ \prod_{j=1}^{m} H_T(t'_j) \Big] \rangle$$

$$+ i \sum_{k=1}^{m} K(t - t'_k) \langle \bar{\mathcal{T}} \Big[ \prod_{i=1}^{n} H_T(t_i) \Big] \hat{I}_B(0) \mathcal{T} \Big[ \hat{I}_B(t'_k) \prod_{\substack{j=1 \\ j \neq k}}^{m} H_T(t'_j) \Big] \rangle$$

(D.10)

The first term comes from the contraction of $j_R$ with $\hat{I}_B^I(0)$. The other two terms are the contractions of $j_R$ with the $H_T$ appearing in the time evolution operators. We plug the total expression Eq. (D.10) back into the summations and integretions in Eq. (D.9). Our next goal is to show that this step results in the following non-equilibrium Ward identity

$$\mathcal{F}(t) = -iQ^2 K(t) \langle H_T^I(0) \rangle - \int_{-\infty}^{0} K(t - t') \langle [\hat{I}_B^I(t'), \hat{I}_B^I(0)] \rangle \, dt' \,.$$

(D.11)

We are interested in the summation and integration over Eq. (D.10), i.e.

$$\sum_{n,m=0}^{\infty} \frac{(i)^n}{n!} \frac{(-i)^m}{m!} \Big[ \prod_{i=1}^{n} \int_{-\infty}^{0} dt_i \Big] \Big[ \prod_{j=1}^{m} \int_{-\infty}^{0} dt'_j \Big] \Big[ \text{Eq. (D.10)} \Big]$$

Consider the first term appearing in Eq. (D.10) (proportional to $Q^2$). It should be straightforward to see that this term results in the first term of Eq. (D.11). Next we consider the second term of Eq. (D.10). The integration over $dt'_j$ and summation over $m$ results in $\mathcal{U}(0, -\infty)$. What remains is

$$\sum_{n=1}^{\infty} \frac{(i)^{n-1}}{n!} \Big[ \prod_{i=1}^{n} \int_{-\infty}^{0} dt_i \Big] \sum_{k=1}^{n} K(t - t_k) \langle \bar{\mathcal{T}} \Big[ I_B(t_k) \prod_{\substack{i=1 \\ i \neq k}}^{n} H_T(t_i) \Big] \hat{I}_B(0) \mathcal{U}(0, -\infty) \rangle$$

(D.12)

By changing integration variables ($t_k \to t'$ and some additional relabeling) we can write this expression as

$$-\int_{-\infty}^{0} dt' K(t-t') \sum_{n=1}^{\infty} \frac{(i)^{n-1}}{(n-1)!} \Big[\prod_{i=1}^{n-1} \int_{-\infty}^{0} dt_i\Big] \langle \bar{\mathcal{T}}\Big[I_B(t') \prod_{i=1}^{n-1} H_T(t_i)\Big] \hat{I}_B(0) \mathcal{U}(0,-\infty)\rangle \quad \text{(D.13)}$$

The final integration and summation results in

$$\sum_{n=0}^{\infty} \frac{(i)^n}{n!} \prod_{i=1}^{n} \int_{-\infty}^{0} dt_i \bar{\mathcal{T}}\Big[I_B(t') \prod_{i=1}^{n} H_T(t_i)\Big] =$$

$$\bar{\mathcal{T}}\Big[\hat{I}_B(t')\mathcal{U}^\dagger(0,-\infty)\Big] = \mathcal{U}^\dagger(t',-\infty)\hat{I}_B(t')\mathcal{U}^\dagger(0,t') . \quad \text{(D.14)}$$

Finally, combining this result with Eq. (D.12) results in

$$[\text{2}^{\text{nd}}\text{ term}] \longrightarrow -\int_{-\infty}^{0} dt' K(t-t')\langle \hat{I}_B^I(t') \hat{I}_B^I(0)\rangle \quad \text{(D.15)}$$

The manipulation of the third and final term in Eq. (D.10) is done along the same lines and results in

$$[\text{3}^{\text{rd}}\text{ term}] \longrightarrow \int_{-\infty}^{0} dt' K(t-t')\langle \hat{I}_B^I(0) \hat{I}_B^I(t')\rangle \quad \text{(D.16)}$$

Putting everything together results in the non-equilibrium Ward identity Eq. (D.11).

Next we look at the Fourier transform of $\mathcal{F}(t)$. To obtain this we require $K(\omega)$. This can be obtained for instance through a contour integral. The result is

$$\int e^{i\omega t} K(t)dt = -e^{-\omega\delta} \frac{e^{\frac{\omega}{T}}}{e^{\frac{\omega}{T}} - 1} = -\frac{1}{2}e^{-\delta\omega}\Big(\coth\big(\frac{\omega}{2T}\big) + 1\Big) \equiv -\frac{1}{2}e^{-\delta\omega} N(\omega) . \quad \text{(D.17)}$$

The frequency representation of the non-equilibrium Ward identity is then (taking $\delta \downarrow 0$)

$$\mathcal{F}(\omega) = \frac{1}{2}N(\omega)\Big[iQ^2\langle H_T^I(0)\rangle + \int_{-\infty}^{0} e^{i\omega t'} \langle [\hat{I}_B^I(t'), \hat{I}_B^I(0)]\rangle dt'\Big] . \quad \text{(D.18)}$$

Note also the appearance of the antisymmetric noise, $R_{I_B}$, in the expression for $\mathcal{F}$. For $\Delta S$ we use Eq. (D.3) and obtain

$$\Delta S(\omega) = N(\omega)R_{I_B}(\omega) . \quad \text{(D.19)}$$

This proves the relation (4.81). We also note the real and imaginary parts of $\mathcal{F}$

$$2\text{Re}\big[\mathcal{F}(\omega)\big] = \Delta S(\omega) \quad \text{(D.20)}$$

$$2\text{Im}\big[\mathcal{F}(\omega)\big] = Q^2 N(\omega)\langle H_T^I(0)\rangle . \quad \text{(D.21)}$$

and so $\mathcal{F}(\omega)^* = e^{\omega/T}\mathcal{F}(\omega)$.

**Multichannel case**

We also comment on the multichannel case. In this case we have a non-equilibrium Ward identity for each channel. The difference is that the current operator of the $i$'th channel only measures a fraction of the total charge of the tunnelling operator $\mathcal{V}$. In particular, expression (D.8) becomes

$$\langle \Delta j_i(t) \cdots H_T(t') \cdots \rangle = i\frac{\kappa_i q_i}{Q} K(t - t')\langle \cdots \hat{I}_B(t') \cdots \rangle + \dots \tag{D.22}$$

The final identity Eq. (D.18) is scaled down by the same factor of $\kappa_i q_i / Q$. In the treatment of the multichannel case we also encounter the following cross correlation which mixes velocities of different channels

$$\Delta S_{ij}(t) = \langle \Delta j_i(x, t + \eta_j x/v_j)\hat{I}_B^I(0)\rangle + \langle \hat{I}_B^I(0)\Delta j_i(x, -(t + \eta_j x/v_j))\rangle \ . \tag{D.23}$$

This requires a bit more care, as we encounter the velocity $v_j$ instead of $v_i$ (compare this to Eq. (D.2)). Using the KMS relation Eq. (4.87) we obtain

$$\Delta S_{ij}(t) = \frac{\kappa_i q_i}{Q}\mathcal{F}\Big(t - x\big(\frac{\eta_i}{v_i} - \frac{\eta_j}{v_j}\big)\Big) + \frac{\kappa_i q_i}{Q}\mathcal{F}\Big(-t - x\big(\frac{\eta_i}{v_i} - \frac{\eta_j}{v_j}\big) - i/T\Big) \tag{D.24}$$

and its Fourier transform

$$\Delta S_{ij}(\omega) = \frac{\kappa_i q_i}{Q}e^{i\omega x\left(\frac{\eta_i}{v_i} - \frac{\eta_j}{v_j}\right)}N(\omega)R_{I_B}(\omega) \ . \tag{D.25}$$

# Bibliography

[1] An, S., P. Jiang, H. Choi, W. Kang, S. H. Simon, L. N. Pfeiffer, K. W. West, and K. W. Baldwin. *Braiding of Abelian and Non-Abelian Anyons in the Fractional Quantum Hall Effect*. ArXiv e-prints URL arXiv:1112.3400

[2] Anderson, P. W. *Absence of Diffusion in Certain Random Lattices*. Phys. Rev. **109**, (1958), 1492. DOI 10.1103/PhysRev.109.1492

[3] Ardonne, E. *A conformal field theory description of fractional quantum Hall states*. PhD. Thesis, University of Amsterdam (2002). URL http://dare.uva.nl/en/record/103471

[4] Ardonne, E. and C. J. M. Schoutens. *New Class of Non-Abelian Spin-Singlet Quantum Hall States*. Phys. Rev. Lett. **82**, (1999), 5096. DOI 10.1103/PhysRevLett.82.5096

[5] Arovas, D., J. R. Schrieffer, and F. Wilczek. *Fractional Statistics and the Quantum Hall Effect*. Phys. Rev. Lett. **53**, (1984), 722. DOI 10.1103/PhysRevLett.53.722

[6] Bais, A. F., B. J. Schroers, and J. K. Slingerland. *Hopf symmetry breaking and confinement in (2+1)-dimensional gauge theory*. Journal of High Energy Physics **2003** (05), (2003), 068. DOI 10.1088/1126-6708/2003/05/068

[7] Balachandran, A. P., L. Chandar, and B. Sathiapalan. *Duality and the fractional quantum Hall effect*. Nuclear Physics B **443** (3), (1995), 465 . DOI 10.1016/0550-3213(95)00122-9

[8] Belavin, A., A. Polyakov, and A. Zamolodchikov. *Infinite conformal symmetry in two-dimensional quantum field theory*. Nuclear Physics B **241** (2), (1984), 333 . DOI 10.1016/0550-3213(84)90052-X

[9] Bena, C. and C. Nayak. *Effects of non-Abelian statistics on two-terminal shot noise in a quantum Hall liquid in the Pfaffian state*. Phys. Rev. B **73**, (2006), 155335. DOI 10.1103/PhysRevB.73.155335

[10] Bena, C. and I. Safi. *Emission and absorption noise in the fractional quantum Hall effect*. Phys. Rev. B **76**, (2007), 125317. DOI 10.1103/PhysRevB.76.125317

[11] Bergholtz, E. J. and A. Karlhede. *Quantum Hall system in Tao-Thouless limit*. Phys. Rev. B **77**, (2008), 155308. DOI 10.1103/PhysRevB.77.155308

[12] Bernevig, B. A. and F. D. M. Haldane. *Model Fractional Quantum Hall States and Jack Polynomials*. Phys. Rev. Lett. **100**, (2008), 246802. DOI 10.1103/PhysRevLett.100.246802

[13] Bid, A., N. Ofek, M. Heiblum, V. Umansky, and D. Mahalu. *Shot Noise and Charge at the 2/3 Composite Fractional Quantum Hall State*. Phys. Rev. Lett. **103**, (2009), 236802. DOI 10.1103/PhysRevLett.103.236802

[14] Bid, A., N. Ofek, H. Inoue, C. L. Heiblum, M. Kane, V. Umansky, and D. Mahalu. *Observation of neutral modes in the fractional quantum Hall regime*. Nature **466**, (2010), 585. DOI 10.1038/nature09277

[15] Bieri, S. and J. Fröhlich. *Physical principles underlying the quantum Hall effect*. Comptes Rendus Physique **12** (4), (2011), 332. DOI 10.1016/j.crhy.2011.02.001

[16] Bieri, S. and J. Fröhlich. *Effective field theory and tunneling currents in the fractional quantum Hall effect*. Annals of Physics **327** (4), (2012), 959. DOI 10.1016/j.aop.2011.10.012

[17] Bishara, W., P. Bonderson, C. Nayak, K. Shtengel, and J. K. Slingerland. *Interferometric signature of non-Abelian anyons*. Phys. Rev. B **80**, (2009), 155303. DOI 10.1103/PhysRevB.80.155303

[18] Bishara, W. and C. Nayak. *Edge states and interferometers in the Pfaffian and anti-Pfaffian states of the $\nu = 5/2$ quantum Hall system*. Phys. Rev. B **77** (16), (2008), 165302. DOI 10.1103/PhysRevB.77.165302

[19] Bishara, W. and C. Nayak. *Odd-even crossover in a non-Abelian $\nu = 5/2$ interferometer*. Phys. Rev. B **80** (15), (2009), 155304. DOI 10.1103/PhysRevB.80.155304

[20] Blanter, Y. and M. M. Büttiker. *Shot noise in mesoscopic conductors*. Physics Reports **336** (1-2), (2000), 1. DOI 10.1016/S0370-1573(99)00123-4

[21] Blok, B. and X.-G. Wen. *Effective theories of the fractional quantum Hall effect at generic filling fractions*. Phys. Rev. B **42**, (1990), 8133. DOI 10.1103/PhysRevB.42.8133

[22] Blok, B. and X.-G. Wen. *Many-body systems with non-abelian statistics*. Nuclear Physics B **374** (3), (1992), 615. DOI 10.1016/0550-3213(92)90402-W

[23] Bonderson, P., A. E. Feiguin, G. Möller, and J. K. Slingerland. *Competing Topological Orders in the* $\nu = 12/5$ *Quantum Hall State.* Phys. Rev. Lett. **108**, (2012), 036806. DOI 10.1103/PhysRevLett.108.036806

[24] Bonderson, P., A. Kitaev, and K. Shtengel. *Detecting Non-Abelian Statistics in the* $\nu = 5/2$ *Fractional Quantum Hall State.* Phys. Rev. Lett. **96**, (2006), 016803. DOI 10.1103/PhysRevLett.96.016803

[25] Bonderson, P., K. Shtengel, and J. K. Slingerland. *Probing Non-Abelian Statistics with Quasiparticle Interferometry.* Phys. Rev. Lett. **97**, (2006), 016401. DOI 10.1103/PhysRevLett.97.016401

[26] Bonderson, P. and J. K. Slingerland. *Fractional quantum Hall hierarchy and the second Landau level.* Phys. Rev. B **78**, (2008), 125323. DOI 10.1103/PhysRevB.78.125323

[27] Boyarsky, A., V. Cheianov, and J. Fröhlich. *Effective-field theories for the* $\nu = 5/2$ *quantum Hall edge state.* Phys. Rev. B **80**, (2009), 233302. DOI 10.1103/PhysRevB.80.233302

[28] Braggio, A., D. Ferraro, M. Carrega, N. Magnoli, and M. Sassetti. *Environmental induced renormalization effects in quantum Hall edge states due to 1/f noise and dissipation.* New Journal of Physics **14** (9), (2012), 093032

[29] Büttiker, M. *Four-Terminal Phase-Coherent Conductance.* Phys. Rev. Lett. **57**, (1986), 1761. DOI 10.1103/PhysRevLett.57.1761

[30] Büttiker, M. *Scattering theory of current and intensity noise correlations in conductors and wave guides.* Phys. Rev. B **46**, (1992), 12485. DOI 10.1103/PhysRevB.46.12485

[31] Caldeira, A. O. and A. J. Leggett. *Quantum tunnelling in a dissipative system.* Annals of Physics **149**, (1983), 374. DOI 10.1016/0003-4916(83)90202-6

[32] Camino, F. E., W. Zhou, and V. J. Goldman. *Realization of a Laughlin quasiparticle interferometer: Observation of fractional statistics.* Phys. Rev. B **72**, (2005), 075342. DOI 10.1103/PhysRevB.72.075342

[33] Cappelli, A., G. V. Dunne, C. A. Trugenberger, and G. R. Zemba. *Conformal symmetry and universal properties of quantum Hall states.* Nuclear Physics B **398** (3), (1993), 531 . DOI 10.1016/0550-3213(93)90603-M

[34] Cappelli, A., C. A. Trugenberger, and G. R. Zemba. *Infinite symmetry in the quantum Hall effect*. Nuclear Physics B **396** (2–3), (1993), 465 . DOI 10.1016/0550-3213(93)90660-H

[35] Carlson, B. C. *Lauricella's hypergeometric function FD*. J. of Math. Analysis and Applications **7** (3), (1963), 452 . DOI 10.1016/0022-247X(63)90067-2

[36] Carrega, M., D. Ferraro, A. Braggio, N. Magnoli, and M. Sassetti. *Anomalous Charge Tunneling in Fractional Quantum Hall Edge States at a Filling Factor $\nu = 5/2$*. Phys. Rev. Lett. **107**, (2011), 146404. DOI 10.1103/PhysRevLett.107.146404

[37] Carrega, M., D. Ferraro, A. Braggio, N. Magnoli, and M. Sassetti. *Spectral noise for edge states at the filling factor $\nu = 5/2$*. New Journal of Physics **14** (2), (2012), 023017. DOI 10.1088/1367-2630/14/2/023017

[38] Chakraborty, T. and P. Pietiläinen. *The Quantum Hall Effects - Fractional and Integral*. Springer, New York (1995)

[39] Chamon, C. and D. E. Freed. *Colored noise in the fractional quantum Hall effect: Duality relations and exact results*. Phys. Rev. B **60**, (1999), 1842. DOI 10.1103/PhysRevB.60.1842

[40] Chamon, C. d. C., D. E. Freed, S. A. Kivelson, S. L. Sondhi, and X.-G. Wen. *Two point-contact interferometer for quantum Hall systems*. Phys. Rev. B **55** (4), (1997), 2331. DOI 10.1103/PhysRevB.55.2331

[41] Chamon, C. d. C., D. E. Freed, and X.-G. Wen. *Tunneling and quantum noise in one-dimensional Luttinger liquids*. Phys. Rev. B **51** (4), (1995), 2363. DOI 10.1103/PhysRevB.51.2363

[42] Chamon, C. d. C., D. E. Freed, and X.-G. Wen. *Nonequilibrium quantum noise in chiral Luttinger liquids*. Phys. Rev. B **53** (7), (1996), 4033. DOI 10.1103/PhysRevB.53.4033

[43] Chamon, C. d. C. and X. G. Wen. *Sharp and smooth boundaries of quantum Hall liquids*. Phys. Rev. B **49**, (1994), 8227. DOI 10.1103/PhysRevB.49.8227

[44] Chang, A. M. *Chiral Luttinger liquids at the fractional quantum Hall edge*. Rev. Mod. Phys. **75**, (2003), 1449. DOI 10.1103/RevModPhys.75.1449

[45] Chen, H., Z.-X. Hu, K. Yang, E. H. Rezayi, and X. Wan. *Quasiparticle tunneling in the Moore-Read fractional quantum Hall state*. Phys. Rev. B **80**, (2009), 235305. DOI 10.1103/PhysRevB.80.235305

[46] Chung, Y. C., M. Heiblum, Y. Oreg, V. Umansky, and D. Mahalu. *Anomalous chiral Luttinger liquid behavior of diluted fractionally charged quasiparticles*. Phys. Rev. B **67**, (2003), 201104. DOI 10.1103/PhysRevB.67.201104

[47] Chung, Y. C., M. Heiblum, and V. Umansky. *Scattering of Bunched Fractionally Charged Quasiparticles*. Phys. Rev. Lett. **91**, (2003), 216804. DOI 10.1103/PhysRevLett.91.216804

[48] Clerk, A. A., M. H. Devoret, S. M. Girvin, F. Marquardt, and R. J. Schoelkopf. *Introduction to quantum noise, measurement, and amplification*. Rev. Mod. Phys. **82**, (2010), 1155. DOI 10.1103/RevModPhys.82.1155

[49] Comforti, E., Y. C. Chung, M. Heiblum, and V. Umansky. *Multiple Scattering of Fractionally Charged Quasiparticles*. Phys. Rev. Lett. **89**, (2002), 066803. DOI 10.1103/PhysRevLett.89.066803

[50] Cooper, N. R. *Rapidly rotating atomic gases*. Advances in Physics **57**, (2008), 539. DOI 10.1080/00018730802564122

[51] Costa, M. E. V. and H. O. Girotti. *Comment on "Self-dual fields as charge-density solitons"*. Phys. Rev. Lett. **60**, (1988), 1771. DOI 10.1103/PhysRevLett.60.1771

[52] Cristofano, G., G. Maiella, R. Musto, and F. Nicodemi. *Topological order in Quantum hall effect and two-dimensional conformal field theory*. Nuclear Physics B **33** (3), (1993), 119 . DOI 10.1016/0920-5632(93)90377-I

[53] Das Sarma, S., M. Freedman, and C. Nayak. *Topologically Protected Qubits from a Possible Non-Abelian Fractional Quantum Hall State*. Phys. Rev. Lett. **94**, (2005), 166802. DOI 10.1103/PhysRevLett.94.166802

[54] Datta, S. *Electronic Transport in Mesoscopic Systems*. Cambridge University Press, Cambridge (1997)

[55] de-Picciotto, R., M. Reznikov, M. Heiblum, V. Umansky, G. Bunin, and D. Mahalu. *Direct observation of a fractional charge*. Nature **389**, (1997), 162. DOI 10.1038/38241

[56] Deser, S., R. Jackiw, and S. Templeton. *Topologically massive gauge theories*. Annals of Physics **140** (2), (1982), 372 . DOI 10.1016/0003-4916(82)90164-6

[57] Devecchi, F. P. and H. O. Girotti. *Chiral bosons and improper constraints*. Phys. Rev. D **49**, (1994), 4302. DOI 10.1103/PhysRevD.49.4302

[58] Di Francesco, P., P. Mathieu, and D. Senechal. *Conformal Field Theory*. Springer, New York (1995)

[59] Dirac, P. A. M. *Lectures on quantum mechanics*. Dover, New York (1964)

[60] Dolev, M., Y. Gross, Y. C. Chung, M. Heiblum, V. Umansky, and D. Mahalu. *Dependence of the tunneling quasiparticle charge determined via shot noise measurements on the tunneling barrier and energetics*. Phys. Rev. B **81**, (2010), 161303. DOI 10.1103/PhysRevB.81.161303

[61] Dolev, M., Y. Gross, Y. C. Chung, M. Heiblum, V. Umansky, and D. Mahalu. *Is The Charge Determined Via Shot Noise Unique?* In J. Ihm and H. Cheong (Editors), *American Institute of Physics Conference Series*, volume 1399, 613–614 (2011). DOI 10.1063/1.3666527

[62] Dolev, M., Y. Gross, M. Heiblum, V. Umansky, A. Stern, and D. Mahalu. *Shot noise measurement at $\nu = 5/2$ quantum Hall state*. In M. Caldas and N. Studart (Editors), *American Institute of Physics Conference Series*, volume 1199, 239–240 (2010). DOI 10.1063/1.3295387

[63] Dolev, M., Y. Gross, R. Sabo, I. Gurman, M. Heiblum, V. Umansky, and D. Mahalu. *Characterizing Neutral Modes of Fractional States in the Second Landau Level*. Phys. Rev. Lett. **107**, (2011), 036805. DOI 10.1103/PhysRevLett.107.036805

[64] Dolev, M., M. Heiblum, V. Umansky, A. Stern, and D. Mahalu. *Observation of a quarter of an electron charge at the $\nu = 5/2$ quantum Hall state*. Nature **452**, (2008), 829. DOI 10.1038/nature06855

[65] Dunne, G. V. *Aspects Of Chern-Simons Theory*. In A. Comtet, T. Jolicoeur, S. Ouvry, and F. David (Editors), *Topological aspects of low dimensional systems*, volume 69, 177–263. Springe (1999). DOI 10.1007/3-540-46637-1_3

[66] Economou, E. N. *Green's Functions in Quantum Physics*. Springer (2010)

[67] Elitzur, S., G. Moore, A. Schwimmer, and N. Seiberg. *Remarks on the canonical quantization of the Chern-Simons-Witten theory*. Nuclear Physics B **326**, (1989), 108

[68] Erdélyi, A. *Higher Transcendental Functions Volume 1*. Robert E. Krieger Publishing Company, Florida (1953)

[69] Fendley, P., M. P. A. Fisher, and C. Nayak. *Dynamical Disentanglement across a Point Contact in a Non-Abelian Quantum Hall State*. Phys. Rev. Lett. **97** (3), (2006), 036801. DOI 10.1103/PhysRevLett.97.036801

[70] Fendley, P., M. P. A. Fisher, and C. Nayak. *Edge states and tunneling of non-Abelian quasiparticles in the $\nu = 5/2$ quantum Hall state and $p + ip$ superconductors*. Phys. Rev. B **75** (4), (2007), 045317. DOI 10.1103/PhysRevB.75.045317

[71] Fendley, P., A. W. W. Ludwig, and H. Saleur. *Exact Conductance through Point Contacts in the $\nu = 1/3$ Fractional Quantum Hall Effect*. Phys. Rev. Lett. **74**, (1995), 3005. DOI 10.1103/PhysRevLett.74.3005

[72] Fendley, P., A. W. W. Ludwig, and H. Saleur. *Exact Nonequilibrium dc Shot Noise in Luttinger Liquids and Fractional Quantum Hall Devices*. Phys. Rev. Lett. **75**, (1995), 2196. DOI 10.1103/PhysRevLett.75.2196

[73] Fendley, P., A. W. W. Ludwig, and H. Saleur. *Exact nonequilibrium transport through point contacts in quantum wires and fractional quantum Hall devices*. Phys. Rev. B **52**, (1995), 8934. DOI 10.1103/PhysRevB.52.8934

[74] Fendley, P. and H. Saleur. *Nonequilibrium dc noise in a Luttinger liquid with an impurity*. Phys. Rev. B **54**, (1996), 10845. DOI 10.1103/PhysRevB.54.10845

[75] Ferraro, D., A. Braggio, N. Magnoli, and M. Sassetti. *Charge tunneling in fractional edge channels*. Phys. Rev. B **82**, (2010), 085323. DOI 10.1103/PhysRevB.82.085323

[76] Ferraro, D., A. Braggio, N. Magnoli, and M. Sassetti. *Multiple-quasiparticle agglomerates at*. Physica E: Low-dimensional Systems and Nanostructures **42** (3), (2010), 580 . DOI 10.1016/j.physe.2009.06.037

[77] Ferraro, D., A. Braggio, N. Magnoli, and M. Sassetti. *Neutral modes' edge state dynamics through quantum point contacts*. New Journal of Physics **12** (1), (2010), 013012. DOI 10.1088/1367-2630/12/1/013012

[78] Ferraro, D., A. Braggio, M. Merlo, N. Magnoli, and M. Sassetti. *Relevance of Multiple Quasiparticle Tunneling between Edge States at $\nu = p/(2np + 1)$*. Phys. Rev. Lett. **101**, (2008), 166805. DOI 10.1103/PhysRevLett.101.166805

[79] Feynman, R. P. and A. R. Hibbs. *Quantum Mechanics and Path Integrals*. McGraw-Hill Companies (1965)

[80] Fidkowski, L. *Double Point Contact in the k=3 Read-Rezayi State*. ArXiv e-prints URL arXiv:0704.3291

[81] Floreanini, R. and R. Jackiw. *Self-dual fields as charge-density solitons*. Phys. Rev. Lett. **59**, (1987), 1873. DOI 10.1103/PhysRevLett.59.1873

[82] Fradkin, E., C. Nayak, A. Tsvelik, and F. Wilczek. *A Chern-Simons effective field theory for the Pfaffian quantum Hall state*. Nuclear Physics B **516** (3), (1998), 704 . DOI 10.1016/S0550-3213(98)00111-4

[83] Freedman, M. H. *P/NP, and the quantum field?computer*. Proceedings of the National Academy of Sciences **95** (1), (1998), 98

[84] Fröhlich, J. and T. Kerler. *Universality in quantum Hall systems*. Nuclear Physics B **354** (2–3), (1991), 369 . DOI 10.1016/0550-3213(91)90360-A

[85] Fröhlich, J., B. Pedrini, C. Schweigert, and J. Walcher. *Universality in Quantum Hall Systems: Coset Construction of Incompressible States*. J. of Stat. Phys. **103**, (2001), 527. DOI 10.1023/A:1010389232079

[86] Fröhlich, J. and A. Zee. *Large scale physics of the quantum hall fluid*. Nuclear Physics B **364** (3), (1991), 517 . DOI 10.1016/0550-3213(91)90275-3

[87] Fujii, T. *New Study of Shot Noise Based on the Nonequilibrium Kubo Formula in Mesoscopic Systems: Application to the Kondo Effect in a Quantum Dot*. J. of the Phys. Society of Japan **79** (4), (2010), 044714. DOI 10.1143/JPSJ.79.044714

[88] Georgiev, L. S. *A universal conformal field theory approach to the chiral persistent currents in the mesoscopic fractional quantum Hall states*. Nuclear Physics B **707** (3), (2005), 347 . DOI 10.1016/j.nuclphysb.2004.11.022

[89] Giamarchi, T. *Quantum physics in one dimension*. Clarendon Press, Oxford (2003)

[90] Ginzburg, V. L. and L. D. Landau. *On the theory of superconductivity*. Zh. Eksp. Teor. Fiz. **20**, (1950), 1064

[91] Girotti, H. O., M. Gomes, V. Kurak, V. O. Rivelles, and A. J. da Silva. *Chiral Bosonization*. Phys. Rev. Lett. **60**, (1988), 1913. DOI 10.1103/PhysRevLett.60.1913

[92] Girvin, S. M. *The Quantum Hall Effect: Novel Excitations and Broken Symmetries*. ArXiv e-prints URL arXiv:cond-mat/9907002v1

[93] Giuliani, G. and G. Vignale. *Quantum Theory of the Electron Liquid.* Cambridge University Press, Cambridge (2005)

[94] Glattli, D. C., V. Rodriguez, H. Perrin, P. Roche, Y. Jin, and B. Etienne. *Shot noise and the Luttinger liquid-like properties of the FQHE.* Physica E: Low-dimensional Systems and Nanostructures **6** (1–4), (2000), 22. DOI 10.1016/S1386-9477(99)00044-2

[95] Glattli, D. C., L. Saminadayar, Y. Jin, and B. Etienne. *Observation of e/3 fractionally charged quasiparticles.* Physica B: Condensed Matter **249–251** (0), (1998), 401 . DOI 10.1016/S0921-4526(98)00142-2

[96] Goerbig, M. O. *Quantum Hall Effects.* ArXiv e-prints URL arXiv:0909.1998

[97] Gogolin, A. O., A. A. Nersesyan, and A. M. Tsvelik. *Bosonization and Strongly Correlated Systems.* Cambridge University Press, Cambridge (1998)

[98] Gradshteyn, I. S. and I. M. Ryzhik. *Table of Integrals, Series, and Products.* Elsevier, Massachusetts, 7th edition (2007)

[99] Greiter, M., X.-G. Wen, and F. Wilczek. *Paired Hall state at half filling.* Phys. Rev. Lett. **66**, (1991), 3205. DOI 10.1103/PhysRevLett.66.3205

[100] Griffiths, T. G., E. Comforti, M. Heiblum, A. Stern, and V. Umansky. *Evolution of Quasiparticle Charge in the Fractional Quantum Hall Regime.* Phys. Rev. Lett. **85**, (2000), 3918. DOI 10.1103/PhysRevLett.85.3918

[101] Haldane, F. D. M. *'Luttinger liquid theory' of one-dimensional quantum fluids. I. Properties of the Luttinger model and their extension to the general 1D interacting spinless Fermi gas.* Journal of Physics C: Solid State Physics **14** (19), (1981), 2585

[102] Haldane, F. D. M. *Fractional Quantization of the Hall Effect: A Hierarchy of Incompressible Quantum Fluid States.* Phys. Rev. Lett. **51**, (1983), 605. DOI 10.1103/PhysRevLett.51.605

[103] Haldane, F. D. M. and E. H. Rezayi. *Spin-singlet wave function for the half-integral quantum Hall effect.* Phys. Rev. Lett. **60**, (1988), 956. DOI 10.1103/PhysRevLett.60.956

[104] Hall, E. H. *On a new action of the magnet on electric currents.* American Journal of Mathematics **2** (3), (1879), 287

[105] Halperin, B. *Theory of the quantized Hall conductance.* Helv. Phys. Acta **56**, (1983), 75

[106] Halperin, B. I. *Quantized Hall conductance, current-carrying edge states, and the existence of extended states in a two-dimensional disordered potential*. Phys. Rev. B **25**, (1982), 2185. DOI 10.1103/PhysRevB.25.2185

[107] Halperin, B. I. *Statistics of Quasiparticles and the Hierarchy of Fractional Quantized Hall States*. Phys. Rev. Lett. **52**, (1984), 1583. DOI 10.1103/PhysRevLett.52.1583

[108] Halperin, B. I., P. A. Lee, and N. Read. *Theory of the half-filled Landau level*. Phys. Rev. B **47**, (1993), 7312. DOI 10.1103/PhysRevB.47.7312

[109] Halperin, B. I., A. Stern, I. Neder, and B. Rosenow. *Theory of the Fabry-Pérot quantum Hall interferometer*. Phys. Rev. B **83**, (2011), 155440. DOI 10.1103/PhysRevB.83.155440

[110] Hansson, T. H., C.-C. Chang, J. K. Jain, and S. Viefers. *Composite-fermion wave functions as correlators in conformal field theory*. Phys. Rev. B **76**, (2007), 075347. DOI 10.1103/PhysRevB.76.075347

[111] Hansson, T. H., C.-C. Chang, J. K. Jain, and S. Viefers. *Conformal Field Theory of Composite Fermions*. Phys. Rev. Lett. **98**, (2007), 076801. DOI 10.1103/PhysRevLett.98.076801

[112] Hansson, T. H., V. Oganesyan, and S. L. Sondhi. *Superconductors are topologically ordered*. Annals of Physics **313** (2), (2004), 497 . DOI 10.1016/j.aop.2004.05.006

[113] Hasan, M. Z. and C. L. Kane. *Colloquium : Topological insulators*. Rev. Mod. Phys. **82**, (2010), 3045. DOI 10.1103/RevModPhys.82.3045

[114] Heiblum, M. *Measuring the fractional charge and its evolution*. In B. Kramer (Editor), *Advances in Solid State Physics*, volume 40, 21 (2000). DOI 10.1007/BFb0108343

[115] Heiblum, M. *Fractionally charged quasiparticles*. Physica E: Low-dimensional Systems and Nanostructures **20** (1-2), (2003), 89 . DOI 10.1016/j.physe.2003.09.024

[116] Heiblum, M. *Quantum shot noise in edge channels*. Physica Status Solidi B Basic Research **243**, (2006), 3604. DOI 10.1002/pssb.200642237

[117] Henneaux, M. and C. Teitelboim. *Quantization of gauge systems*. Princeton university press (1994)

[118] Hu, Z.-X., E. H. Rezayi, X. Wan, and K. Yang. *Edge-mode velocities and thermal coherence of quantum Hall interferometers*. Phys. Rev. B **80**, (2009), 235330. DOI 10.1103/PhysRevB.80.235330

[119] Hunter, J. D. *Matplotlib: A 2D graphics environment*. Computing In Science and Engineering **9** (3), (2007), 90. URL http://matplotlib.org/

[120] Iyoda, E. and T. Fujii. *Analysis of Shot Noise at Finite Temperatures in Fractional Quantum Hall Edge States*. Journal of the Physical Society of Japan **80** (7), (2011), 073709. DOI 10.1143/JPSJ.80.073709

[121] Jackiw, R. *(Constrained) Quantization Without Tears*. ArXiv High Energy Physics - Theory e-prints URL arXiv:arXiv:hep-th/9306075

[122] Jain, J. K. *Composite-fermion approach for the fractional quantum Hall effect*. Phys. Rev. Lett. **63**, (1989), 199. DOI 10.1103/PhysRevLett.63.199

[123] Jain, J. K. *Incompressible quantum Hall states*. Phys. Rev. B **40**, (1989), 8079. DOI 10.1103/PhysRevB.40.8079

[124] Jain, J. K. *Composite Fermions*. Cambridge University Press, Cambridge (2007)

[125] Jentschura, U. D., P. J. Mohr, S. G., and E. J. Weniger. *Convergence acceleration via combined nonlinear-condensation transformations*. Comp. Phys. Comm. **116** (1), (1999), 28 . DOI 10.1016/S0010-4655(98)00111-8

[126] Ji, Y., Y. Chung, D. Sprinzak, M. Heiblum, D. Mahalu, and H. Shtrikman. *An electronic Mach-Zehnder interferometer*. Nature **422**, (2003), 415. DOI 10.1038/nature01503

[127] Johansson, F. et al. *mpmath: a Python library for arbitrary-precision floating-point arithmetic (version 0.17)* (2010)

[128] Jr., C. C. and J. Harvey. *Anomalies and fermion zero modes on strings and domain walls*. Nuclear Physics B **250** (1-4), (1985), 427 . DOI 10.1016/0550-3213(85)90489-4

[129] Kadanoff, L. P. and G. Baym. *Quantum statistical mechanics: Green's function methods in equilibrium and nonequilibrium problems*. Benjamin (1962)

[130] Kane, C. L. and M. P. A. Fisher. *Transmission through barriers and resonant tunneling in an interacting one-dimensional electron gas*. Phys. Rev. B **46** (23), (1992), 15233. DOI 10.1103/PhysRevB.46.15233

[131] Kane, C. L. and M. P. A. Fisher. *Nonequilibrium noise and fractional charge in the quantum Hall effect*. Phys. Rev. Lett. **72** (5), (1994), 724. DOI 10.1103/PhysRevLett.72.724

[132] Kane, C. L. and M. P. A. Fisher. *Contacts and edge-state equilibration in the fractional quantum Hall effect.* Phys. Rev. B **52**, (1995), 17393. DOI `10.1103/PhysRevB.52.17393`

[133] Kane, C. L., M. P. A. Fisher, and J. Polchinski. *Randomness at the edge: Theory of quantum Hall transport at filling ν=2/3.* Phys. Rev. Lett. **72**, (1994), 4129. DOI `10.1103/PhysRevLett.72.4129`

[134] Kauffman, L. H. *Knots and Physics.* World Scientific Publishing Company (2012)

[135] Kitaev, A. and J. Preskill. *Topological Entanglement Entropy.* Phys. Rev. Lett. **96**, (2006), 110404. DOI `10.1103/PhysRevLett.96.110404`

[136] Kitaev, A. Y. *Fault-tolerant quantum computation by anyons.* Annals of Physics **303** (1), (2003), 2 . DOI `10.1016/S0003-4916(02)00018-0`

[137] Kitaev, A. Y. *Anyons in an exactly solved model and beyond.* Annals of Physics **321** (1), (2006), 2 . DOI `10.1016/j.aop.2005.10.005`

[138] Klitzing, K. v., G. Dorda, and M. Pepper. *New Method for High-Accuracy Determination of the Fine-Structure Constant Based on Quantized Hall Resistance.* Phys. Rev. Lett. **45** (6), (1980), 494. DOI `10.1103/PhysRevLett.45.494`

[139] Knizhnik, V. G. and A. B. Zamolodchikov. *Current algebra and Wess-Zumino model in two dimensions.* Nucl. Phys. B **247** (1), (1984), 83. DOI `10.1016/0550-3213(84)90374-2`

[140] Laarhoven, P. J. M. v. and T. A. C. M. Kalker. *On the computation of Lauricella functions of the fourth kind.* J. of Comp. and Appl. Math. **21** (3), (1988), 369 . DOI `10.1016/0377-0427(88)90320-2`

[141] Landau, L. D. *Diamagnetismus der Metalle.* Zeitschrift für Physik **64** (9-10), (1930), 629. DOI `10.1007/BF01397213`

[142] Landau, L. D. and E. M. Lifshitz. *Quantum Mechanics, Non-Relativistic Theory: Vol. 3 of Course of Theoretical Physics.* Pergamon Press, Oxford (1958)

[143] Landauer, R. and T. Martin. *Equilibrium and shot noise in mesoscopic systems.* Physica B: Condensed Matter **175** (1-3), (1991), 167 . DOI `10.1016/0921-4526(91)90710-V`

[144] Laughlin, R. B. *Quantized Hall conductivity in two dimensions.* Phys. Rev. B **23**, (1981), 5632. DOI `10.1103/PhysRevB.23.5632`

[145] Laughlin, R. B. *Anomalous Quantum Hall Effect: An Incompressible Quantum Fluid with Fractionally Charged Excitations.* Phys. Rev. Lett. **50** (18), (1983), 1395. DOI 10.1103/PhysRevLett.50.1395

[146] Lauricella, G. *Sulle funzioni ipergeometriche a piu variabili.* Rendiconti del Circolo Matematico Di Palermo **7** (1), (1893), 111 . DOI 10.1007/BF03012437

[147] Lee, D.-H. and X.-G. Wen. *Edge excitations in the fractional-quantum-Hall liquids.* Phys. Rev. Lett. **66**, (1991), 1765. DOI 10.1103/PhysRevLett.66.1765

[148] Lee, S.-S., S. Ryu, C. Nayak, and M. P. A. Fisher. *Particle-Hole Symmetry and the $\nu = \frac{5}{2}$ Quantum Hall State.* Phys. Rev. Lett. **99**, (2007), 236807. DOI 10.1103/PhysRevLett.99.236807

[149] Leinaas, J. M. and J. Myrheim. *On the theory of identical particles.* Il Nuovo Cimento B Series 11 **37** (1), (1977), 1. DOI 10.1007/BF02727953

[150] Lesovik, G. B. *Excess quantum noise in 2D ballistic point contacts.* Soviet Journal of Experimental and Theoretical Physics Letters **49**, (1989), 592

[151] Levin, M., B. I. Halperin, and B. Rosenow. *Particle-Hole Symmetry and the Pfaffian State.* Phys. Rev. Lett. **99**, (2007), 236806. DOI 10.1103/PhysRevLett.99.236806

[152] Levin, M. A. and X.-G. Wen. *String-net condensation: A physical mechanism for topological phases.* Phys. Rev. B **71**, (2005), 045110. DOI 10.1103/PhysRevB.71.045110

[153] Levkivskyi, I. P., A. Boyarsky, J. Fröhlich, and E. V. Sukhorukov. *Mach-Zehnder interferometry of fractional quantum Hall edge states.* Phys. Rev. B **80**, (2009), 045319. DOI 10.1103/PhysRevB.80.045319

[154] Lopez, A. and E. Fradkin. *Fractional quantum Hall effect and Chern-Simons gauge theories.* Phys. Rev. B **44**, (1991), 5246. DOI 10.1103/PhysRevB.44.5246

[155] MacDonald, A. H. *Introduction to the Physics of the Quantum Hall Regime* URL arXiv:cond-mat/9410047

[156] MacDonald, A. H. and P. Středa. *Quantized Hall effect and edge currents.* Phys. Rev. B **29**, (1984), 1616. DOI 10.1103/PhysRevB.29.1616

[157] Martin, T. *Noise in mesoscopic physics.* In H. Bouchiat and et al. (Editors), *Nanophysics: coherence and transport: Les Houches summer school*, 283–359. Elsevier, Amsterdam (2005)

[158] Martin, T. and R. Landauer. *Wave-packet approach to noise in multichannel mesoscopic systems*. Phys. Rev. B **45**, (1992), 1742. DOI 10.1103/PhysRevB.45.1742

[159] Mathai, A., R. Saxena, and H. Haubold. *The H-Function: Theory and Applications*. Springer (2009)

[160] Milovanović, M. and N. Read. *Edge excitations of paired fractional quantum Hall states*. Phys. Rev. B **53**, (1996), 13559. DOI 10.1103/PhysRevB.53.13559

[161] Moon, K., H. Yi, C. L. Kane, S. M. Girvin, and M. P. A. Fisher. *Resonant tunneling between quantum Hall edge states*. Phys. Rev. Lett. **71**, (1993), 4381. DOI 10.1103/PhysRevLett.71.4381

[162] Moore, G. and N. Read. *Nonabelions in the fractional quantum hall effect*. Nuclear Physics B **360**, (1991), 362. DOI 10.1016/0550-3213(91)90407-O

[163] Moore, G. and N. Seiberg. *Polynomial equations for rational conformal field theories*. Physics Letters B **212** (4), (1988), 451 . DOI 10.1016/0370-2693(88)91796-0

[164] Moore, J. E. *The birth of topological insulators*. Nature **464**, (2010), 194. DOI 10.1038/nature08916

[165] Nayak, C., S. H. Simon, A. Stern, M. Freedman, and S. Das Sarma. *Non-Abelian anyons and topological quantum computation*. Rev. Mod. Phys. **80**, (2008), 1083. DOI 10.1103/RevModPhys.80.1083

[166] Nayak, C. and F. Wilczek. *2n-quasihole states realize $2^{n-1}$-dimensional spinor braiding statistics in paired quantum Hall states*. Nuclear Physics B **479** (3), (1996), 529 . DOI 10.1016/0550-3213(96)00430-0

[167] Nazarov, Y. V. and Y. M. Blanter. *Quantum Transport*. Cambridge University Press, Cambridge (2009)

[168] Nobel Media AB Nobelprize.org. *Press Release: The 1985 Nobel Prize in Physics* (2013). URL http://www.nobelprize.org/nobel_prizes/physics/laureates/1985/press.html

[169] Nobel Media AB Nobelprize.org. *Press Release: The 1998 Nobel Prize in Physics* (2013). URL http://www.nobelprize.org/nobel_prizes/physics/laureates/1988/press.html

[170] Oliphant, T. E. *Python for Scientific Computing*. Computing in Science and Engineering **9** (3), (2007), 10

[171] Oshikawa, M., Y. B. Kim, K. Shtengel, C. Nayak, and S. Tewari. *Topological degeneracy of non-Abelian states for dummies*. Annals of Physics **322**, (2007), 1477. DOI 10.1016/j.aop.2006.08.001

[172] Overbosch, B. J. *Edge tunneling and transport in non-abelian fractional quantum Hall systems*. PhD. Thesis, Massachusetts Institute of Technology (2008)

[173] Overbosch, B. J. and X.-G. Wen. *Dynamical and scaling properties of nu=5/2 interferometer*. ArXiv e-prints URL arXiv:0706.4339

[174] Pan, W., J.-S. Xia, V. Shvarts, D. E. Adams, H. L. Stormer, D. C. Tsui, L. N. Pfeiffer, K. W. Baldwin, and K. W. West. *Exact Quantization of the Even-Denominator Fractional Quantum Hall State at $\nu = 5/2$ Landau Level Filling Factor*. Phys. Rev. Lett. **83** (17), (1999), 3530. DOI 10.1103/PhysRevLett.83.3530

[175] Peskin, M. E. and D. V. Schroeder. *An Introduction To Quantum Field Theory*. Westview Press (1995)

[176] Peterson, P. *F2PY: a tool for connecting Fortran and Python programs*. Int. J. of Computational Science and Engineering **4** (4), (2009), 296 . URL http://www.f2py.com/

[177] Prange, R. E. and S. M. Girvin (Editors). *The Quantum Hall Effect*. Springer-Verlag, New York (1987)

[178] Preskill, J. *Lecture notes on quantum computation* (1998). URL http://www.theory.caltech.edu/people/preskill/ph229

[179] Pruisken, A. M. M. *Universal Singularities in the Integral Quantum Hall Effect*. Phys. Rev. Lett. **61**, (1988), 1297. DOI 10.1103/PhysRevLett.61.1297

[180] Rammer, J. *Quantum Field Theory of Non-Equilibrium States*. Cambridge Univ., Cambridge (2007)

[181] Read, N. *Order Parameter and Ginzburg-Landau Theory for the Fractional Quantum Hall Effect*. Phys. Rev. Lett. **62**, (1989), 86. DOI 10.1103/PhysRevLett.62.86

[182] Read, N. *Excitation structure of the hierarchy scheme in the fractional quantum Hall effect*. Phys. Rev. Lett. **65**, (1990), 1502. DOI 10.1103/PhysRevLett.65.1502

[183] Read, N. and G. Moore. *Fractional Quantum Hall Effect and Nonabelian Statistics*. Progress of Theoretical Physics Supplement **107**, (1992), 157. DOI 10.1143/PTPS.107.157

[184] Read, N. and E. Rezayi. *Beyond paired quantum Hall states: Parafermions and incompressible states in the first excited Landau level.* Phys. Rev. B **59**, (1999), 8084. DOI 10.1103/PhysRevB.59.8084

[185] Regnault, N. and B. A. Bernevig. *Fractional Chern Insulator.* Phys. Rev. X **1**, (2011), 021014. DOI 10.1103/PhysRevX.1.021014

[186] Rezayi, E. H. and N. Read. *Non-Abelian quantized Hall states of electrons at filling factors 12/5 and 13/5 in the first excited Landau level.* Phys. Rev. B **79**, (2009), 075306. DOI 10.1103/PhysRevB.79.075306

[187] Reznikov, M., R. D. Picciotto, T. G. Griffiths, M. Heiblum, and V. Umansky. *Observation of quasiparticles with one-fifth of an electron's charge.* Nature **399**, (1999), 238. DOI 10.1038/20384

[188] Rosenow, B. and B. I. Halperin. *Nonuniversal Behavior of Scattering between Fractional Quantum Hall Edges.* Phys. Rev. Lett. **88**, (2002), 096404. DOI 10.1103/PhysRevLett.88.096404

[189] Rosenow, B. and B. I. Halperin. *Influence of Interactions on Flux and Back-Gate Period of Quantum Hall Interferometers.* Phys. Rev. Lett. **98**, (2007), 106801. DOI 10.1103/PhysRevLett.98.106801

[190] Rosenow, B., B. I. Halperin, S. H. Simon, and A. Stern. *Bulk-Edge Coupling in the Non-Abelian $\nu = 5/2$ Quantum Hall Interferometer.* Phys. Rev. Lett. **100**, (2008), 226803. DOI 10.1103/PhysRevLett.100.226803

[191] Rosenow, B., B. I. Halperin, S. H. Simon, and A. Stern. *Exact solution for bulk-edge coupling in the non-Abelian $\nu = 5/2$ quantum Hall interferometer.* Phys. Rev. B **80**, (2009), 155305. DOI 10.1103/PhysRevB.80.155305

[192] Safi, I., C. Bena, and A. Crépieux. *ac conductance and nonsymmetrized noise at finite frequency in quantum wires and carbon nanotubes.* Phys. Rev. B **78**, (2008), 205422. DOI 10.1103/PhysRevB.78.205422

[193] Saminadayar, L., D. C. Glattli, Y. Jin, and B. Etienne. *Observation of the $e/3$ Fractionally Charged Laughlin Quasiparticle.* Phys. Rev. Lett. **79**, (1997), 2526. DOI 10.1103/PhysRevLett.79.2526

[194] Schottky, W. *Small-Shot Effect and Flicker Effect.* Phys. Rev. **28**, (1926), 74. DOI 10.1103/PhysRev.28.74

[195] Slingerland, J. and F. Bais. *Quantum groups and non-Abelian braiding in quantum Hall systems*. Nuclear Physics B **612** (3), (2001), 229 . DOI 10.1016/S0550-3213(01)00308-X

[196] Smits, O. *Numerical implementation of the R function* (2013). URL http://github.com/olafSmits/rfunction

[197] Sreejith, G. J., C. Tőke, A. Wójs, and J. K. Jain. *Bipartite Composite Fermion States*. Phys. Rev. Lett. **107**, (2011), 086806. DOI 10.1103/PhysRevLett.107.086806

[198] Steinhardt, P. J. *Problems of quantization in the infinite momentum frame*. Annals of Physics **128** (2), (1980), 425 . DOI 10.1016/0003-4916(80)90327-9

[199] Stern, A. and B. I. Halperin. *Proposed Experiments to Probe the Non-Abelian $\nu = 5/2$ Quantum Hall State*. Phys. Rev. Lett. **96**, (2006), 016802. DOI 10.1103/PhysRevLett.96.016802

[200] Stone, M. *Edge waves in the quantum Hall effect*. Annals of Physics **207** (1), (1991), 38 . DOI 10.1016/0003-4916(91)90177-A

[201] Stone, M. *Vertex operators in the quantum Hall effect*. International Journal of Modern Physics B **05** (03), (1991), 509. DOI 10.1142/S0217979291000316

[202] Sundermeyer, K. *Constrained Dynamics*. Springer-Verlag (1982)

[203] Suorsa, J., S. Viefers, and T. H. Hansson. *Quasihole condensates in quantum Hall liquids*. Phys. Rev. B **83**, (2011), 235130. DOI 10.1103/PhysRevB.83.235130

[204] Thouless, D. *Introduction to Topological Quantum Numbers*. In A. Comtet, T. Jolicoeur, S. Ouvry, and F. David (Editors), *Topological aspects of low dimensional systems*, volume 69, 767–841. Springer, Berlin (1999). DOI 10.1007/3-540-46637-1_11

[205] Thouless, D. J., M. Kohmoto, M. P. Nightingale, and M. den Nijs. *Quantized Hall Conductance in a Two-Dimensional Periodic Potential*. Physical Review Letters **49**, (1982), 405. DOI 10.1103/PhysRevLett.49.405

[206] Trauzettel, B., P. Roche, D. C. Glattli, and H. Saleur. *Effect of interactions on the noise of chiral Luttinger liquid systems*. Phys. Rev. B **70**, (2004), 233301. DOI 10.1103/PhysRevB.70.233301

[207] Treiman, S. B., R. Jackiw, B. Zumino, and E. Witten. *Current Algebra and Anomalies*. Princeton University Press (1985)

[208] Tsui, D. C., H. L. Stormer, and A. C. Gossard. *Two-Dimensional Magnetotransport in the Extreme Quantum Limit*. Phys. Rev. Lett. **48** (22), (1982), 1559. DOI `10.1103/PhysRevLett.48.1559`

[209] von Delft, J. and H. Schoeller. *Bosonization for beginners - refermionization for experts*. Annalen der Physik **7**, (1998), 225. DOI `10.1002/(SICI)1521-3889(199811)7:4<225::AID-ANDP225>3.0.CO;2-L`

[210] Wang, C. and D. E. Feldman. *Fluctuation-dissipation theorem for chiral systems in nonequilibrium steady states*. Phys. Rev. B **84**, (2011), 235315. DOI `10.1103/PhysRevB.84.235315`

[211] Wang, C. and D. E. Feldman. *Chirality, Causality, and Fluctuation-Dissipation Theorems in Nonequilibrium Steady States*. Phys. Rev. Lett. **110**, (2013), 030602. DOI `10.1103/PhysRevLett.110.030602`

[212] Wang, Z. *Topological quantum computation*. American Mathematical Society, Providence, Rhode Island (2010)

[213] Wen, X.-G. *Chiral Luttinger liquid and the edge excitations in the fractional quantum Hall states*. Phys. Rev. B **41**, (1990), 12838. DOI `10.1103/PhysRevB.41.12838`

[214] Wen, X.-G. *Topological order in rigid states*. International Journal of Modern Physics B **04** (02), (1990), 239. DOI `10.1142/S0217979290000139`

[215] Wen, X.-G. *Edge transport properties of the fractional quantum Hall states and weak-impurity scattering of a one-dimensional charge-density wave*. Phys. Rev. B **44**, (1991), 5708. DOI `10.1103/PhysRevB.44.5708`

[216] Wen, X.-G. *Gapless boundary excitations in the quantum Hall states and in the chiral spin states*. Phys. Rev. B **43**, (1991), 11025. DOI `10.1103/PhysRevB.43.11025`

[217] Wen, X.-G. *Theory of the Edge States in Fractional Quantum Hall Effects*. International Journal of Modern Physics B **6**, (1992), 1711. DOI `10.1142/S0217979292000840`

[218] Wen, X.-G. *Topological orders and edge excitations in fractional quantum Hall states*. Advances in Physics **44**, (1995), 405. DOI `10.1080/00018739500101566`

[219] Wen, X.-G. *Quantum field theory of many-body systems*. Oxford University Press, Oxford (2004)

[220] Wen, X.-G. *An Introduction of Topological Orders* (2012). URL `http://dao.mit.edu/~wen/topartS3.pdf`

[221] Wen, X.-G. *Topological order: from long-range entangled quantum matter to an unification of light and electrons.* ISRN Condensed Matter Physics **2013** (198710), (2013), 239. DOI 10.1155/2013/198710

[222] Wen, X.-G. and Q. Niu. *Ground-state degeneracy of the fractional quantum Hall states in the presence of a random potential and on high-genus Riemann surfaces.* Phys. Rev. B **41**, (1990), 9377. DOI 10.1103/PhysRevB.41.9377

[223] Wen, X.-G. and Z. Wang. *Classification of symmetric polynomials of infinite variables: Construction of Abelian and non-Abelian quantum Hall states.* Phys. Rev. B **77**, (2008), 235108. DOI 10.1103/PhysRevB.77.235108

[224] Wen, X.-G. and A. Zee. *Classification of Abelian quantum Hall states and matrix formulation of topological fluids.* Phys. Rev. B **46**, (1992), 2290. DOI 10.1103/PhysRevB.46.2290

[225] Wilczek, F. *Fractional statistics and anyon superconductivity.* World Scientific Publishing Co. Pre. Ltd, Singapore (1990)

[226] Willett, R., J. P. Eisenstein, H. L. Störmer, D. C. Tsui, A. C. Gossard, and J. H. English. *Observation of an even-denominator quantum number in the fractional quantum Hall effect.* Phys. Rev. Lett. **59**, (1987), 1776. DOI 10.1103/PhysRevLett.59.1776

[227] Willett, R. L., C. Nayak, K. Shtengel, L. N. Pfeiffer, and K. W. West. *Magnetic field-tuned Aharonov-Bohm oscillations and evidence for non-Abelian anyons at $\nu = 5/2$.* ArXiv e-prints URL arXiv:1301.2639

[228] Willett, R. L., L. N. Pfeiffer, and K. W. West. *Measurement of filling factor 5/2 quasiparticle interference with observation of charge e/4 and e/2 period oscillations.* PNAS **106**, (2009), 8853. DOI 10.1073/pnas.0812599106

[229] Willett, R. L., L. N. Pfeiffer, and K. W. West. *Alternation and interchange of e/4 and e/2 period interference oscillations consistent with filling factor 5/2 non-Abelian quasiparticles.* Phys. Rev. B **82** (20), (2010), 205301. DOI 10.1103/PhysRevB.82.205301

[230] Willett, R. L., L. N. Pfeiffer, and K. W. West. *Magnetic field induced resistance properties at filling factor 5/2 consistent with non-Abelian e/4 quasiparticles in multiple sized interferometers.* ArXiv e-prints URL arXiv:1204.1993

[231] Willett, R. L., L. N. Pfeiffer, K. W. West, and M. Manfra. *Aharonov-Bohm effect and coherence length of charge $e/4$ quasiparticles at 5/2 filling factor measured in multiple small Fabry-Perot interferometers.* ArXiv e-prints URL arXiv:1301.2594

[232] Willett, R. W. *The quantum Hall effect at 5/2 filling factor*. Reports on Progress in Physics **76** (7), (2013), 076501. DOI 10.1088/0034-4885/76/7/076501

[233] Witten, E. *Quantum field theory and the Jones polynomial*. Comm. in Math. Phys. **121**, (1989), 351

[234] Xia, J. S., W. Pan, C. L. Vicente, E. D. Adams, N. S. Sullivan, H. L. Stormer, D. C. Tsui, L. N. Pfeiffer, K. W. Baldwin, and K. W. West. *Electron Correlation in the Second Landau Level: A Competition Between Many Nearly Degenerate Quantum Phases*. Phys. Rev. Lett. **93**, (2004), 176809. DOI 10.1103/PhysRevLett.93.176809

[235] Yang, K. *Field Theoretical Description of Quantum Hall Edge Reconstruction*. Phys. Rev. Lett. **91**, (2003), 036802. DOI 10.1103/PhysRevLett.91.036802

[236] Yoshioka, D. *The Quantum Hall Effect*. Springer, New York (2002)

[237] Zee, A. *Quantum Hall Fluids*. In H. Geyer (Editor), *Field Theory, Topology and Condensed Matter Physics*, 99–153. Springer, New York (1995)

[238] Zhang, S. C., T. H. Hansson, and S. Kivelson. *Effective-Field-Theory Model for the Fractional Quantum Hall Effect*. Phys. Rev. Lett. **62**, (1989), 82. DOI 10.1103/PhysRevLett.62.82

[239] Zhang, Y., D. T. McClure, E. M. Levenson-Falk, C. M. Marcus, L. N. Pfeiffer, and K. W. West. *Distinct signatures for Coulomb blockade and Aharonov-Bohm interference in electronic Fabry-Perot interferometers*. Phys. Rev. B **79**, (2009), 241304. DOI 10.1103/PhysRevB.79.241304

[240] Zirnstein, H.-G. and B. Rosenow. *Cancellation of quantum anomalies and bosonization of three-dimensional time-reversal symmetric topological insulators*. ArXiv e-prints URL arXiv:1303.2644